GA-A12916
UC-77

HTGR BASE PROGRAM

QUARTERLY PROGRESS REPORT FOR THE PERIOD ENDING FEBRUARY 28, 1974

Prepared under
Contract AT(04-3)-167
Project Agreement No. 17
for the
San Francisco Operations Office
U.S. Atomic Energy Commission

GENERAL ATOMIC PROJECT 317 DATE PUBLISHED - MARCH 29, 1974

GENERAL ATOMIC

GENERAL ATOMIC COMPANY
P.O. BOX 81608
SAN DIEGO, CALIFORNIA 92138

QUARTERLY REPORT SERIES

GA-4072-December, 1962, through February, 1963
GA-4350-March, 1963, through May, 1963
GA-4569-June, 1963, through August, 1963
GA-4937-September, 1963, through November, 1963
GA-5104-December, 1963, through February, 1964
GA-5366-March, 1964, through May, 1964
GA-5618-June, 1964, through August, 1964
GA-5866-September, 1964, through November, 1964
GA-6113-December, 1964, through February, 1965
GA-6418-March, 1965, through May, 1965
GA-6671-June, 1965, through August, 1965
GA-6869-September, 1965, through November, 1965
GA-7010-December, 1965, through February, 1966
GA-7181-March, 1966, through May, 1966
GA-7396-June, 1966, through August, 1966
GA-7553-September, 1966, through November, 1966
GA-7801-December, 1966, through February, 1967
GA-7981-March, 1967, through May, 1967
GA-8200-June, 1967, through August, 1967
GA-8356-September, 1967, through November, 1967
GA-8530-December, 1967, through February, 1968
GA-8662-March, 1968, through May, 1968
GA-8860-June, 1968, through August, 1968
GA-9090-September, 1968, through November, 1968
GA-9227-December, 1968, through February, 1969
GA-9372-March, 1969, through May, 1969
GA-9660-June, 1969, through August, 1969
GA-9815-September, 1969, through November, 1969
GA-9944-December, 1969, through February, 1970
GA-10088-March, 1970, through May, 1970
GA-10288-June, 1970, through August, 1970
GA-10399-September, 1970, through November, 1970
GA-10501-December, 1970, through February, 1971
GA-10661-March, 1971, through May, 1971
Gulf-GA-A10784-June, 1971, through August, 1971
Gulf-GA-A10930-September, 1971, through November, 1971
Gulf-GA-A10999-December, 1971, through February, 1972
Gulf-GA-A12150-March, 1972, through May, 1972
Gulf-GA-A12222-June, 1972, through August, 1972
Gulf-GA-A12422-September, 1972, through November, 1972
Gulf-GA-A12515-December, 1972, through February 1973
Gulf-GA-12599-March, 1973, through May, 1973
Gulf-GA-A12725-June, 1973, through August, 1973
Gulf-GA-A12818-September 1973, through November, 1973

ABSTRACT

This publication continues the quarterly report series on the HTGR Base Program. The Program covers items of the base technology of the High-Temperature Gas-cooled Reactor (HTGR) system. The development of the HTGR system will, in part, meet the greater national objective of more effective and efficient utilization of our national resources. The work reported here includes studies of basic fission-product distribution mechanisms, recycle fuel studies (including designing and testing of recycle test elements) and exploration of head-end reprocessing methods (as part of a national recycle plan and of a recycle fuel plan), and physics and fuel management studies. Materials studies include irradiation and analysis of fuel particles in capsules to evaluate fuel systems, and basic studies of control materials and of carbon and graphite. Experimental procedures and results are discussed and, where appropriate, the data are presented in tables, graphs, and photographs. More detailed descriptions of experimental work are presented in topical reports, and these are listed at the end of the report for those concerned with the field.

INTRODUCTION

This report covers the work performed by the General Atomic Company under U.S. Atomic Energy Commission Contract AT(04-3)-167, Project Agreement No. 17. This Project Agreement calls for support of basic technology associated with gas-cooled, nuclear power reactor systems. The program is based on the concept of the High-temperature Gas-cooled Reactor (HTGR) developed by the General Atomic Company.

Large HTGR systems will be placed in operation starting in the late 1970's following the operation of the 330-MW(e) prototype in 1973. Characteristics of these advanced systems include:

1. A single-phase gas coolant allowing generation of high-temperature, high-pressure steam with consequent high-efficiency energy conversion and low thermal discharge.

2. A prestressed concrete reactor vessel (PCRV) offering advantages in field construction, primary system integrity, and stressed member inspectability.

3. Graphite core material assuring high-temperature structural strength, large temperature safety margins, and good neutron economy.

4. Thorium fuel cycle leading to U-233 fuel which allows good utilization of nuclear resources and minimum demands on separative work.

CONTENTS

FIGURES

TABLES

TASK IV
FISSION PRODUCT MECHANISMS

VAPOR PRESSURE STUDIES

Cesium Isotherm Measurements

The pressure-versus-concentration cesium isotherms have shown a downward break at low concentrations (see earlier Quarterly Progress Report Gulf-GA-A12515). This behavior has not been observed for strontium. Past experiments provided inadequate data to explain the break. Recent experiments utilizing an interconnected double Knudsen cell, where loading and unloading could be simultaneously observed, have yielded significant results (see earlier Quarterly Progress Reports Gulf-GA-A12599 and Gulf-GA-A12725). The results of these experiments lead to the conclusion that the pressure break is due to a rapid change of vaporization kinetics at low concentrations. Although it is conjectured that this effect (i.e., slow vaporization kinetics) will also occur in the reactor, it is not yet used in present FIPER code calculations for fission product transport from the core.

Cesium isotherms, shown in Fig. 4-1, have been measured for H-451 graphite (44 to 74 μm size) using the Knudsen cell - mass spectrometric technique. The results are identical, within the precision of the measurements, to those for H-327 graphite.

Sorption Measurements

A program to obtain information on the sorption of cesium and strontium on various unirradiated carbon materials is under way. This

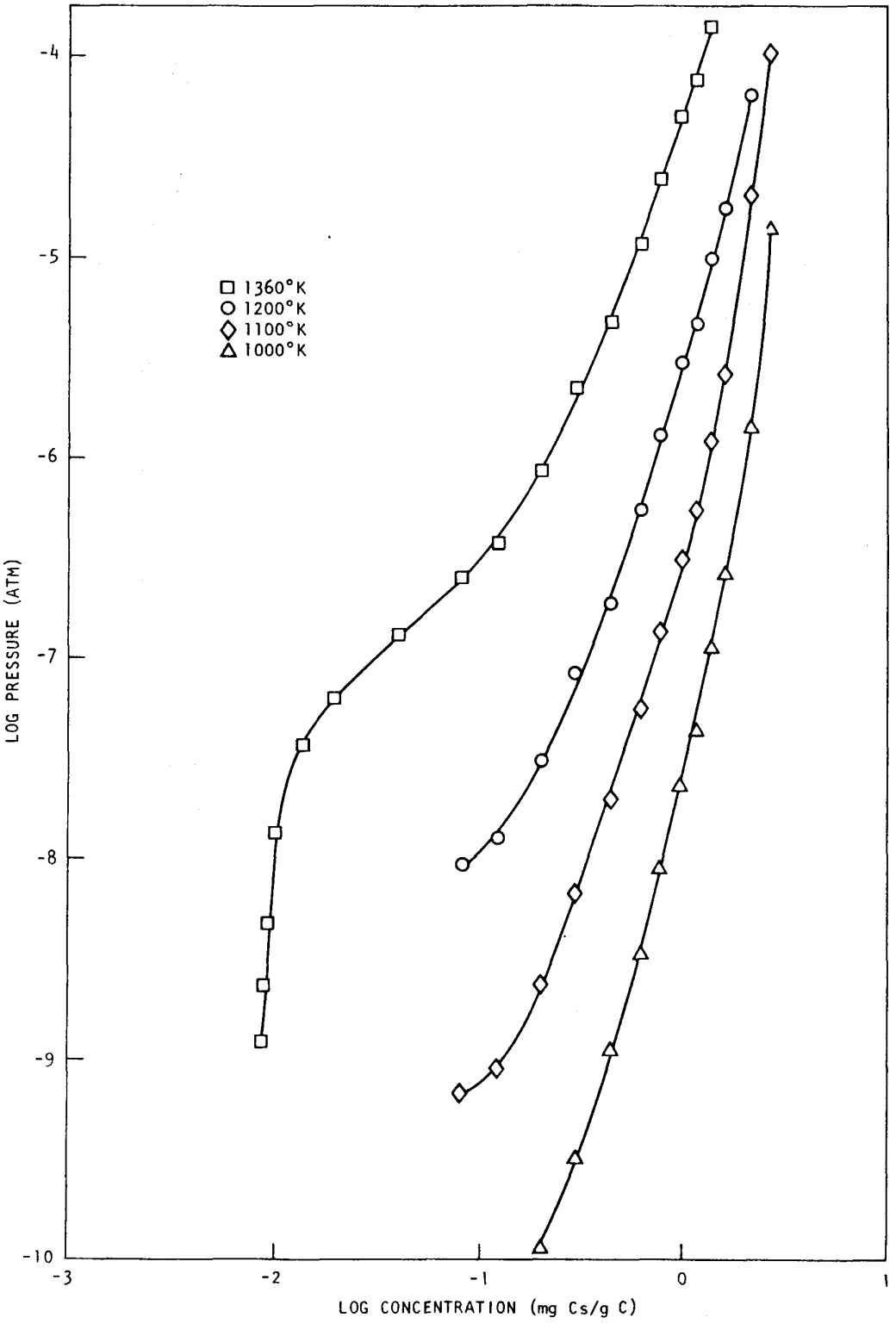

Fig. 4-1. Vapor pressure of cesium over H-451 graphite

work will provide data on ϕ, the sorption ratio, which is defined as the ratio of fission product metal concentration in the fuel matrix to that in the graphite.

The measurements were made by annealing the samples for 8 hours at 1200°C (for cesium) or 1400°C (for strontium) in sealed tantalum cells containing cesium or strontium sources. These sources were prepared by loading H-327 graphite of 44 to 74-μm particle size with the element nitrate containing a small amount of Cs-137 or Sr-85 tracer. The relative sorptivity of each sample with respect to powder H-327 graphite was deduced from the weights of the sample and the H-327 graphite source and their cesium or strontium concentrations. The results of these measurements are shown in Tables 4-1 through 4-4.

The following conclusions can be drawn from these measurements:

1. Both resin-type and pitch-type cokes are good sinks for strontium.

2. Although coal tar and petroleum pitch cokes do not take up cesium as well as strontium, two resin-type cokes, furfuryl alcohol coke and Resinox 50-50 (50% wt % phenolic resin and 50 wt % graphite powder), are good cesium sinks.

3. The addition of graphite filler tends to deteriorate the cesium sorptivity of Resinox coke but not pitch-type cokes.

4. The sorptivity of strontium does not change significantly with the particle size of the H-327 graphite, while the sorptivity of cesium decreases by a factor of 2.2 between the 44-74 μm powder and the bulk graphite.

5. There is evidence that the cesium sorptivity on matrix material does not change significantly from fine powder to bulk material.

TABLE 4-1

CESIUM SORPTION ON UNIRRADIATED PITCH COKES AND MATRIX MATERIALS

Run	Final Cs Source Concentration (mg Cs/g C)	Sample	Sample Conc. / Source Conc.
S-1	0.59	M-205 matrix, 44-74 μm, petroleum pitch	5.8
S-2	0.49	M-156 matrix, 44-74 μm, petroleum pitch	6.5
S-3	0.94	M-266 matrix, 44-74 μm, Lanza filler, petroleum pitch	3.8
S-4	1.22	M-259 matrix, rod cured in Al_2O_3, 44-74 μm, petroleum pitch	4.3
S-4	1.22	A-240 "Ashland oil" petroleum pitch, not sieved	5.0
S-7	0.16	B018 "boron oil" petroleum pitch, 44-74 μm	8.4
S-2	0.47	FSV production matrix, 44-74 μm, coal tar pitch	6.0
S-3	0.94	FSV production matrix, 3-mm chunks, coal tar pitch	4.7
S-2	0.47	M-155 laboratory prepared FSV matrix, 44-74 μm, coal tar pitch	6.9
S-9	0.76	M-224 matrix made with "Koppers" coal tar pitch, 44-74 μm	5.3

TABLE 4-2

CESIUM SORPTION ON UNIRRADIATED RESIN COKES

Run	Final Cs Source Concentration (mg Cs/g C)	Sample	Sample Conc. / Source Conc.
S-1	0.59	Furfuryl alcohol coke, 62-144 μm, old sample	186.0
S-7	0.16	Furfuryl alcohol coke, 44-74 μm, powder fired	98.1
S-11	0.88	Furfuryl alcohol coke, 44-74 μm, rod fired at 1100°C	110.0
S-11	0.88	Furfuryl alcohol coke, 44-74 μm, rod fired at 1800°C	49.3
S-7	0.16	A-3, HOBEG matrix, 44-74 μm, various firings, phenolic resin	6.8
S-10	0.61	Resinox 80-20 (filler resin), 44-74 μm, phenolic resin, powder fired	9.6
S-10	0.61	Resinox 50-50, 44-74 μm, phenolic resin	62.2
S-11	0.88	Resinox 80-20, 44-74 μm, rod fired	9.8

TABLE 4-3

CESIUM SORPTION ON MISCELLANEOUS UNIRRADIATED CARBON MATERIALS

Run	Final Cs Source Concentration (mg Cs/g C)	Sample	Sample Conc. / Source Conc.
S-4	1.22	H-327 graphite, 149-250 μm	0.74
S-5	1.39	H-327 graphite, 250-420 μm	0.74
S-8	0.035	H-327 graphite, 149-250 μm	0.71
S-8	0.035	H-327 graphite, 420-841 μm	0.51
S-8	0.035	H-327 graphite, 1.7-3.3 mm	0.46
S-1	0.59	H-327 graphite, 44-74 μm	1.5
S-3	0.94	Matrix, pre-core 1, 44-74 μm	5.4
S-10	0.61	Matrix, Allied Chemical H.O.I.P. (GA M-001) pitch, 44-74 μm	2.5
S-5	1.39	FO-115, impregnated Lanza shim, not sieved	2.8
S-5	1.39	FO-136, impregnated Great Lakes Carbon Company shim, not sieved	2.7

TABLE 4-4

STRONTIUM SORPTION ON UNIRRADIATED CARBON MATERIALS

Run	Final Sr Source Concentration (mg Sr/g C)	Sample	Sample Conc. / Source Conc.
S-6	0.017	FSV production matrix, 44-74 μm, coal tar pitch	36.0
S-6	0.017	M-205, new matrix, 44-74 μm petroleum pitch	46.0
S-6	0.017	Furfuryl alcohol coke, 62-149 μm, old sample	99.0
S-6	0.017	FO-115, impregnated, Lanza shim, not sieved	3.8
S-6	0.017	H-327 graphite, 44-74 μm	1.0
S-6	0.017	H-327 graphite, 250-450 μm	0.7
S-6	0.017	H-327 graphite, 450-841 μm	1.1
S-6	0.017	H-327 graphite, 1.7-3.3 mm	1.1

Variations of cesium sorptivity among the various fuel-rod matrix materials shown in Tables 4-1 through 4-4 suggested the need for a correlation between structural properties of carbonaceous materials and their sorptivity with respect to cesium. As a first step, four samples of well characterized carbon blacks were obtained through the courtesy of Dr. Medalia of the Cabbot Corporation. Two of these were commercial carbon blacks differing greatly in particle size and therefore BET surface areas. The other two were derived from these two by graphitization at 2700°C, which affected the BET surface areas only negligibly but greatly changed the electron-microscopic appearance of the particles from smooth-surfaced and homogeneous to angular and layered. Their X-ray diffraction also changed greatly during graphitization, but the low-area Sterling sample gave a clearly sharper X-ray diffraction pattern than the low-area Vulcan sample when the two ungraphitized and the two graphitized samples were compared.

When equilibrated against cesium containing H-327 graphite at 1200°C for 8 hours, the relative sorptivities shown in Table 4-5 were found.

TABLE 4-5

CESIUM SORPTION ON WELL CHARACTERIZED UNIRRADIATED CARBON MATERIALS

Sample	Relative Cs Sorptivity	BET N_2 Surface Area (m^2/g)
Vulcan (ungraphitized)	226	81
Sterling (ungraphitized)	114	6.2
Vulcan (graphitized)	14	73
Sterling (graphitized)	3.1	8.1

The order is clearly that of the relative sharpness of the X-ray diffraction pattern and not of particle size or surface area, showing

that cesium is sorbed at graphite defects not necessarily accessible to nitrogen. This conclusion leads to the conjucture that neutron irradiation, such as will occur in the reactor, will increase the sorptivity of graphite and matrix materials by creation of many new defects or active sites.

FISSION PRODUCT PLATEOUT AND LIFTOFF STUDIES

A deposition loop, assembled at GAC, is being used to study the plateout characteristics of cesium, strontium, and iodine under conditions similar to HTGR conditions. Helium at 350 psia circulates in the loop with Reynolds numbers of around 15,000 and temperatures varying from 150° to 320°C. The type of steel used for the loop tubing is representative of steel used in the steam generators of HTGRs. Surface temperatures in the loop vary from 200° to 400°C. The source of fission products in the loop is obtained by heating graphite crucibles within the loop that are loaded with the fission products sorbed on graphite matrix material.

The objectives of the loop work are to obtain plateout distribution data and to obtain liftoff data by subjecting sections of the loop to conditions of higher shear ratios than obtained in the loop. The plateout data are used to test and refine the PAD code. The liftoff data are used for safety analyses associated with HTGR depressurization accidents.

As reported in the previous Quarterly Progress Report (Gulf-GA-A12818), loop No. 5 (Sr tagged with Sr-85) was compromised by very low strontium release and dust generated by graphite corrosion due to impurities (H_2O, O_2) in the helium. Therefore, counting statistics of the blowdown tests were so poor that the results were qualitative at best.

Efforts began this quarter to repeat the strontium transport experiment with modifications to eliminate the problems present in loop No. 5. A new electrical resistance source heater was built using Kanthal windings rather than Nichrome to facilitate higher source temperatures (2000° to 2200°F); the heater design was further improved by increasing the purge flow of helium over the graphite crucibles containing the source material. In addition, the helium supply will be purified by passage through charcoal in liquid nitrogen to decrease the gaseous impurity levels.

A number of new difficulties have been encountered in the present efforts, including failure of the blower which necessitated a rather long delay in replacement and reinstallation. However, in spite of the delays, the experiment (loop No. 6) is currently being started and should be completed by the end of March 1974.

REACTIONS OF COOLANT IMPURITIES WITH FUEL MATERIALS

Oxidation of Uranium Dicarbide by Carbon Monoxide

Introduction

The fissile particle for the HTGR is the TRISO coated UC_2 particle, which constitutes about 5% of the fuel inventory; the remaining 95% is the fertile ThO_2 particle. If the individual coatings on the fissile particles become cracked or otherwise fail during reactor operation, the possibility exists that the kernel could react with carbon monoxide impurity in the helium coolant (see earlier Quarterly Progress Report Gulf-GA-A12599) according to the reaction

$$UC_2 + 2CO = UO_2 + 4C \quad .$$

Thermodynamic calculations for this reaction show that when the partial pressure of CO is 4.7×10^{-4} atm (i.e., 10 ppm at 47 atm), which corresponds to the maximum level or technical specification limit for oxygen-containing impurities in the HTGR, conversion to oxide will occur at temperatures below 1322°C. Furthermore, even at concentrations of CO approaching 0.1 ppm, UC_2 oxidation is feasible at temperatures below 1100°C.

Because the oxidation product, $UO_2 + 4C$, has a greater molecular weight and a lower density than the original UC_2, oxidation could cause increased fission gas release, R/B, and expansion of the fuel rods. Expansion effects will be small, however, since only about 5% of the fuel consists of UC_2. In view of these considerations there is a need to measure the rate of reaction of UC_2 with carbon monoxide as a function of temperature, CO pressure, and fuel burnup.

Method

A series of samples of UC_2 are reacted with various partial pressures of CO at different temperatures and for different times. The samples to be used are as follows:

1. Bare loose unirradiated kernels.

2. Laser-drilled* irradiated loose particles.

3. Cracked irradiated loose particles.

4. Laser-drilled* particles in rods.

5. Bare unirradiated kernels in rods.

*Laser drilling of coated particles is a technique used to create representative failures in fuel particles. The laser holes are about 20 μm in diameter.

The extent of reaction after various times will be determined by (1) hydrolyzing the remaining UC_2 and measuring the hydrolysis product, ethane, and (2) standard metallographic techniques.

Apparatus

The reaction apparatus being used to conduct the oxidation is shown in Fig. 4-2. Since uranium dicarbide reacts readily with O_2, CO_2, and water, precautions are necessary to remove these impurities from the He/CO gas mixture. Accordingly, the gas is prepurified by passing it through an activated charcoal trap at -78°C to remove water, through an Ascarite trap to remove CO_2, and finally through a copper-gauze O_2 getter at 600°C.

The oxidation reaction is carried out in a quartz tube heated by an electric clamshell furnace. Temperatures are measured inside the quartz heater tube using a chromel-alumel thermocouple.

Procedure

The samples of UC_2 were weighed on a Cahn Electric microbalance and then transferred to graphite crucibles, which had previously been dried and stored in a vacuum desiccator. The samples were placed in the heater tube directly under the thermocouple, and the apparatus was immediately evacuated. After a 30-min evacuation, a helium flow was established, and the He/CO flow was vented to ensure saturation of the charcoal scrubber. The kinetic run was initiated by discontinuing the helium flow and starting the He/CO flow. When a kinetic sample was removed, the He/CO flow was stopped and the system was evacuated, which effectively quenched the reaction. To prevent back diffusion of atmospheric gases when the vessel was opened, a helium flow ($\sim$1 ℓ/min) was established and the sample was then removed. The exit end cap was replaced and the system was again evacuated to remove any atmospheric gas. The He/CO flow was then started. This procedure was repeated for each reaction time.

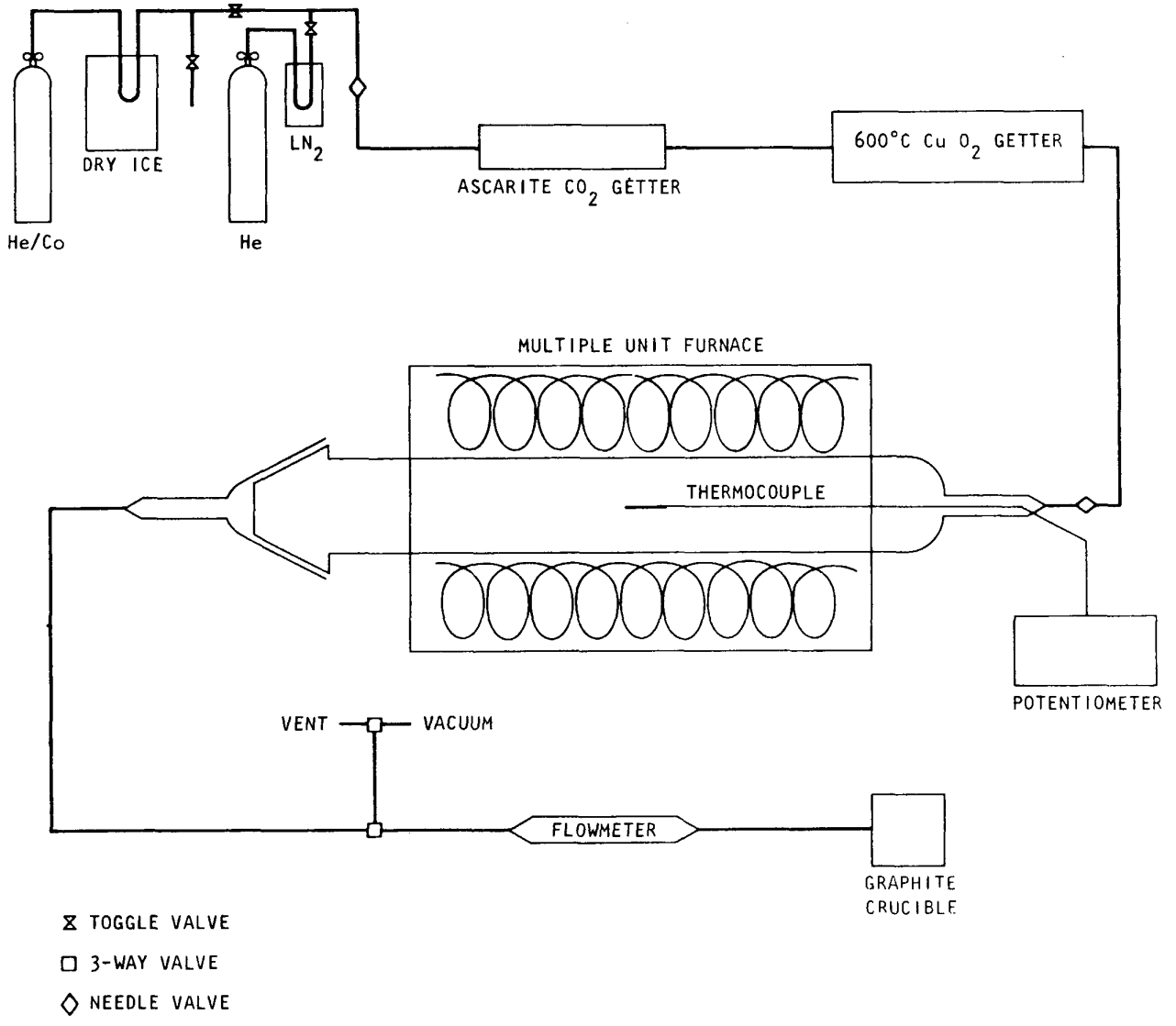

Fig. 4-2. Oxidation apparatus

The extent of reaction was measured by hydrolyzing the remaining UC_2 using the standard "carbide hydrolysis" method, which involves exposing a given sample in a pressure vessel at ∿115°C and to ∿1 atm steam. After a 90-min hydrolysis time, the amount of ethane produced is collected and determined by vapor phase chromatography. The amount of carbide in the sample is then calculated by comparison to known standard or control runs.

Results

To date, one preliminary experiment has been conducted. The results of this initial run are shown in Table 4-6. Using a gas mixture containing 500 ppm CO in He, at a temperature of 1150°C ± 5°C, it has been found that 70% of the bare unirradiated UC_2 has reacted in 161.5 hr. The data are plotted in Figure 4-3, assuming pseudo first-order kinetics. As can be seen there is a wide variation in the data, which is not unanticipated in heterogeneous reactions of this sort. Refinements in the apparatus and experimental techniques are expected to improve the precision of the kinetic data.

TABLE 4-6

REACTION OF UNIRRADIATED UC_2 BARE KERNELS WITH CO
(500-μatm CO in helium, 1150°C ± 5°C)

Sample No.	Accumulated Reaction Time (hr)	UC_2 Remaining (%)
1	0	98.7
2	20.8	84.3
3	44.1	83.3
4	69.3	46.8
5	90.1	78.8
6	161.7	29.7

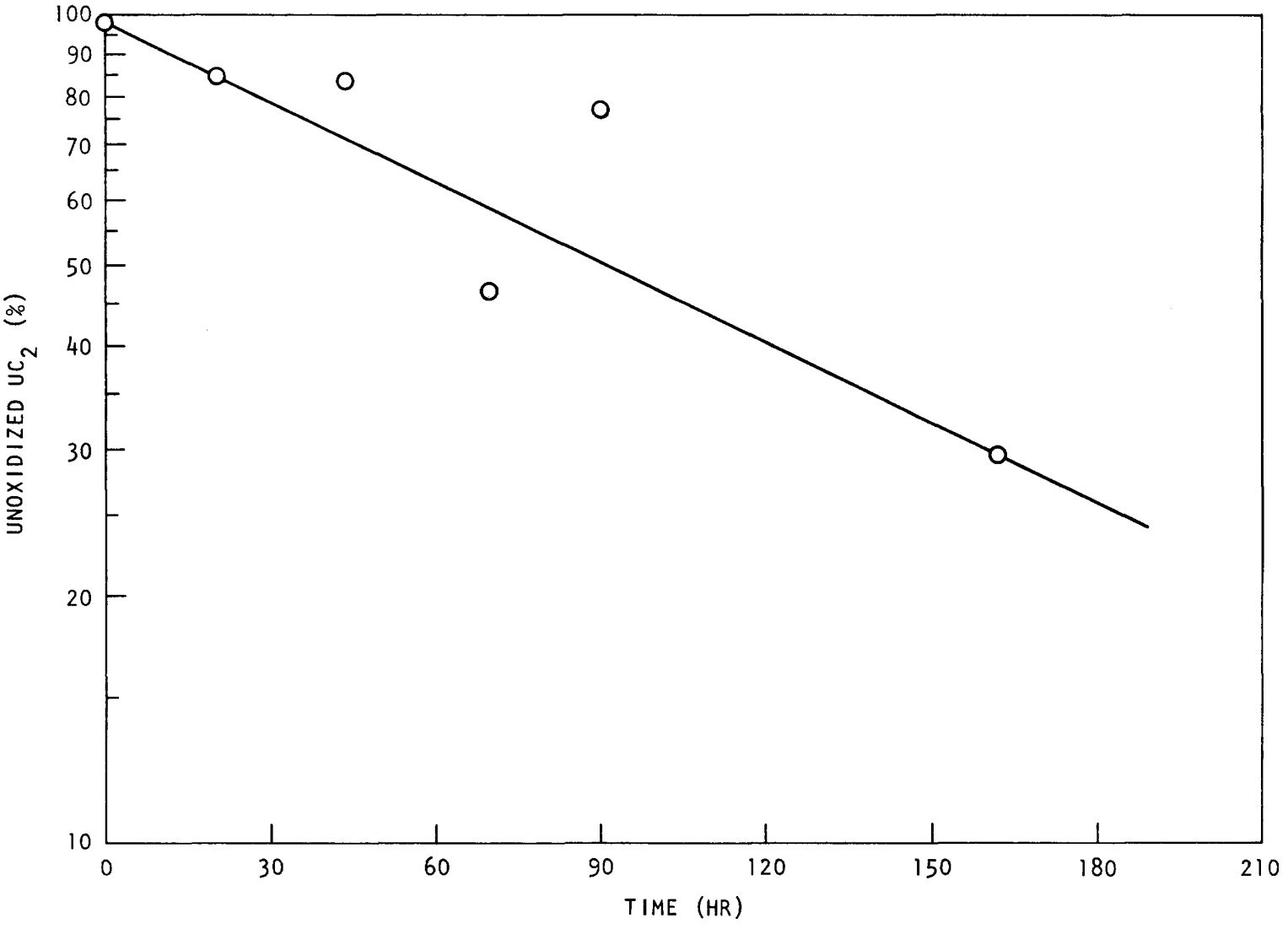

Fig. 4-3. Reaction of unirradiated UC_2 with CO at 1150°C and 500 μatm CO

Effect of Fuel Hydrolysis on Fission Gas Release (R/B)

Introduction

Hydrolysis of failed fissile (UC_2) fuel particles may proceed according to the reaction:

$$UC_2 + H_2O(g) = UO_2 \cdot XH_2O + H_2(g) + \text{hydrocarbon gases} \quad .$$

Exposure of fuel to water vapor can occur due to (1) small steady-state steam leaks whereby total coolant impurities ($CO + H_2O + CO_2$) may reach the technical specification limit of 10 ppm (500 μatm), or (2) large leaks such as tube ruptures, in which case the reactor would be rapidly shut down. In the latter case, however, steam pressures $\geq$1 atm could result. Hydrolysis of the fertile fuel will not occur to a significant extent because the fertile ThO_2 particles, even if they are failed, are stable to temperatures of about 1400°C, which is well above the normal maximum fuel temperature.

The immediate effect of UC_2 hydrolysis is a decrease in the density of the kernel material which causes: (1) an instantaneous release of stored fission gas from the hydrolyzed fraction, and (2) an increase in R/B, the steady-state fission gas release. The work presently being conducted at GAC concerning the effect of water vapor on the steady-state release of fission gas from carbide kernel materials is discussed below.

Method

Fuel rods have been prepared which contain small known amounts of unirradiated, uncoated $(Th,U)C_2$ kernels. This configuration should give pessimistic results because (1) the rate of hydrolysis of $(Th,U)C_2$ is faster than UC_2, (2) irradiation tends to reduce the hydrolysis rate, and (3) the use of uncoated kernels is a gross exaggeration of failed coated particles. These rods have been exposed to a wet argon atmosphere

for up to 2500 hr at two different temperatures. At several intervals during the exposure, the steady-state Kr-85m release rate at 1100°C was measured.

Experimental

Fabrication of Fuel Rods. In order to ensure easy location of the carbide kernels (for subsequent metallographic analysis), fuel rods 0.5 in. in diameter by 1 in. long were prepared in the following manner: the holes in a six-rod jig were half filled with PyC coated ZrO_2 dummy (i.e., unfueled) particles, the bare $(Th,U)C_2$ kernels were added, and then the remainder of the hole was filled with additional dummy particles. Injection of matrix material at 350°F with subsequent cooling resulted in a green rod with the test kernels located approximately at the center. The green rods were then placed in graphite crucibles and carbonized by firing in an argon atmosphere to 1200°C using the standard programmed rate of 10°C/min. The rods were held at 1200°C for 1 hr, fired at 1800°C for an additional hour, and then cooled to room temperature.

Apparatus and Hydrolysis Procedure. The apparatus used to conduct the hydrolysis reaction is shown in Fig. 4-4. A Venturi capillary diffusion vessel was used to provide approximately 100 ppm water vapor in an argon carrier gas. The concentration of water vapor was continuously measured using a Meeco (Manufacturers Engineering and Equipment Corporation) Model W electrolytic-type water analyzer. The fuel rods in their graphite crucibles were hydrolyzed inside a quartz heater tube with heat being supplied by a Kanthal-wound furnace connected to a Wheelco temperature controller. Temperatures were measured with a chromel-alumel thermocouple located in the annulus between the quartz heater tube and the furnace, midway from the furnace ends. The carrier gas flow was continuously monitored with a rotameter located at the exit end of the reaction tube.

To conduct a test run, the rod, contained in a graphite crucible, was placed in the furnace tube; the wet argon flow was established; and

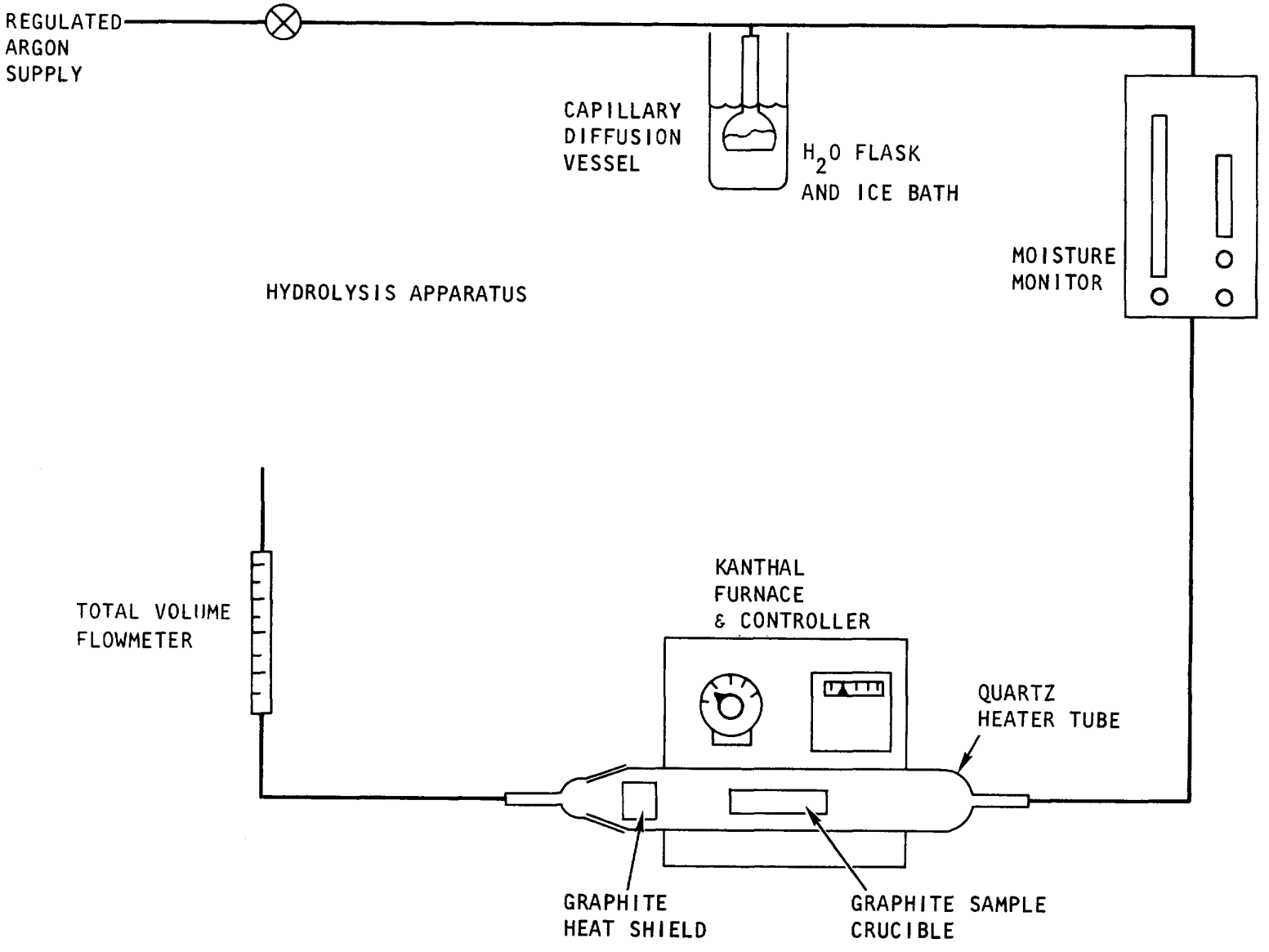

Fig. 4-4. Fuel hydrolysis apparatus

the furnace was then heated to the run temperature (800° or 900°C). After the appropriate time, the furnace was gradually cooled, the sample was removed, and an R/B determination was made using the TRIGA King furnace facility.

Results

The graphical representation of the data in Fig. 4-5 shows the effect of hydrolysis on R/B for bare unirradiated kernels in a fuel rod as a function of time at two hydrolysis temperatures. It is seen that a maximum in R/B occurs after about 600 hours exposure. Additional long-term annealing in the moist argon caused a slight decrease in R/B.

These experiments are not truly representative of HTGR fuel, but are part of a test program designed to understand the basic effects of hydrolysis on fission gas release. These data must be compared with hydrolysis tests on an irradiated FTE-3 fuel rod (see earlier Quarterly Progress Report Gulf-GA-A12725) which showed quite small increases in R/B after long-term exposure to 100-ppm water vapor. These results corroborate the expectation that hydrolysis of bare unirradiated uncoated UC_2 particles is more severe than hydrolysis of irradiated failed coated particles. Further studies in this series of experiments will include hydrolysis of test rods made from laser-drilled carbide particles (irradiated and unirradiated) and irradiated fuel rods or compacts with known failure fractions.

TRITIUM TRANSPORT STUDIES

This task consists of a joint effort by Los Alamos Scientific Laboratory (LASL) and General Atomic Company (GAC) to determine the retention of tritium in irradiated HTGR core materials. General Atomic Company has selected and characterized samples and LASL will do the tritium analyses, taking advantage of the excellent facilities and capable staff at LASL.

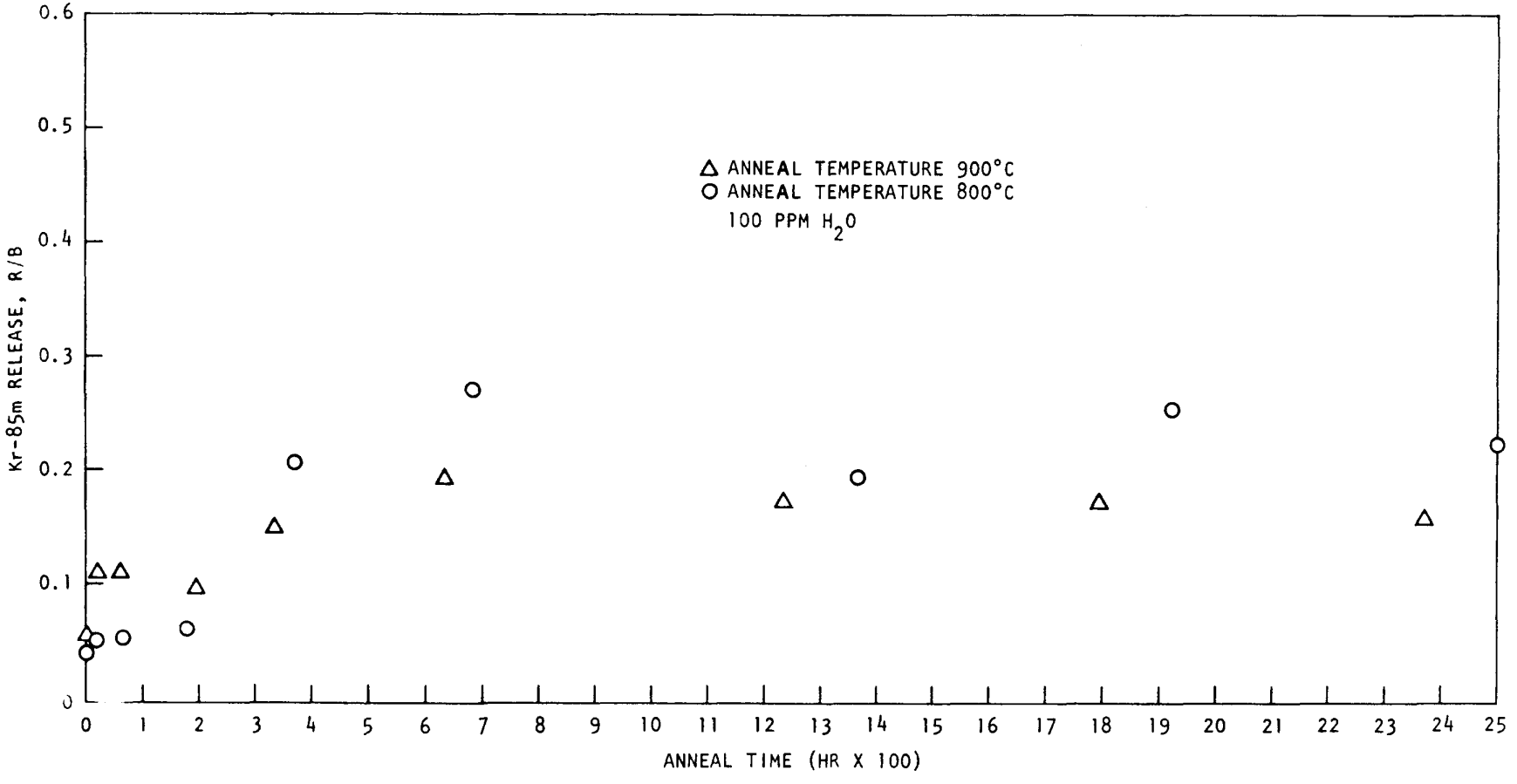

Fig. 4-5. Effect of hydrolysis on steady-state Kr-85m release (R/B) at 1100°C from fuel rods containing uncoated $(Th,U)C_2$ kernels

The principal sources of tritium in HTGR systems are ternary fission and neutron activation of (1) He-3 present in the helium coolant, (2) Li-6 and Li-7 present as impurities in the core and reflector materials, and (3) B-10 in the control rods and reflector materials.

The results of work at GAC and elsewhere generally indicate that tritium is retained in fuel materials at normal operating temperatures and that the retention decreases with increasing temperature.

Studies of tritium retention in graphite indicate that most of the tritium formed in the core graphite is retained there and that even an appreciable fraction of tritium produced from He-3 may be trapped by core materials. A small amount of work has been done on the concentration of tritium in irradiated control materials, and the results indicate appreciable tritium retention by these materials. Work on tritium retention in graphite and control materials is of particular importance because in present predictions it is conservatively assumed that all the tritium formed in these materials escapes into the helium coolant.

Several tritium surveys have been performed at the Peach Bottom HTGR. This work has yielded valuable data which are being used as a basis for estimating tritium behavior and release in FSV and large plants. These data indicate that tritium born in Peach Bottom core materials is largely held there, but further substantiation and explanation of this observation is needed.

Twenty coated fuel particles were selected from irradiation capsules and sent to LASL for tritium analyses. The particles were first micro-radiographed at GAC using an X-ray technique to determine coating integrity and were then gamma-counted to determine fission product activity. The number of fissions was calculated from the concentrations of Zr-95,

Ru-106, Cs-137, and other suitable radionuclides and the concentration of tritium in the particles was calculated using a ternary fission yield of 0.87×10^{-4}. The particle samples have been sent to LASL for tritium analyses.

Five samples of irradiated graphite were submitted to LASL for determination of lithium and tritium contents. The lithium content is needed to determine the amount of tritium produced.

Five samples of irradiated control materials (B_4C compacts) were submitted to LASL for tritium analyses. In this case, the amount of tritium produced can be calculated from the neutron flux during the irradiation or determined from B-10 burnout. Determination of the B-10 burnout requires a mass spectrometric analysis of the B-10/B-11 ratio.

The results of the analyses at LASL will be reported as they become available.

FISSION METAL RELEASE STUDIES

Introduction

The reference fissile and fertile particles for the large plant are TRISO coated fissile UC_2 particles and BISO coated ThO_2 particles, respectively. Both TRISO and BISO coatings retain fission gases, including iodine. The silicon carbide layer in the TRISO coating effectively retains the volatile fission product metals (cesium, barium, and strontium). On the other hand, the volatile metals have appreciable diffusivities in pyrolytic carbon and may be released in varying degrees from intact BISO particles.

One formulation that has been used in the FIPER codes for treating the release of fission metals from coated fuel particles is the release constant model described by the equation

$$\frac{DN}{dt} = P - (\lambda + R)N,$$

where N is the inventory within the fuel particle, t is the time, P is the production rate, λ is the decay constant, and R is the release constant. Release constant values are derived from observed fission metal release data. Another method for treating release from coated particles is to simply assign fractional release values for fission metals. A third and more rigorous method was described in the previous Quarterly Progress Report (Gulf-GA-A12818) and utilizes diffusion coefficient data for kernel and coating.

The first two methods are based on simple empirical fits to observed release data. The third method utilizes experimentally measured diffusion coefficient data for the metals in kernel and coating materials. The objective of this subtask is to provide the needed diffusion coefficient data.

Earlier studies indicate that the release rates of strontium and barium from BISO particles are controlled by diffusion in the kernel and that the diffusivity of these two metals in oxide kernels is lower than in carbide kernels. The release of cesium from BISO particles appears to be controlled by diffusion in the coating, although the data here are inconclusive and additional experiments are needed.

Description of Work

The procedure in these tests is to anneal well-characterized coated particles and bare kernels irradiated to various burnup levels. The anneals are carried out at temperatures in the range of 1200° to 1800°C. During the anneals, released metal nuclides are collected for radioassay and the accumulated fractional release data are plotted as a function of the square root of time. Diffusion coefficient data for the metals in the coatings are then calculated from delay or break-through times.

Experimental Procedure

BISO coated fuel particles are first selected from previous irradiation capsule inventories. The particles are then carefully screened by initial X-radiography, gamma counting, and measurements for fission gas release (R/B)* using the TRIGA King furnace facility. These three screening tests evaluate coating integrity and Cs inventory prior to starting the fission metal release anneals. Recently an acid leach step has been tried as an addition to the particle screening procedure. The leach process removes surface contamination from the sample and also effectively removes particles with cracked or failed coatings, which might otherwise go undetected, by dissolution of kernel material causing coatings to open up and fragment. The failed coating fragments and dissolved kernel material can then be easily removed from the sample.

The particles are loaded into graphite crucibles, 3/8 in. in diameter by 3/8 in. long, and then gamma counted using a Li-drifted germanium detector and accompanying electronics coupled with an XDS Sigma II computer. This gives an initial fission metal inventory for the start of the anneal and provides further insight into coating integrity by comparing the measured Cs inventory with the calculated inventory based on measurements of refractory (i.e., nonmobile) species such as Zr-95 or Ru-106. Only particles that have retained essentially all the Cs are used in these tests. The sample crucibles are then placed in the tantalum containment tubes which are positioned in the graphite tube furnace. The furnace and containment tube arrangement is shown schematically in Figs. 4-6 and 4-7. The furnace is resistance heated utilizing a graphite tube positioned between two low-voltage electrodes. Furnace power is varied by changing the current supplied from an SCR controller through a step-down transformer.

---

*R/B = release rate/birth rate of a gaseous nuclide at steady state.

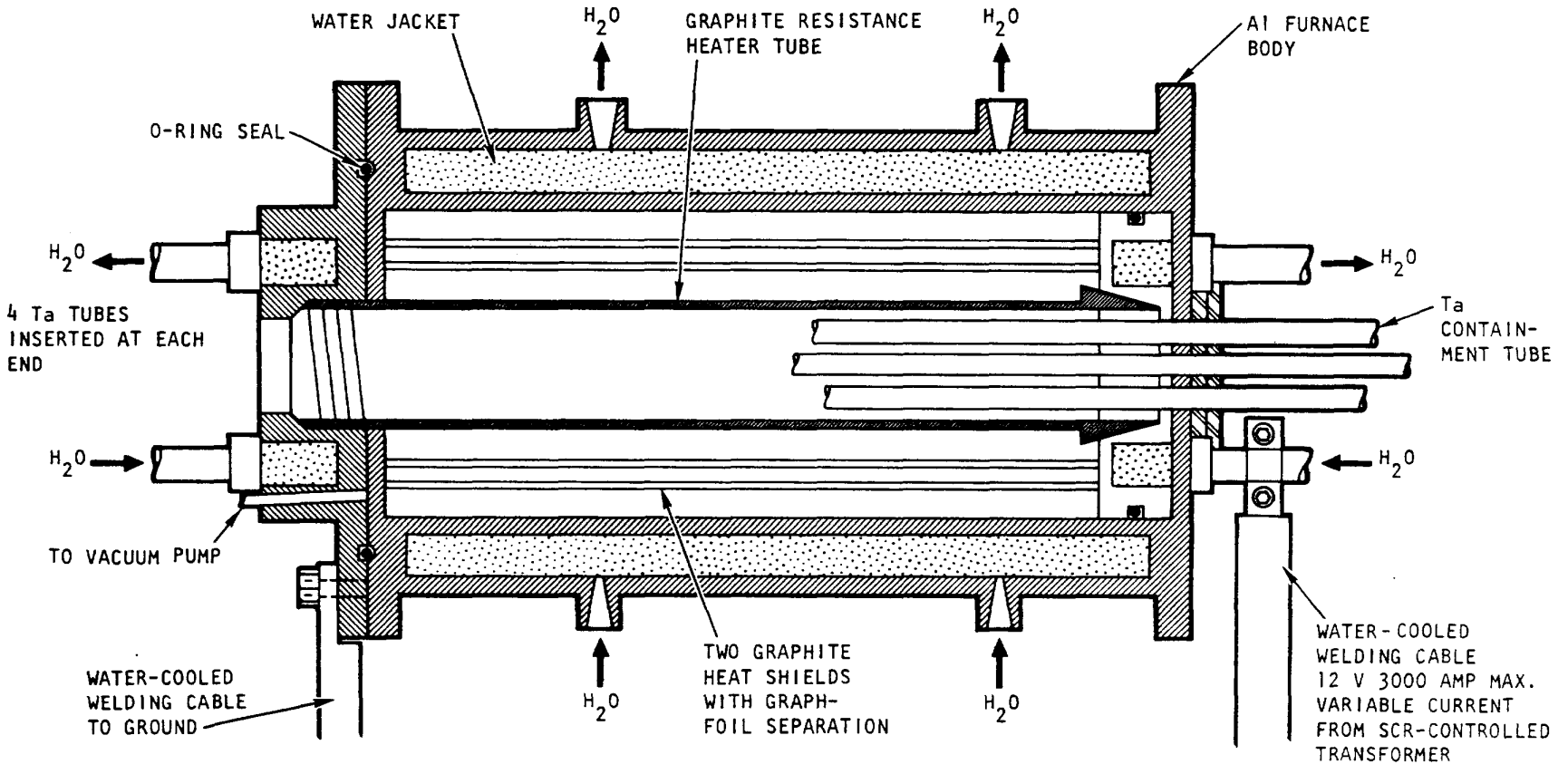

Fig. 4-6. Furnace for fuel particle anneals

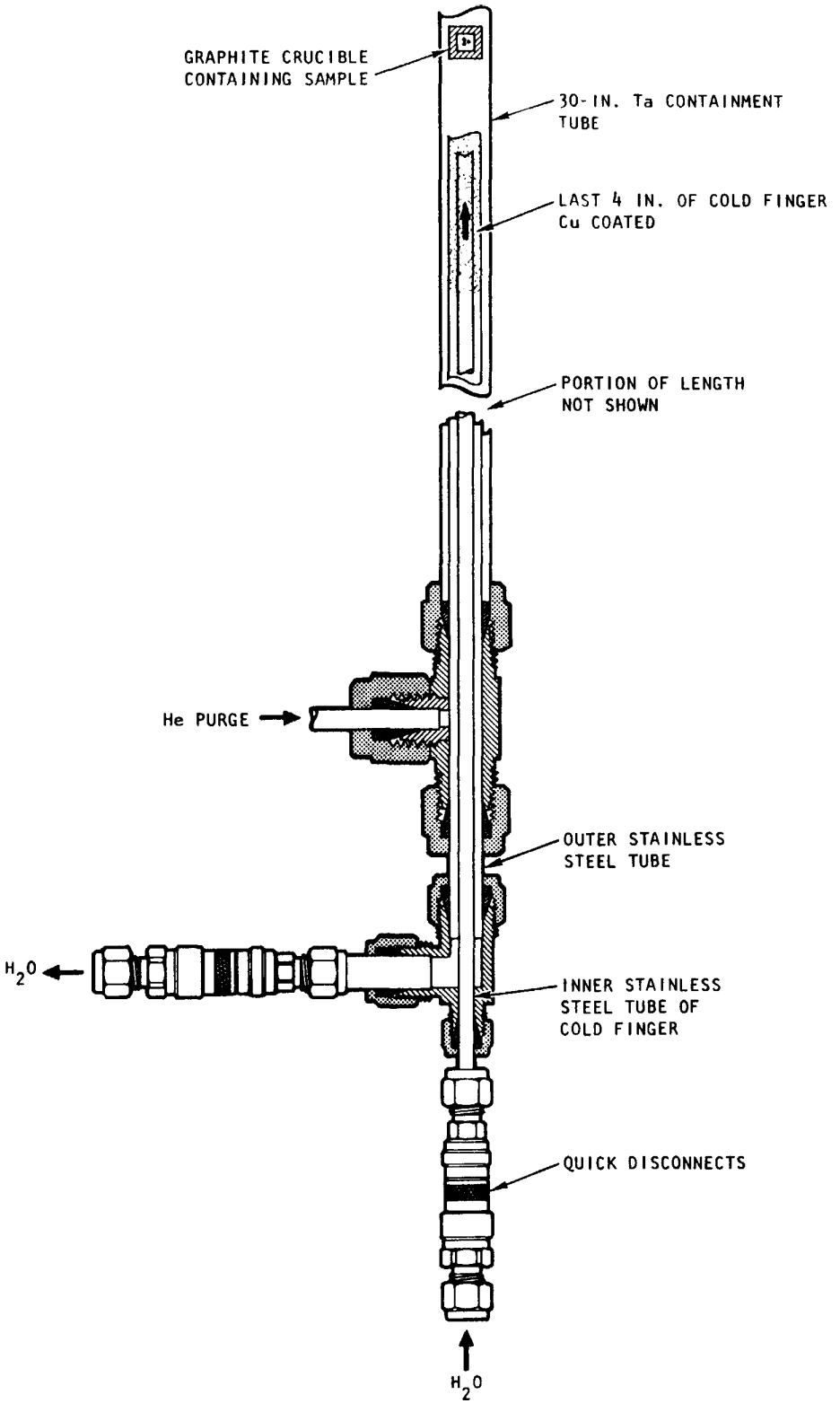

Fig. 4-7. Tantalum container tube and cold finger

The temperature is controlled through a Barber Coleman proportional controller connected to a type K stainless steel clad thermocouple located in the low-temperature (~1000°C) region of the furnace. The actual temperature of the sample is obtained by viewing the graphite crucible with an optical pyrometer. Insertion of the cold finger into the furnace hot zone reduces the temperature to some extent, and a correction factor is applied to the observed optical measurement.

The interior of the furnace is kept under a high vacuum, and the tantalum containment tubes are maintained with static helium at approximately 5 psig. As many as eight tantalum containment tubes (four from each end) are in each furnace, allowing six separate anneals since their position in the hot zone can be shifted to vary their temperature. One of the spare tubes is used for the control thermocouple and the other for sighting with the pyrometer.

A water-cooled stainless steel cold finger is inserted down the tantalum tube to within 1/2 to 1 in. of the graphite crucible, as shown in Fig. 4-7. The last 4 in. of the cold finger is electroplated with Cu, which provides a surface for condensation of fission metals that is easily removed by washing with nitric acid.

The cold fingers are periodically changed by separation at the disconnects, and clean, freshly copper plated cold fingers are quickly substituted for the contaminated ones. This operation is normally done without interrupting furnace power. The removed cold fingers are immersed in three consecutive nitric acid washes. The wash solutions are combined in a 4-dram polyvial, which is topped off to a prescribed level with nitric acid, sealed, and placed inside another vial for double containment. The washed cold fingers are then checked to determine if any residual activity remains that would require repeated washings.

The cold finger solutions are counted and analyzed. Geometry and quenching corrections are incorporated into the computer program by

analyzing known Cs-137 solutions in the same vials containing similar cupric nitrate concentrations.

During the anneals cesium nuclides (Cs-134 and Cs-137), having high mobility in graphite at these elevated temperatures, collect primarily on the cold finger, whereas other metal species such as Sr, Ba, and Ce collect primarily in the graphite crucible. The particles are counted periodically during the anneals to obtain normalization factors for mass balance of the data obtained from analysis of the cold fingers. The graphite crucibles are also analyzed at this time for Sr, Ce, and other species that may be present. The cumulative fractions released are plotted versus the square root of time, as in the example in Fig. 4-8, and diffusion coefficient data are calculated. The calculation for the diffusion coefficient in the coating, D_c, is made using the equation $D_c = \chi^2/6t_D$, where χ is the coating thickness and t_D is the delay time. The delay time is obtained by extrapolation of the initial release slope to the time axis.

Representative coating diffusion coefficient data are shown in Fig. 4-9, which is an Arrhenius plot of D_c versus 1/T for Cs. The physical data characterizing each sample are listed in Table 4-7. The diffusion coefficients were obtained from anneals of BISO LTI particles having burnups of $\leq$10% FIMA. The straight line is the least squares fit of the data and the curved lines are 95% confidence hyperbolae as calculated by the computer code CONFID. The hyperbolae give confidence levels for the position and slope of the least-squares line.

Extrapolation of the least-squares line to a temperature of about 1070°C (which is well above the average fuel temperature of $\sim$900°C) yields a D_c (cesium) of 10^{-13} cm^2/sec. Using the formula $t_D = \chi^2/6D_c$, where the coating thickness = 8×10^{-3} cm, t_D is calculated to be 4 years (assuming 80% duty factor), which is the fuel lifetime. It can be concluded from these results that Cs release from most of the BISO coated fertile particles in the HTGR will be quite low.

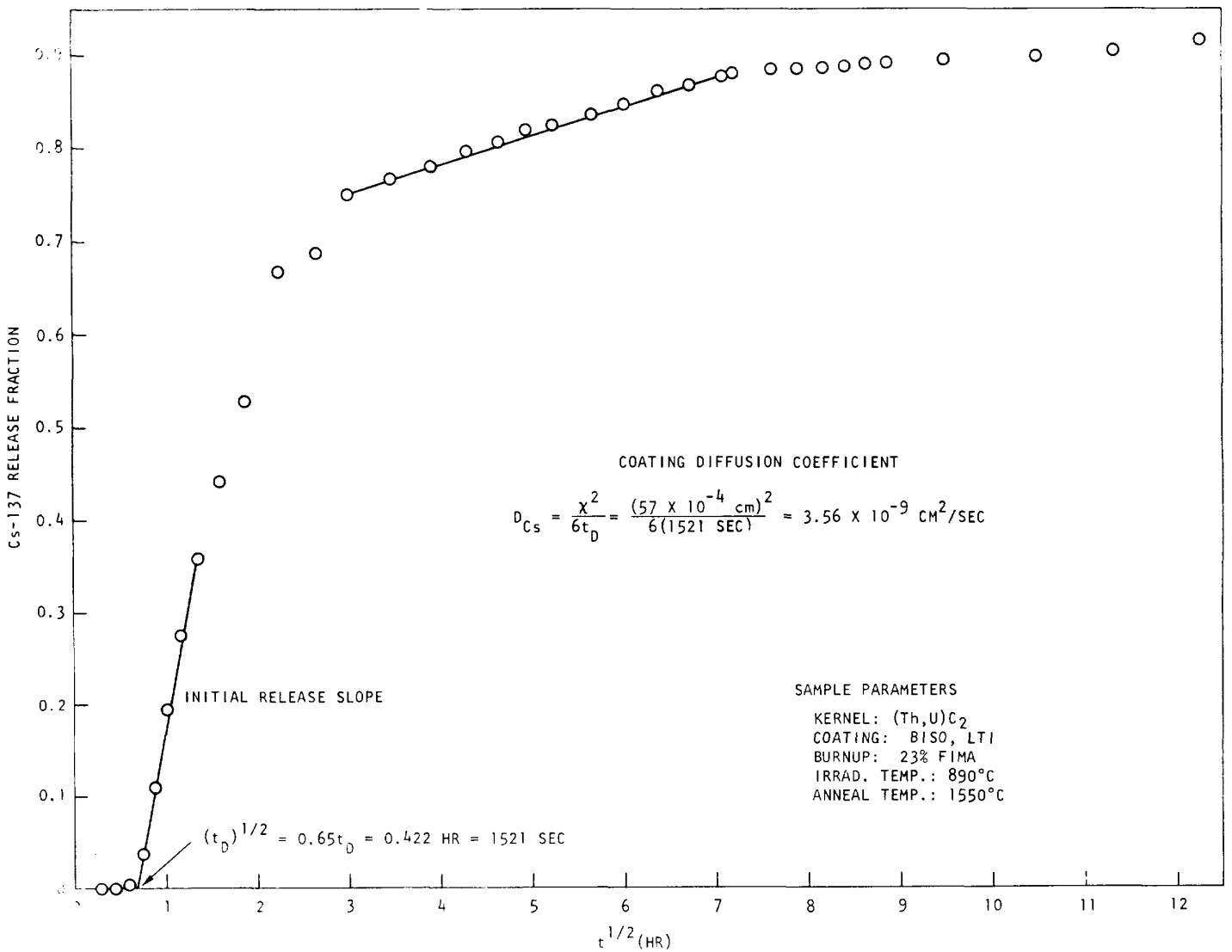

Fig. 4-8. Cumulative Cs-137 fraction release versus anneal time, $t^{1/2}$

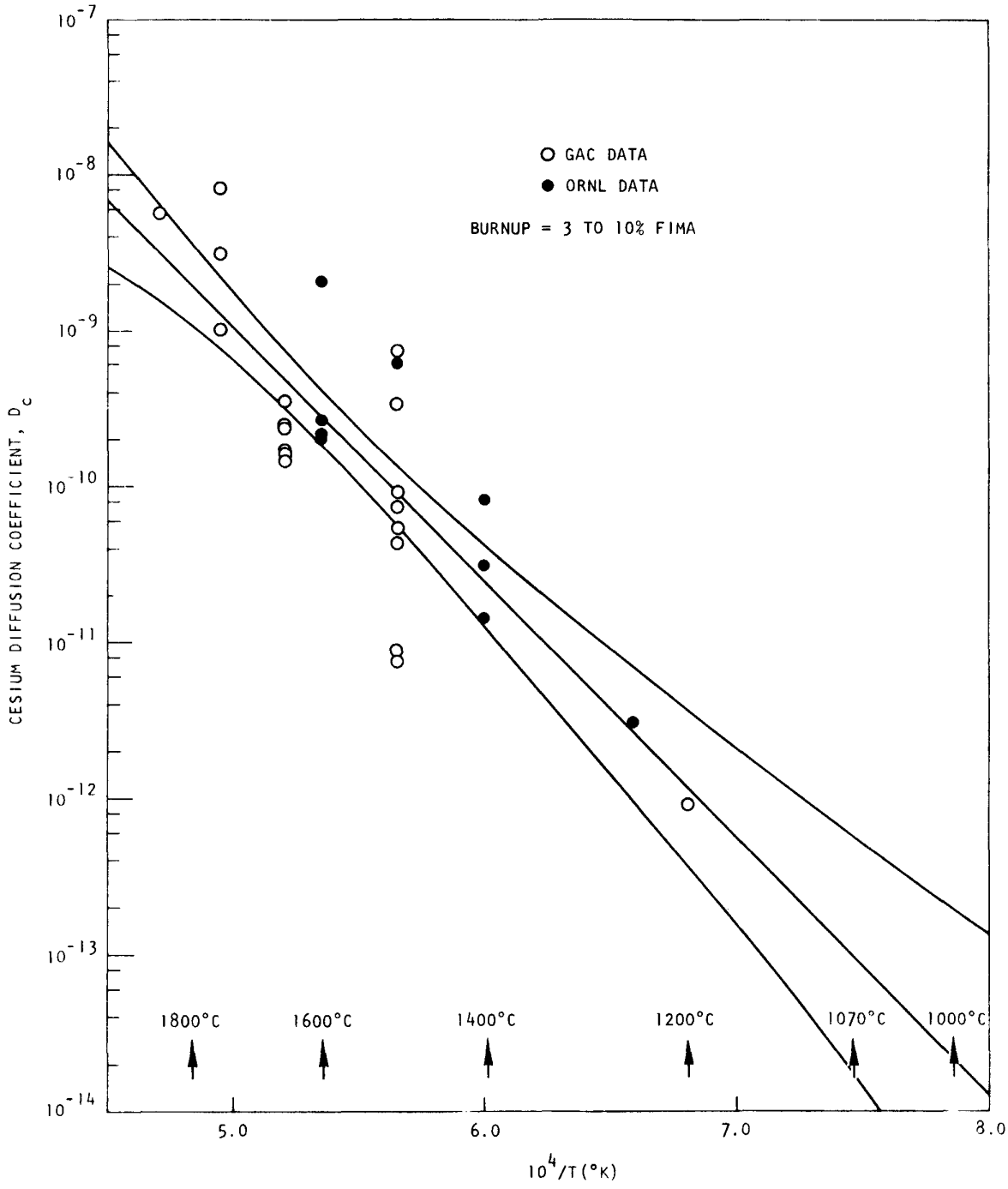

Fig. 4-9. Cesium diffusion from intact BISO (LTI) fuel particles

TABLE 4-7

CHARACTERISTICS OF LTI COATED FUEL PARTICLES

Lot Number	Coating Type	Thickness (μm)	Density (g/cm^3)	Anisotropy Factor	Type	Th:U Ratio	Size (μm)	Test	Temp (°C)	Burnup (% FIMA)	Fast Fluence (10^{21} n/cm^2)	Anneal Temp (°C)	D_{Cs} in Coating (cm^2/sec)
3363-117E	LTI	39	2.03	1.21	$(Th,U)C_2$	7.8	300-420	P16	1310	5.7	2.1	1850 1200	5.6×10^{-9} 9.0×10^{-13}
4000-339	LTI	81	1.78	1.09	ThO_2	---	350-450	HT-8	750	10.5	8.3	1750 1650 1500	8.5×10^{-9} 1.8×10^{-10} 7.5×10^{-10}
4000-339	LTI	81	1.78	1.09	ThO_2	---	350-450	HT-8	1050	10.7	8.3	1750 1500	1.1×10^{-9} 3.4×10^{-10}
4000-323	LTI	68	1.85	1.10	ThC_2	---	351 (avg)	P13M	1300	3.5	6.5	1750 1650 1500	3.3×10^{-9} 2.8×10^{-10} 4.3×10^{-11}
4000-334	LTI	61	1.90	1.17	ThC_2	---	300-450	HT-8	1050	10.0	8.3	1750 1650 1500	1.1×10^{-9} 2.3×10^{-10} 7.0×10^{-11}
4413-75	LTI	85	1.89	1.02	ThO_2	---	576 (avg)	P13L	1325	7.0	7.0	1650 1500	3.7×10^{-10} 9.5×10^{-12}
4000-660E	LTI	58	1.66	1.00	$(Th,U)C_2$	2.5	150-250	P19	975	13.0	2.5	1550 1400	5.0×10^{-10} 1.8×10^{-11}
4000-632E	LTI	57	2.01	1.04	$(Th,U)C_2$	2.5	150-250	P19	890	23.0	6.4	1750 1650 1550 1400	1.2×10^{-6} 1.6×10^{-8} 4.6×10^{-9} 3.0×10^{-9}
4503-53(53P)	LTI	124	1.64		$(Th,U)O_2$	2.0	360	FTE-1	1100	10.6	1.2	1500 1650	7.4×10^{-11} 1.5×10^{-10}
4503-53(52P)	LTI	124	1.64		$(Th,U)O_2$	2.0	360	FTE-2	999	8.26	1.8	1500 1650	5.5×10^{-11} 1.7×10^{-10}
4503-53(57P)	LTI	124	1.64		$(Th,U)O_2$	2.0	360	FTE-2	971	19.4	1.8	1500 1650	9.4×10^{-11} 1.5×10^{-10}

Present emphasis is on long-term anneals in the low-temperature region (1200° to 1500°C) to fill in the scarcity of data near representative HTGR temperatures. Even so, extrapolations to all temperatures below approximately 1200°C must be made because of the long test times involved at low temperatures. For example, experiments at 1200°C must be carried out for times exceeding approximately 5000 hr before meaningful data are obtained.

In addition, bare kernel anneals are planned to determine coefficients for the kernel diffusivity. Also a new laser technique is being used to drill small holes (approximately 20 μm diameter) through PyC coatings, thus providing representative "failed" fuel particles which can be used to measure "effective" diffusion coefficients.

Fuel Test Element FTE-3

Details of the postirradiation examination of FTE-3 metallic diffusion samples in spine positions will be published in a forthcoming topical report.

STEAM-GRAPHITE REACTIONS

Work is in progress to determine the effects of selected variables on the steam-graphite reaction, i.e., temperature, water vapor partial pressure, extent of graphite burnoff, and helium pressure. The purpose of these studies is to collect rate data on candidate graphites for input in the GOP and OXIDE computer codes, which are used for integrated HTGR core oxidation calculations.

Low-Pressure Studies

The effects of temperature, graphite burnoff, and steam partial pressure on the reaction rate of steam with graphite at a total pressure of 1 atm are being investigated. This work is being carried out to verify

previously reported rate data for the reference H-327 graphite, to characterize potential candidate graphites such as H-451, and to extend the number and range of parameters studied in the H_2O-C reaction.

Apparatus and Procedures

Several recording microbalances have recently been put into operation, enabling rapid continuous determination of oxidation rates as a function of temperature and other parameters. These instruments operate by continuously recording the instantaneous weight of graphite samples, with an accuracy in the submilligram range.

Thin slabs of virgin graphite 0.5 in. by 1.0 in. by 0.125 in. have been used in this work to minimize effects of in-pore diffusion. The samples are suspended in a quartz reaction tube via a platinum wire from one arm of the balance (Fig. 4-10). The tube is positioned within a resistively heated furnace controlled by a temperature SCR power controller combination. Sample temperatures are monitored with a potentiometer and a chromel-alumel thermocouple located adjacent to the sample. Nominal helium flows of 100 cm^3/min, as measured with a rotameter, are allowed to pass upward over the sample. Partial pressures of water in helium from 0 to 30,000 ppm can be introduced by purging with the dry or water-saturated helium.

Initial degassing of the sample is carried out under moderate vacuum at 1000°C. After a stable weight has been attained, and the background oxidation rate measured at the selected temperature, moist helium is flowed over the sample and the weight of the sample is continuously recorded on a strip chart recorder. Rate data are calculated from sample weight losses divided by the appropriate time increment.

Results

Figure 4-11 is an Arrhenius plot of oxidation rate of the present reference H-327 graphite at from 835° to 1050°C with 30,000 ppm H_2O in

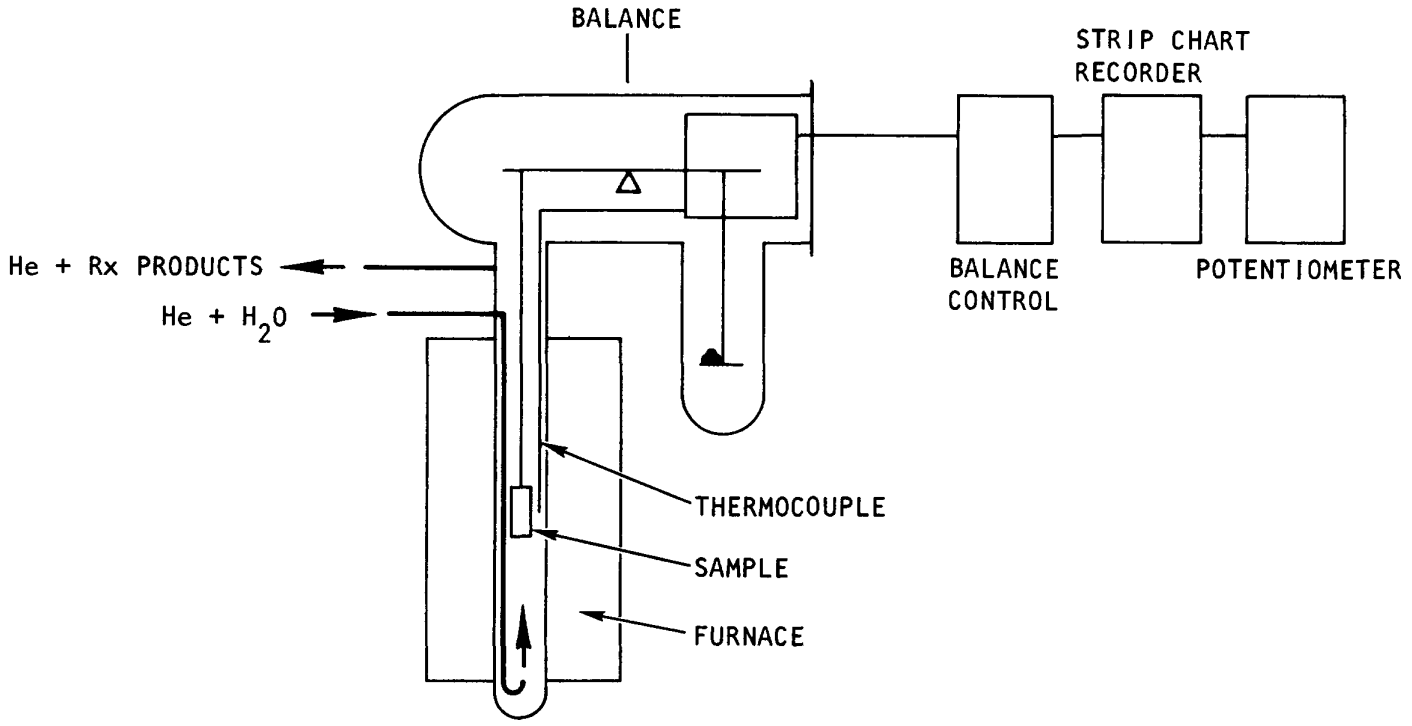

Fig. 4-10. Automatic recording microbalance for steam-graphite reaction rate studies

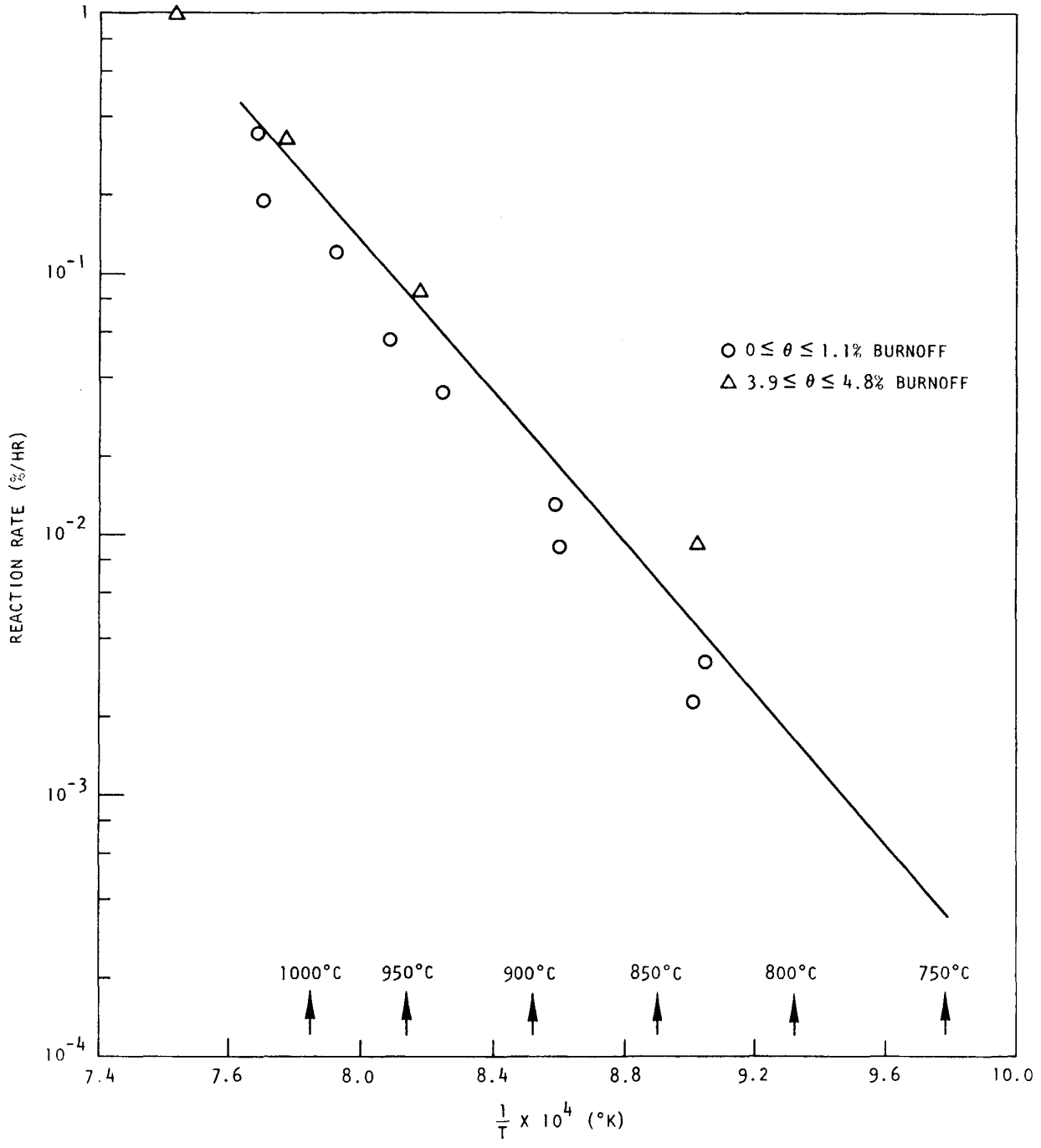

Fig. 4-11. Arrhenius plot of oxidation rate of reference H-327 graphite

helium. The straight line plot represents previously reported data for graphite samples with 5% burnoff.* Good agreement is seen between the two independent sets of data, with comparable activation energies of 40 ± 2 kcal/mole. Figure 4-12 shows similar oxidation rate data for preproduction samples of H-451, which is a near-isotropic graphite and is presently being qualified for use in the HTGR. Occasional anomalously high values at the lower temperatures are felt to be experimental artifacts, since a positive change in slope in this region is unexpected. Further reaction rate data on additional samples with different sizes and surface-to-volume ratios should improve low-temperature rate data precision.

Experiments planned for the next quarter include the determination of the effects of reduced H_2O partial pressure and variable burnoff on the reaction rate.

High-Pressure Studies

Theoretical predictions of the effect of helium pressure on the reaction rate of steam with graphite indicate a $P^{-1/2}$ dependence. Work is in progress to ascertain if these predictions are indeed verified by experimental evidence. Previously reported data have indicated the rate is approximately dependent on $P^{-1/2}$, but precise results have been hampered by inordinately high oxidation rates, indicating the presence of catalysts. Current efforts are aimed toward more precisely defining the pressure dependence.

Prior experience indicated high reaction rates resulted when samples were contained directly within Inconel tubes. The possibility of nickel catalyzing the reaction, perhaps in the form of $Ni(CO)_4$, was postulated.

*Public Service Company of Colorado 330-MW(e) High-Temperature Gas-Cooled Reactor Research and Development Program, Quarterly Progress Report for the Period Ending March 31, 1970, USAEC Report GA-10010, General Atomic Company, April 30, 1970.

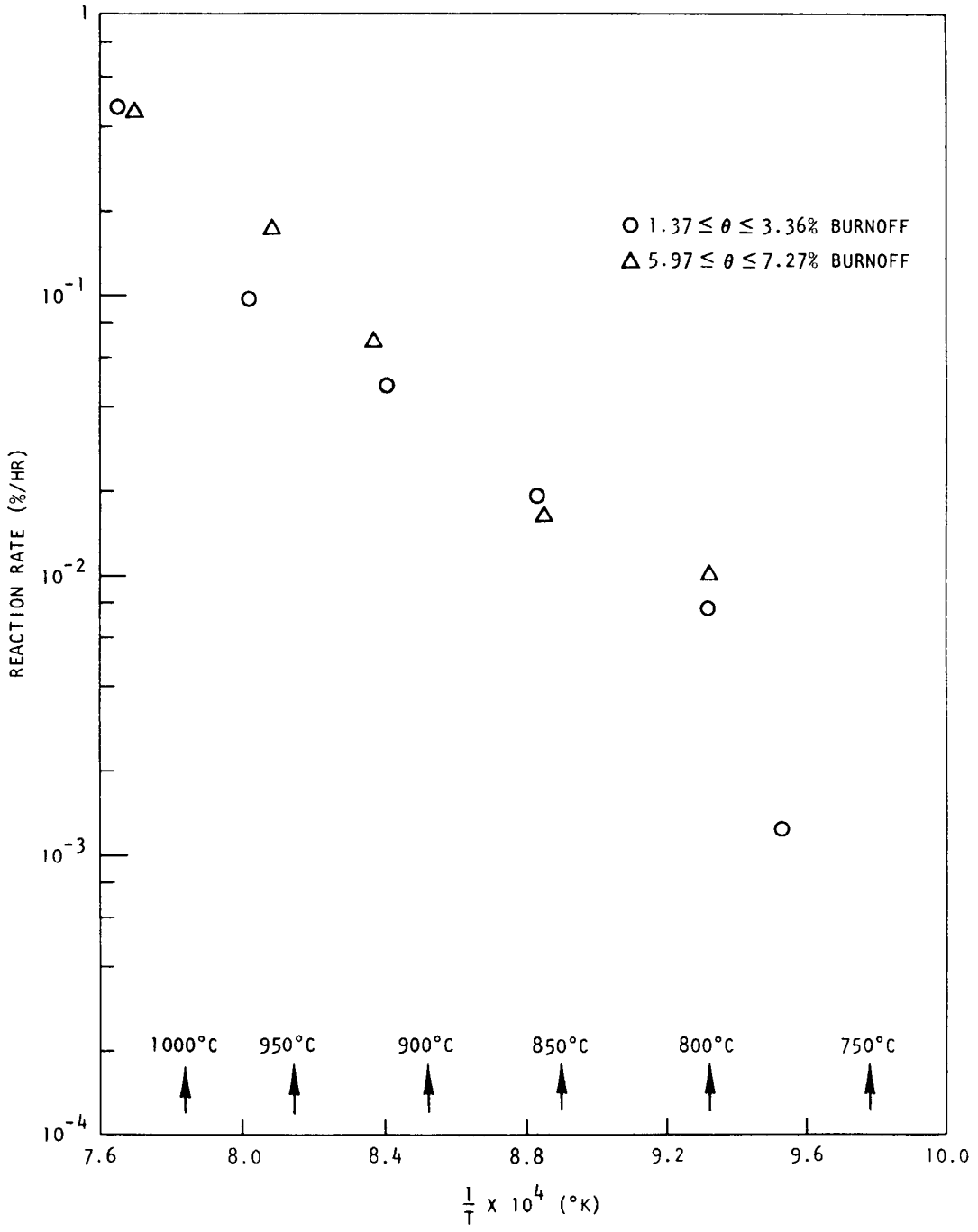

Fig. 4-12. Arrhenius plot of oxidation rate of preproduction samples of H-451 graphite

Insertion of a quartz liner within the inner chamber of the furnace reduced, but apparently did not eliminate, the effects of catalysis, as high oxidation rates were still observed. Recent changes in the apparatus have included the insertion of a closed-end quartz finger in the inner tube, along with a redesigned helium inlet system. As a result of these changes, moist helium is introduced and contained by nonreactive quartz material in the hot zone of the apparatus and thus at no time comes in contact with high-temperature metal surfaces. This design change has yielded a secondary benefit of significantly lowered air inleakage rates.

Recent data collected with this apparatus have shown reasonable agreement with previously reported data. However, oxidized samples have shown indications of pitting, probably resulting from iron impurities present after machining of graphite samples. Since the catalytic effect of iron is a surface effect, catalyzed oxidation is unlikely to be affected by a varying helium pressure (which affects the rate of transport of molecular species within the subsurface pores of the graphite). The high carbon monoxide production at iron catalyzed pits can conceivably mask the apparent pressure dependence of the in-pore reaction rate. New samples are being prepared with special attention being given to avoiding trace Fe impurities. These samples will be used to further investigate the pressure dependence at varying temperature, sample burnoff, and H_2O partial pressure.

TASK V
RECYCLE FUEL STUDIES

HTGR FUEL RECYCLE PLANT STUDY

Design Criteria for Commercial Reprocessing Plant

A draft of this document, "Design Criteria - Commercial Reprocessing Plant: Requirements" (DC-20201), was completed by the end of the reporting period.

Liaison with National Laboratories and AEC

Representatives of ORNL visited GAC in December 1973 to review the refabrication development program. A series of agreements were reached and considerable design information was exchanged. Additional process information for fresh fuel development has been transmitted to ORNL as a follow-on to this meeting.

A meeting was held in Idaho Falls in January 1974 to discuss the schedule and technical progress of the HTGR prototype reprocessing facility.

A meeting was held at ORNL in February 1974 to discuss the selection of the reference recycle kernel and manufacturing process for refabricated fuel. A joint recommendation was developed to designate the UC_2 kernel derived from a resin process.

Conceptual Flowsheets and Material Balances for Refabrication*

The conceptual design of a commercial-scale HTGR fuel recycle facility is being developed to guide the development program toward providing the

---

*Bibliography on page 162.

technology to allow the commercial recycle of HTGR fuel. The reference size plant reprocesses 50,000 HTGR fuel blocks/year from which will be recovered sufficient U-233 to refabricate 20,000 recycle fuel elements.

As a part of the examination of candidate processes for refabrication of U-233 fuel in HTGR fuel elements, flowsheets, material balances and equipment lists have been prepared for the ORNL-developed SOLEX process for the preparation of mixed $(TH,U)O_2$ microspheres. In order to provide greater operating reliability, three parallel streams of 1/3 capacity each were specified. Representative flowsheets for one of the three parallel systems are shown in Figs. 5-1 through 5-3. Material balances for 4.25/1 thorium/uranium ratios in the mixed oxide kernel are shown in Tables 5-1 through 5-3. A summary equipment list for the SOLEX process is given in Table 5-4.

Guidelines for Process Design for Remote Operations

The following general guidelines were used in developing a flowsheet for operation in a shielded refabrication facility:

1. The greatest costs are caused by process downtime.
2. The most important process/equipment characteristic is reliability.
3. Provide numerous indicating instruments with automatic alarms.
4. Provide numerous sampling points.
5. Automate the safety-criticality-contamination/radiation control equipment.
6. Automatic data logging is desirable but do not over-automate the process control functions.
7. Provide for getting off-specification material-in-process out of main processing line as soon as possible.
8. Minimize the number of moving parts in-cell.
9. Prefer slow-moving parts over fast-moving parts in-cell.
10. Prefer piping and other vessel penetrations through the head of in-cell vessels, rather than through the side or bottom.
11. Prefer vacuum over pressure.

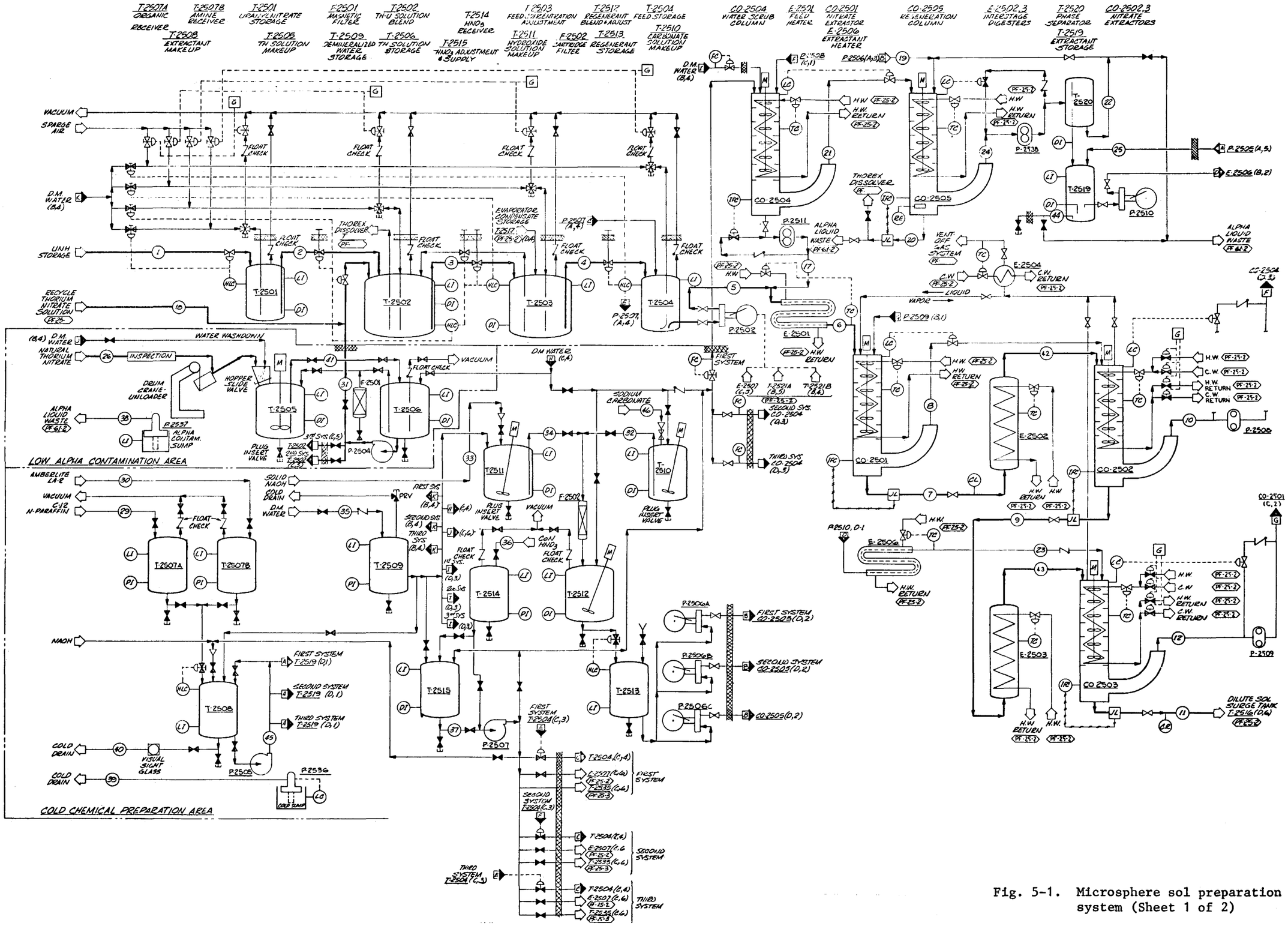

Fig. 5-1. Microsphere sol preparation system (Sheet 1 of 2)

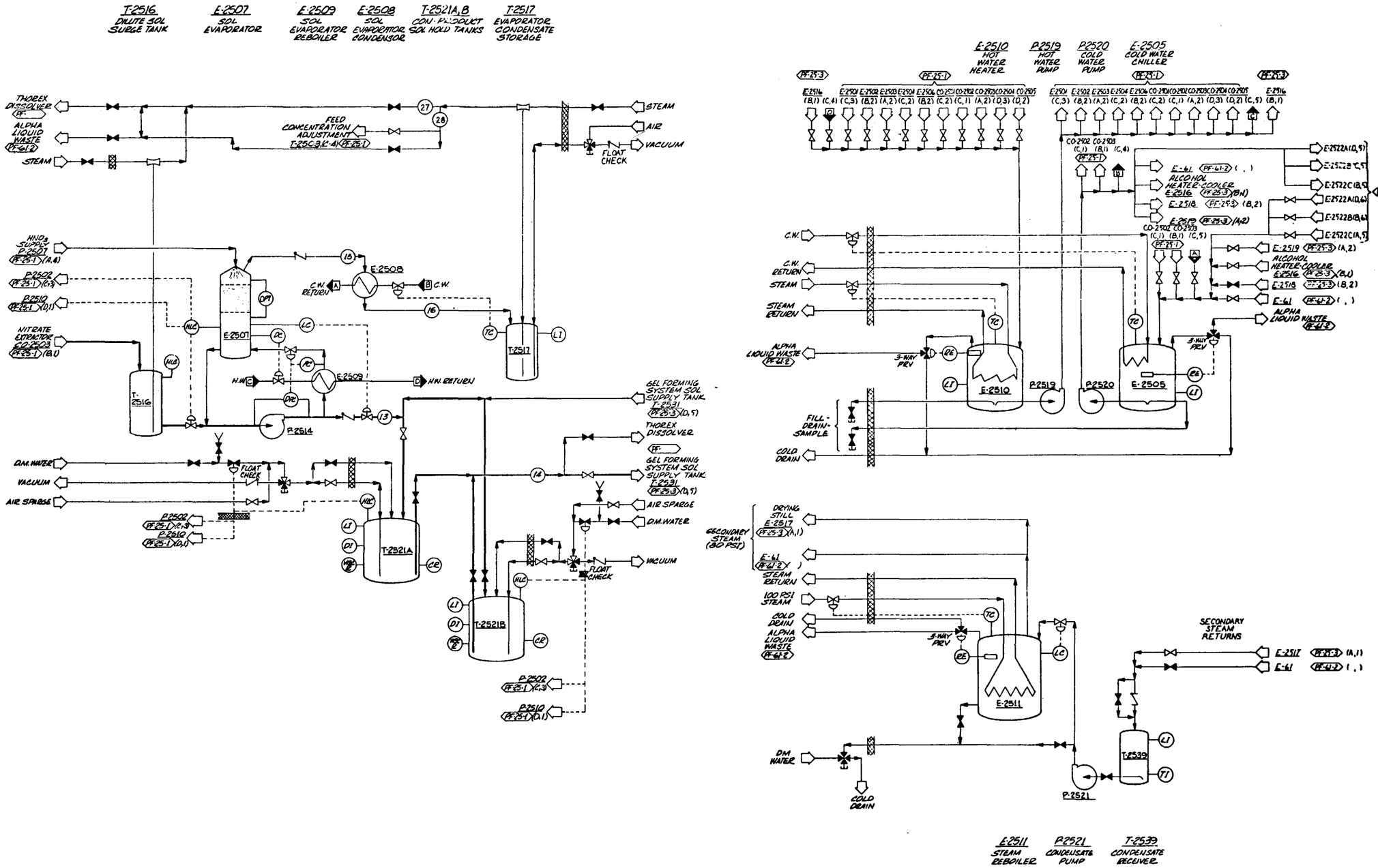

Fig. 5-1. Microsphere sol preparation system (Sheet 2 of 2)

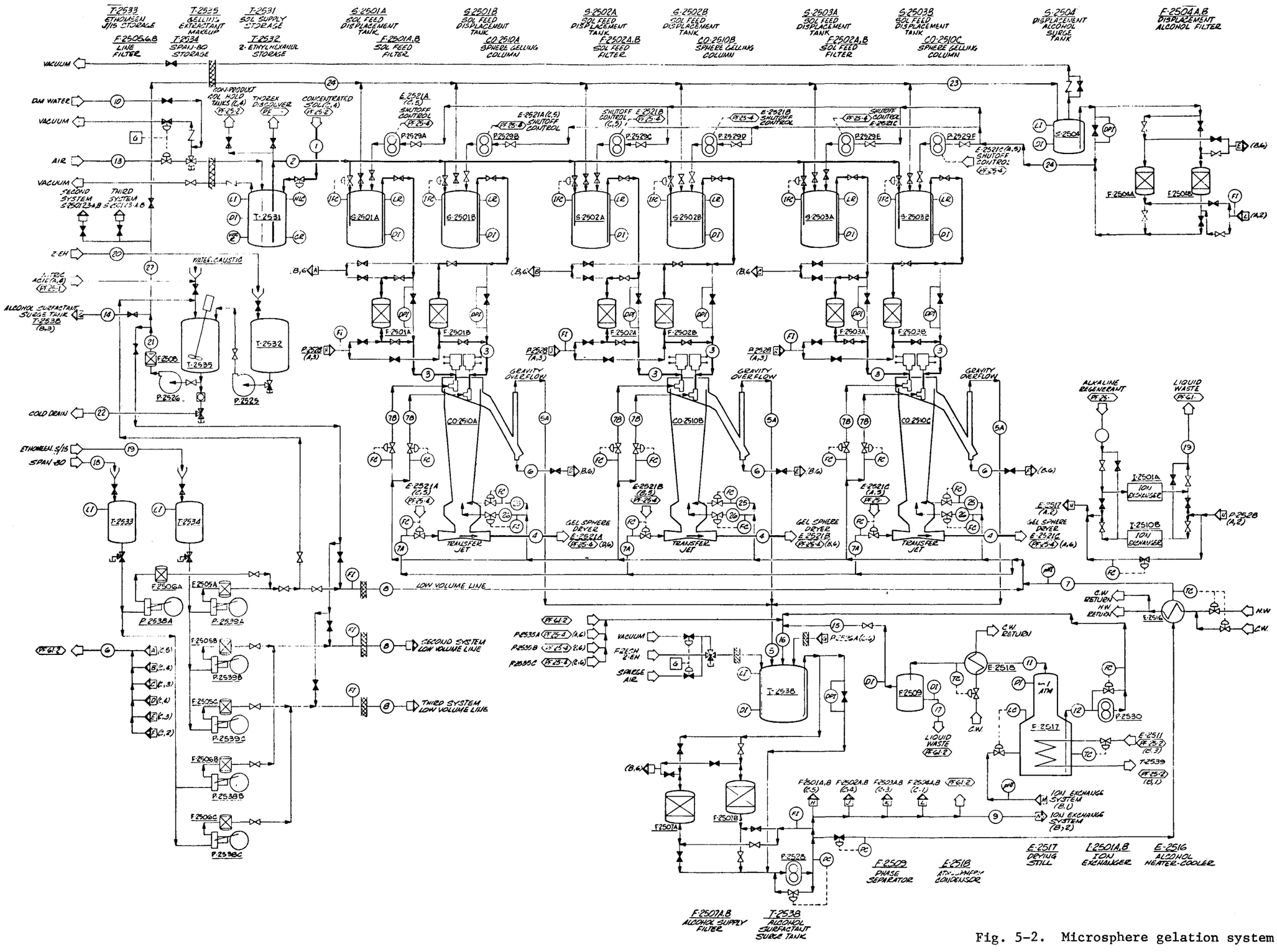

Fig. 5-2. Microsphere gelation system

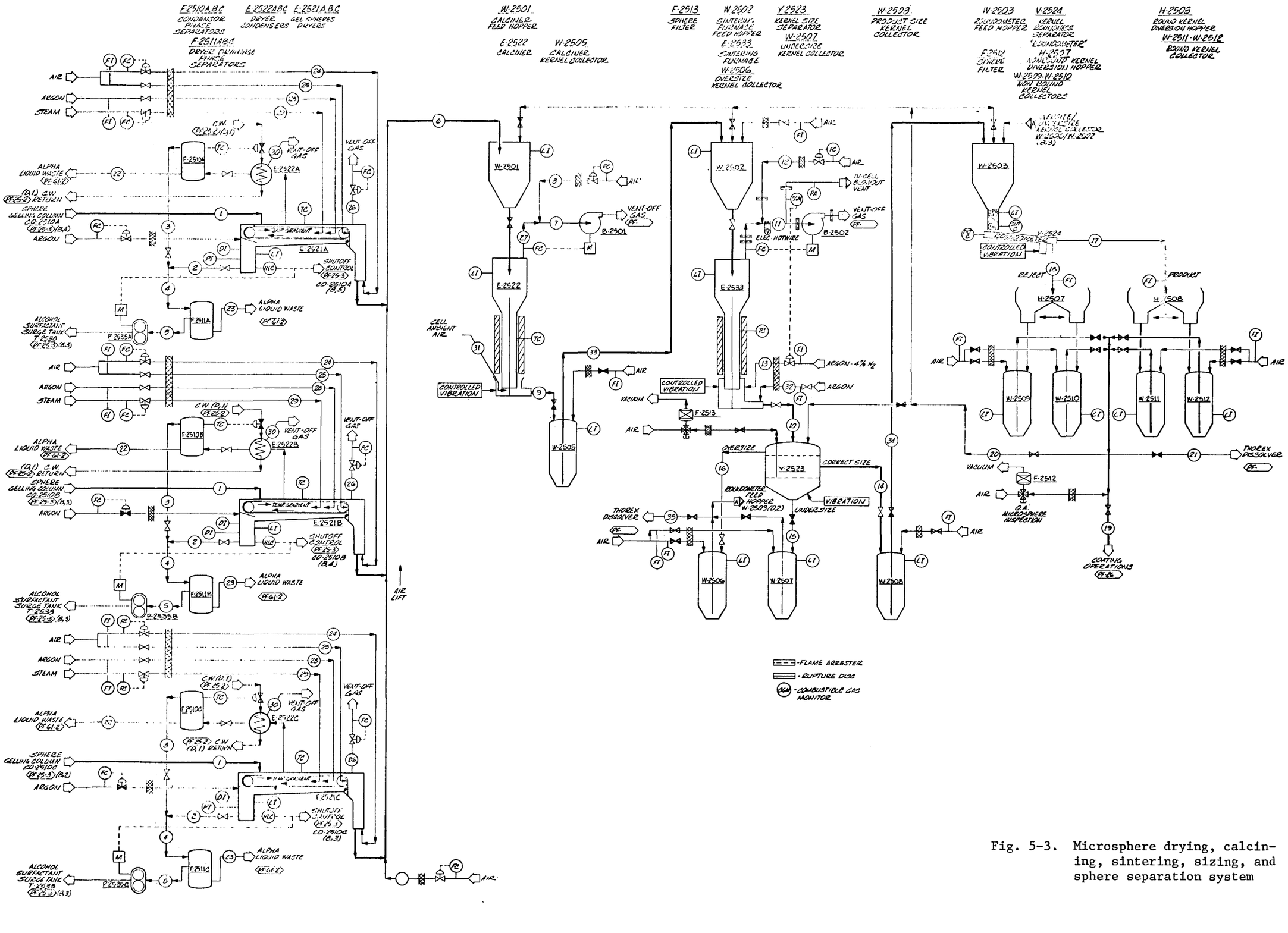

Fig. 5-3. Microsphere drying, calcining, sintering, sizing, and sphere separation system

TABLE 5-1

MATERIAL BALANCES AND PROCESS CONDITIONS FOR FIG. 5-1

		FLOWRATES *					CONCENTRATION, MOLARITY									
STREAM NUMBER	STREAM DESCRIPTION	TOTAL LITERS/HR	HEAVY METAL KG/HR	U KG/HR	Th KG/HR	NITRATE MOLES/HR	HEAVY METAL	U	Th	NITRATE	FREE NITRIC ACID	TOTAL EXTRACTANT	FREE EXTRACTANT	SODIUM CARBONATE	SODIUM HYDROXIDE	REMARKS
1	URANIUM INPUT	21-8	7.4-8	7.4-8	T	100-8	1.5	1.5	T	4.7	1.7	-	-	-	-	
2	ASSAYED URANIUM	21-8	7.4-8	7.4-8	T	100-8	1.5	1.5	T	4.7	1.7	-	-	-	-	
3	MIXED THORIUM/URANIUM	64-8	29.5-8	7.4-8	22-8	525-8	2.0	0.5	1.5	8.5	1.2	-	-	-	-	
4	ADJUSTED SOLUTION FEED	350-8	29.5-8	7.4-8	22-8	525-8	0.36	0.09	0.27	1.5	0.22	-	-	-	-	
5	ASSAYED SOLUTION FEED	44	3.7	0.93	2.8	66	0.36	0.09	0.27	1.5	0.22	-	-	-	-	
6	HEATED/DILUTED FEED	56	3.7	0.94	2.8	67	0.29	0.07	0.22	1.2	0.17	-	-	-	-	
7	FIRST COL. AQ. OUTPUT	56	3.7	0.94	2.8	12	0.29	0.07	0.22	0.22	8×10^{-5}	-	-	-	-	60°C FOR 20 MIN.
8	FIRST COL. ORG. OUTPUT	120	T	T	T	59	T	T	T	0.5	-	0.70	0.20	-	-	60°C FOR 20 MIN.
9	SECOND COL. AQ. OUTPUT	56	3.7	0.94	2.8	5	0.29	0.07	0.22	0.09	T	-	-	-	-	60°C FOR 20 MIN.
10	SECOND COL. ORG. OUTPUT	120	0.019	9×10^{-3}	0.01	65	8×10^{-4}	3×10^{-4}	5×10^{-4}	0.55	-	0.70	0.15	-	-	60°C FOR 20 MIN.
11	THIRD COL. AQ. OUTPUT	51	3.7	0.93	2.8	2	0.31	0.08	0.23	0.04	2×10^{-5}	-	-	-	-	60°C FOR 20 MIN.
12	THIRD COL. ORG. OUTPUT	120	T	T	T	4	T	T	T	0.04	-	0.70	0.66	-	-	60°C FOR 20 MIN.
13	SOL EVAPORATOR OUTPUT	10	3.7	0.93	2.8	2	1.6	0.40	1.2	0.2	$\sim10^{-4}$	-	-	-	-	~100°C
14	ASSAYED CON SOL	80-8	29.5-8	7.4-8	22-8	16-8	1.6	0.40	1.2	0.2	$\sim10^{-4}$	-	-	-	-	~ROOM TEMP.
15	SOL EVAPORATOR VAPOR	7×10^{4}	-	-	-	T	-	-	-	T	T	-	-	-	-	100°C
16	SOL EVAPORATOR CONDENSATE	41	-	-	-	T	-	-	-	T	T	-	-	-	-	<45°C
17	SCRUB SOL AQ. OUTPUT	12	0.019	9×10^{-3}	0.01	0.30	7×10^{-3}	3×10^{-3}	4×10^{-3}	0.02	-	-	-	-	-	60° C FOR 30 MIN.
18	REPRO THORIUM INPUT	43-8	22-8	T	22-8	425-8	2.3	T	2.3	10	1	-	-	-	-	GAMD-8382, P.104
19	REGENERATION COL. AQ. INPUT	36	-	-	-	-	-	-	-	-	-	-	-	1.0	1.0	
20	REGENERATION COL. AQ. OUTPUT	41	≤2.3 MG/HR	≤1.3 MG/HR	≤1.0 MG/HR	64	≤58 PPM	≤32 PPM	≤26 PPM	1.5	-	-	-	0.55	T	60° C FOR 25 MIN.
21	SCRUB COL. ORG. OUTPUT	120	~1.4 MG/HR	~0.9 MG/HR	~0.5 MG/HR	65	~12 PPM	~7 PPM	~5 PPM	0.55	-	0.70	0.15	-	-	60°C FOR 30 MIN.
22	PHASE SEP. AQ. RETURN	N.S.	N.S	N.S.	N.S.	N.S.	≤58 PPM	≤32 PPM	≤26 PPM	1.5	-	-	-	0.55	T	
23	THIRD COL. ORG. INPUT	110	-	-	-	0.1	-	-	-	0.01	-	0.73	0.72	-	-	60°
24	REGENERATION COL. ORG. OUTPUT	110	-	-	-	0.1	-	-	-	0.01	-	0.73	0.72	-	-	60°C FOR 25 MIN.
25	ACID-CLEANOUT SOLUTION	NI	-	-	-	NI	-	-	-	4 TO 8	4 TO 8	-	-	-	-	
26	NATURAL THORIUM NITRATE	NI	NI	T	NI	NI	40 wt %	T	40 wt %	43 wt %	T	-	-	-	-	
27	WATER SOL EVAP. CONDENSATE	42-8	-	-	-	T	-	-	-	T	T	-	-	-	-	
28	RECYCLE SOL EVAP. CONDENSATE	286-8	-	-	-	T	-	-	-	T	T	-	-	-	-	
29	C-12N-PARAFFIN DILUTENT	NI	-	-	-	-	-	-	-	-	-	0	-	-	-	
30	AMBERLITE LA-12	NI	-	-	-	-	-	-	-	-	-	2.3	2.3	-	-	
31	NATURAL THORIUM INPUT	NI	NI	T	NI	NI	1.5	T	1.5	6.0	~0.08	-	-	-	-	
32	CARBONATE SOLUTION	440-24	-	-	-	-	-	-	-	-	-	-	-	2	-	
33	SODIUM HYDROXIDE	35kg-24	-	-	-	-	-	-	-	-	-	-	-	-	100 wt %	
34	HYDROXIDE SOLUTION	440-24	-	-	-	-	-	-	-	-	-	-	-	-	2	
35	DEMINERALIZED WATER	~1000-24	-	-	-	-	-	-	-	-	-	-	-	-	-	
36	CON NITRIC ACID	NI	-	-	-	-	-	-	-	15.8	15.8	-	-	-	-	
37	DILUTE NITRIC ACID	NI	-	-	-	-	-	-	-	≤15.8	≤15.8	-	-	-	-	
38	ALPHA SUMP WASTE	NI	-	-	-	-	-	-	-	-	-	-	-	-	-	
39	COLD SUMP WASTE	NI	-	-	-	-	T	T	T	-	-	-	-	-	-	
40	EXTRACTANT PRETREATMENT WASTE	NI	-	-	-	NI	-	-	-	-	-	-	-	-	-	
41	THORIUM STOCK SOLUTION	NI	-	-	-	-	3	T	3	~0.1	~0.1	-	-	-	-	
42	FIRST DIGESTER AQ. OUTPUT	56	3.7	0.94	2.8	12	0.29	0.07	0.22	6×10^{-3}	6×10^{-3}	-	-	-	-	100°C FOR 30 MIN
43	SECOND DIGESTER AQ. OUTPUT	56	3.7	0.94	2.8	5	0.29	0.07	0.22	2×10^{-3}	2×10^{-3}	-	-	-	-	100°C FOR 30 MIN
44	ORG. SUPPLY AQ. HEEL	NS	NS	NS	NS	-	T	T	T	-	-	-	-	T	-	
45	MAKEUP EXTRACTANT	NI	-	-	-	-	-	-	-	-	-	0.74	0.74	-	-	
46	SODIUM CARBONATE	92kg-24	-	-	-	-	-	-	-	-	-	-	-	100%	-	

T = TRACE
NI = NORMALLY INFREQUENT
NS = NORMALLY SMALL

ALL PROCESS PRESSURES ARE AT VENT-OFF GAS PRESSURE, SLIGHTLY BELOW AMBIENT TEMPERATURES ARE AMBIENT UNDER SPECIFICALLY INDICATED OTHERWISE

* PARTS OF THE SYSTEM OPERATED BATCHWISE SHOW BATCH AMOUNT - TIME INTERVAL.

ONE-THIRD OF 50,000 FUEL ELEMENTS/YEAR

TABLE 5-2

MATERIAL BALANCES AND PROCESS CONDITIONS FOR FIG. 5-2

		FLOW RATES †								CONCENTRATIONS							
STREAM NUMBER	STREAM DESCRIPTION	TOTAL LITERS/HR	HEAVY METAL kg/hr	U kg/hr	Th kg/hr	2-EH LITERS/HR	WATER LITERS/HR	SPAN-80 LITERS/HR	ETHOMEEN S-15 LITERS/HR	HEAVY METAL M	U M	Th M	2-EH WT%	WATER WT%	SPAN-80 WT%	ETHOMEEN S-15 VOL%	REMARKS
1	SOL INPUT	80-8	29.8	7.4-8	22-8	–	77-8	–	–	1.6	0.4	1.2	–	70	–	–	SEE ORNL-4095, P.17
2	ARRAYED SOL	13-1.3	4.8-1.3	1.2-1.3	3.7-1.3	–	13-1.3	–	–	1.6	0.4	1.2	–	70	–	–	
3	METERED SOL FEED	1.7	0.62	0.16	0.46	0.002	1.6	T	T	1.6	0.4	1.2	0.1	70	T	T	
4	GELLED SPHERES *	1.5 kg/hr.	1.2	0.32	0.92	0.3*	0.4	T	T	66 wt%	17 wt%	49 wt%	10	13	0.02	0.1	RESIDENCE TIME ~ 3/4 HR
5	COMBINED WET 2-EH	15,000	T	T	T	15,000	160	7.5	30	T	T	T	99	1.5	0.05	0.2	STARTUP SURFACTANT CONC.
5A	2-EH COLUMN OVERFLOW	5,000	T	T	T	5,000	55	2.5	10	T	T	T	99	1.5	0.05	0.2	
6	WET SOLIDS-FINES *	0.5 kg-8	0.5-8	0.1-8	0.4-8	0.07-8	0.1-8	T	T	60 wt%	15 wt%	45 wt%	13	16	0.02	0.1	
7	2-EH COLUMN FEEDS	5,000	T	T	T	5,000	50	2.5	10	T	T	T	99	1.4	0.05	0.2	~ 10^{-4} M HNO_3 (ORNL-TM-3226)
7A	TRANSPORT 2-EH	60	T	T	T	60	0.6	0.03	0.12	T	T	T	99	1.4	0.05	0.2	
7B	NOZZLE 2-EH	600	T	T	T	600	6	0.3	1.2	T	T	T	99	1.4	0.05	0.2	
8	SURFACTANTS INPUT	0.07	–	–	–	–	–	0.05	0.02	–	–	–	–		70	30	SEE ORNL-4398, P.33
9	ION EXCHANGER FEED	1300	T	T	T	1,300	18	0.7	3	T	T	T	99	1.5	0.05	0.2	
10	DEMINERALIZED WATER	NI	–	–	–	–	–	–	–	–	–	–	–	100	–	–	
11	2-EH STILL VAPOR	75,000	T	T	T	200**	13**	–	–	T	T	T	94	6	–	–	COMPOSITION IS IN DOUBT
12	2-EH STILL BOTTOMS	1200	T	T	T	1200	9	0.6	2.6	T	T	T	99	0.7	0.05	0.2	TEMP. ≃ 155°C
13	SPARGE AIR	60	–	–	–	–	–	–		–	–	–	–	–			
14	2-EH MAKEUP	NI	–	–	–	NI	NS	NS	NS	–	–	–	97	2.7			
15	2-EH CONDENSATE	190	T	T	T	190	5	T	T	T	T	T	97	2.7			
16	2-EH RETURNS	1700	T	T	T	1700	14	0.8	3.2	T	T	T	99	0.8	0.05	0.2	
17	STILL AQUEOUS WASTE	8.5	T	T	T	0.1	8.4	T	T	T	T	T	0.1	99.9			
18	SPAN-80 INPUT	0.05	–	–	–	–	–	0.05	–	–	–	–	–	–	100	–	
19	ETHOMEEN S-15 INPUT	0.02	–	–	–	–	–	–	0.02	–	–	–	–	–	–	100	
20	2-EH RAW INPUT	NI††	–	–	–	NI	–	–	–	–	–	–	100	–	–	–	
21	TREATED 2EH SUPPLY	NI††	–	–	–	NI	–	NI	NI	–	–	–	97	2.7	0.05	0.2	
22	2-EH TREATMENT WASTE	NI	–	–	–	NS	NI	–	–	–	–	–	0.1	99.9	–	–	
23	DISPLACEMENT 2EH RETURN	10 Avg.	T	T	T	10 Avg.	0.3 Avg.	0.005 Avg.	0.02 Avg.	T	T	T	97	2.7	0.05	0.2	
24	DISPLACEMENT 2-EH FEED	10 Avg.	T	T	T	10 Avg.	0.3 Avg.	0.005 Avg.	0.02 Avg.	T	T	T	97	2.7	0.05	0.2	
25	COLUMN SWIRL 2-EH	1900	T	T	T	1900	19	1	4	T	T	T	99	1.0	0.05	0.2	
26	COLUMN UPFLOW 2-EH	1900	T	T	T	1900	19	1	4	T	T	T	99	1.0	0.05	0.2	
27	DISPLACEMENT 2-EH SUPPLY	NI	–	–	–	NI	NS	NS	NS	–	–	–	97	2.7	0.05	0.2	

T = TRACE
NI = NORMALLY INFREQUENT
NS = NORMALLY SMALL

† PARTS OF THE SYSTEM OPERATED BATCHWISE SHOW BATCH AMOUNT-TIME INTERVAL

* 2-ETHYL HEXANOL FLOW FOR TRANSPORTING THE GELLED SOLIDS IS NOT INCLUDED IN THIS LINE OF THE TABLE. THE DENSITY OF THE GEL IS ABOUT 3 g/cm³. FLOW OF 2-EH FOR TRANSPORTING GEL SOLIDS DEPENDS ON PIPE SIZE. FOR ~ 1/2" PIPE, THE TRANSPORT FLOW MIGHT BE ~ 1 TO 2 LITERS/MIN. THE FLOW IN THE GELLED SPHERES TRANSFER JETS IS CONTINUOUS. FILTER BACKWASH FLOW IS INTERMITTENT.

†† THE DAILY LOSS OF 2-EH AS FILTRATE BACKWASH TO THE LIQUID WASTE SYSTEM, PF-61-2, MIGHT BE ABOUT 40-50 LITERS/DAY, IF THE 2-EH IS NOT RECOVERED AND RETURNED TO PF-25-3. WITH BACKWASH 2-EH RECOVERY THE LOSS MIGHT BE CUT TO 10-15 LITERS/DAY.

** THESE ARE THE VOLUMES OF THE CONDENSED LIQUIDS WHICH ARE EQUIVALENT TO THE VAPORS.

TABLE 5-3

MATERIAL BALANCES AND PROCESS CONDITIONS FOR FIG. 5-3

		FLOWRATES*								COMPOSITIONS							
STREAM NUMBER	STREAM DESCRIPTION	TOTAL LITERS/h	HEAVY METAL kg/h	U kg/h	Th kg/h	2-EH LITERS/h	WATER kg/h	ARGON LITERS/h	AIR LITERS/h	HEAVY METAL WT%	U WT%	Th WT%	2-EH WT%	WATER WT%	ETHO-MEEN VOL%	SPAN-80 VOL%	REMARKS
1	GELLED KERNELS †	1.5 kg/hr	1.2	0.32	0.92	0.3	0.4	-	-	66	17	49	10	15	0.1	0.02	
2	DRAINED 2-EH	59	T	T	T	58	1	-	-	T	T	T	98	2	0.2	0.05	<100°C †
3	CONDENSED 2-EH	1	-	-	-	1	0.02	-	-	-	-	-	98	2	0.2	0.05	<40°C †
4	COMBINED 2-EH	60	T	T	T	59	1	-	1	T	T	T	98	2	0.2	0.05	<100°C †
5	RECYCLED 2-EH	60	T	T	T	59	1	-	1	T	T	T	98	2	0.2	0.05	<100°C †
6	DRIED KERNELS	4.2 kg/h	3.6	0.91	T	0.04	0.04	-	-	85	21	64	1 ††	1	0.01 ††	0.003 ††	200°C. MAX; 37 HRS IN TEMP GRADIENT
7	DILUTED CALCINER OFF-GAS	≤7500	T	T	T	-	T	-	≤7500	T	T	T	-	T	-	-	300°C
8	CALCINER DILUTION AIR	2800	-	-	-	-	-	-	2800	-	-	-	-	-	-	-	
9	CALCINED KERNELS	4.1 kg/h	3.6	0.91	2.7	-	T	-	-	88	22	66	-	T	-	-	1000°C MAX; 4 HRS IN TEMP GRADIENT
10	SINTERED KERNELS	4.1 kg/h	3.6	0.91	2.7	-	-	-	-	88	22	66	-	-	-	-	<350°C. AFTER 1200°C MAX, 4 HRS.†
11	DILUTED FURNACE OFF-GAS	21000 †††	T	T	T	-	-	6300	15000	T	T	T	-	-	-	-	
12	FURNACE DILUTION AIR	11000	-	-	-	-	-	-	11000	-	-	-	-	-	-	-	
13	ARGON - 4% H_2	4800	-	-	-	-	-	4800	-	-	-	-	-	-	-	-	
14	PRODUCT SIZE KERNELS	4 kg/h	3.5	0.90	2.6	-	-	-	-	88	22	66	-	-	-	-	
15	UNDERSIZE KERNELS	0.05 kg/h	0.044	0.011	0.033	-	-	-	-	88	22	66	-	-	-	-	
16	OVERSIZE KERNELS	0.05 kg/h	0.044	0.011	0.033	-	-	-	-	88	22	66	-	-	-	-	
17	SPHERES	3.9 kg/h	3.4	0.85	2.5	-	-	-	-	88	22	66	-	-	-	-	
18	NONSPHERES	0.1 kg/h	0.088	0.022	0.066	-	-	-	-	88	22	66	-	-	-	-	
19	SPHERE PRODUCT KERNELS	3.9 kg/h	3.4	0.85	2.5	-	-	-	-	88	22	66	-	-	-	-	
20	NONSPHERE RECYCLE	N.I.	-	-	-	-	-	-	-	88	22	66	-	-	-	-	
21	NONSPHERE REJECT	0.1 kg/h	0.088	0.022	0.066	-	-	-	-	88	22	66	-	-	-	-	
22	WASTE CONDENSATE	3.7	-	-	-	-	-	-	-	-	-	-	0.1	99.9	-	-	40°C
23	ENTRAINED WATER REJECT	N.S.	T	T	T	-	-	-	-	T	T	T	0.1	99.9	-	-	
24	PURGE AIR	30	-	-	-	-	-	-	600	-	-	-	-	-	-	-	
25	BLAST AIR	600	-	-	-	-	-	-	30	-	-	-	-	-	-	-	
26	DRYER HOPPER OFF-GAS	630	-	-	-	-	T	T	630	-	-	-	-	-	-	-	
27	CALCINER OFF-GAS	<4700	T	T	T	-	-	-	<4700	T	T	T	-	-	-	-	<1000°C †
28	DRYER PURGE ARGON	1300	-	-	-	-	-	1300	-	-	-	-	-	-	-	-	
29	DRYER STEAM INPUT	8000	-	-	-	-	11	-	-	-	-	-	-	100	-	-	~200°C †
30	CONDENSER OFF-GAS	1500	T	T	T	-	<0.06	1500	-	T	T	T	-	<3	-	-	<40°C †
31	CALCINER INPUT AIR	1100 ***	-	-	-	-	-	-	1100	-	-	-	-	-	-	-	
32	FURNACE HOPPER ARGON	1	-	-	-	-	-	1	-	-	-	-	-	-	-	-	
33	BATCHED CALCINED SPHERES	32 kg-8	29 kg-8	7.3 kg-8	22 kg-8	-	-	-	-	85	21	64	-	-	-	-	
34	BATCHED SINTERED SPHERES	31 kg-8	29 kg-8	7.3 kg-8	22 kg-8	-	-	-	-	88	22	66	-	-	-	-	
35	OFFSIZE KERNELS REJECT	0.8 kg-8	0.7 kg-8	0.18 kg-8	.52 kg-8	-	-	-	-	88	22	66	-	-	-	-	
36	DRYED GEL AIRLIFT	~100 CFH	-	-	-	-	-	-	100 CHF	-	-	-	-	-	-	-	

* PARTS OF THE SYSTEM OPERATED BATCHWISE SHOW BATCH AMOUNT-TIME.

** TEMPERATURES ARE NOMINALLY AMBIENT, ~27°C, UNLESS SPECIFICALLY INDICATED OTHERWISE.

*** FLOW IS 100% EXCESS OVER MAX. POSSIBLE CHEMICAL DEMAND.

\+ REFERS TO THE GELLED PARTICLES ONLY. AN ACCOMPANING 2-EH FLOW FOR TRANSPORTING THE PARTICLES DEPENDS ON TRANSPORT PIPE SIZE. IN A 3/8" DIA. PIPE THE TRANSPORT 2-EH FLOW MIGHT BE ABOUT 1 LITER/MIN. (60 LITERS/HR.

†† ORGANICS WILL PROBABLY BE MORE OR LESS CARBONIZED.

††† STREAM CONTAINS TRACES OF H_2O AND H_2; ABOUT 0.6 VOL % OF EACH.

50,000 FUEL ELEMENTS /YEAR

TABLE 5-4

EQUIPMENT LIST FOR SOLEX FLOWSHEET

OUT-OF-CELL COLD PREPARATION EQUIPMENT FOR
FLOWSHEET PF-25-1 (FIG. 5-1, SHEET 1) (ONE SET REQUIRED)

Item No.	Code No.	Description	Capacity[a]	Instruments	
1	T-2507	Organic Solvent Supply	2400 liters (634 gal)	LI	PI
2	T-2507B	Amberlite LD-2 Supply	500 (132)	LI	PI
3	T-2509	Demin. Water Storage	4000 (1060)	LI	PI
4	T-2508	Extractant Makeup	800 (211)	LI	HLC
5	T-2514	Conc. Nitric Acid Supply	100 (26)	LI	PI
6	T-2515	Nitric Acid Adjustment	400 (106)	LI	DI
7	T-2511	Hydroxide Makeup	2400 (634)	LI	DI
8	T-2510	Carbonate Makeup	2400 (634)	LI	DI
9	T-2512	Regenerant Blending	2400 (634)	LI	DI
10	T-2513	Regenerant Feed	2400 (634)	LI	HLC

Item No.	Code No.	Description	Capacity[a]		Type
11	P-25	Cold Sump	100 lpm (25 gpm)		Submersible
12	P-2505	Fresh Extractant Transfer	50	13	Centrifugal
13	P-2507	Nitric Acid Transfer	50	13	Centrifugal
14	P-2506A	Regenerant Metering	0-1	0-1/2	Pos. Displ.
15	P-2506B	Regenerant Metering	0-1	0-1/2	Pos. Displ.
16	P-2506C	Regenerant Metering	0-1	0-1/2	Pos. Displ.

Item No.	Code No.	Description	Capacity[a]	Type
17	(T-2511)	Hydroxide Makeup Stirrer	1 hp	Offset-angled propeller; through top
18	(T-2510)	Carbonate Makeup Stirrer	1 hp	Offset-angled propeller; through top
19	(T-2512)	Regenerant Blending Stirrer	1 hp	Turbine, tight seal through side

Item No.	Code No.	Description	Number
20-collective	N/A	In-Line Hand Valves	37
21-collective	N/A	Sample Valves	8
22-collective	N/A	Plug Insert Sample Valves	2
23-collective	N/A	Automatic Valves, Level	5
24-collective	N/A	Float-Check Valves	4
25	N/A	Pressure Relief	1
26	N/A	Automatic Valves, Flow	3

Item No.	Code No.	Description
27	F-2502	Filter, Replaceable Cartridge Type
28	N/A	Sump Level Control

(a) Tank capacities are working volumes.

TABLE 5-4 (Continued)

OUT-OF-CELL, LOW ALPHA CONTAMINATION EQUIPMENT FOR FLOWSHEET PF-25-1 (FIG. 5-1, SHEET 1) (ONE SET REQUIRED)

Item No.	Code No.	Description	Capacity[a]		Instruments	
1	T-2505	Thorium Nitrate Dissolver	600 liters	(160 gal)	LI	DI
2	T-2506	Thorium Nitrate Storage	600	(160)	LI	DI
					Type	
3	P-2504	Thorium Nitrate Transfer	20 lpm	5 gpm	Centrifugal	
4	P-25--	Alpha Contam. Sump	20 lpm	5 gpm	Submersible	
					Type	
5	(T-2505)	Th. Nitrate Diss. Stirrer	1 hp		Vertical propeller; through top	
			Number			
6-collective	N/A	In-Line Hand Valves	8			
7-collective	N/A	Sample Valves	1			
8-collective	N/A	Plug Insert Sample Valves	1			
9-collective	N/A	Float Check Valves	1			
10-collective	(T-2505)	Hopper Slide Valve	1			
11	F-2501	Replaceable, Magnetic Element Filter, one required				
12	N/A	Crane-Type Drum Unloader, one required				
		PF-25-3				
		OUT-OF-CELL: EQUIPMENT FOR GEL-SPHERE FORMING				
13	T-2532	2-Ethylhexanol Storage	1200 liters	(200 gal)		
14	T-2533	2-Ethylhexanol Makeup	400	(100)		
15	T-2534	Ethoneen Storage	20	(5)		
16	T-2535	SPAN-80 Storage	20	(5)		
17	P-2525	Raw 2-EH Transfer	20 lpm	(5 gpm)	Centrifugal	
18	P-2526A	Treated 2-EH Transfer	20 lpm	(5 gpm)	Centrifugal	
19	F-2508	On-Line Filter	20 lpm	(5 gpm)	Replaceable Cartridge Paper	
			No. Reqd.			
20-collective	N/A	In-Line Manual Valves	13			
21-collective	N/A	3-Way Sample Valves	4			
22	N/A	In-Line Right Glass	1			

[a] Tank capacities are working volumes.

TABLE 5-4 (Continued)

IN-CELL FEED MAKEUP SYSTEM(S) FOR FLOWSHEET PF-25-1 (FIG. 5-1, SHEET 1)
(THREE SETS REQUIRED)

Item No.	Code No.	Description	Capacity[a]	Instruments
1	T-2501	Uranyl Nitrate Storage	63 liters(17 gal)	LI DI HLC
2	T-2502	Th-U Solution Blend	85 (23)	LI DI HLC
3	T-2503	Feed Conc. Adjust	350 (93)	LI DI HLC
4	T-2504	Feed Storage	350 (93)	LI HLC
				Type
5	P-2502	Column Feed Metering	0-1.5 lpm 0-1/2 gpm	Pos. Displ.
			Number	
6-collective		In-Line Manual-Control Valves	6	
7-collective		In-Line Manual-Automatic Valves	3	
8-collective		In-Line Automatic Valves	2	
9-collective		Float-Check Valves	4	

OUT-OF-CELL EQUIPMENT ASSOCIATED WITH IN-CELL EQUIPMENT

		Number
10-collective	Four-Way Sample Valves	4
11-collective	Float-Check Valves	4
12-collective	Manual-Automatic Valves	12

[a] Tank capacities are working volumes.

TABLE 5-4 (Continued)

IN-CELL SOLVENT EXTRACTION SOL-MAKING SYSTEM(S) FOR FLOWSHEET PF-25-1 (FIG. 5-1, SHEET 1) (THREE SETS REQUIRED)

Item No.	Code No.	Description	Capacity or Dia. x Ht.	Instruments		
1	CO-2501	1st Nitrate Extractor	10 cm x 250 cm (4" x 8')	LC	TC	IFC
2	CO-2502	2nd Nitrate Extractor	10 x 250 (4" x 8')	LC	TC	IFC
3	CO-2503	3rd Nitrate Extractor	10 x 250 (4" x 8')	LC	TC	IFC
4	CO-2504	Water Scrub Column	10 x 250 (4" x 8')	LC	TC	IFC
5	CO-2504	Regeneration Column	10 x 250 (4" x 8')	LC	TC	IFC
6	T-2519	Extractant Storage	500 liters (132 gal)	LI	DI	

Item No.	Code No.	Description	Capacity or Dia. x Ht.	Type
7	P-25--	Scrub Recycle Input	1/2 lpm 1/8 gpm	Pos. Displ.
8	P-2508	2nd Ext. Col. Extractant Transfer	4 1	Pos. Displ.
9	P-2509	3rd Ext. Col. Extractant Transfer	4 1	Pos. Displ.
10	P-2510	Regenerated Extractant Metering	0-4 0-1	Pos. Displ.
11	P-25--	Regenerated Extractant Transfer	4 1	Pos. Displ.

Item No.	Code No.	Description	Capacity or Dia. x Ht.	Output Typ.	Temp. Max.	Input Typ.	Temp. Min.
12	E-2501	Feed Heater[b]	100 kcal/min 400 Btu/min	60°C	100°C	25	10
13	E-2502	Digester[b]	100 400	100	100	60	25
14	E-2503	Digester[b]	100 400	100	100	60	25
15	E-2504	Off Gas Condenser	1(?) 4(?)	30	40	<100	25
16	E-2506	Extractant Heater	100 400	60	100	25	10

Item No.	Code No.	Description	Capacity or Dia. x Ht.	No. Reqd.
17	T-2502	Phase Separator	4 lpm extractant, max. rate (1 gpm extractant)	
18-21	N/A	Four Interface Control Jockley-Pressure Pots		
22	N/A	Flow Controller (1 reqd.)	0-1/2 lpm 0-1/8 gpm	
23-collective	N/A	In-Line Manual Control Valves		12
24-collective	N/A	Automatic Control Valves		19
25-29	(CO-2501-5)	Five Variable Speed Stirrers	0-600 RPM, 1/4 hp	
30	N/A	Output Sol. Conductivity	0-10 millimho/cm	
31	N/A	In-Line Density Measurement		
32	(CO-2505)	Outlet Radiation Detector		
33		Out-of-Cell Sample Valve for 2-2519		
34		Out-of-Cell Flow Controller for Aqueous Scrub Input		

(b) Useful input only; no allowance for heat losses.

TABLE 5-4 (Continued)

IN-CELL SOL CONCENTRATION AND SECONDARY HEAT EXCHANGE SYSTEMS FOR FLOWSHEET PF-25-2 (FIG. 5-1, SHEET 2) (THREE SETS REQUIRED)

Item No.	Code No.	Description	Working Capacity		Instruments	
1	T-2516	Dilute Sol. Surge	500 liters	(130 gal)	HLC	
2	T-2521A	Conc. Sol. Storage-Assay	100	(25)	HLC, LI, DI, CR, VISC. R.	
3	T-2521B	Conc. Sol. Storage-Assay	100	(25)	HLC, LI, DI, CR, VISC. R.	
4	T-2517	Condensate Storage	500	(130)		
					Type	
5	P-2514	Evaporation Recirculation	40 lpm	10 gpm	Centrifugal	DPC
6	E-2509	Evaporation Reboiler	1000 kcal/min	(4000 Btu/min		PC
7	E-2508	Sol. Evap. Condenser				
8	E-2507	Sol. (Flash) Evaporator	Volumetric vapor flowrate = 1200 lpm		HLC, LC, DC, DPI	
9-10	(T-2516,17)	Steam Ejectors	20 lpm (5 gpm) liquid ejection rate		LI	
					No. Reqd.	
11-collective	N/A	In-Line Manual Valves			10	
12-collective	N/A	Automatic Control Valves			5	
13-collective	N/A	Check Valves			2	
		OUT-OF-CELL ASSOCIATED EQUIPMENT				
14-collective	N/A	In-Line Manual Valves			12	
15-collective	N/A	4-Way Sample Valves			3	
16-collective	N/A	Float-Check Valves			3	
17-collective	N/A	Automatic Control Valves			2	
18	T-2539	Sec. Condensate Receiver	200 liter	50 gal		
19	E-2505	Sec. Cold Water Chiller	3000 kcal/min[c]		LI, TC, RE (≈ 0 psig 4°C)	
20	E-2510	Sec. Hot Water Heater	1500 kcal/min		LI, TC, RE (50 psig, 140°C)	
21	E-2511	Sec. Steam Reboiler	1500 kcal/min 6000 Btu/min		LC, TC, RE (160 psi, 184°C)	
					Type	
22	P-2519	Hot Water Circulation	50 lpm	12 gpm	Centrifugal	
23	P-2520	Cold Water Recirculation	25 lpm	6 gpm	Centrifugal	
24	P-2521	Boiler Feed	10 lpm	3 gpm	Centrifugal	
					No. Reqd.	
25-collective	N/A	In-Line Manual Valves			19	

[c] No allowance made for direct heating-cooling losses from liner/tanks, etc.

TABLE 5-4 (Continued)

Item No.	Code No.	Description	No. Reqd.
26-collective	N/A	3-Way Pressure Relief Valves	3
27-collective	N/A	Automatic Control Valves	1
28	N/A	Radiation Detection Elements	3
29	N/A	Check Valves	1
		OUT-OF-CELL ASSOCIATED EQUIPMENT	
30	N/A	Automatic Control Valves	3
31	N/A	Sample Valves	2
32	N/A	4-Way Sample Valves	1

TABLE 5-4 (Continued)

SPHERE FORMING SYSTEM FOR FLOWSHEET PF-25-3 (Fig. 5-2)
(THREE SETS REQUIRED)

Item No.	Code No.	Description	Capacity	Instruments
1	N/A	Travelling T.V. Camera		
2	T-2531	Conc. Sol Storage	100 liters (25 gal)	LI, HLC, DI, CR, VISC.R.
3	T-2538	Drying Alcohol Surge	400 (100)	LI, DI
4-9	S-2501A-3B	Feed Development	30 (8)	LR, DI, IFC
10	S-2504	Displacement Alcohol Surge	200 (50)	
11-16	F-2501A-3B	Sol Filters	50 ml/min thru 100 mesh	DPI
17-18	F-2507A, B	Alcohol Supply Filters	300 lpm (75 gpm), ΔP max., ≈2 psi	
19-20	F-2504A, B	Displacement Alcohol Filters	10 lph (3 gph), through 100 mesh	
21	F-2509	Condensate Phase Separator	4 lpm (1 gpm) input	
22	E-2517	Alcohol Still	1500 kcal/min, 6000 Btu/min	LC, TC, PI
23	E-2518	Still Overheads Condenser	120 cal/min, 500 Btu/min	TC
24	E-2516	Feed Alcohol Heat Exchanger	±1000 kcal/min for 250 lpm alcohol flow	TC
25-27	CO-2510A, B, C,	Gelling Columns	Tapered; max. dia. ≈20 cm (8") x ≈250 cm (8') ht.	
28-33	N/A	Sol Dropper Heads	50 ml/min (1 gph) Pulse Frequency Slope and Amplitude Control	
34-35	I-2510A, B	Ion Exchanger	10 liters = 10 miles HNO_3 each	
				Type
36	P-2528	Alcohol Feed Pump	300 lpm (75 gpm)	Pos. Displ.
37-42	P-2529A-F	Displ. Metering	0 -0.1 lpm, 0 - 1-1/2 gph	Pos. Displ.
			No. Reqd.	
43-collective	N/A	In-Line Hand Valves	78	
44-collective	N/A	Automatic Valves, Level	8	
45-collective	N/A	Automatic Valves, Flow	17	
46-collective	N/A	Automatic Valves, Temp.	4	
47-collective	N/A	Automatic Valves, Pressure	2	
48-collective	N/A	Float Check Valve	1	
49-collective	N/A	In-Line Flow Indicators	5	
50-collective	N/A	In-Line Flow Controller	8	
51-collective	N/A	In-Line Pressure Controllers	2	
52-collective	N/A	In-Line Density Indicators	2	
53-collective	N/A	In-Line pH Indication	2	

TABLE 5-4 (Continued)

OUT-OF-CELL EQUIPMENT ASSOCIATED WITH GEL SPHERE FORMING FOR FLOWSHEET PF-25-3 (Fig. 5-2) (THREE SETS REQUIRED)

Item No.	Code No.	Description	Capacity	No. Reqd.	Type
1	N/A	In-Line Manual Valves		9	
2	P-2526B	Span-80 Metering	0-0.1 lph		Pos. Displ.
3	P-2526C	Ethoneen Metering	0-0.05 lph		Pos. Displ.
4	F-2505	In-Line Filter	1 lph		Replaceable Cartridge, Paper
5	F-2506	In-Line Filter	1 lph		Replaceable Cartridge, Paper
6	N/A	3-Way Sample Valves		2	
7	N/A	4-Way Sample Valves		1	
8	N/A	Float-Check Valves		1	
9	N/A	Automatic Control Valves		2	

TABLE 5-4 (Continued)

IN-CELL EQUIPMENT FOR FLOWSHEET PF-25-4 (FIG. 5-3)
(THREE SETS REQUIRED)

Item No.	Code No.	Description	Capacity or Size	Instruments
1-3	E-2521A, B & C	Belt Dryer(s)	Max. Temp. ≈ 200°C Heat Load = 25 kcal/min Belt 3' x 10'	LI, HLC, PI, DI, TI
4-6	E-2522A, B & C	Dryer Off Gas Condenser(s)	HT Load = 25 kcal/min, efflux temp. $\leq$ 40°C	
7	E-2522	Calciner	10 kw, ≈8' tall x 1' dia.	TI
8	E-2533	Sintering Furnace	10 kw, ≈8' tall x 1' dia.	TI
9	W-2501	Calciner Feed Hopper	30 liters (7 gal)	LI
10	W-2502	Sintering Feed Hopper	30 liters (7 gal)	LI
11	W-2503	Roundometer Feed Hopper	30 liters (7 gal)	LI, SLIT C
12	W-2505	Calciner Kernels Collector	10 liters (2-1/2 gal)	LI
13	W-2506	Oversize Kernel Collector	10 liters (2-1/2 gal)	LI
14	W-2507	Undersize Kernel Collector	10 liters (2-1/2 gal)	LI
15	W-2508	Product Size Kernel Collector	10 liters (2-1/2 gal)	LI
16	W-2509	Non-round Kernel Array Coll.	10 liters (2-1/2 gal)	LI
17	W-2510	Non-round Kernel Array Coll.	10 liters (2-1/2 gal)	LI
18	W-2511	Round Kernel Array Coll.	10 liters (2-1/2 gal)	LI
19	W-2512	Round Kernel Array Coll.	10 liters (2-1/2 gal)	LI
20-21	H-2507 & 08	Diversion Hoppers	To handle 4 kg MO_2/hr from V-2524	
22	Y-2523	Vibrating Sieves	Est. overall equip. size for 4 kg MO_2/hr, ≈2' x 2' x 2', 1 hp motor, each screen even 2'.	
23	V-2524	Roundometer(s)	Est. table area ≈100'^{2}	Tilts, vib. freq. and amplitude
24-26	F-2510A, B & C	Phase Separator(s)	5 lph input	TC
27-29	F-2511A, B & C	Phase Separator(s)	1 lph input	
30-31	F-2512 & 13	Filters[d]	≈6 lpm air flow, cartridge type, replaceable element	
			No. Reqd.	
32-collective		In-Line Manual Valves	26	
33-collective		In-Line Automatic Valves	6	
34-collective		In-Line Flow Controllers	5	
35-37	P-2535A, B & C	2-EH Return	2 lpm (1/2 gpm)	
38	B-25--	Calciner Off Gas Blower	7500 lph @ 300°C	

[d] These are out-of-cell, not in-cell.

TABLE 5-4 (Continued)

Item No.	Code No.	Description	Capacity or Size	Instruments
39	B-25--	Furnace Off Gas Blower	21,000 lph @ 300°C	
40-42	N/A	Automatic Motor Controls	5	
43	N/A	Calciner Product Hopper Vibrator	1 reqd., controlled freq. & ampl.	
44	N/A	Furnace Product Hopper Vibrator	1 reqd., controlled freq. & ampl.	
45	N/A	Combust. Gas Monitor	1 reqd.	
46-50	N/A	Flame Arresters	5 reqd., 2 for 80 lpm, 1200°C Argon-1% H_2 3 for 350 lpm, 300°C air-25%(AR-H_2)	
51	N/A	Rupture Pin	"Very low" pressure blowout	
52	N/A	Hot Wire Demister	1 reqd.	
		OUT-OF-CELL ASSOCIATED EQUIPMENT		
53-collective		In-Line Manual Valves	26 reqd.	
54-collective		Flow Indicators	23 reqd.	
55-collective		4-Way Sample Valves	2 reqd.	

12. Prefer gravity flow in-cell only if it does not create an additional and otherwise unnecessary submerged penetration of a vessel.
13. Provide parallel redundancy.
14. For out-of-cell, noncontaminated equipment prefer regular operational ease, low item cost, and low operating manpower requirement (but in-cell prefer reliability over all of these).
15. Avoid centrifugal pumps where suction lift is required.

These general guidelines were disregarded in particular circumstances. When they were disregarded, it was for particular reasons. There is no sharp cutoff between "operability" and "inoperability" as any of these rules and ideas are more or less disregarded, but if more than a few are generally disregarded, process realiability and operability suffer.

In many cases, some particular piece of equipment was chosen mainly for the sake of specificity in illustration. Some examples of this are the use of pressure-pot jacklegs to control interface levels and vac-wash-sparge samples systems. Other alternatives, with differing combinations of advantages and disadvantages, are possible. In changing these or other parts of system, however, it is suggested that the following two valid ways of improving a process be used with restraint:

1. Lowering the process equipment cost by either specifying a cheaper or simpler device or by combining functions in a single device.
2. Lowering of manpower requirements by automating routine process control functions.

It is difficult to know how much restraint in these matters is enough. An example of such a question, regarding(1) above, is the use of belt dryers in Fig. 5-3. The single greatest problem encountered during the SOLEX demonstration run reported in Ref. 5-1 was cracking in the drying-calcining step.

The pot-batch dryer/calciner used at ORNL differs radically from a belt dryer, and the reported ORNL drying conditions (a 36-hr schedule with a change of atmosphere) result in a complex and slow-moving belt dryer. Direct modeling of the ORNL pot dryer/calciners leads, however, to replacing each of the belt dryers shown with 6 pots (36 per production line; 108 for a 3-line refabrication plant). Large bench-scale or small-unit operation-scale experimental testing of belt drying of SOLEX gel spheres would be required before the process could be constructed on the scale required for a commercial recycle facility.

Flowsheet Design

Instrumentation and control functions on in-cell equipment are shown as if these equipment items were wholly in-cell. Actual readouts and setpoint controls must be located outside the cells. Process variable control functions should normally include an indication of the controlled variable, for example, designation of level control (LC) includes a level indicator (LI). Sometimes LI is shown explicitly in addition to LC to emphasize the presence of both functions.

In cases where an indicating instrument is specified, it would be desirable, but perhaps not essential, to have automatic recording readout or other automatic data logging. Cases where automatic recording is essential are specifically shown. Alarm functions are now shown, but in general most control and indicating functions should also have alarms.

Tanks and other equipment items should have a closable connection to the vent-offgas system. This connection is omitted from the flowsheet except where a defined process gas load into the offgas system or other special consideration exists. The equipment decontamination-cleanout system is, similarly, shown only in a few special cases, but, in general, a decontamination cleanout and spray system should also be provided throughout the process line.

Microsphere Sol Preparation System (Fig. 5-1, Sheet 1, Drawing No. PF-25-1)

Alpha Contamination Area. The low-alpha area may be either deleted in subsequent flowsheets or considered only as a backup alternative, if a firm decision to use directly recycled thorium in refabrication were made. Some possible fuel management options involve extended storage of the reprocessed thorium, in which case provision for introducing virgin thorium would be needed.

Cold Chemical Preparation Area. Sample valves on the cold makeup tanks are shown at bottom-center to pick up the dirtiest (most conservative) sample for analytical determinations. Tanks receiving undissolved solid inputs should have plug insert type bottom valves.

Hot Feed Makeup. T-2501 could be eliminated if proper storage capacity, concentration, assaying, and volume transfer control were provided in the uranium product portion of the reprocessing plant. A separate Th/U mixing tank (T-2502) and an overall concentration adjustment tank (T-2503) are specifically recommended in Ref. 5-1. Having two tanks eases the assaying scheduling problems and correction of mistakes in Th/U ratio. T-2503 has water addition capability but does not need water removal capability for a credible dilution error. Accidentally high heavy metal concentration can create a severe problem, gelation in the extractors and/or digesters, but accidental dilution to any reasonably expectable extent merely decreases heavy metal throughout and increases the water load on the sol evaporator.

Sol Making Extraction System. A variety of different types of extractors has been tried for making sols. Spray columns, either unpacked or packed, might be used. However, the stirred chamber column was the first tried for these sol systems at ORNL, and it has the longest history of successful operation.

The phase separator, T-2520, is a conceptual addition to the actual ORNL prototype equipment. A recommendation has been made by ORNL personnel to add a water wash column after the regeneration column (CO-2505). A future

revision of Fig. 5-1 (PF-25-1) should substitute a CO-2506 for T-2520.

The solubility of water in the organic extractant is slightly variable with temperature and the degree of regeneration. In the past, there has been an occasional tendency for an aqueous heel to collect in the regenerated organic supply tank (T-2519). This accumulation is not a problem if allowance is made for its detection and removal.

The heavy metal concentration in the aqueous feed to CO-2501 normally is somewhat lower than the concentration leaving CO-2503 as sol. This is an advantageous effect in a purely process sense. It takes a little of the load off the subsequent sol evaporation step. Most of this concentration effect is probably due to water takeup by the organic extractant as it extracts nitrate, but an unknown fraction may be due to evaporation to the offgas from the heated columns. The unknown and potentially variable evaporative loss of volume is an inconvenience in a remote system under tight inventory definition and control. The offgas condenser, E-2504, was added to eliminate questions concerning evaporative volume loss versus leakage. It is a convenience for inventory measurement rather than a process necessity.

The extraction system is shown as having seven pumps associated with it (three metering and four transfer). The actual number and types of pumps needed, and their locations in association with the columns, can be varied depending on assumptions made about overall column heights and the headroom available in the cell. The illustrative scheme chosen for Fig. 5-1 (PF-25-1) assumed that gravity cascading of the aqueous stream is possible for CO-2501, -2502, and -2503, and that the regeneration system columns are gravity-cascaded for the organic in a separate train, where CO-2504 is level with or above CO-2502. P-2508 may be eliminated if CO-2504 can be placed below CO-2502, for example.

The ORNL prototype system contains no equipment corresponding to E-2501, E-2503, and E-2506. The system can operate without these items, but then the system would contain some looseness of process definition and control. Some poorly understood variabilities have occurred in the sols made in the

ORNL prototype system. The foregoing additions may be needed to improve process control.

Microsphere Sol Preparation System (Fig. 5-1, Sheet 2, Drawing No. PF-25-2)

The left hand side of this flowsheet is a continuation of the in-cell sol-making extraction equipment of Fig. 5-1, Sheet 1 (PF-25-1).

Sol-Evaporation System. The evaporator arrangement comprised of E-2507, E-2508, E-2509, and P-2514 closely models the ORNL system except for specifying hot water instead of steam to E-2509; i.e., with care steam may be used, but excessive temperatures on the heat transfer surfaces can cause bakeout of the sol as a difficult-to-remove cake. The pressure difference across P-2514 is a significant control variable. When this pressure difference rises, it signals that the sol is becoming viscous and is liable to gelation in the equipment. Malfunction of the sol-making equipment can lead to sols which gel at abnormally low heavy metal concentrations.

While properly made SOLEX-type sols are storable for days and weeks, it is not difficult to make SOLEX sols which will slowly thicken and finally gel if stored for a long time after being concentrated. The indicated viscometric instrumentation is needed to ensure that the content of these tanks do not gel in the event of unexpected equipment outage downstream. These viscometers should be of a low shear intensity type, since thixotropy is a common property of slightly "off" sols while they are undergoing slow thickening.

Secondary Heating and Cooling. The purpose of these systems is mainly to isolate possible radioactive leakage from the in-cell process equipment to the steam/water systems outside the cells. The only slightly special features of these systems are radiation monitors which switch the pressure relief valves from cold waste to alpha waste (to recovery or to radioactive waste disposal).

Most or all heating functions could be served in principle by electrical heaters; however, electrical heaters fix the heat flux instead of the temperature and are more subject to abrupt total failure than a well-designed fluid recirculation system.

Microsphere Gelation System (Fig. 5-2, Drawing No. PF-25-3)

Conceptually, Fig. 5-2 (PF-25-3) contains only two operations: sphere gelation and alcohol recirculation. These operations are not simple. The former operation requires a complex balance of flows and compositions, whereas the latter operation contains a variety of substeps. No single process adjustment or substep is especially difficult, at least in a contact plant, but orchestrating all the interrelationships into simultaneous satisfactory overall operation requires skill and experience. Since much of the operation of this portion of the system is somewhat of an artistic balancing act, it is also the most difficult for which to define the process parameters. Published reports of these operations define some of the more accessible operating parameters in empirical terms for a particular apparatus or for a particular campaign, but there is little definition, at least in easily accessible documents, of the parameters needed for scaleup design. For example, the dryness of the 2-EH is defined as a direct, simple function of still operating temperature in the ORNL prototype still. However, no vapor-liquid equilibria data versus composition are given for the 2-EH water system, and parameters such as the heat load of the still or the wet 2-EH condensate rate from the phase separator are not given. In the absence of such data, genealized correlations were used to estimate the material balances and stream compositions.

The material balances, equipment sizes, and heat loads for Fig. 5-2 (PF-25-3) are, by far, the least well defined and most uncertain in the overall SOLEX process.

Sol Displacement System. This system is based on the recommendations in Ref. 5-2. The displacement pumps are Zenith Corporation viscose filament spinneret gear pumps, pumping 2-ethylhexanol. The sol is too corrosive to pump directly in stainless steel pumps. In a contact plant, the filters in the pump discharge are optional, since removing or cleaning a clogged needle in the dropping nozzle is not difficult. Other pumping systems are possible, and a small piston-syringe pump has been used at ORNL for small volume, light duty, laboratory-scale dropping systems. HOBEG uses, in its contact plant, a pressure-regulated blowcase through a needle valve.

Considerable thought and effort have gone into ganging several nozzles to the discharge of a single pump or other feed device, but such ganging has typically led to problems in keeping the flow to each nozzle equal to that of every other nozzle. All displacement and blowcase systems involve stopping the nozzle during a refill cycle. Originally, Fig. 5-2 (PF-25-3) was drawn with a dual displacement system for each nozzle, so as to minimize the time the nozzle was not operating. However, the added complications of piping, valving, and additional pumps and tanks seemed excessive for an in-cell operation, in relation to a comparatively small percentage gain in nozzle on-stream time.

Dropping Nozzles. It is assumed that the pulsed fluid nozzles will be those described in Ref. 5-3. The size yields reported for these nozzles are somewhat better than those assumed in the material balances to allow for start, stop, and malfunction of these in-cell nozzles. The result of in-cell operation is seldom as favorable as with contact operations.

Dehydration Column. The advantages of the tapered gelling column are low headroom requirement and high throughput. The disadvantage is "touchiness" in operation. One must balance properly an upflow rate, a swirl flowrate, two surfactant concentrations, a water concentration, and possibly the column acidity. Another possibly significant, but relatively unexplored, variable is column temperature. The control of column temperature

and acidity has not been studied extensively in ORNL development. E-2516 is a conceptual addition to the ORNL prototype system to permit temperature control in the columns.

The various aspects of acidity control are fairly complicated. Sometimes acidity need not be closely controlled, but, especially for in-cell operation of a fairly touchy system, it seems best to control acidity. The most direct effect of acidity as nitric acid is to degrade oxidatively the surfactant(s) in the 155°C drying still. These "degradation products" have been another undefined variable in the surface active properties of the ORNL system. General principles suggest minimizing this undefined variable by removing the acid, to at least some extent, by ion exchange columns I-2501 A and B before imposing a 155°C temperature on the organic stream.

Organic Drying System. The system shown in that used in the ORNL prototype. The major items of equipment are qualitatively defined and have a long history of operation, but some of the details needed for equipment design, such as boilup rates and vapor composition, are not defined explicitly in the available reports. The definition of sizes, flowrates, and such are given only empirically or implicitly for particular operations in the ORNL prototype equipment.

The ORNL distillation is effective and can, with care, work safely in-cell with high activity uranium feeds. Although problems of fire and explosion hazard are surmountable, more effort is needed to minimize these potential hazards. One alternative which is suggested for further evaluation is drying by ion exchange resins at room temperature and then regenerating with some nonexplosive purge gas(es) at the higher temperatures (Ref. 5-4). If the latter approach for dessication is technically feasible, its potential for an accidental release of hot, undiluted, organic vapor-mist into the cell is much less than with distillation.

Drying, Firing, and Product Quality Assurance (Fig. 5-3, Drawing No. PF-25-4)

The operations and equipment which appear in Fig. 5-3 (PF-25-4) are common to virtually all sol-gel or gel-supported processes for making HTGR fuel kernels. The significant difference among flowsheets in the processing steps indicated schematically in Fig. 5-3 are the operating conditions to be attained in the equipment rather than in the gross, overall identity of the type of unit operations to be performed.

Drying. Drying is the least understood, least developed, least satisfactory step in the overall SOLEX flowsheet. A history of difficulties and of great sensitivity to drying conditions has been reported in Ref. 5-1. The currently recommended drying process conditions involve long times (37 hr) and intricate temperature-atmosphere scheduling.

Some informal information at GAC suggests that drying conditions which are more reasonable and practical for in-cell operation may exist (Ref. 5-5). However, there is agreement that the drying step requires further experimental research and development before suitable in-cell equipment can be designed (Refs. 5-6 and 5-7).

Calcining. A calcining step is required to burn out residual carbon left by the cracking to carbon of adsorbed 2-ethylhexanol during drying and/or other heating under nonoxidizing conditions. If the kernels were pure thoria, steam stripping of the alochol in the dryer might be a practical possibility, but with the uranium present, which holds 2-ethylhexanol more tightly than thoria, the occurrence of stripping without cracking becomes dubious. It is conservative to leave the oxidative calcination step in the flowsheet.

Sintering-Reduction. The sintering-reduction furnace indicated would be an adaptation of a design by Haws and Snider of ORNL (Ref. 5-8). At ORNL, bridging problems with the irregular sol-gel ThO_2-UO_3 shards caused

cracking of the furnace tube when cold gel fell suddenly into the hot zone. Experiments at GAC using sol-gel ThO_2 in a vertical tube furnace have shown that spheroidal particles do not exhibit the bridging behavior of shards and that a vibrating hopper (Syntron Corporation) moves the particles easily, controllably, and without particle damage. The vertical tube furnace used experimentally at GAC is almost a full-scale prototype for the calcining furnace, E-2522, discussed under Calcining above.

Sieving. The main problems expected with sieving are: (1) finding a small enough commercially available continuous siever, and (2) unblinding the screens remotely. It is not difficult to find commercial, continuous sievers which are about 4 in. x 4 in. x 4 in. in overall dimensions, but the capacity of a unit this size would be in large excess of what is needed. Sprout, Waldron and Company, Muncy, Pennsylvania, makes a well designed, but oversized, continuous siever (Sani-Sizer 4323). However, special provision for cleaning, changing, and unblinding the screens remotely may necessitate developing special equipment in-house instead of purchasing any commercial unit. The problem here is more nearly one of mechanical design rather than process development.

"Roundometer" Shape Separation. A vibrating tilted table is specified for separating spheres from other shapes. This type device has a low throughput for the area required and does not readily lend itself to direct scaleup.

It is more difficult to define objectively the operation and adjustment of the vibrating tables than it is to operate and adjust them. Proper setting of vibration intensity, sphere feed rate, and table tilts in two directions depend strongly on how many nonspheres are present, the balance between cleanliness and yield in the product cut, the shape of the nonspheres, and the size of the spheres and nonspheres. Whether or not control of the tabling parameters could be automated (left unattended for extended periods

of time after being set up) will depend crucially on how variable the particle shape is as a function of time. Based on general experience, it is doubtful that this operation can be fully automated or left unattended for extended periods of time.

The illustration of the "roundometer" apparatus is the only equipment item which does not show the actual number of equipment items expected in each of the three lines. A preliminary evaluation indicates that there would be about 12 separate, identical tables represented by the single device shown as V-2524 in Fig. 5-3 (PF-25-4).

Product Collection and Transfer Systems. Items W-2505 through W-2512 are sphere and nonsphere collection vessels which can be valved off, pressurized, and blown out through a dip tube. The spheres are entrained and transported pneumatically with the gas blow. This method of transfer of dry particles has been demonstrated and reported at ORNL (Refs. 5-1 and 5-9).

Material Balances (Tables 5-1 through 5-3)

The material balances were divided to fit three instead of four flow diagrams. Parts of the system originally intended to appear on PF-25-1 were placed on PF-25-2 to relieve visual congestion. The numerical values entered in the tables have been rounded from calculations having more significant figures than shown. In some cases this rounding produces apparent discrepancies in balances on a particular component, especially when the component is a small difference in two larger streams.

Particularly on the material balances related to the 2-ethylhexanol flows, the data contain guesswork. The operation of the sphere-forming columns and the drying still are defined mainly in narrow empirical terms which are well defined only for the particular equipment constructed at ORNL. For example, no data are given in the listed references for the vapor-liquid equilibrium of 2-ethylhexanol and water. The still vapor rates, composition, and heats of vaporization were calculated by using various generalized estimates and approximations.

Equipment Lists (Table 5-4)

The equipment lists for the process contain major equipment items which are also sized.

The calculated heat loadings specified for some equipment items, mainly those associated with the 2-ethylhexanol drying system on the sphere dryers, were based on very preliminary estimates made without firm data. Additionally, the heat load specifications refer only to process load, not external losses. All heat load data would need re-evaluation for detailed design purposes.

Waste Handling and Recycle

Throughout these flowsheets, waste handling has been disregarded except for indicating that it shall be removed to a radioactive liquid facility designated by PF-61-2.

The PF-61-2 flowsheet is a preliminary sketch rather than a "PF" document in the sense of its conforming fully to all the standards given in the GAC Standards Manual, Series G. The existing PF-61-2 flowsheet would need further development to safely handle some of the special requirements of the SOLEX waste, such as the occasional charge-out of the entire 2-ethylhexanol inventory when it becomes contaminated with potentially hazardous oxidized or nitrated organic species.

Recycle of uranium-rich material is directed to a thorex-type dissolving step in all cases. Whether or not this is "the" dissolver for the main reprocessing plant is a possibility for consideration, but it should probably be a special auxiliary dissolver, since it would be desirable to keep potentially nitratable organics out of the main dissolver. Dissolved recycle U/Th in a conservative processing scheme would go to the 1AF stream of the reprocessing plant but might go to the SOLEX extraction columns feed, if the extraction processing conditions were suitably adjusted.

No allowance for recycle of off-specification uranium-bearing materials is made in the material balances for the flowsheet. With respect to the flowsheet, all waste and all "recycle" materials are treated as if they go to permanent storage.

HEAD-END REPROCESSING

Summary

Interim development reports were written relating the experimental results obtained from the primary, secondary, and tertiary crushers. Preparation of these unit crushers for tests utilizing reject FSV fuel rods is continuing. The design of a full-scale integrated crusher system is proceeding.

Installation of the air classifier was completed and parametric studies evaluating its operating characteristics are proceeding. The air classifier is an integral part of the pneumatic transport systems being installed; the first system (secondary burner product to leachers) is completed and ready for testing.

Fuel particle crushing continues to be evaluated, with the recent addition of several roll pairs enabling parametric studies to be performed.

Batch operation of a primary fluidized-bed burner with in-vessel filters was successfully demonstrated utilizing operating procedures similar to those used in continuous operation. Continuous primary burner operation was concentrated on improving the solids transport systems associated with feeding and product removal.

Secondary burning of crushed fertile particles continued successfully. Evaluation of distributor plate designs was performed and shakedown of the temperature control system was completed.

Evaluation of the presence of whole fissile particles on the dissolution of crushed burned-back TRISO fissile particles indicated some detrimental effects, which will require further study. Four alloys were fabricated in corrosion coupons and installed in the 13-cm-diameter leacher for future inspection at selected intervals. A satisfactory ash feeding

system was developed for the dissolvers. The preliminary design of the evaporator/stripper for feed adjustment to solvent extraction was completed.

Preliminary studies were completed evaluating the effects of synthetic fission products and soluble neutron poisons on dissolution and feed adjustment. Problems were defined that will require further study.

Crushing

Fuel Element Crushing

Interim reports were written to relate the experimental results obtained from the primary, secondary, and tertiary crushers.

Each of these crushers is presently being fitted with a total enclosure in preparation for crushing tests using standard fuel elements and reject FSV fuel rods. In these tests, two half-length fuel elements will be loaded with reject rods and subsequently crushed in the primary, secondary, and tertiary crushers. The intent of these tests is to quantify the fissile and fertile particle breakage incidental to the crushing of standard fuel elements.

Full-Scale Crusher System

A full-scale integrated crusher system is to be built according to the configuration of Fig. 5-4. This system will be built from standard parts and is expected to provide the following advantages: (1) minimized total number of parts, and (2) remote maintainability.

For the most part, simplification will be provided via the Pitman assembly shown in Fig. 5-5. In this assembly the Pitman, toggle, and pushing block remain attached, thereby eliminating the need for a tension rod and spring. Attaching the pushing block to the top of the Pitman with a cable or bracket should enable the entire assembly to be removed from the frame as a single unit.

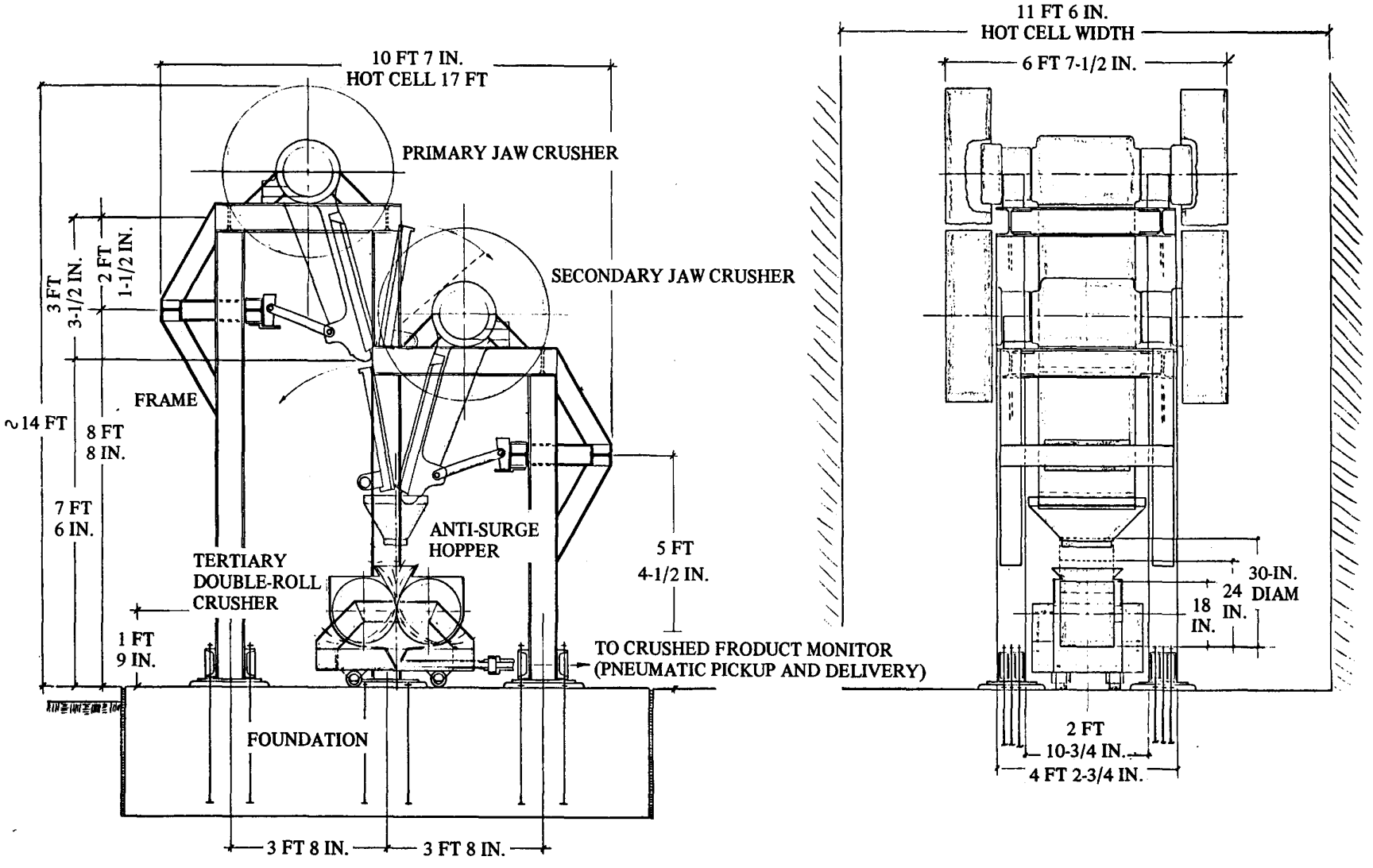

Fig. 5-4. UNIFRAME crusher system

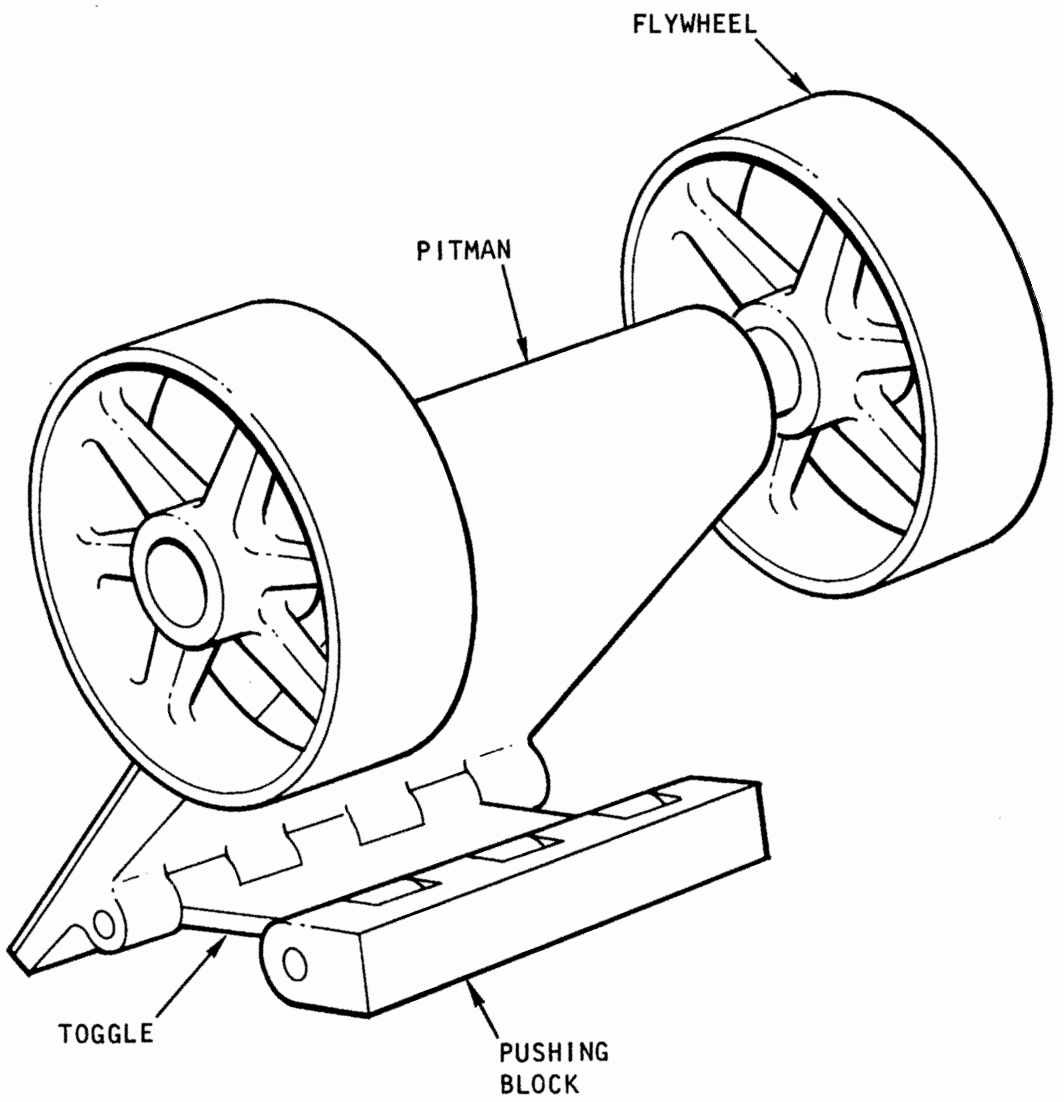

Fig. 5-5. Pitman assembly for UNIFRAME structure

The UNIFRAME concept provides the gravity flow between each crusher with an antisurge hopper located between the secondary and tertiary crushers.

Even though the three-stage crushing system will operate without recycle, a provision for recycle will be provided. The recycle system will, in fact, be part of a crushed product monitoring device, which is intended to take the full flow of the crushed product.

As shown in Fig. 5-6, the full flow of crushed product issued from the terminal crushing stage will be handled by the crushed product monitor. The monitor will separate that material which is of the correct size from the oversize material; the correct-size material will be pneumatically transported to the primary burner storage bin and the oversize material will be reduced to the correct size by an in-line pulverizer.

The in-line pulverizer will be sized to accept up to approximately 20 wt % of the total flow at any given tertiary crusher reduction ratio. Moreover, the pulverizer would be sized to accommodate the largest particle that could be issued from the secondary crusher.

For the case where the tertiary crusher has been adjusted to the point of providing the maximum reduction ratio and for quantities of oversize material greater than 20 wt %, operation of the recycle system would enable the entire crusher system to perform at its rated capacity.

Solids Handling

Pneumatic Transport Systems

Of the three pneumatic conveyance systems previously reported (see Quarterly Progress Report Gulf-GA-A12725), the "secondary burner product to leacher" system has been completely installed. This system will be evaluated in conjunction with secondary burner operations. The general configuration of the system is shown in Fig. 5-7.

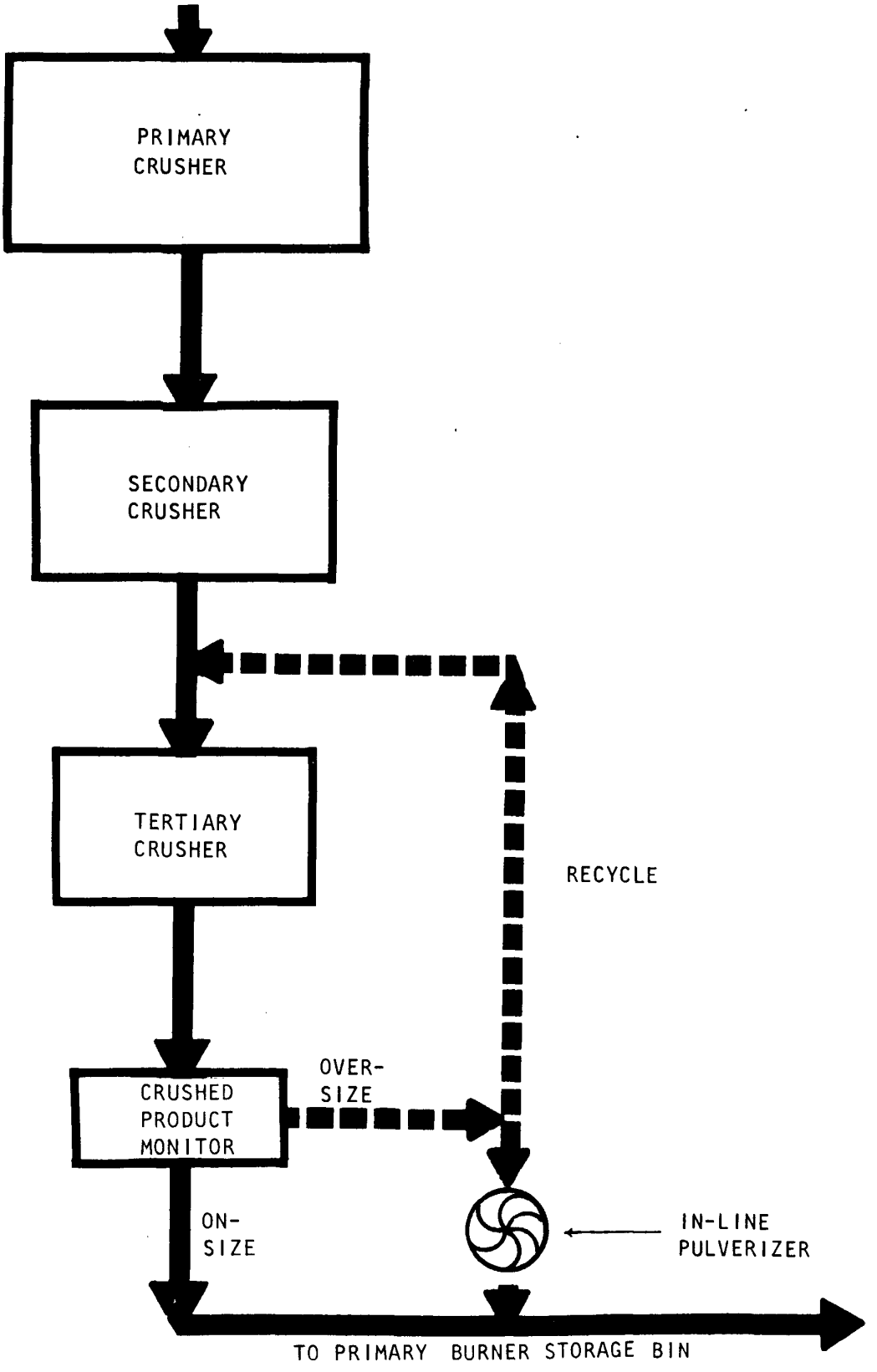

Fig. 5-6. Crushed product monitoring system

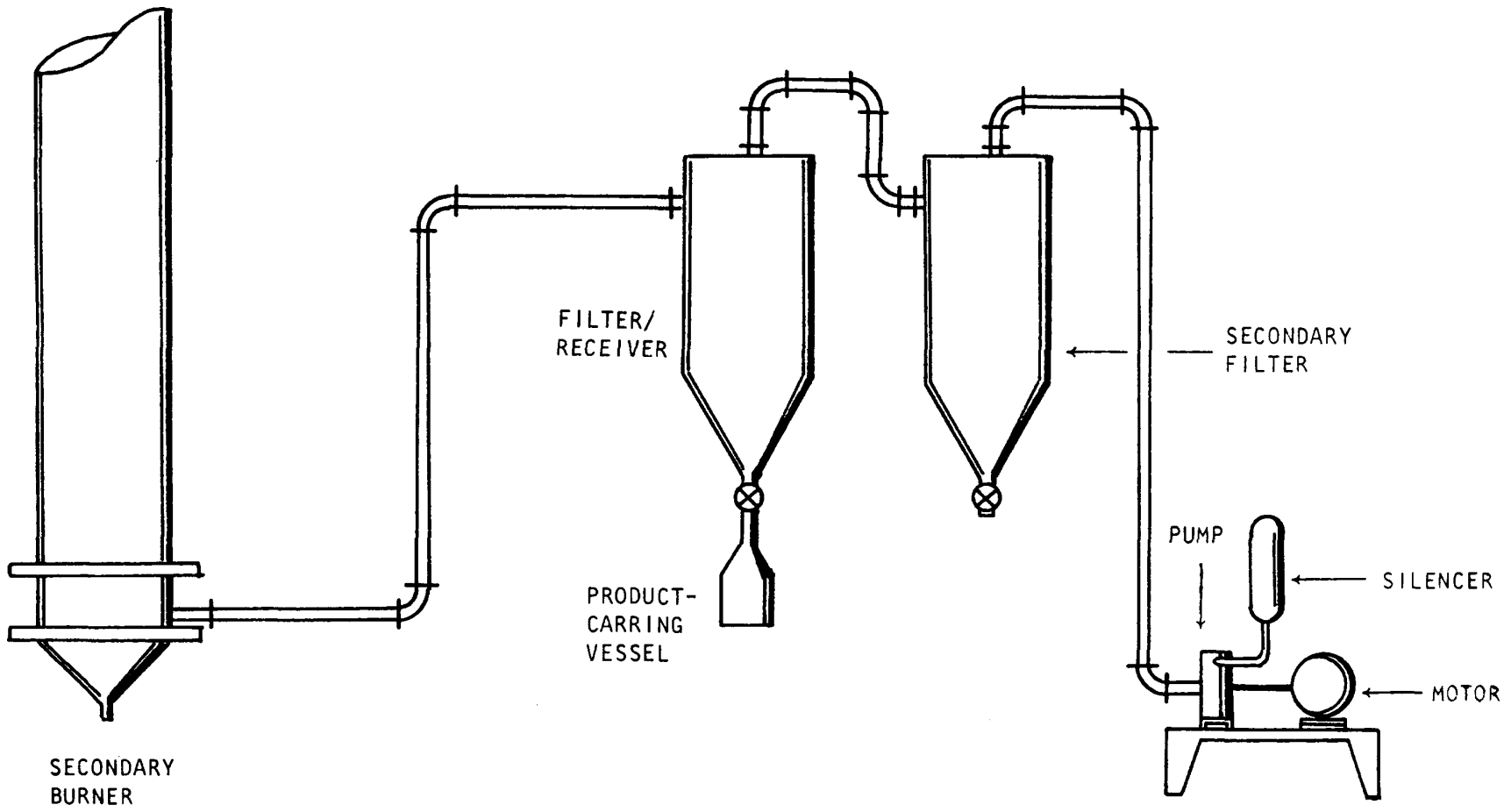

Fig. 5-7. Pneumatic conveyer (secondary burner product to leachers)

The pneumatic transport system is connected to the secondary fluidized-bed burner via the previously reported high-temperature bed removal system (see Quarterly Progress Report Gulf-GA-A12725).

Air Classification

Experiments are in progress to quantify the degree to which several feed and product streams of the head-end flowsheet can be separated into their respective components. The principal objectives are to learn the parametric relationships that exist between the solids feed rate, gas flow rate, and separation efficiency. The experimental apparatus that has been constructed to accomplish the task is shown in Fig. 5-8.

Fuel Particle Crushing

The particle crushing system previously reported (see Quarterly Progress Report Gulf-GA-A12818) is shown in Fig. 5-9, and the individual crusher is shown in Fig. 5-10.

Particle crushing experiments are aimed at obtaining suitable feed for the secondary fluidized-bed burner and as such are conducted and coordinated with burner experiments. Several roll pairs have been ordered, which are expected to provide a number of alternative roll gap dimensions.

Primary Fluidized-Bed Burner

During the past quarter, all the experimental work on primary fluidized-bed burners has been with 10-cm-diameter beds. Two batch runs and five semicontinuous runs were made during this period. A preliminary Design Criteria for the prototype primary burner was drafted.

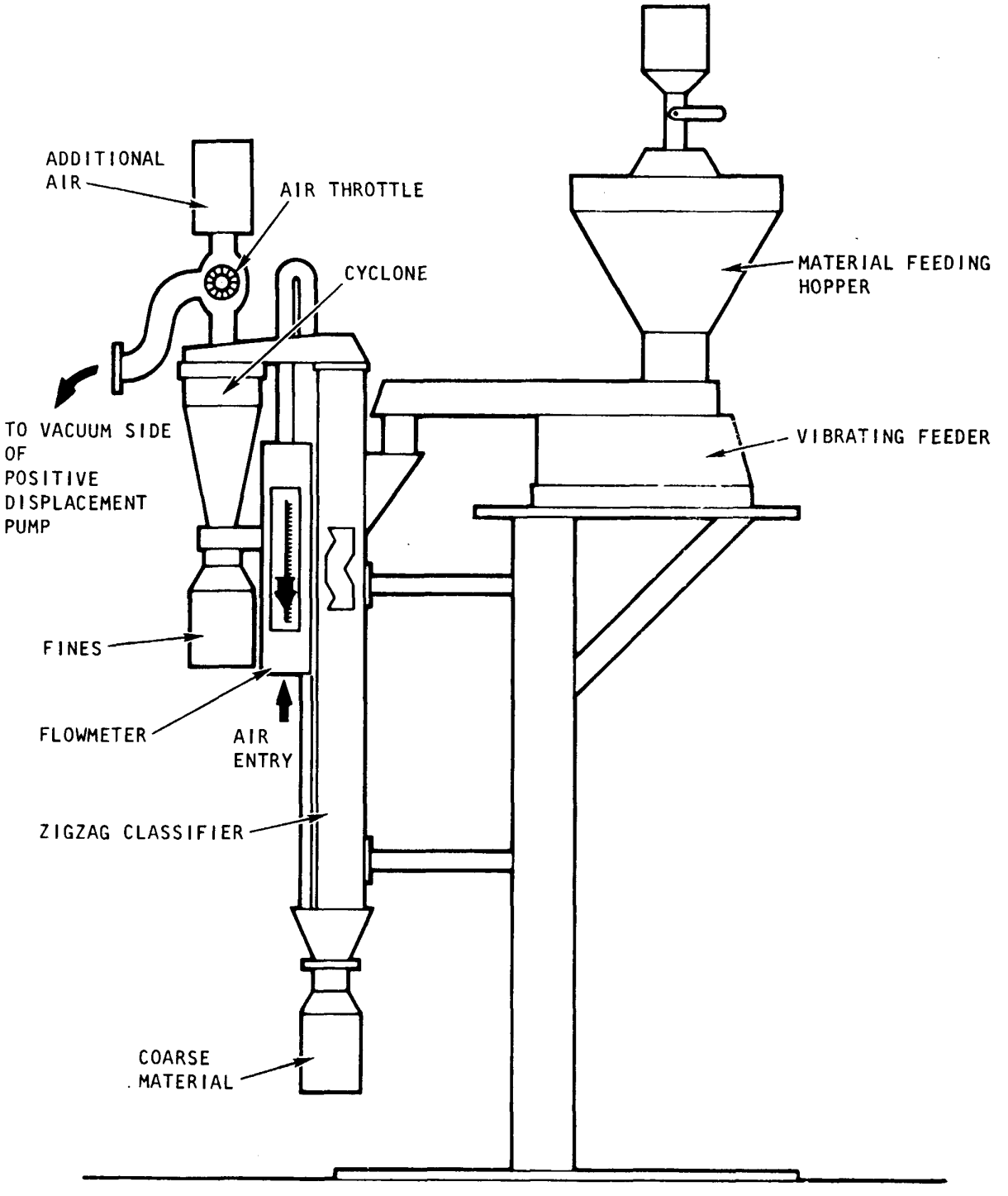

Fig. 5-8. Air classifier

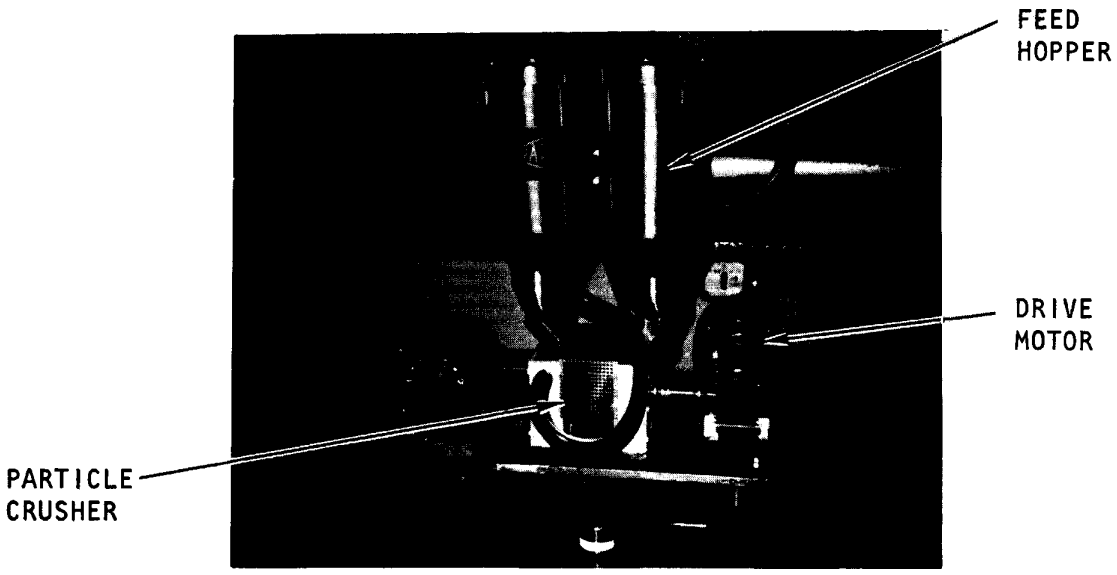

Fig. 5-9. Crusher mounting stand

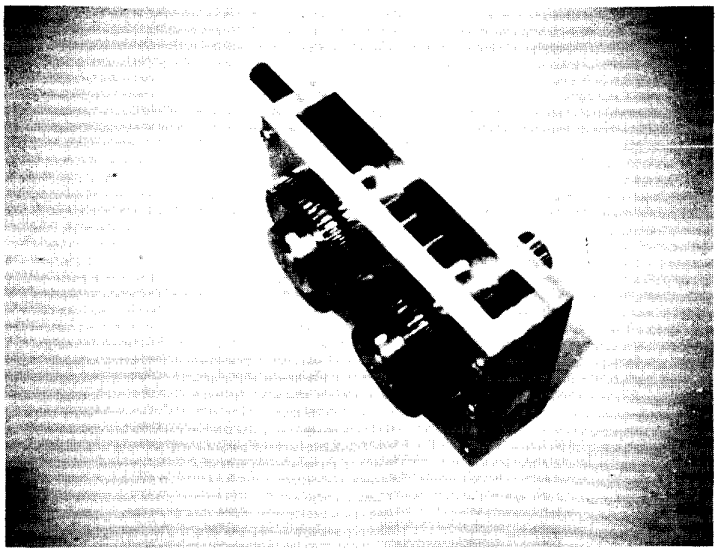

Fig. 5-10. Crusher

Batch Primary Burner

The batch primary burner concept is an attempt to simplify the equipment associated with disposing of elutriated fines. By using in-vessel filters to contain fines, the equipment associated with the primary burner [defined as burning the (crushed) fuel elements down to particles] would be simplified by eliminating the equipment presently used to handle fines. Conceptually the run would operate until the bed of particles was built to an arbitrary size, the flow rate would then be lowered to allow burning the fines, and the batch would be dumped. This would eliminate the need for a bed size control loop.

The initial test of this concept utilized a "whole bed" startup technique - feeding 5 kg of fresh feed to a hot burner tube (950°C). Two run attempts were made in the 10-cm secondary burner tube (Fig. 5-11) using the pneumatic feeder and a distributor plate (see Quarterly Progress Report Gulf-GA-A12515, Fig. 5-9). In both attempts the bed segregated during startup, with the static bed burning at the bottom of the burner. Hot spots formed, which resulted in the formation of agglomerates and failure of burner components. In the first attempt the tube was heated to 1000°C, the feed was added, and then N_2 flow was begun; in the second attempt the feed was added with 20 liters/min [~19 cm/sec (0.6 ft/sec) superficial velocity] of N_2 flowing through the reactor. It was concluded that whole-bed startup (defined as ignition of a whole bed of feed as obtained from the crushing chain) was not possible with the present burner configuration.

Runs 25 and 26 were made to evaluate batch operation without attempting whole-bed startup. Four kilograms of particles mixed with 400 g of coke was used as a startup bed for these two runs. The bed was added to the burner with 20 liters/min of N_2 flowing through the burner and the centerline temperature at ~900°C. Run 25 demonstrated that the burner could be operated successfully with in-bed filters containing the fines in the burner for a "batch" period of 9.6 kg of feed. The feed was added intermittently (with 2.25-sec pulses, ~370 g/pulse) using a pneumatic feeder. The run continued

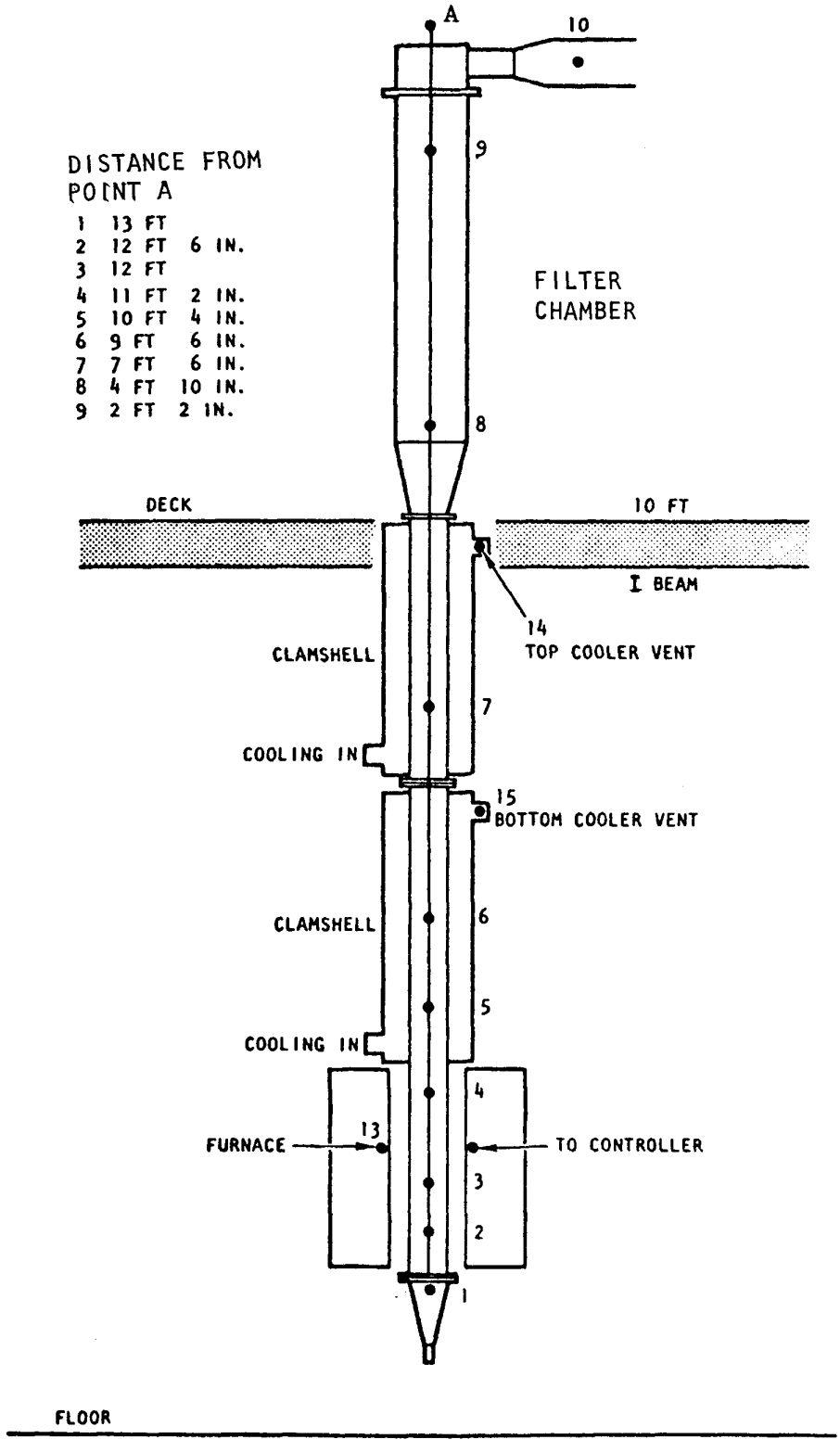

Fig. 5-11. 10-cm secondary burner

until an instability, presumably resulting from the fall-back of fines into the burner, extinguished combustion and caused rapid cooling of the burner (a "flame-out"), after which the run was terminated. The maximum burn rate, 51.4 g C/min, was maintained for 96 min. After 207 min the first fines fall-back occurred, which resulted in a small temperature excursion; after 288 min a second fall-back occurred, which extinguished the bed. During this run 9.6 kg of feed (of 15 kg added to the feed hopper) were burned. Approximately 6.2 kg of the material was burned at the maximum burn rate.

Table 5-5 summarizes Run 25, and Fig. 5-12 gives the final bed size distribution. The high burnable carbon content of the fluidized bed, coupled with the large weight fraction of fines (~7%) and a rapid change in filter ΔP at the end of the run, supports the contention that fines fall-back terminated the run. It appears that batch burning with containment of fines is a viable concept; however, with a 10-cm burner and two filters (39 in. x 3-in. diameter), the batch size apparently cannot exceed ~10 kg when burning at nominal rates of ~50 g C/min.

Run 26 was made to evaluate whether the fines contained by the in-vessel filters during batch operation could be burned at the end of a run. This run was made feeding 5.3 kg of material, burning until the temperature dropped, reducing the flow rate to allow the fines to reenter the combustion area, and burning the fines. The pneumatic feeder was used with 1-sec pulses (187 g/pulse); pulses were added periodically at a rate that kept the bed carbon content high enough to maintain combustion. The pulse rate was controlled by watching for changes in the CO and CO_2 concentrations. Startup was accomplished by heating the burner tube to 950°C and then adding a bed of particles and coke (4.0 kg of burned-back SiC coated fertiles mixed with 400 g of coke). For this run startup was slow because the resistance heater was damaged; one of the two elements had broken electrical leads. Table 5-6 summarizes the run conditions, and Fig. 5-13 is a plot of the final bed size analysis. Feed was added over the first 103 min of the run, during which time the bed and fines level built up (as the fines build up, the filter ΔP and the temperature of thermocouple No. 15 builds up). After the bed had

TABLE 5-5
SUMMARY OF RUN 25 - BATCH PRIMARY BURNER

Average burn rate	28.6 g C/min
Maximum burn rate	51.4 g C/min (80 liters/min O_2 at 6.5 psig)
Final bed	6.63 kg
	19.2% burnable carbon
	3.9% broken particles (% <550 μm after tray burning)
	d_{sv} = 289 μm
Startup bed	4-kg particles
	400 g coke

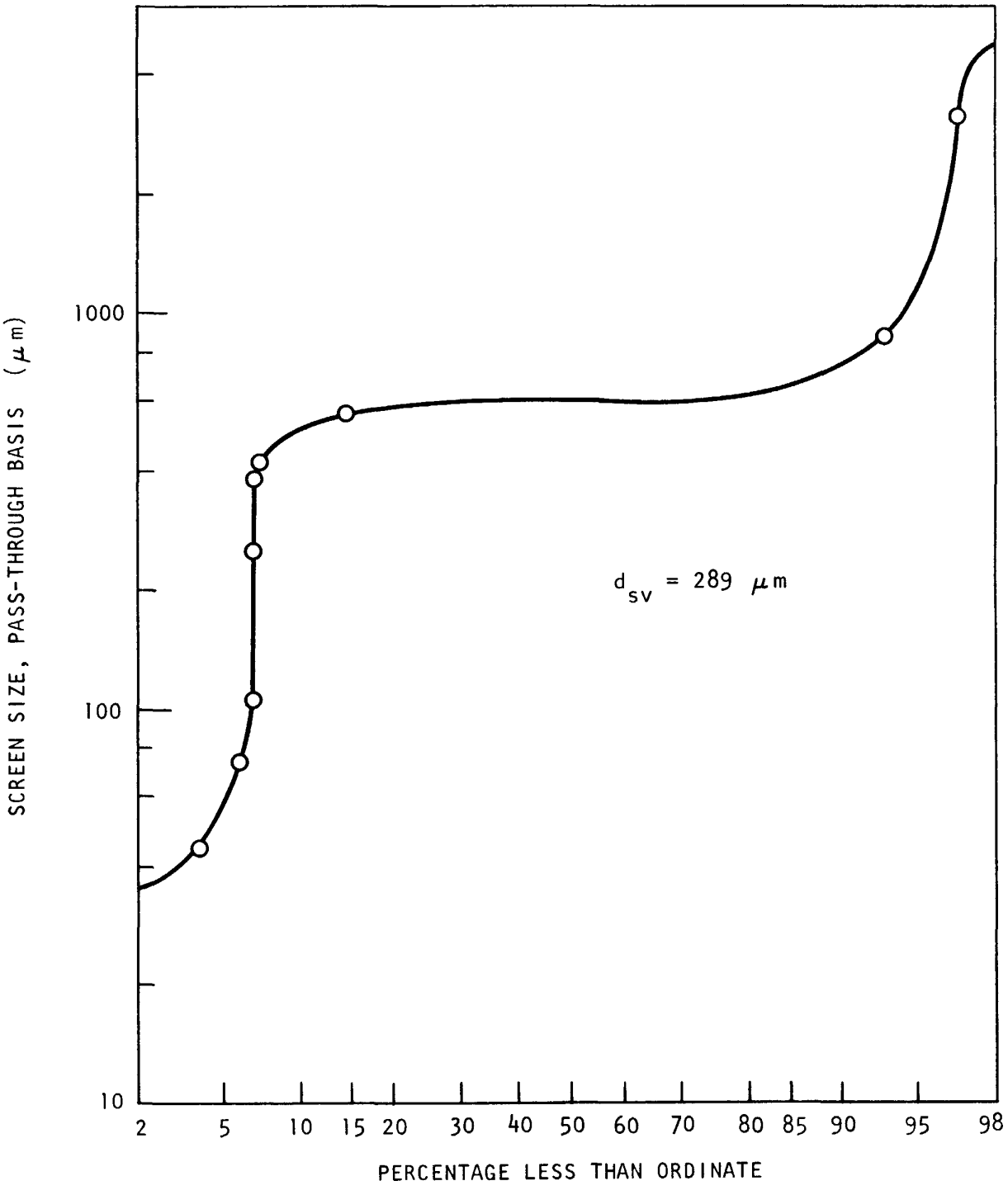

Fig. 5-12. Size distribution, final bed, run 25

TABLE 5-6
SUMMARY OF RUN 26 - BATCH PRIMARY BURNER

Average burn rate	22.4 g C/min
	178-min run time
Maximum burn rate	45.0 g C/min
Final bed	5.2 kg
	1.9% burnable carbon
	2.2% broken particles
	d_{sv} = 647 μm
Startup bed	4.4 kg
	(10:1 particles and coke)

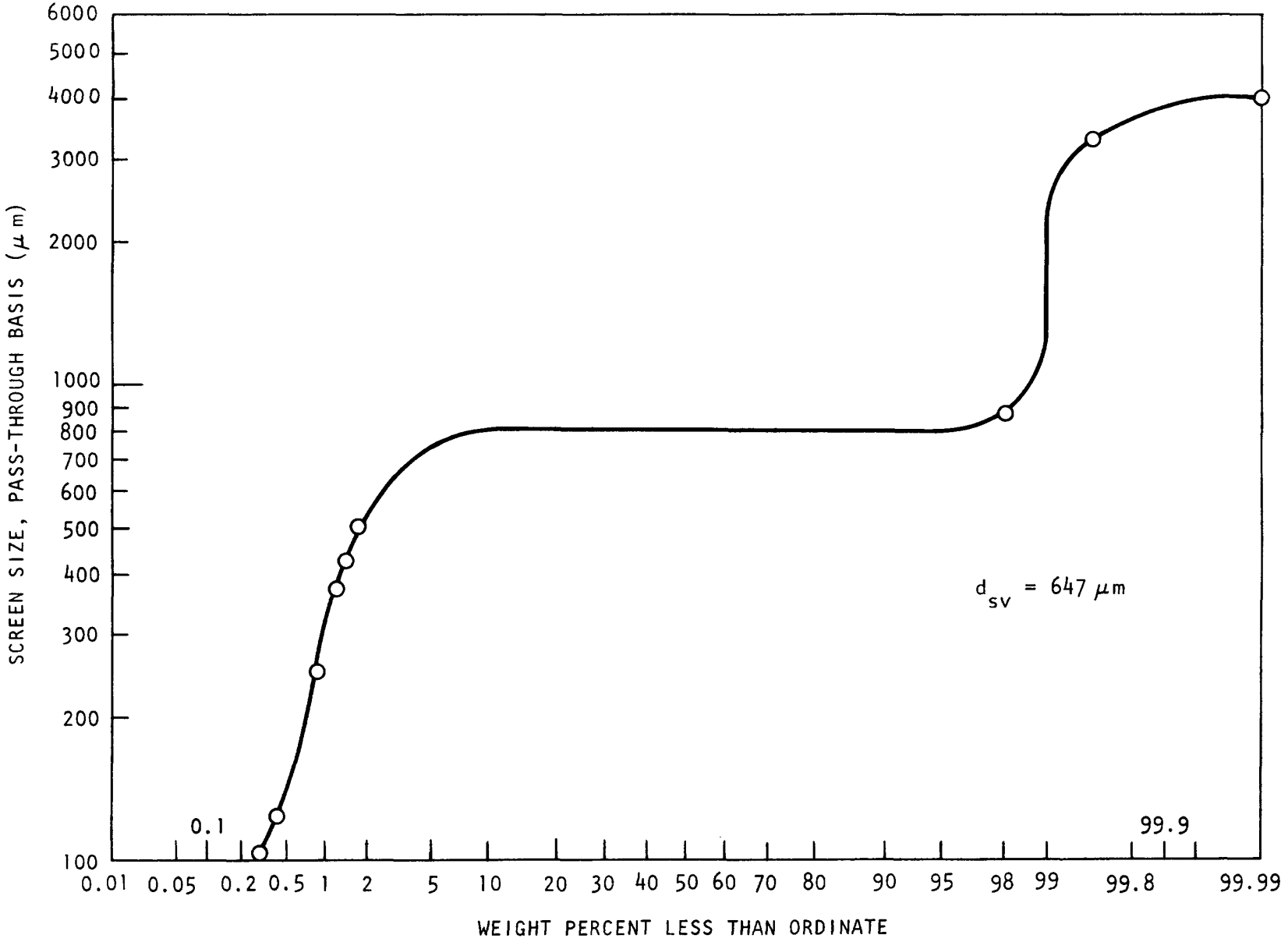

Fig. 5-13. Product size analysis of final bed, run 26

built up, feed addition was stopped, the resistance heater was turned on, and the gas flow was lowered to 30 liters/min (~20 g C/min).

The results of the run indicate that the primary burner can be operated with in-vessel filters to contain fines, and that these fines can be burned at the end of the batch by supplying external heating and adding gas at a low flow rate. Operating in this manner indicates that in-vessel fines containment in a batch-operated burner, followed by fines burnup, is a possible alternative to fines recycle or use of a separate fines burner. In Run 25 a maximum batch size of 9.5 kg in a 10-cm-diameter burner was given as a preliminary batch operating limit. In this run fines cleanup at the end of a batch was established although the average burn rate, including startup and fines cleanup, was low (22 g C/min). However, the operating procedures were not well established (this was a scoping study), and better performance can be expected.

Further data will be obtained at a future date to establish more typical operating conditions and to allow a better evaluation of this concept in comparison with other primary burner operating modes.

10-cm Semicontinuous Primary Burner

Five runs were made on the 10-cm primary burner during the past quarter. Runs 27, 28, and 29 were made utilizing the burner feed and product removal devices shown in previous Quarterly Progress Reports (Gulf-GA-A12818 and Gulf-GA-A12725), except that the auger feed system (see Gulf-GA-A12818, Fig. 5-3) was modified to incorporate 2-in.-diameter pipe tees and a 2-in.-i.d. bellows to provide better pickup of material by the bottom auger. During Run 27 the automatic temperature control loop was operated for 5 hr with a 950°C set point for the bed temperature control thermocouple.

Runs 27, 28, and 29 were used to evaluate the auger feed system during actual operation and to obtain information on the rate of fines elutriation and general burner performance. Based on data obtained from these three

runs, it was concluded that the hopper-auger system did not provide consistent delivery rates for fresh feed mixed with recycled elutriated fines.

The auger system had been developed around fresh feed, which has a surface-to-volume average particle size (d_{sv}) of 363 μm and a size variation [the screen size that 80% of the material will pass through divided by the screen size that the smallest 20% of the material will pass through ($d_{80\%}/d_{20\%}$)] of 6.4. As material (mixed fresh feed and elutriated fines) was augered from the hopper, variations were observed in both the size distribution of the product and the delivery rate. Visual observation of the hopper indicated "rat-hole" flow that is characterized by material segregation and bridging, both of which contribute to erratic delivery. In these tests the size distribution of fresh feed mixed with elutriated fines had a d_{sv} between 92 and 123 μm and a size variation ($d_{80\%}/d_{20\%}$) between 23 and 32; at 30 rpm the auger discharge rate varied between 30 and 110 g/min.

Based on earlier bench tests with hopper-auger systems, a mass-flow hopper was installed to help solve the segregation and bridging problems and to provide constant flow. Also, a larger auger (tapered over the hopper-exit auger-pickup length) was used to provide higher delivery (feed) rates. The auger was changed to a 3.2-cm (1-1/4-in.) diameter auger, 1.27-cm (0.5-in.) diameter core in a 5-cm (2-in.) pipe (Fig. 5-14). The upper auger is 91 cm (36 in.) long and is supported by bearings at both ends; the bottom auger is 34 cm (13-1/2 in.) long and is suspended at one end by a bearing. The new metal bellows, 5.3-cm stroke, has a metal sleeve similar to the old one and has a similar spring constant (29 lb/in. compared to 21 lb/in.). Using a flexible bellows and bearings on the augers helps to maintain alignment of the auger in the housings and to minimize application of torque to the burner wall during thermal expansion (which would bend the hot burner wall); the burner (304 SS) expands about 2.5 cm (1 in.) and the bellows expands 1.7 cm (5/8 in.), maintaining alignment of the bottom auger within 1.6° during thermal expansion (see Fig. 5-14). Figure 5-15 shows the delivery rate of fresh feed (-4.8 mm mixed 4:1 with SiC coated fertile particles) as a function of the auger rotation speed for both the new auger

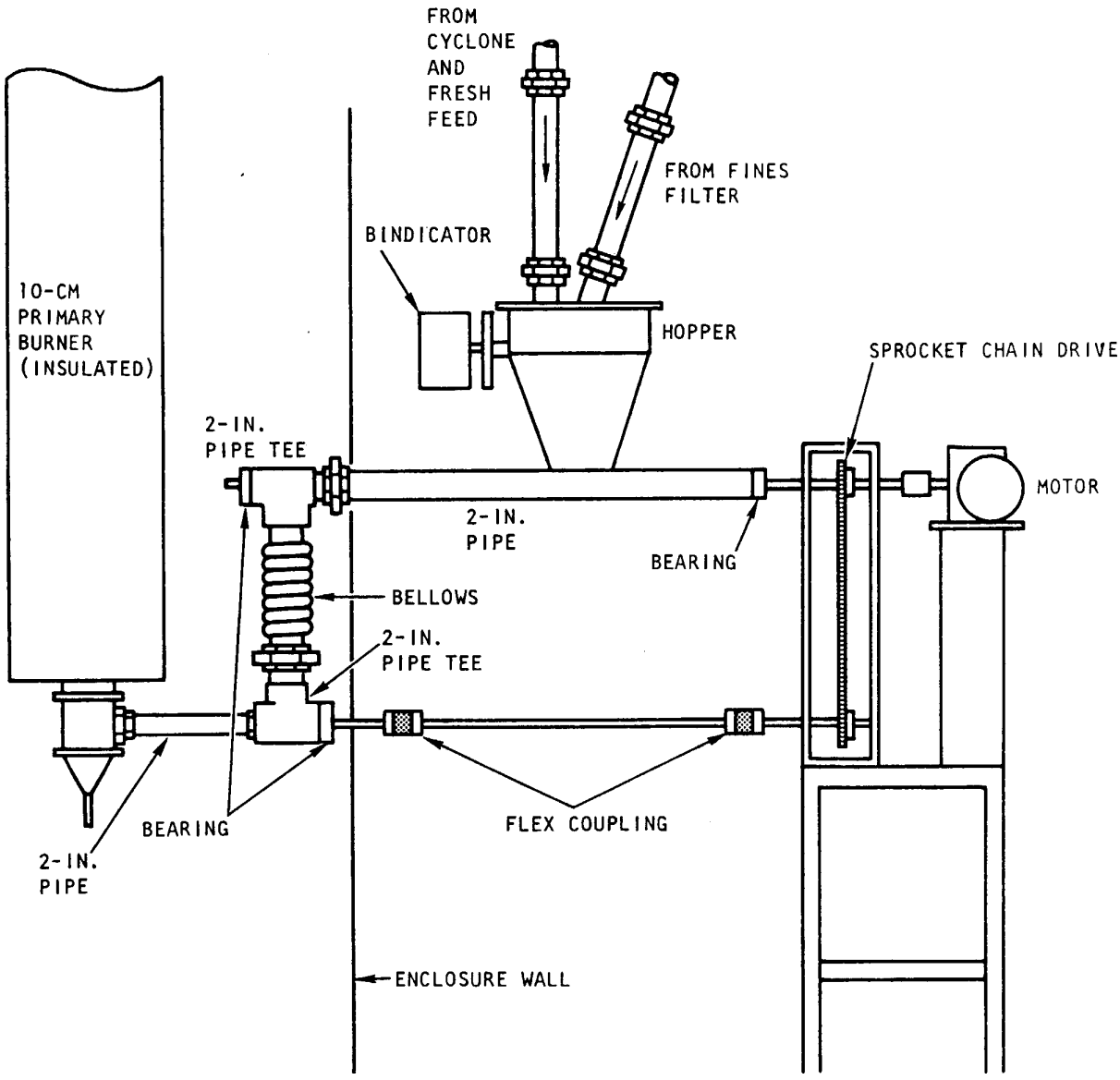

Fig. 5-14. 10-cm primary burner bottom feed system

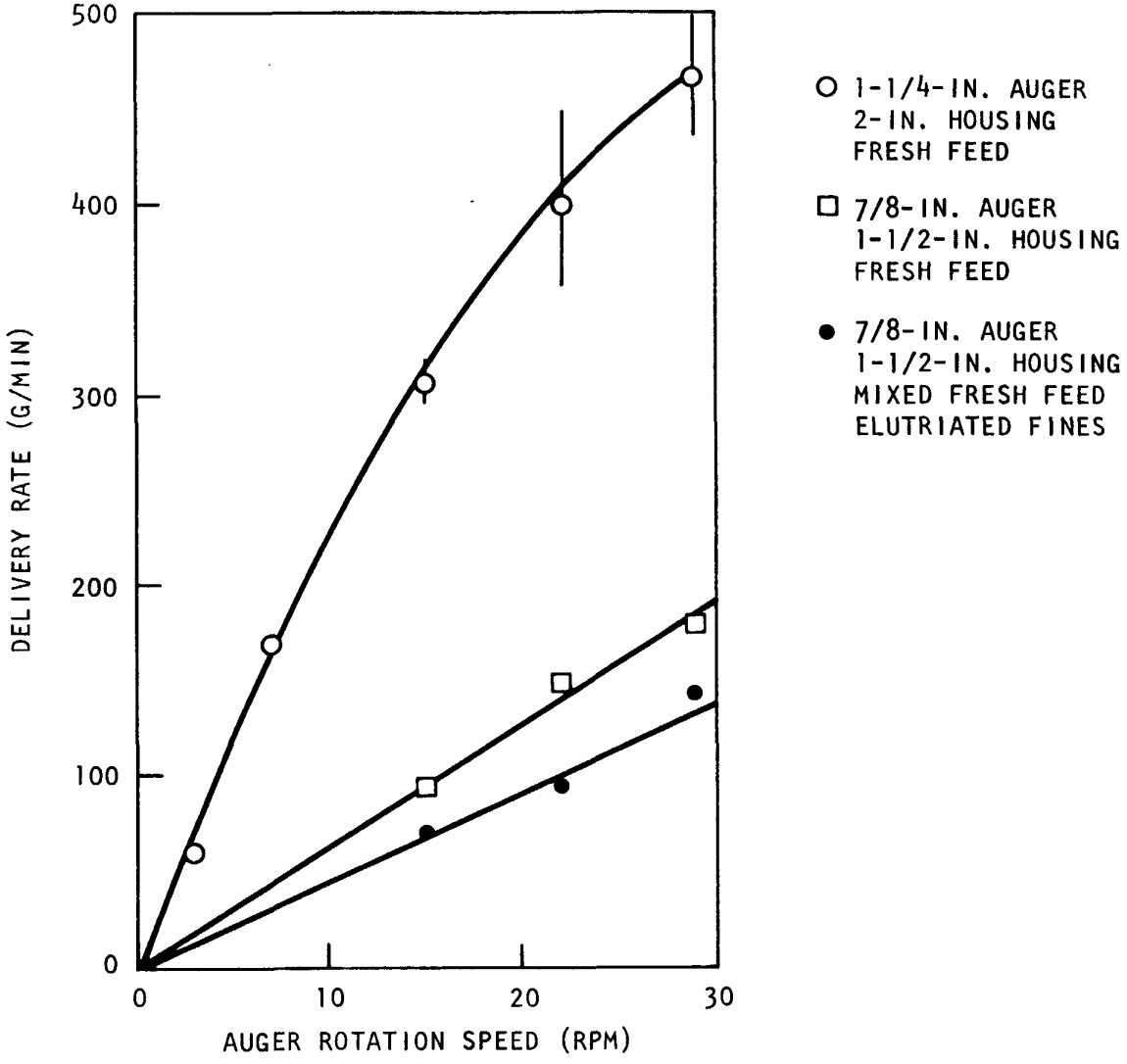

Fig. 5-15. Bottom feed system delivery rate versus auger speed - mass flow hopper

(1-1/4-in. auger in a 2-in. housing) and the old auger (7/8-in. auger in a 1-1/2 in. housing) using the mass-flow hopper shown in Fig. 5-16.

The present bottom feed system confirms the results of earlier bench auger tests:

1. Use of a mass-flow hopper to obtain a constant discharge density.

2. Use of a tapered auger pickup (in-flow region) to maintain active flow from the entire hopper discharge region. This further helps prevent any tendency for "rat-holing" in the hopper and promotes stable hopper discharge rates.

3. Use of a longer pitch (larger helix angle) to increase the volumetric flow per revolution and decrease the flight pressure which compresses the material.

4. Bigger auger-housing clearances to decrease material degradation and decrease variations in discharge rates.

Earlier feed systems were characterized by erratic discharge rates (Fig. 5-17) and binding of the auger (possibly caused by compaction of material in the auger barrel (see Quarterly Progress Report Gulf-GA-A12422). Auger binding has not been a problem with the augers having a higher pitch angle and problems with erratic delivery rates have apparently been solved by the mass-flow hopper. Table 5-7 characterizes the present and previous auger feed systems. The present mass-flow hopper, tapered-end auger provides consistent delivery rates equal to the swept volume times the bulk density of the feed (see Table 5-7). The lower delivery rate of fresh feed mixed with fines can be characterized by the drop in bulk density; the delivered weight per swept volume for fresh feed is ~1.0 g/cm^3 (bulk density = 1.1 g/cm^3); for mixed fresh feed and fines (Fig. 5-15) it is 0.87 g/cm^3.

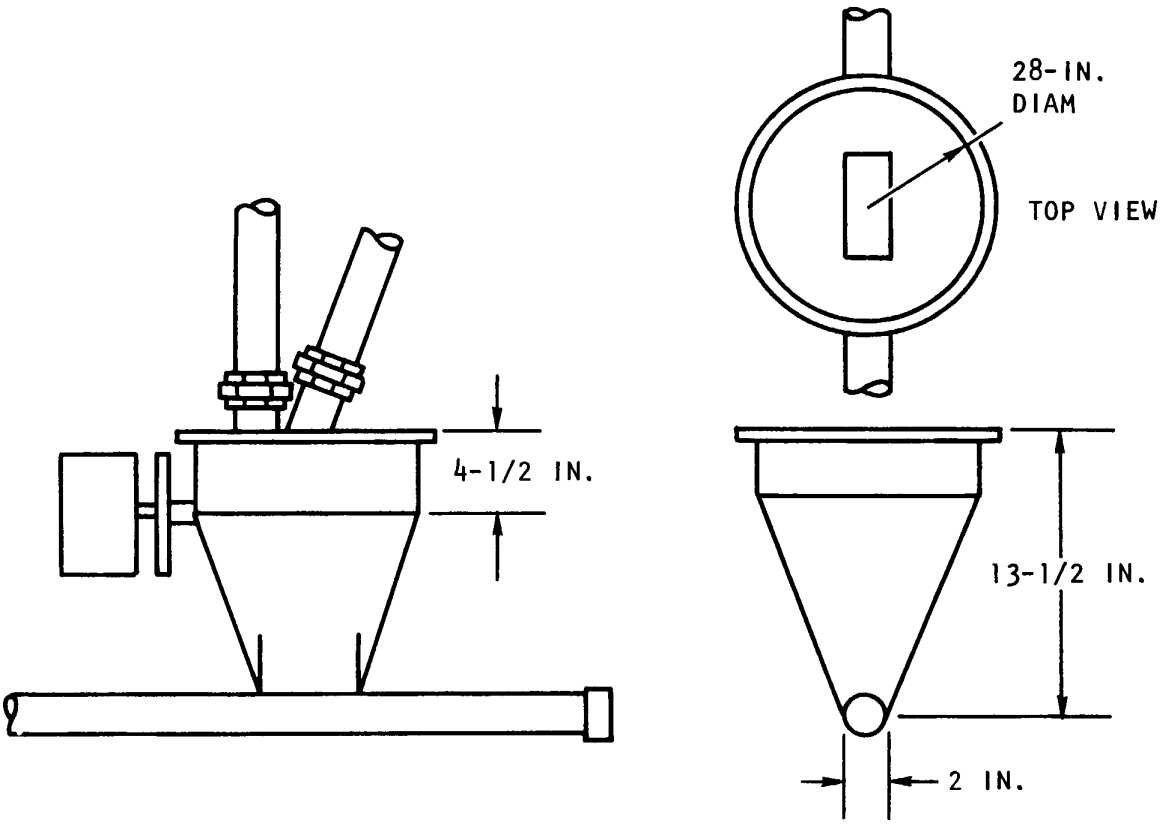

Fig. 5-16. Bottom feed hopper

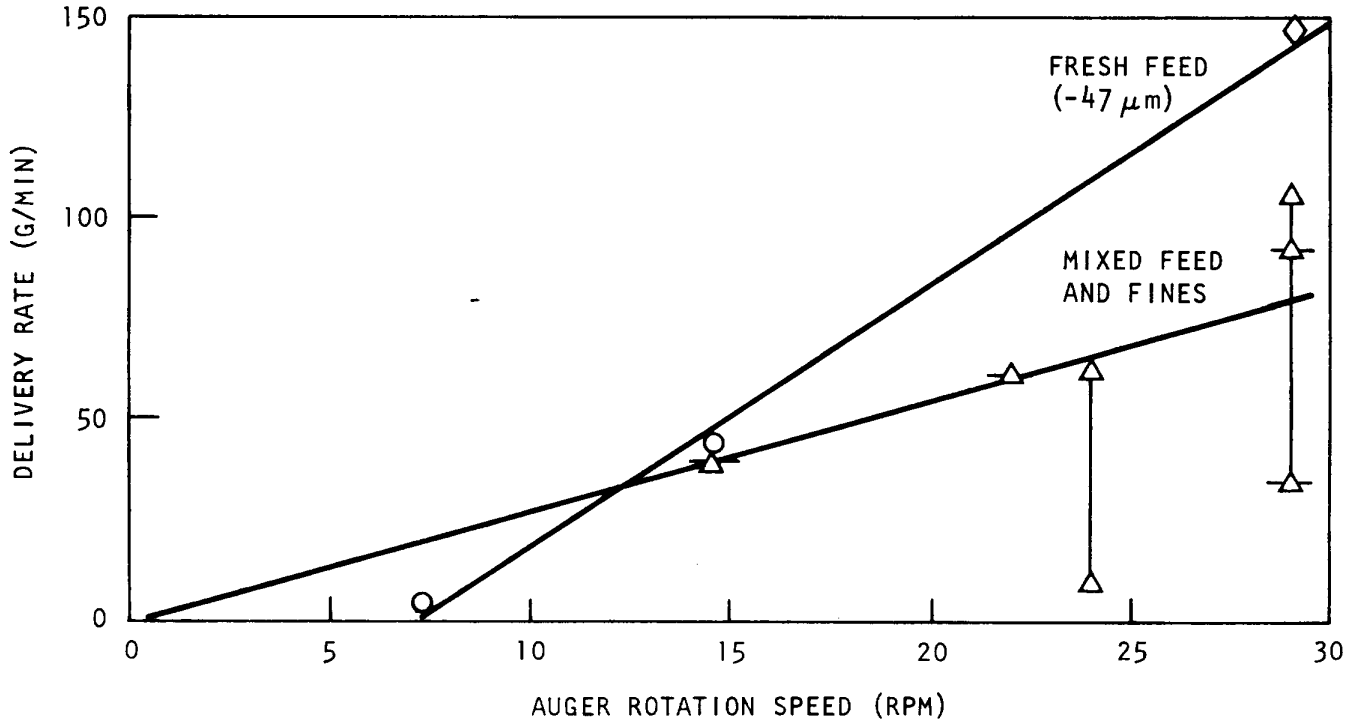

Fig. 5-17. 10-cm primary burner auger performance, installed, 7/8-in. core auger in a 1-1/4 in. diameter barrel, rectangular hopper

TABLE 5-7
AUGER FEED SYSTEMS

Identification	Auger Diam (in.)	Core Diam (in.)	Helix Angle (degrees)	Pitch (in.)	V_{swept} (in^3/rev)	$\bar{W}_{delivery}$, Fresh Feed, 29 rpm (g/rev)	$\bar{W}/V^{(a)}$ (g/cm^3)	Remarks
Quarterly Progress Report Gulf-GA-A12725 August 1973: rectangular hopper, ship's auger	1.0	-	-	-	-	8.0	-	Erratic feed binding
Quarterly Progress Report Gulf-GA-A12818 (Fig. 5-3), November 1973: tapered end, rectangular hopper	0.87	0.5	21.0	0.86	0.34	5.1	0.91	Erratic delivery of mixed feed
	0.87	0.5	21.0	0.86	0.34	6.2	1.11	Consistent flow
	1.25	0.5	18.0	0.95	0.98	16.0	1.00	Consistent flow
Quarterly Progress Report Gulf-GA-A12422 November 1973: old 20-cm burner auger, no taper, rectangular hopper	1.97	1.12	13.0	1.1	2.37	4.5	0.16	Erratic feed binding

(a) $\rho_{taper} \approx 1.2$ g/cm^3, $\rho_{bulk} \approx 1.1$ g/cm^3.

Runs 30 and 31 were made to obtain further operating data and to test equipment modifications. Run 30 was made with a 7.24-kg bed. The final bed was high in carbon. This is explained by the previously observed flotation of large pieces of graphite on the top of the bed (see Quarterly Progress Report Gulf-GA-A12599, Table 5-5), and the rapid graphite-oxygen reaction. With the large bed, graphite in the top of the bed is above the oxygen zone and over the course of the run (6 hr), the carbon content of the bed became higher than that of the initial bed (67% compared to 90%). During Run 31 gas samples taken 10 cm above the bottom spool piece adapter (feed system entry adapter, Fig. 5-14) were mixed with the filter off-gas samples; these results indicate nearly complete oxygen utilization has taken place at this point. From Runs 30 and 31 it can be concluded that there is no advantage in operating a tall bed, except for heat transfer caused by axial mixing of the slugging bed. The present feed port injects fines halfway between the oxygen inlet and the position where the oxygen is completely utilized. The fines rate can probably be lowered by use of a second, higher oxygen port, which will be tested at a later date. During Run 31 the overall heat transfer coefficients were calculated as 13 Btu/hr-ft^2-°F at the top and 10 Btu/hr-ft^2-°F (±2 Btu/hr-ft^2-°F) with 92% closure on the heat balance (Fig. 5-18).

After Run 31 it was determined that the 10-cm burner must be rebuilt because a crack in the bottom-flange/burner-wall weld created a leak. Samples from the old tube (1/16 in. thick, 304 SS) have been taken for metallographic interpretation. (This tube had been operated for ~1000 hr with about 200 thermal cycles.) A new burner is being fabricated from Schedule 40 Hastelloy X.

The rotary product valve (see Quarterly Progress Report Gulf-GA-A12715, Fig. 5-11) is being modified to allow higher throughputs at the same rotation speed by increasing the rotor diameter to allow more rapid decreases in bed size. The capacity is being increased rather than the speed of rotation to help maintain low levels of particle damage. The minimum constriction (top opening) is being enlarged to 1 cm to allow use with larger sized feed; the product removal device

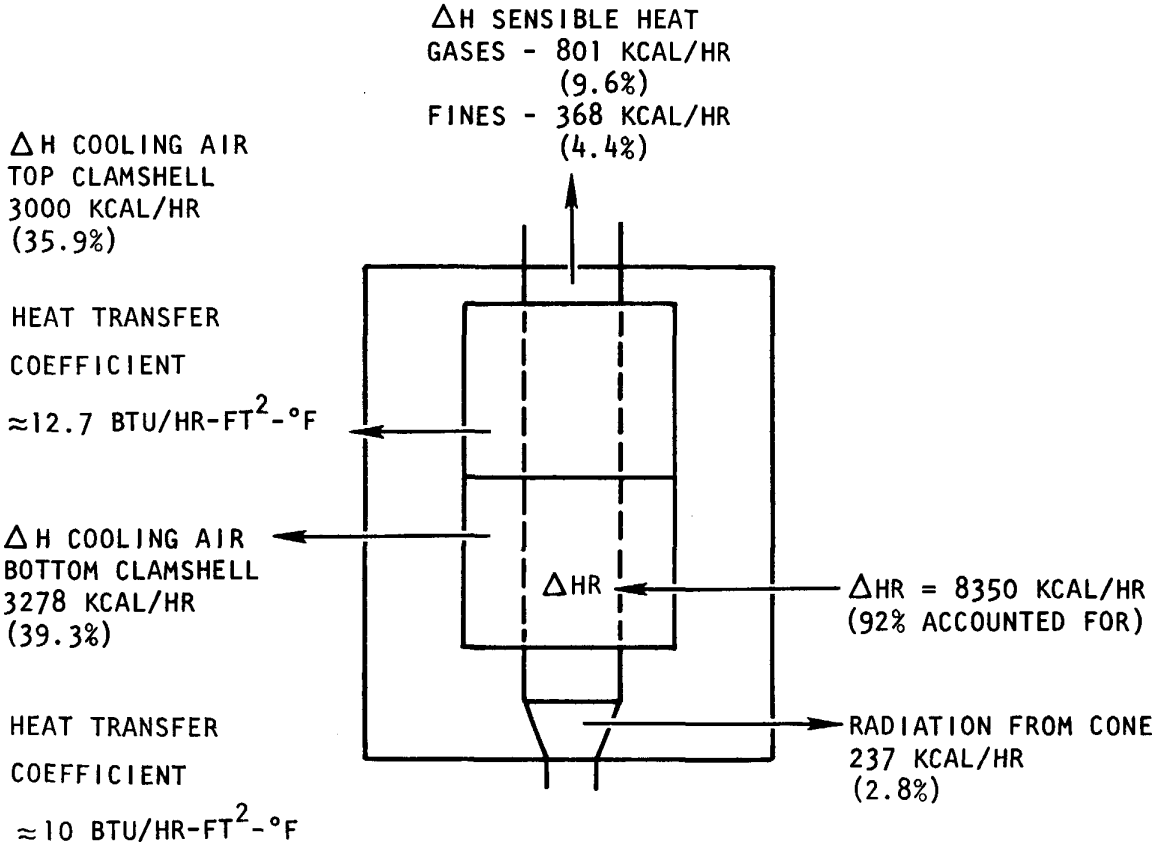

CLAMSHELL (TOTAL)	- 5.5-IN. OD X 36 IN. (AREA = 0.0777 FT^2)
CONE	- 4-IN. OD X 4-IN.
SPOOL	- 4-IN. OD X 4-IN.

Fig. 5-18. Heat balance, 10-cm primary burner

must be able to accommodate any size piece of graphite particle found in the feed or bridging will result and the bed level cannot be controlled.

Table 5-8 summarizes operating data on runs made when fines elutriation rates were measured. Table 5-9 gives the correlations for fines elutriation for both fines recycle with the present burner configuration (Quarterly Progress Report Gulf-GA-A12715, Fig. 5-13) and no fines recycle (Quarterly Progress Report Gulf-GA-A12599, Table 5-3). Attempts were made to correlate fines elutriation data with all other measured (or calculated) process data, including the static and maximum slugging bed heights, bed temperature, and superficial velocity in the bed. The two correlations shown in Table 5-9 are the only statistically significant correlations. Data taken during the runs, as well as data from Table 5-8, were used to develop the correlation for fines recycle.

Secondary Fluidized-Bed Burner

Crushed Fertile Particle Combustion

Nine batches of FSV-type TRISO fertile particles were crushed in a double-roll crusher and oxidized in the 10-cm secondary burner (see Fig. 5-11). Data concerning these burn runs are given in Tables 5-10 through 5-12.

The operating method for these runs is as follows:

1. Crush entire batch of fertile particles to expose the inner coatings and the ThC_2 kernel.

2. Load the batch into the burner tube through a gravity-pneumatic feeder.

3. Allow fluidized batch (fluidized on a distributor plate with N_2) to heat to >500°C using the resistance heater.

TABLE 5-8
SUMMARY OF CONTINUOUS 10-CM PRIMARY BURNER RUNS 18 TO 31

Run No.	Average Burn Rate (g C/min)	Bed Temperature[a] (°C)	Fluidizing Gas [SLPM (% O_2)]	Superficial Velocity, Bed (cm/sec)	Superficial Velocity, Top of Bed[b] (cm/sec)	Bed Size (kg)	Bed Height[c]		Fines Elutriation Rate (g C/min)	Off-Gas Composition ($\%O_2$, $\%CO_2$, %CO)	Final Bed	
							Max. (cm)	Min. (cm)			% Carbon	d_{sv} (μm)
18	32	1015	70 (87)	64	45	5.5	93	61	40	0, 83, 4.5	6.3	600
19	38	995	78 (88)	78	65	5.9	117	77	81	0, 80, 8	10.9	576
20	52	975	97 (91)	85	94	6.5	134	90	256	0, 82, 8.2	23.2	655
21	24	1020	70 (88)	64	52	5.4	93	61	112	0.7, 83, 1.2	0.5	606
22	40	1010	88 (90)	80	64	6.0	119	78	48	0, 88, 1.5	3.9	--
27	28	950	58 (82)	54	40	3.3	55	29	36	0, 71, 8	17.1	532
28	20	985	53 (80)	48	39	3.5	53	31	36	0, 69, 7	11.9	477
30	26	1000	75 (58)	66	41	7.2	134	96	48	0, 53, 10	62.7[d]	440
31	22	915	63 (58)	53	41	4.2	69	43	38	0.5, 48, 16	2.0	674

[a] At 15 cm from cone apex.

[b] At 119 cm from cone apex; total 10-cm burner length = 171 cm.

[c] Based on slugging bed calculations.

[d] Product 4%.

TABLE 5-9
FINES ELUTRIATION CORRELATIONS[a]
(Significant at 95% Confidence Level)

No recycle

$$f = 89.2 - 0.1064\ (T_1) + 0.6112\ (V_5) \pm 2.4$$

Range of V_5 = 38 to 58 cm/sec

Range of f = 9 to 25 g/min

Recycle

$$f = 3.368\ (V_5) - 100.4 \pm 28.3$$

Range of V_5 = 34 to 94 cm/sec

Range of f = 14 to 256 g/min

(a) f = fines carryover rate (g/min).
T_1 = thermocouple reading 15 cm from cone base (°C).
V_5 = superficial velocity 119 cm from cone base (cm/sec).

TABLE 5-10
CRUSHED FEED ANALYSIS

Run No.	Initial Bed Weight (kg)	Uncrushed Feed d_{sv} (μm)	Roll Crusher Gap (in.)	Crushed Feed d_{sv} (μm)	ThC_2 (%)	Carbon (%)	SiC and Unbroken Particles (%)	Crushed Feed Bulk Density (g/cm^3)	Crushed Feed Tap Density (g/cm^3)	Crushed Feed Angle of Repose (degrees)
26	10	642	0.019	227	69.5	17.3	13.2	2.02	2.43	31
27	12	642	0.019	227	69.5	17.3	13.2	2.02	2.43	31
29	13	622	0.020	222	61.0	17.9	21.1	2.00	2.30	--
30	14	607	0.021	259	62.0	16.6	21.4	2.46	3.01	--
31	15	607	0.022	259	62.0	16.6	21.4	2.46	3.01	--
32	15	569	0.023	291	52.4	21.6	26.0	1.90	2.20	--
33	17	569	0.024	291	52.4	21.6	26.0	1.90	2.20	--
34	18.5	569	0.017	111	52.3	20.6	27.1	--	--	40
35	20	569	0.019	--	52.3	20.6	27.1	--	--	--

TABLE 5-11
SECONDARY BURNER COMBUSTION CHARACTERISTICS

Run No.	Ignition Temperature (°C)	Max. Filter $\Delta P/A$ (in. H_2O/cm^2)	Average Burn Rate (g/min)	Peak Burn Rate (g/min)	Burn Rate at Shutdown (g/min)
26	650	0.0020	21	33	0.2
27	625	0.0008	14	26	0.5
29	550	0.0020	26	41	0.2
30	500	0.0012	21	36	1.1
31	550	0.0012	23	48	0.2
32	500	0.0025	23	43	1.5
33	600	0.0055	28	49	1.0
34	500	0.0114	22	42	0.8
35	550	0.0085	31	40	0.7

TABLE 5-12
SECONDARY BURNER PRODUCT CHARACTERISTICS AND ANALYSIS

Run No.	Product Weight (kg)	Product d_{sv} (μm)	ThO_2 (%)	Carbon (%)	SiC and Unbroken Particles (%)	Product Bulk Density (g/cm^3)	Product Tap Density (g/cm^3)	Product Angle of Repose (Degrees)
26	8,482	56	84.0	0.7	15.3	2.92	3.22	40
27	10,100	53	83.2	0.7	16.1	2.80	3.20	40
29	11,009	59	74.2	0.8	25.0	--	--	--
30	11,722	56	76.7	0.5	22.8	2.46	3.01	--
31	12,356	51	75.7	0.3	24.0	--	--	--
32	12,386	48	68.7	0.4	30.9	2.4	2.8	--
33	13,655	49	65.6	0.3	34.1	--	--	--
34	14,636	31	75.4	0.1	24.5	2.5	2.9	--
35	16,362	45	76.1	0.7	23.2	--	--	--

4. Introduce O_2 in addition to N_2 to cause combustion. Increase O_2 gradually until the fluidized bed reaches the control temperature (900°C).

5. Begin air cooling through annular jackets above the resistance heater; shut heater off.

6. When the carbon in the bed begins to be depleted (as evidenced by a decline in combustion products in the off-gas), reduce superficial velocity (and hence burn rate) to allow fine carbon particles to descend into the bed from the filter chamber.

7. After the burn rate falls to a predetermined value, stop combustion by fluidizing with N_2 only.

8. Open product removal valve until the bed ΔP-cell indicates no further reduction in bed differential pressure. This terminates the run.

During the entire run, the off-gas filters (located directly above the bed) are periodically reverse jet blown-back by recirculated off-gas. This reduces the fines buildup on the filters and prevents excessive pressure drop through the filters. The maximum filter ΔP/A reported in Table 5-11 is essentially the steady-state value that is attained in the early stages of burning and is reduced only during the end of the run when carbon fines are being removed via combustion.

Filters presently used are 1/8-in.-thick, 3-in.-diameter, 36-in.-long sintered stainless steel cylinders with a 5-μm mean pore size. Two are installed, yielding a total area of 4378 cm^2.

Distributor Plate Evaluation

Several different distributor plate designs have been tried. The various distributor plates were designed according to the following criteria:

$$\text{Minimum plate } \Delta P = \text{maximum } (0.1 \times \text{bed } \Delta P,\ 35 \text{ cm } H_2O,\ 100\ \Delta P \text{ of expansion into vessel}),$$

which was recommended in Ref. 5-10.

The first design was a flat, 1/4-in.-thick stainless steel plate with 21 holes, each 1/16 in. in diameter. This design gave good fluidization properties with the normal >10 kg bed sizes, but would not fluidize the bed when it became shallow [as during product removal (see Fig. 5-19)].

Davidson and Harrison (Ref. 5-11) presented a method for calculating jet penetration in fluidized beds. Given the fluid density and velocity through the orifices, this method yields a ratio of jet penetration depth to orifice diameter.

For this first plate design, a jet penetration depth of 10 cm (2260 g of product) at 20 liters/min is predicted, which is quite close to the actual amount noted (2174 g). Thus, the reason the entire bed was not removed is that it defluidized after being reduced to the depth where the jets would completely penetrate the bed.

To reduce this "heel" of product, a distributor plate made of stainless steel wire mesh laminate was tried. This plate buckled during burning, presumably due to thermally induced stresses, and was thus evaluated as unsuitable.

The third design, which had 95 drilled holes each 1/32 in. in diameter, significantly reduced the heel to $\sim$1.0 kg. This design was used for all subsequent runs and gave approximately the same weight of heel regardless of the total product weight.

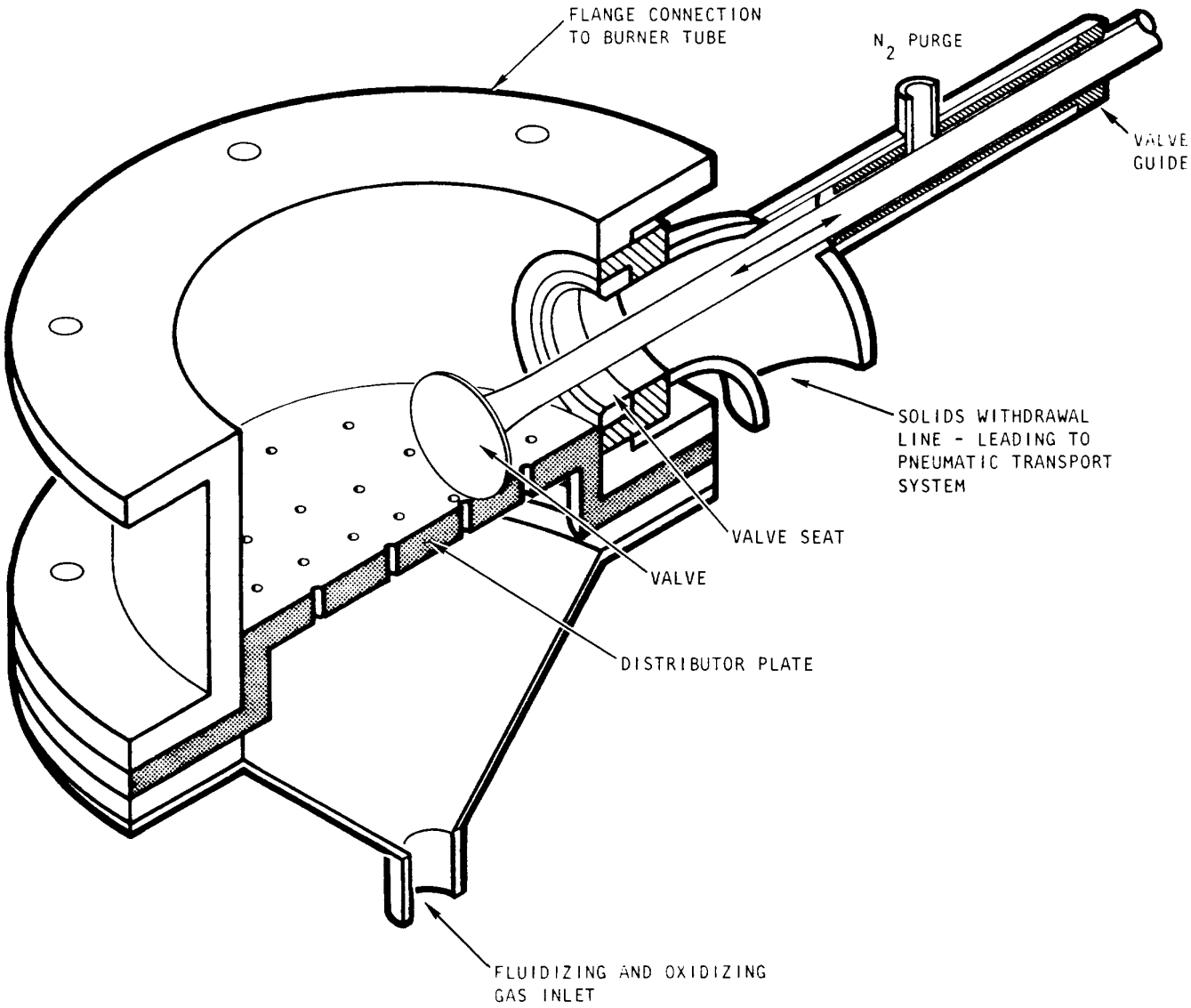

Fig. 5-19. High-temperature bed removal system for 10-cm secondary fluid bed burner

Elimination of the heel is expected when the vacuum pneumatic transport system is used in conjunction with the high-temperature bed removal system. This will cause a transverse sweep of gas across the distributor plate, thus eliminating the holes pierced by the jets. The bed will therefore stay fluidized during the entire product removal step.

Automatic Temperature Control Loop

An automatic temperature control system was tuned to keep bed centerline temperatures constant within ±15°C. As shown in Fig. 5-20, the three-mode controller receives the bed temperature as input. Output is positioning of a pneumatic O_2 control valve. High temperatures as input cause lower O_2 flow rates to the burner, resulting in a negative feedback situation. The temperature variations noted are well within tolerable limits, which indicates suitable controller settings. This control system will be utilized in all future runs.

Leaching

Experimental Leaching Runs

Leaching Runs 72 through 78 were conducted to investigate the dissolution of crushed burned-back TRISO fertile particles in the presence of whole SiC coated fissile particles. This flowsheet option could exist in a head-end reprocessing flowsheet described previously (see Quarterly Progress Report Gulf-GA-A12599). It was established that the presence of the whole particles adversely affects the overall batch dissolution and increases the difficulty of subsequent liquid-solid separation. The results are shown graphically in Fig. 5-21. These and other results are discussed in more detail under "Conclusions and Recommendations."

Summary of Leach Runs. Six test runs were conducted with the 13-cm-diameter leacher. All of the tests were made on a batch basis using a mixture of whole particles and secondary burner product (resulting from burning

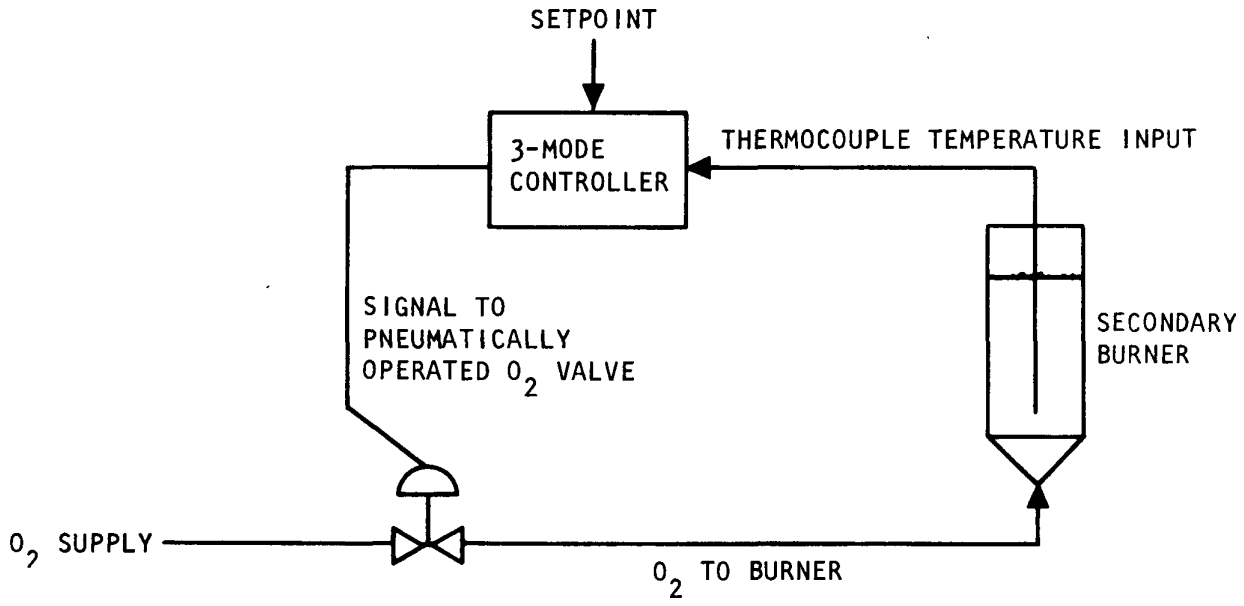

Fig. 5-20. 10-cm secondary burner temperature control loop

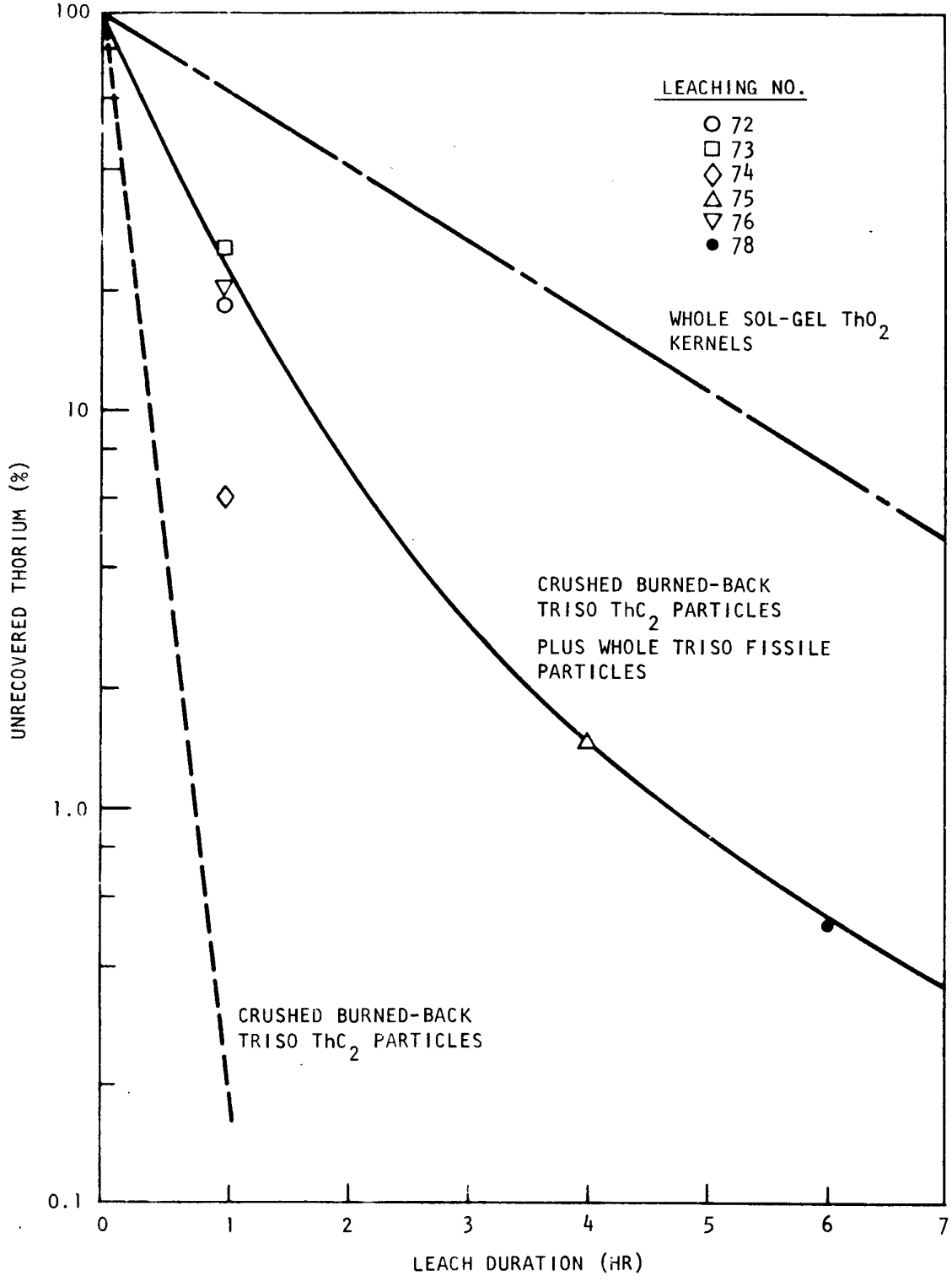

Fig. 5-21. Dissolution of secondary burner ash in presence of whole TRISO fissile particles

crushed TRISO ThC_2 particles). The size distribution and other properties of the burner ash have been recorded previously (Quarterly Progress Report Gulf-GA-A12818, p. 55). All tests were conducted with about 3.25 liters of Thorex (13M HNO_3/0.05M HF/0.1M $Al(NO_3)_3$) per kilogram of secondary burner product. Operating data are shown in Table 5-13.

Runs 72 and 73 were made using 4:1 Th/U-238 TRISO coated particles as the whole particle portion of the feed. The size distributions and chemical analysis for these particles are included in Tables 5-14 and 5-15, respectively. Runs 74, 75, 76, and 78 were made using glass beads to simulate the whole fissile particles. The glass beads had a size distribution of 45 wt % 250 to 300 μm particles and 55 wt % 450 to 500 μm particles. All tests were conducted with 1.88 kg of whole particles and 2 kg of secondary burner ash.

The steam-jet ejector system was not used for transfer of liquids because of an inadequate steam system (see Quarterly Progress Report Gulf-GA-A12599). All liquid transfers were accomplished with a peristaltic pump.

The liquid-solid separation of the leacher product was accomplished with a batch basket centrifuge. Centrifuge data for all runs are as follows:

1. 30-cm-diameter perforate basket.
2. Polypropylene filter bag (5 to 6 μm openings).
3. 1100 gravities purging force at basket sheet (2500 rpm).
4. After washing filter cake, spin dry for about 5 min.

The quantity and specific gravity of liquids in all storage tanks and the leacher were continuously and automatically monitored and recorded. Tank calibration relationships were not utilized for material balance purposes. All volumetric determinations for liquids were accomplished with graduated cylinders. Analyses of samples are given in Table 5-16. These data were utilized in the material balance calculations in Table 5-17.

TABLE 5-13
OPERATING DATA FOR 13-CM-DIAMETER LEACHER

	72[a]	73	74	75	76	78
Whole particles charged, kg	1.88	1.88	1.88	1.88	1.88	1.88
Burner ash charged, kg	2.00	2.00	2.00	2.00	2.00	2.00
Thorex charged, liters	6.50	6.50	6.50	6.50	6.50	6.50
Air sparge rate, liters/min	4.72	14.16	14.16	14.16	14.16	14.16
Leaching time at boiling point, hr	1.0	1.0	1.0	4.0	1.0	6.0
Insolubles after leach (dry wt),[b] g	2362.0	2361.0	2592.0	2198.0	2547.0	0
Mother liquor,[c] liters	6.930	7.575	6.525	11.196	8.374	0

[a] Leach run number. (Leach run 77 was a cleanup run for about 10 previous runs, i.e., a run to remove any soluble Th from insoluble SiC hulls.)

[b] Includes whole particles.

[c] Includes some wash water.

TABLE 5-14
SIZE DISTRIBUTION OF TRISO FISSILE PARTICLES USED
IN LEACH RUNS 72 AND 73
(OUTER PyC REMOVED IN SECONDARY BURNER RUN F4RHB-M25)

Screen Fraction (μm)	Wt %
420 - 495	44.45
350 - 420	49.53
250 - 350	6.02

TABLE 5-15
CHEMICAL ANALYSIS OF TRISO FISSILE PARTICLES

	Weight Percent[a]	
	Sample 1	Sample 2
Th	16.05	35.72
U	4.15	9.09
SiC	22.76	24.17

[a] Based on weight as uncrushed TRISO fissile particle with outer PyC removed, i.e., just as fed to leacher.

TABLE 5-16
SAMPLE ANALYSIS RESULTS FOR 13-CM-DIAMETER LEACHER

	72[a]	73	74	75	76	78
Burner ash, wt % Th	71.3	71.3	71.3	71.3	71.3	71.3
Insolubles,[b] wt % Th	12.28	11.79	14.36	0.89	11.50	0.32
Insolubles, wt % U	1.96	1.75	--	--	--	--
Mother liquor,[c,d] g Th/liter	169.3	176.20	164.0	120.8	135.3	261.9
Mother liquor, g U/liter	0.08	0.14	--	--	--	--

[a] Leach run number.

[b] "Insolubles" are not crushed prior to analysis; thus, analysis indicates only soluble metal content.

[c] Mother liquor analysis is based on gravimetric determination by oxalate precipitation; mother liquor includes some wash water.

TABLE 5-17
THORIUM MATERIAL BALANCE RESULTS FOR 13-CM-DIAMETER LEACHER

	72[a]	73	74	75	76	78[b]
Thorium input, g						
Burner ash	1426.0	1426.0	1426.0	1426.0	1426.0	1426.0
Thorium output, g						
Mother liquor[c]	1173.0	1335.0	1070.0	1352.0	1133.0	--
Insolubles	290.0	278.0	372.2	19.56	293.0	7.23
Total output	1463.0	1613.0	1442.0	1372.0	1426.0	--
Material balance closure,[d] wt %	102.6	113.0	101.1	96.2	100.0	--
Thorium recovery,[e] wt %	82.2	93.6	74.2	98.5	79.45	99.5

[a] Leach run number.

[b] Mother liquor analysis suspected of error and quantity of mother liquor was unrecorded.

[c] Includes some wash water.

[d] Output/input.

[e] Based on outlet quantities.

Conclusions and Recommendations. The following conclusions and recommendations can be made based on data from the six test runs:

1. The addition of whole fissile particles reduces the overall batch dissolution rate for crushed burned-back TRISO ThC_2 particles. This is thought to be the result of ineffective agitation of leacher contents.

2. The TRISO coats on the fissile particles are being damaged at some point within the dissolution system (see uranium analysis, Table 5-16). Based on the following observations, it is suspected that the breakage is occurring within the liquid-solid separation step:

   a. Tests made on two samples of the whole fissile particles indicated only 0.87 to 1.43 wt % of the particles were broken prior to feeding into the leacher.

   b. The quantity of uranium found in the mother liquor after the leach corresponded to 0.32 to 1.36 wt % broken fissile particles.

   c. The soluble uranium contained in the insolubles indicated that from 24.1 to 59.3 wt % of the fissile particles were broken after the liquid-solid separation step. Further testing will be conducted to study this phenomenon.

3. In leaching Runs 73 and 74, problems were encountered in gravity dumping the leacher contents to the centrifuge. When the dump valve was opened, there was no flow of slurry to the centrifuge. Heat was applied to the bottom section of the leacher cone, which apparently reduced the apparent plug and allowed the leacher contents to be dumped.

4. Problems were also encountered in leaching Runs 74, 75, and 78 with the liquid-solid separation. In these runs, the high concentration of solids in the initial slurry fed to the centrifuge resulted in excessive vibration of the centrifuge. It is felt that the difficulty in feeding the high solids content at a consistent flow rate caused "off-loading" of the centrifuge. The use of a dilution tube to reduce the solids concentration (and therefore "off-loading") has been described previously (Quarterly Progress Report Gulf-GA-A12725, pp. 120-122). The problem will be studied further.

5. The problems with particle breakage discussed above resulted in the use of glass beads instead of TRISO fissile particles. The main objective of this work was to investigate the effects of whole fissile particles on dissolution rates. As can be seen from Fig. 5-21, the use of glass beads to simulate the effect on dissolution of whole fissile particles seems acceptable. Further testing is under way and will be reported at a later date.

System for Feeding Burner Ash to Dissolvers

Summary of Results. Information and results concerning the feeding of burner ash to the 13-cm-diameter and 20-cm-diameter dissolvers are discussed in the section. The recommended batch-gravity feed system (shown in Figs. 5-22 and 5-23) has been tested and has demonstrated satisfactory performance. This sytem will be utilized until further development work is completed and indicates a change is necessary, or operational problems necessitate modifications.

Development Details. The main development effort initially undertaken with respect to the dissolvers was concerned with preliminary definition of the effects of operating variables on dissolution rates. The manner in which materials were fed to, or removed from, the dissolution apparatus was

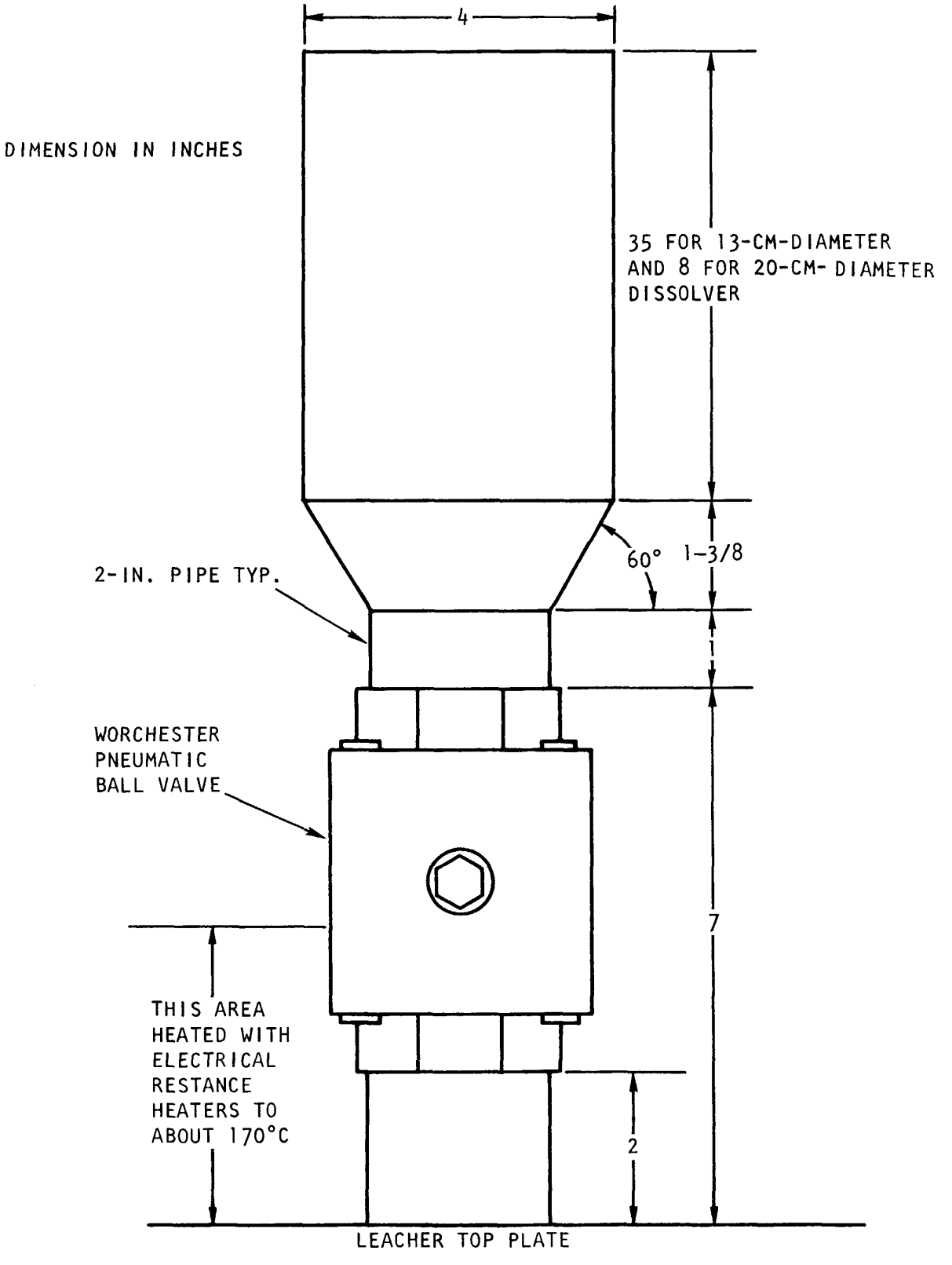

Fig. 5-22. 13-cm-diameter and 20-cm-diameter feed hopper

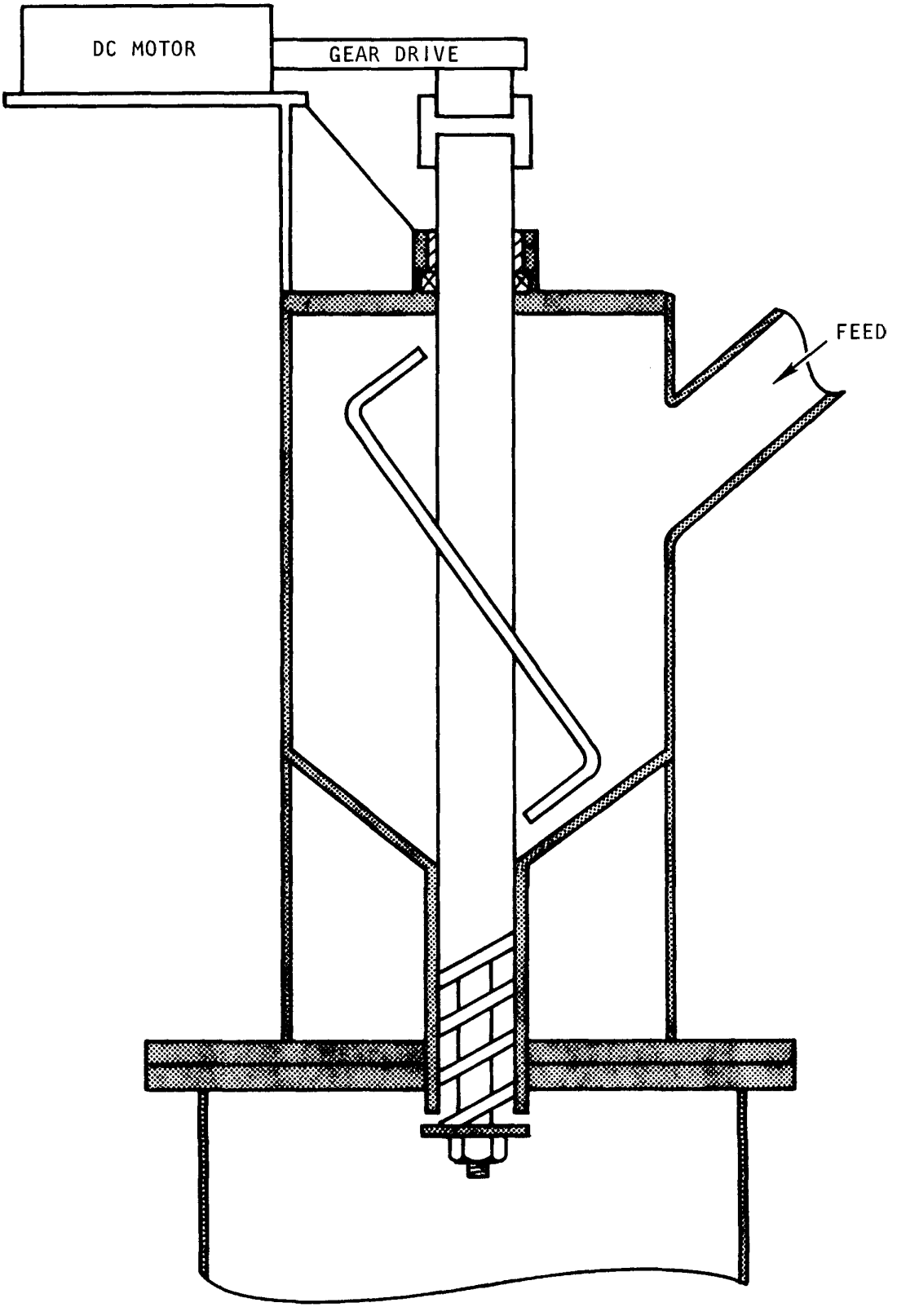

Fig. 5-23. Vertical screw feeder for 5-in.-diameter leacher

of secondary importance. Materials were initially fed into the equipment by hand using a small funnel. Because of the time consuming nature of feeding solids by hand, this method gave way to other attempts.

One of these first efforts resulted from development work on an existing dissolver. This equipment is depicted in Figs. 5-23 and 5-24. The vertical screw feeder originally installed on this equipment was designed for a different service and was found to be unacceptable for secondary burner ash (see Quarterly Progress Report Gulf-GA-A12150, p. 58). Feed addition was not dependable, and the seals of the feeder were damaged as a result of the high-temperature nitric acid atmosphere. In addition to mechanical failures of the feed system, the leacher depicted in Fig. 5-24 was found to have the added problem of excess carryover of condensables due to the use of a vertical condenser. Thus, the leacher was modified as shown in Fig. 5-23.

The next attempts to feed solids to the leachers were directed toward a gravity dump system. This type of feed system offered added reliability through reduction of mechanical devices. However, from the very first, problems were encountered in feeding the burner ash to the leachers (see Quarterly Progress Report Gulf-GA-A12599, p. 63). Specifically, a 1-in.-diameter outlet section on the feed hopper was initially tried. This did not allow free flow of solids to the leacher, and it was necessary to tap the side of the feed hopper before the flow of solids would start. The feed line and valve were electrically heated and maintained at about 170°C. Thus, the problem was not thought to be a result of wet solids buildup. It was thought that bridging of solids in the hopper or feed line caused the problem. In an attempt to eliminate this problem in some of the subsequent dissolution runs, an internal insert was fitted along the sides of the hopper (from top to bottom) to provide an unsymmetrical surface area inside the hopper. However, this did not eliminate the problem. Increasing the hopper outlet line diameter was also considered as a possible solution to the problem. Thus, a separate feed hopper test setup was assembled in a fume hood on an "as-time-permits" basis.

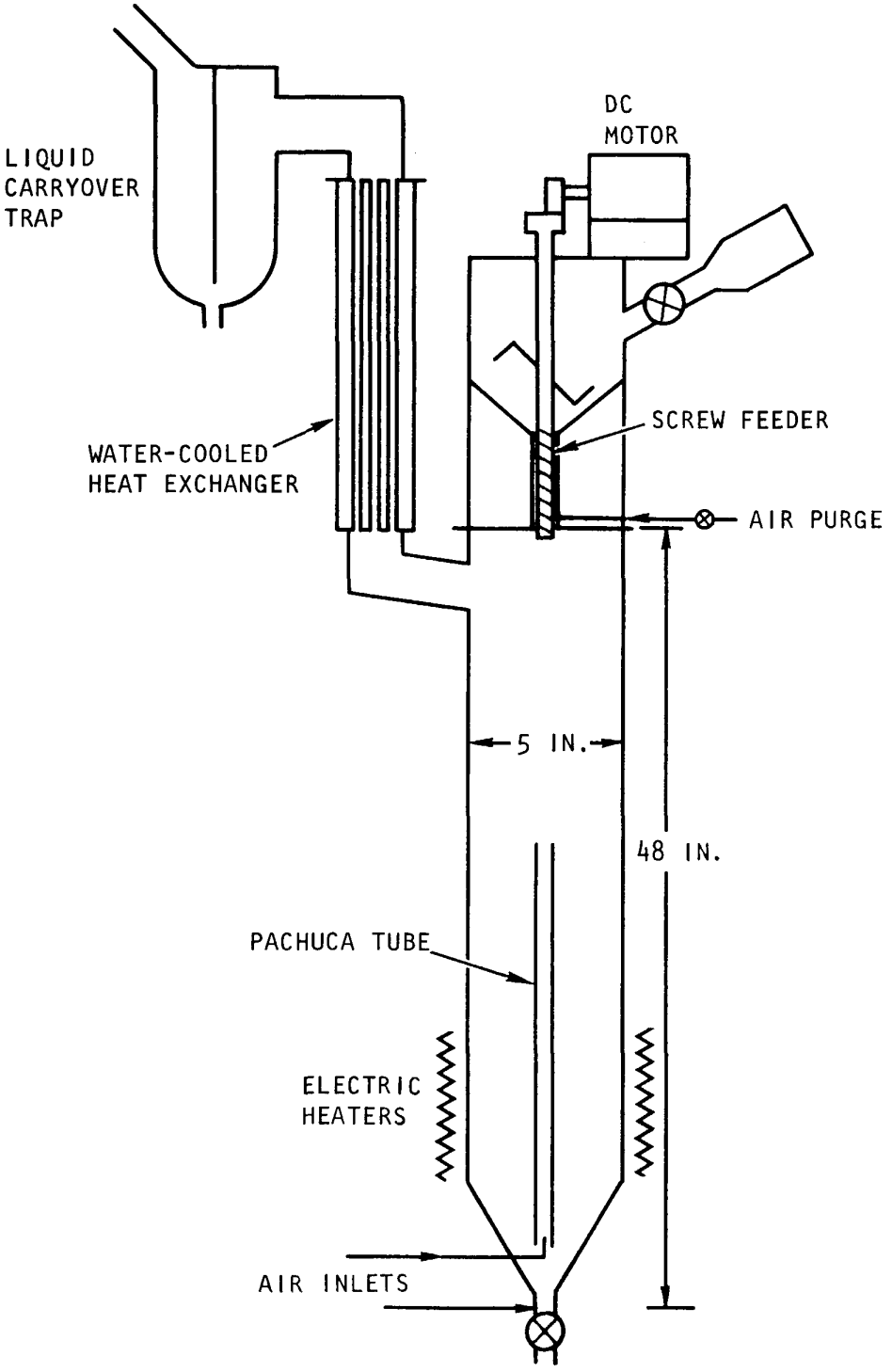

Fig. 5-24. 5-in.-diameter stainless steel leacher

Bench Unit Tests. Secondary burner ash resulting from burning crushed TRISO ThC_2 particles was used in all feed hopper tests. A description of the burner ash (composite of burner runs F4RHB-M3-14, -15, -20, -21, -22, and -23) was given previously (Quarterly Progress Report Gulf-GA-A12725, p. 61). Three cylindrical feed hoppers were tested, differing in design only in the size of the hopper outlet. The hopper outlet sizes tested were 1-in., 1-1/2 in., and 2-in. in diameter. The top section of each hopper was 4 in. in diameter and each had a 60° cone angle (as shown in Fig. 5-22). The testing procedure utilized was qualitative in nature and was directed toward observing either a flow or no-flow condition. From 1 to 4 kg of burner ash was placed in the feed hoppers. Flow of ash out of the hoppers was controlled with a 1/4-in.-thick piece of plexiglas placed over the outlet line. The plexiglas was moved out of the way (as with a gate valve), and the flow or no-flow condition observed. Based on the observed results (Table 5-18), feed hoppers with 2-in.-diameter outlets were installed on both the 13-cm-diameter and 20-cm-diameter leachers (see Fig. 5-24). No difficulties have been experienced with this system.

The 2-in.-diameter feed hopper was tested further. About 10 kg of the burner ash was charged to the feed hopper. Lead weights were used to compact the ash into the feed hopper. After a designated time period, the plexiglas retainer on the bottom of the hopper was pulled out of the way. The solids flow characteristics from the hopper were then recorded. A slight variation of this procedure was then carried out by recompacting the burner ash in the hopper. In this case, the lead weights were removed just prior to dumping the compacted ash. The conditions for the tests are recorded in Table 5-19. In every case, the burner ash gravity dumped smoothly and completely.

To supplement these qualitative tests, some determinations were also made on the differences between the initial and final bulk density of the burner ash when exposed to these types of compressive forces. In these tests, a cylindrical canister with a diameter of 5.75 in. and a length of 6.75 in. was utilized. As in the previous feed hopper tests, lead weights

TABLE 5-18
RESULTS OF BENCH UNIT TESTS ON SYSTEM FOR FEEDING BURNER ASH TO DISSOLVERS

Feed Hopper Outlet Diameter (in.)	Results
1	On almost every occasion, the flow of solids was severely restricted. It was necessary to tap the side of the hopper vigorously before any solids flow would occur. Continual tapping was required to maintain flow. In several cases, the flow of solids began without tapping the hopper but stopped before the hopper was empty.
1-1/2	Results were considerably better than with the 1-in.-diameter outlet. Flow of solids started in every attempt; however, in several cases the flow stopped when approximately 2/3 of the solid had dumped from the hopper. It was necessary to tap the side of the hopper to remove the remaining burner ash. Also, the rate of solids discharge was not consistent. In some tests the solids dumped smoothly, while in others the discharge rate oscillated from fast to slow.
2	There was no hesitation with flow. Solids dumped smoothly and completely.

TABLE 5-19
CONDITIONS OF BENCH UNIT TESTS ON
SYSTEM FOR FEEDING BURNER ASH TO DISSOLVERS

Compacted Weights Utilized (lb)	Time Under Completion (hr)	Compactive Force of Lead Weights (lb/in^2)
12.5	6	1
	24	1
	63	1
25	30	2
	50	2
50	30	4
	50	4
	120	4

were placed on top of a compaction cylinder. The weight of this fixed-volume canister (both before and after compaction) was utilized to determine the bulk density of the burner ash. Results of these tests are given in Table 5-20. A plot of the difference between the initial and final bulk density as a function of time and compaction weight is given in Fig. 5-25. The data could be of use in future design considerations for solids feed hoppers.

Preliminary Results of Effect of Feed Adjustment, Synthetic Fuel Dissolution, and Stability of Neutron Poisons on Leaching System

This section summarizes the preliminary investigations conducted in bench-scale glassware with regard to: (1) feed adjustment, (2) synthetic fuel dissolution, and (3) stability of neutron poisons in the leaching system. A proposed outline for further investigations and details of the experimental procedures are also included.

Results of Preliminary Investigation. Preliminary feed adjustment studies of 1M Th solutions were carried out to determine the extent to which these solutions must be evaporated and steam-stripped in order to achieve an acid-deficient condition of at least -0.1M NO_3. Acid-deficient solutions are defined as solutions in which the ratio of nitrate ion to metal ions is less than the stoichiometric value (Refs. 5-12 through 5-15). Figure 5-26 illustrates that acid deficiency was obtained for 1M Th solutions that were evaporated to 135°C (pot temperature), which corresponds to a volume that is 30% of the original volume, and subsequently steam-stripped at that temperature and volume until the volume in the condensate was at least 100% of the original volume. The 1M Th solutions that were evaporated to 40% or more of their original volume were not stable with regard to thorium precipitation upon cooling. Precipitation from these solutions was prevented by dilution with water to their original volume. Data for these solutions are given in Table 5-21.

Attempts at dissolution of a synthetic fuel (composition 89.9% Th, 10.1% fission products) were not successful. A considerable portion

TABLE 5-20
BULK DENSITY AS A FUNCTION OF TIME AND COMPACTIVE FORCE

Compaction Weight Utilized (lb)	Time Under Compaction (hr)	Bulk Density (lb/ft^3)		Difference Between Final and Initial Bulk Density (lb/ft^3)
		Initial	Final	
100	90.25	166.88	182.33	15.45
100	24.00	165.73	182.88	17.15
100	48.00	165.39	182.97	17.58
75	94.00	165.68	181.91	16.52
75	48.00	167.33	183.10	15.77
75	24.00	167.22	182.31	15.09
50	24.00	165.96	179.38	13.42
25	24.00	165.79	176.38	10.59
25	48.00	165.95	183.28	13.33
25	94.00	167.36	181.21	13.85

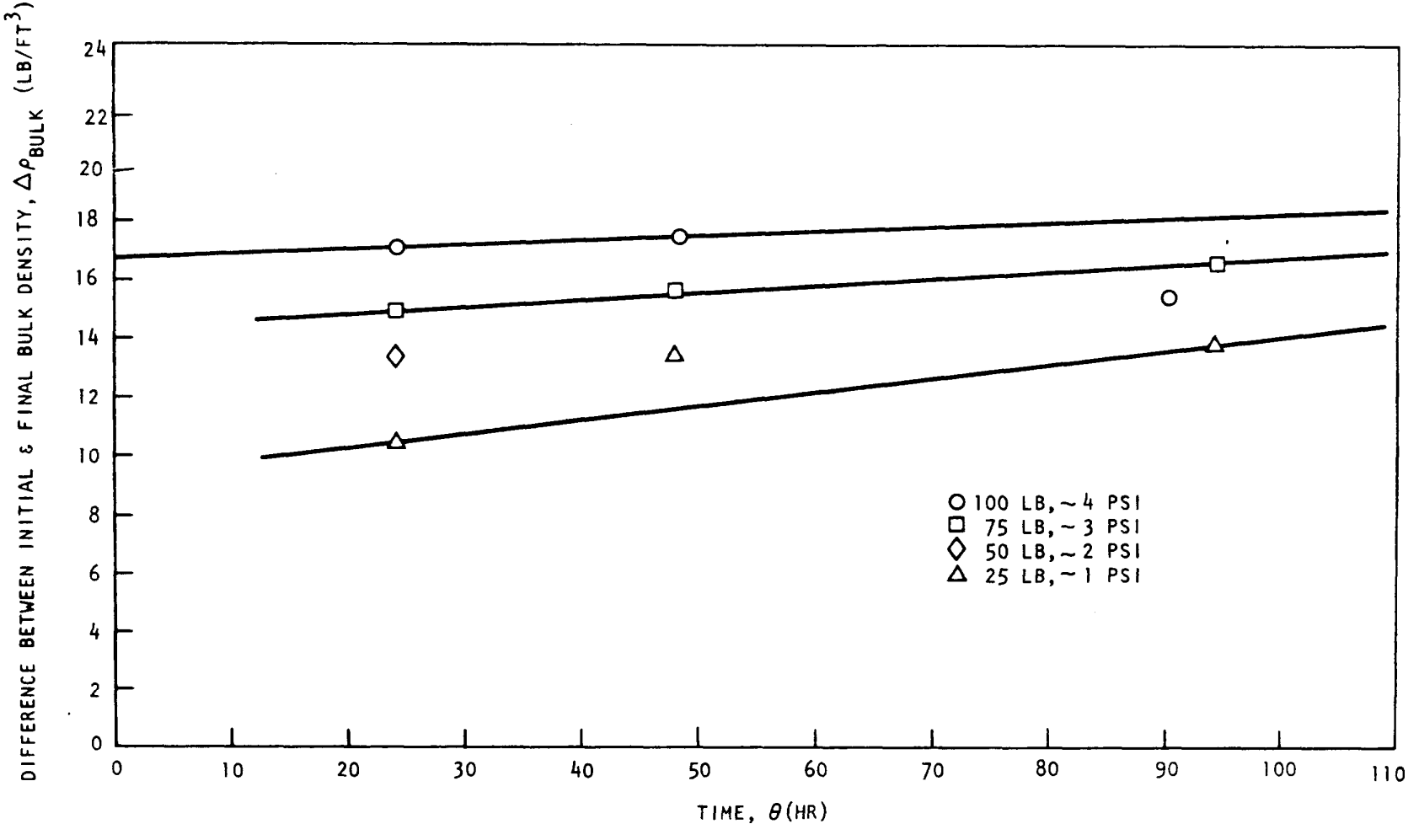

Fig. 5-25. Effect of compressive force on burner ash bulk density as a function of time

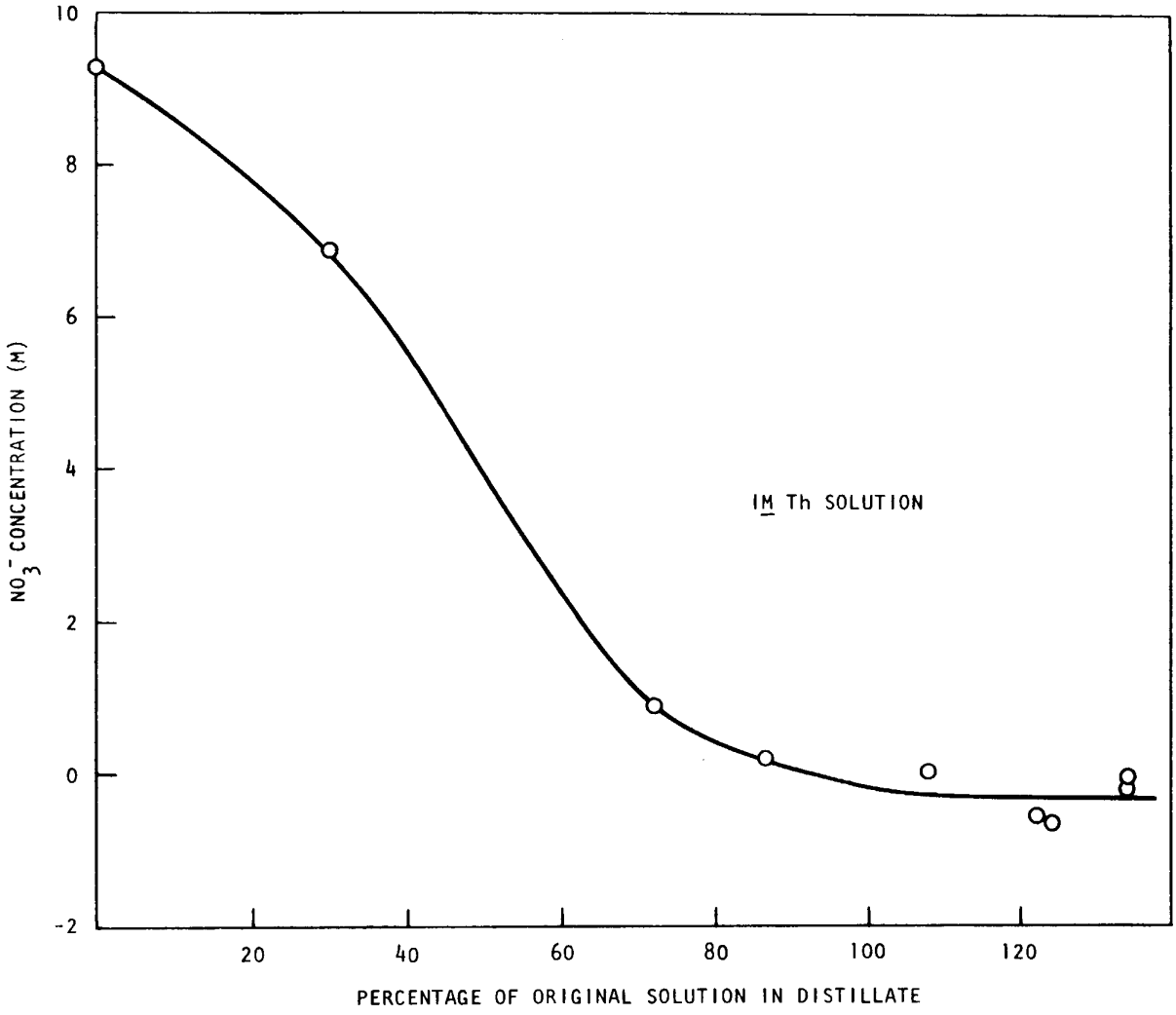

Fig. 5-26. Percentage of original solution in distillate versus NO_3^- ion concentration

TABLE 5-21
FEED ADJUSTMENT DATA TABLE

Sample No.	Volume Collected in Distillate (ml)	Total NO_3^- Conc.[a] (M)	Thorium Conc. (g/l)	Free NO_3^- Conc.[b] (M)	Remarks
FAD-1	0	14.17	233.8	9.87	Solution 1 (1M Th) Original samples 100 ml
FAD-2	8.5	13.40	232.3	9.10	
FAD-3	19.5	12.60	238.1	8.30	
FAD-4	40.0	9.90	239.0	5.60	
FAD-5	59.0	7.17	243.2	2.87	
FAD-6	70.0	5.83	249.3	1.53	
FAD-7	102.0	4.67	243.4	0.37	(c)
FAD-8	117.0	4.50	234.7	0.20	(c)
FAD-9	0	13.63	228.5	9.33	Solution 2 (1M Th) Original samples 100 ml
FAD-10	30.0	11.17	-	6.87	
FAD-11	71.5	5.17	-	0.87	
FAD-12	87.0	4.50	-	0.20	
FAD-13	108.0	4.33	-	0.03	
FAD-14	121.5	4.00	-	-0.30	Acid deficient
FAD-15	124.0	3.97	-	-0.33	Acid deficient
FAD-16	134.0	4.27	-	-0.03	Acid deficient
FAD-17	134.0	4.17	-	-0.13	Acid deficient
FAD-18	-	4.33	-	-	Evaporated to 165°C[d]

[a] Total nitrate ion concentration determined by ultraviolet spectrophotometry.

[b] Free nitrate ion concentration determined by assuming 4M of nitrate associated with Th and 0.3M of nitrate.

[c] Acid deficiency was not obtained due to inefficient steam-stripping.

[d] Literature states that solutions evaporated to 165°C are acid deficient (Ref. 5-13).

(approximately 47%) of the fission product spikes remained undissolved after as long as 1 week reflux in Thorex [(13M HNO_3/0.05M HF/0.1M $Al(NO_3)_3$]. Preliminary indications are that this is the result of the high refractory nature of the commercial oxides of Zr, Mo, Ce, and Ba. The oxides available for Th and Sr readily go into Thorex solution. Data presently available for these synthetic fuel solutions are listed in Tables 5-22 and 5-23. Feed adjustment to acid deficiency was attempted and precipitate formation was observed after dissolution and after steam-stripping for one of the synthetic fuel solutions (Table 5-22). The results are not sufficiently complete at this time to know if these solutions are acid deficient, and the Th/Mo and the Sr/Ba precipitates are attributed to the fact that this particular solution is greater than 1M Th concentration.

The solubility of the neutron poison CdO was determined as a function of temperature in Thorex and 1M Th solutions (Fig. 5-27 and Table 5-24). The solubilities of CdO in Thorex and in a 1M Th solution at 25°C were found to be 0.61M and 1.33M, respectively. Literature values for other Cd salts under somewhat similar conditions range from 0.16M to 1.34M (Ref. 5-16).

Conclusions and Recommendations. The commercially available fission product oxides were found to be unacceptable for dissolution rate determinations. Fission product oxides for future work will be prepared from the nitrates of the metals. The dissolution rates thus obtained would be representative of the secondary burner product. Dissolution rates have been determined for the secondary burner product. Consequently, it is recommended that the dissolution rate for the synthetic fuel with the greatest fission product content, for the same synthetic fuel plus CdO, and for the secondary burner product plus CdO be determined and compared with the secondary burner product rate previously determined. The literature states that the neutron poison boron does not affect the dissolution rate of thorium (Ref. 5-17).

Acid deficiency for the 1M Th solutions resulted when these solutions were evaporated to 30% of their original volume and then steam-stripped until the condensate was greater than 100% of the original volume. The resulting solutions must be diluted to prevent thorium precipitation upon

TABLE 5-22
SYNTHETIC FUEL DISSOLUTION - FEED ADJUSTMENT DATA

Sample No.	Volume Collected in Distillate (ml)	Total NO_3^- Conc. (M)	Th (g/l)	Zr (g/l)	Ce (g/l)	Mo (g/l)	Sr (g/l)	Ba (g/l)	Remarks
FAD-19	0	15.17	267.1						Synthetic fuel No. 1, precipitate
FAD-19P	-	-	-	-	-	-	>1%	>1%	formed from FAD-19P upon standing
FAD-20	98	6.63	-	-	-	-	-	-	
FAD-20P	-	-	>1%	-	-	>1%	-	-	Precipitate formed from FAD-20P after steam-stripping
FAD-21	0	13.80							Synthetic fuel No. 2 (5 hr reflux),
FAD-21S	-								28.97 g wt insolubles, evaporated
FAD-22	70	5.25							to 135°C, steam-stripped
FAD-23	124				Data not available				
FAD-24	0	13.80			at present time				Synthetic fuel No. 3 (23 hr reflux),
FAD-24S	-								22.91 g wt insolubles, evaporated
FAD-25	69	5.58							to 135°C, steam-stripped
FAD-26	127	4.0							
FAD-27	0								Synthetic fuel No. 4 (184 hr reflux),
FAD-28	-								13.91 g wt insolubles

TABLE 5-23
SYNTHETIC FUEL COMPOSITION
(89.9% Th, 10.1% FISSION PRODUCTS)

	Synthetic Fuel No. 4 (g/l)	Synthetic Fuel No. 3 (g/l)	Synthetic Fuel No. 2 (g/l)	Synthetic Fuel No. 1 (g/l)
Th	232.0	232.0	232.0	370.27[a]
Zr	7.4551	7.4602	7.4614	7.4534
Mo	4.7304	4.7294	4.7309	4.7286
Ce	13.6540	13.6562	13.6550	13.6541
Sr	1.9110	1.9095	1.9089	1.9107
Ba	1.8213	1.8215	1.8201	1.8222
Total fission products	29.5718	29.5768	29.5763	29.5690
Total	261.5718	261.5768	261.5763	399.8390

[a] Secondary burner product which is 71.3% Th.

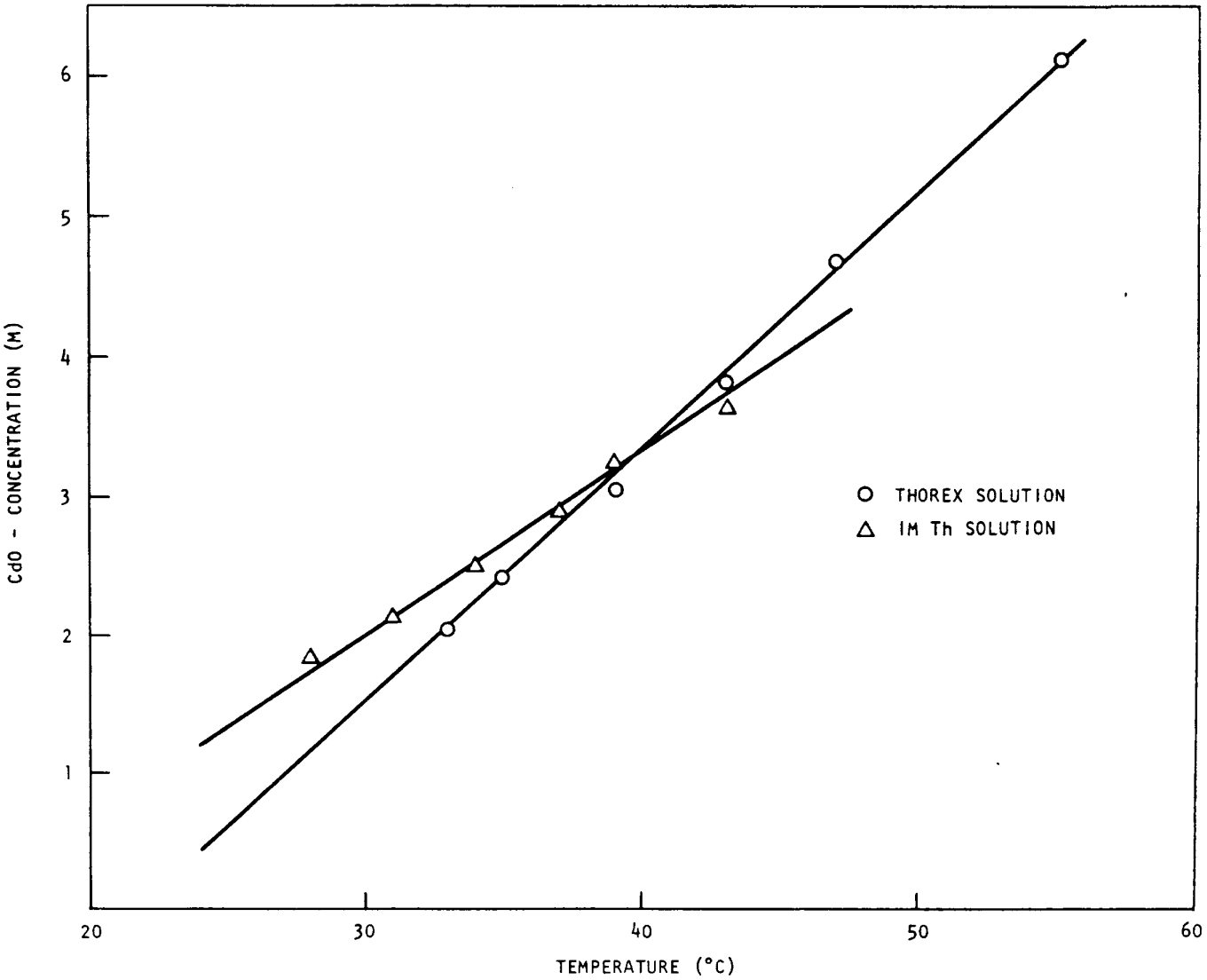

Fig. 5-27. Solubility of CdO in Thorex and 1M Th

TABLE 5-24
SOLUBILITY DATA (CdO in THOREX AND 1M Th SOLUTIONS)

Weight CdO (g)	Volume (ml)	Temp. of Precipitate Formation (°C)	CdO Conc. (M)
		CdO in Thorex Solution	
7.90	10	55	6.15
7.90	13	47	4.73
7.90	16	43	3.84
7.90	20	39	3.07
7.90	25	35	2.46
7.90	30	33	2.05
		CdO in 1M Th Solution	
7.09	15	43	3.68
7.09	17	39	3.25
7.09	19	37	2.90
7.09	22	34	2.51
7.09	26	31	2.12
7.09	30	28	1.84

cooling. Since it is desirable to know the effect of the addition of fission products on the extent of feed adjustment to acid deficiency and the possible formation of precipitation products after adjustment, it is recommended that a range of synthetic fuel compositions be investigated. The present synthetic fuel composition is based on data from Fort St. Vrain, which defines Th, U, and fission product composition for 1- and 6-year irradiation times as follows:

	1 yr	6 yr
Th	88.3%	81.9%
U	9.0%	8.0%
Fission products	2.7%	10.1%

Assuming a linear relationship between fuel composition and irradiation times (flux $\sim$ fission product production), it is proposed that fuels under investigation have the following composition and that each be investigated to determine the extent to which it must be steam-stripped and the extent and identity of any precipitate formation (Table 5-25).

TABLE 5-25
COMPOSITION OF FUELS (%) TO BE INVESTIGATED FURTHER

	1 Yr	2 Yr	3 Yr	4 Yr	5 Yr	6 Yr
Th	88.3	87.0	85.7	84.4	83.2	81.9
U	9.0	8.8	8.6	8.4	8.2	8.0
Fission products	2.7	4.2	5.7	7.2	8.6	10.1

The solubility of the neutron poison CdO is more than adequate for criticality control in 1M Th solutions. However, the literature recommends that the stability of neutron poisons be determined in process solutions (Ref. 5-16). Consequently, the solubility of cadmium and also boron will be determined in the 6-year irradiated synthetic fuel solution as a function of temperature. The neutron poisons gadolinium and samarium have been omitted since they are improbable candidates due to their cost relative to boron and cadmium (Ref. 5-16).

Experimental Procedures. The details of the experimental procedure are outlined below, with the completion time estimated to be 2 to 3 months.

1. Feed Adjustment. A total of six solutions, having the thorium and fission product compositions listed in Table 5-25, will be prepared. Each of these solutions will have a thorium concentration of 1M. The oxides for the fission product spikes of Zr, Ce, Sr, and Ba will be prepared by firing the nitrates at 900°C for 2 hr. With each of the six solutions, two feed adjustments will be carried out. One of these solutions will be evaporated to 135°C, diluted back to its original volume, and sent to Analytical Chemistry for analysis. The second of these solutions will be evaporated to 135°C and then steam-stripped at constant temperature and volume until 120% of the original volume is collected in the condensate. This solution will also be diluted and sent foranalysis. Steam will be supplied by a steam generator consisting of a 1000-ml flask, which will be connected to the three-neck 250-ml round bottom flask through the distillation head adaptor. Constant temperature and volume will be maintained during steam-stripping by slowly dripping water into the reaction mixture through a side arm of the flask. If any precipitate formation occurs after steam-stripping and dilution, the solution will be

filtered and the precipitate sent for analysis. Solutions which are feed adjusted will be analyzed for Th, Al, Zr, Ce, Sr, Ba, Mo, and total nitrate ion content. Calculations made to determine acid deficiency are illustrated in Table 5-26. Results will be tabulated listing the fission product composition, the degree of stripping required, the acid-deficient concentration, and the extent and identity of any precipitate formation.

TABLE 5-26
CALCULATIONS OF ACID DEFICIENCY

A	B	Σ(A x B)	C	C - [Σ(A x B)]
Metal ion conc. (M) at the volume of solution in the residue.	Stoichiometry of the NO_3 ion associated with the metal ion, e.g., 3 for Al, 4 for Th.	The summation of all the metal ions times the stoichiometry of the associated NO_3 ion. This gives conc. (M) of NO_3 ions tied up with the metal ions.	Total NO_3 conc. conc. (M) determined experimentally at the volume of solution in the residue.	If difference is negative, solution is acid deficient.

2. Neutron Poisons. The solubility of the neutron poisons cadmium and boron will be determined in the 6-year irradiated synthetic fuel as a function of temperature. The solubility at each temperature will be determined by heating a mixture of the salt and the synthetic fuel solution to a temperature at which the mixture forms an unsaturated solution, and then cooling and observing the temperature at which crystals just appear. A dilution will be made with the synthetic fuel and the process

repeated. The solubility determinations will be carried out in a test tube containing a thermometer and a small wire with a loop on its end to agitate the mixture. The test tube will be placed in a water bath for temperature control. Data will be collected over a temperature range of 20° to 60°C.

3. Dissolution Rates. Dissolution rates will be determined under reflux conditions for the 6-year irradiated synthetic fuel, the synthetic fuel with CdO, and the secondary burner fuel with CdO. The results will be expressed as percentage undissolved thorium versus time. The concentration of cadmium will be 0.2M and all thorium concentrations will be 1M. Mixtures of each fuel will be prepared and refluxed for a given amount of time, at the end of which the reaction will be terminated. The solution will be filtered and the filtrate analyzed for thorium content. In this manner, at least three determinations at different time intervals will be made for each of the fuels under consideration.

Preliminary Design of Evaporator/Stripper for Feed Adjustment to Solvent Extraction

Summary. A pilot-plant-size coil-type evaporator/stripper with a deentrainment tower will be constructed to accomplish the acid reduction from a 6M HNO_3 concentration to a 0.5M acid-deficient product. The maximum and minimum batch capacities of the system are about 30 to 10 liters, respectively. Continuous capacity is about 10 liters/hr with a holdup volume of about 8 liters required for total heater immersion.

Heat is supplied in the form of condensing steam in two coils. Additional evaporation and temperature control is accomplished by using a low-pressure (~25 psia) steam sparger.

Adequate instrumentation and control devices are supplied for the complete remote operation of the system.

Design Criteria. Design criteria for the feed adjustment step to the Thorex solvent extraction process call for the attainment of an acid-deficient product. Dissolver feed to this unit will normally be about 6M in nitric acid and 1M in thorium. The desired product should be about 0.5M deficient in nitrate ion and remain at 1M in thorium.

Based on these primary requirements, along with a proposed capacity of 25% of that indicated for the ICPP hot demonstration, a feed adjustment process was designed. The feed and product stream compositions used for the design basis are tabulated in Table 5-27.

General Flow. The major piece of equipment in the feed adjustment step is the evaporator/stripper. An overall flow diagram of the evaporator/stripper system is shown in Fig. 5-28. The evaporator/stripper is supplied with feed from a feed surge tank, which in turn receives feed from storage. Within the evaporator/stripper, the nitric acid is removed by evaporation using condensing steam in two coils mounted in the vessel body. Additional acid removal is accomplished by steam-stripping the solution via a sparger mounted in the vessel.

The overhead vapors from the evaporator/stripper vessel are passed through a deentrainment tower where the entrained liquid is separated and returned to the evaporator vessel. The nitric acid and steam vapors are then routed to a water-cooled condenser where they are condensed and cooled. The cooled condensate is routed to an existing storage tank. Any noncondensable gases are separated from the condensate by means of an existing vent system on the condensate storage tank. The vent system also provides for subatmospheric operation of the evaporator/stripper unit.

The concentrated product is withdrawn from the evaporator/stripper vessel and routed to a mixing tee, where it is diluted with water to obtain

TABLE 5-27
EVAPORATOR/STRIPPER DESIGN BASIS FLOWS

	Feed[a]		Steam as Liquid		Condensate		Concentrate		Dilution Water		Solvent Extraction Feed	
	1	2	1	2	1	2	1	2	1	2	1	2
Rate, liters/hr	10.0	10.0	5	4	12.0	12.5	3.0	1.5	7	3.5	10.0	5.0
Specific gravity[b]	1.66	1.44	1	1	1.2	1.18	2.42	2.42	1	1.0	1.43	1.43
Composition, g/hr												
Thorium (Th)	2320.00	1160.00	-	-	-	-	2320.00	1160.00	-	-	2320.00	1160.00
Nitrate ion (NO_3^-)	6240.00	5000.00	-	-	4000.00	3880.00	2240.00	1120.00	-	-	2240.00	1120.00
Thorium nitrate [$Th(NO_3)_4$]	4800.00	2400.00	-	-	-	-	4335.00	2168.00	-	-	4335.00	2168.00
Hydrogen ion (H^+)	60.00	60.00	-	-	60.00	60.00	-	-	-	-	-	-
Free water (H_2O)	7980.00	8180.00	5000	4000	10280.00	10830.00	2700.00	1350.00	7000	3500.0	9700.00	4850.00

[a] Feed 1 corresponds to 1.0M Th solution from dissolver; feed 2 corresponds to 0.5M Th solution from dissolver.

[b] Specific gravities of feed and concentrate are based on bench-scale testing.

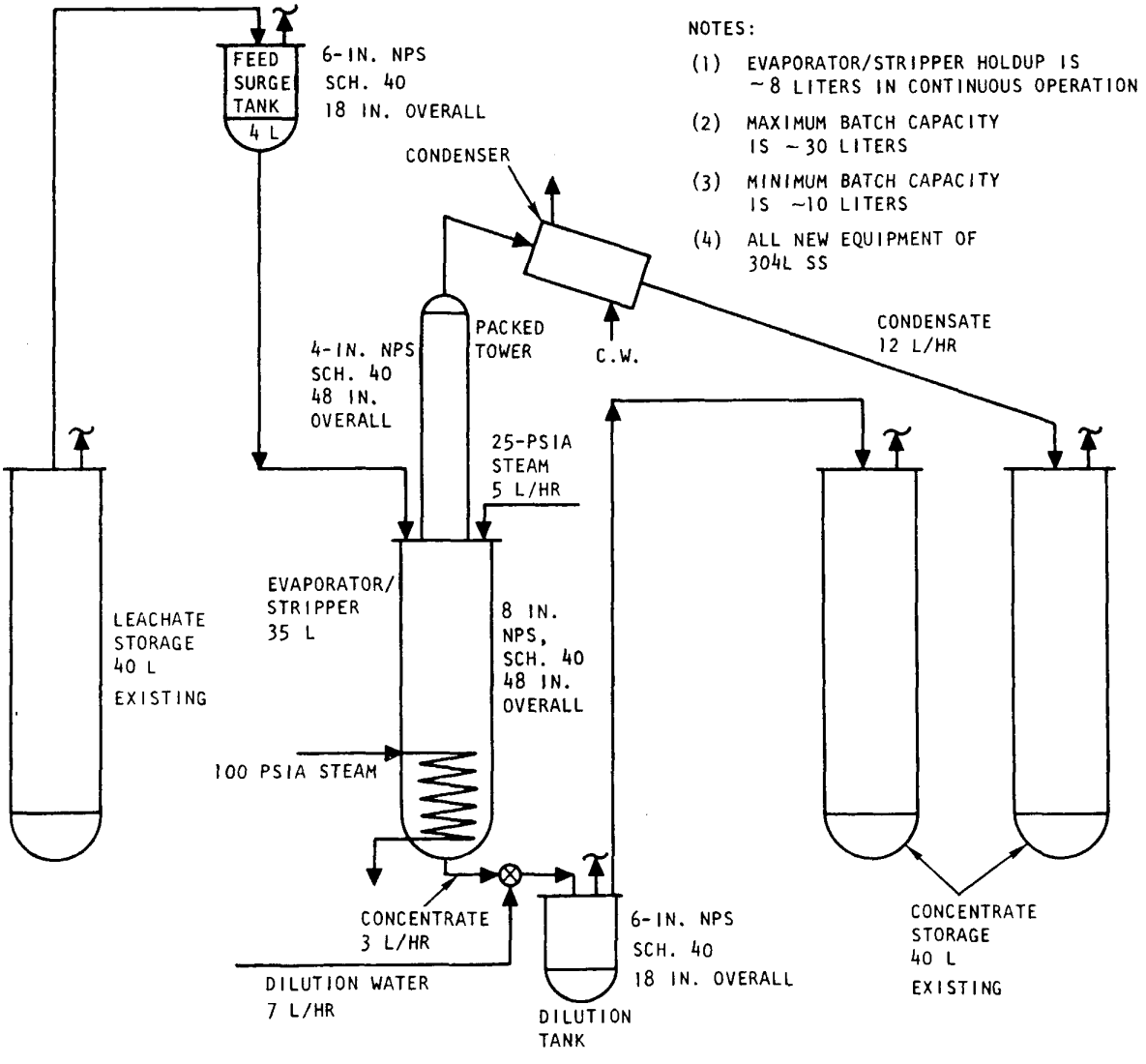

Fig. 5-28. General flow diagram for evaporator/stripper

a 1M concentration in thorium. The mixture then enters a surge tank, from which it is transferred to an existing storage tank.

Proposed Design. Initial considerations indicate the desirability of using a coil-type evaporator for the preliminary testing and data acquisition. The unit is designed for initial batch-wise operation with the future capability of continuous operation. The proposed design of the evaporator/stripper and its auxiliary equipment is as follows:

1. Vessel. The evaporator/stripper vessel will consist of a 4-ft length of nominal 8-in.-diameter, Schedule 40, type 304L stainless steel pipe. The bottom will consist of an ellipsoidal head with a 4-in. length of 2-in.-diameter, Schedule 40, type 304L stainless steel centered and protruding from the head. The top of the vessel will be equipped with a standard 150-lb flange. A 150-lb flange will also be supplied on the 2-in. bottom pipe (see Fig. 5-29).

2. Spool Piece. The spool piece will consist of a 4-in. section of standard 4-in.-diameter, Schedule 40, type 304L stainless steel with a 150-lb flange on one end. The other end will have a modified flange capable of connecting the spool piece to the 8-in.-diameter NPS vessel. This flange will be constructed of 1/2-in.-thick, type 304L stainless steel plate. The bottom piece will be drilled and tapped to make appropriate connections (see Fig. 5-29).

3. Deentrainment Tower. The deentrainment tower consists of a 40-in. length of standard 4-in.-diameter, Schedule 40, type 304L stainless steel pipe with 150-lb flanges at both ends. Two modified flange pieces with heavy stainless mesh welded in the openings will be attached

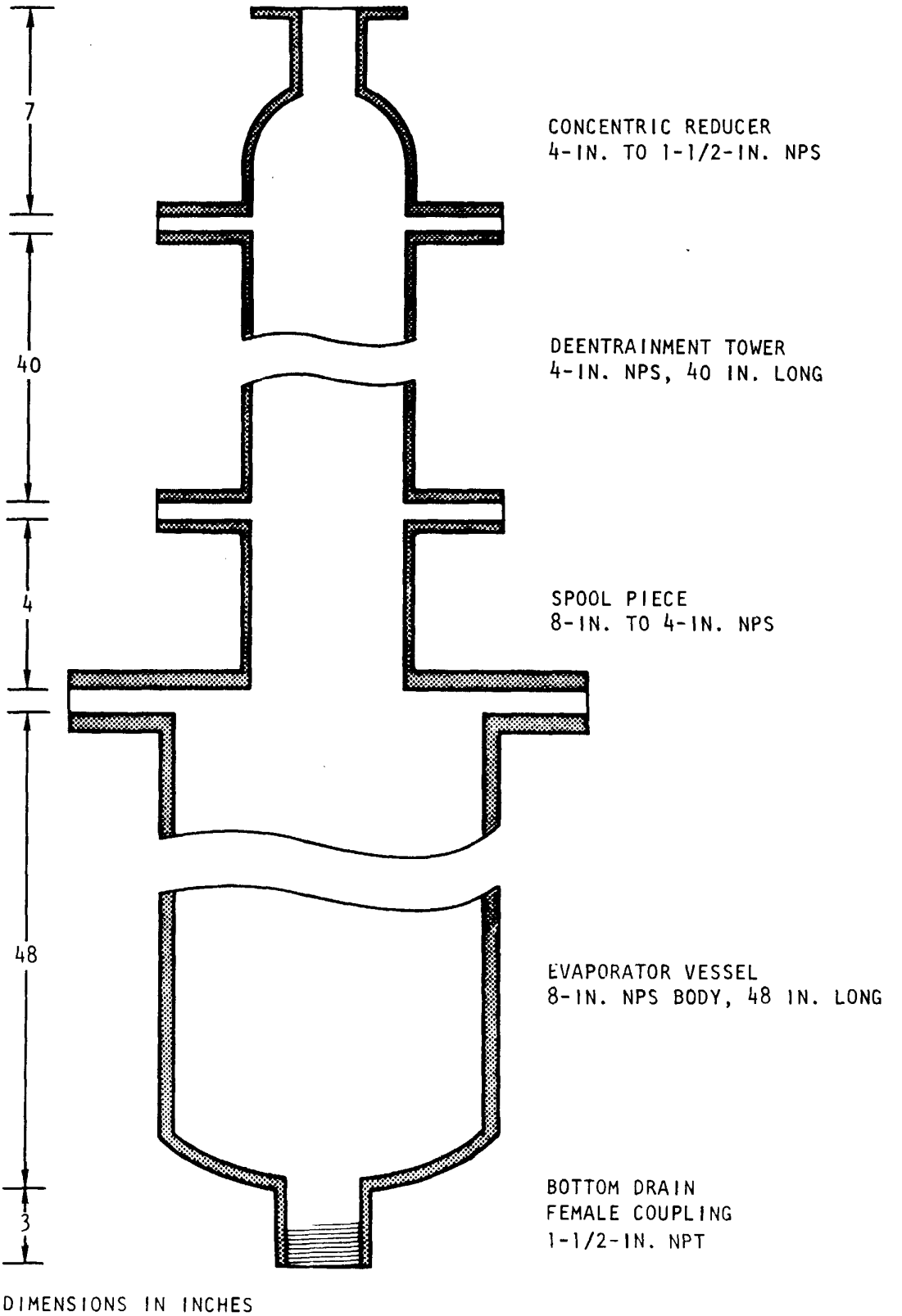

Fig. 5-29. Evaporator stripper, tower, and spool piece

at both ends of the tower. The tower top will be connected to a flanged 4-in. NPS to 1-1/2-in. NPS reducer (see Fig. 5-29).

4. Internals. The evaporator/stripper vessel will be supplied with two heating coils fabricated from 1/2-in.-o.d., 1/16-in. wall, type 304L stainless steel tubing. One coil will be 6-in. o.d. and 5-in. i.d., and the other will be 4-in. o.d. and 3-in. i.d. Both coils will have a center-to-center coil spacing of 7/8 in. and will contain 9-1/2 coils each. The total effective area is approximately 3 ft^2. A steam sparger will also be supplied. The sparger will consist of a single 5-in.-o.d. coil plugged at one end. The coil will have 1/32-in.-diameter holes drilled in the bottom to allow passage and distribution of sparging steam. This coil will also be constructed of 1/2-in.-o.d., 1/16-in. wall, type 304L stainless steel tubing. The evaporator/stripper internals are shown in Fig. 5-30.

5. Feed Surge and Product Dilution Tanks. Both the feed surge and product dilution tanks will consist of a standard 6-in.-diameter, Schedule 40, type 304L stainless steel pipe with an ellipsoid bottom and top flange. Each tank will also be supplied with a modified solid flange piece to cover the tank and to allow drilling and tapping for necessary connections. One tank will be supplied with a 1-in. NPS female fitting centered on the bottom (see Fig. 5-31).

6. Condenser. The overhead condenser will be a prefabricated unit supplied by American Standard Company. The unit is constructed of type 316 stainless steel and will have a heat transfer area of about 11 ft^2.

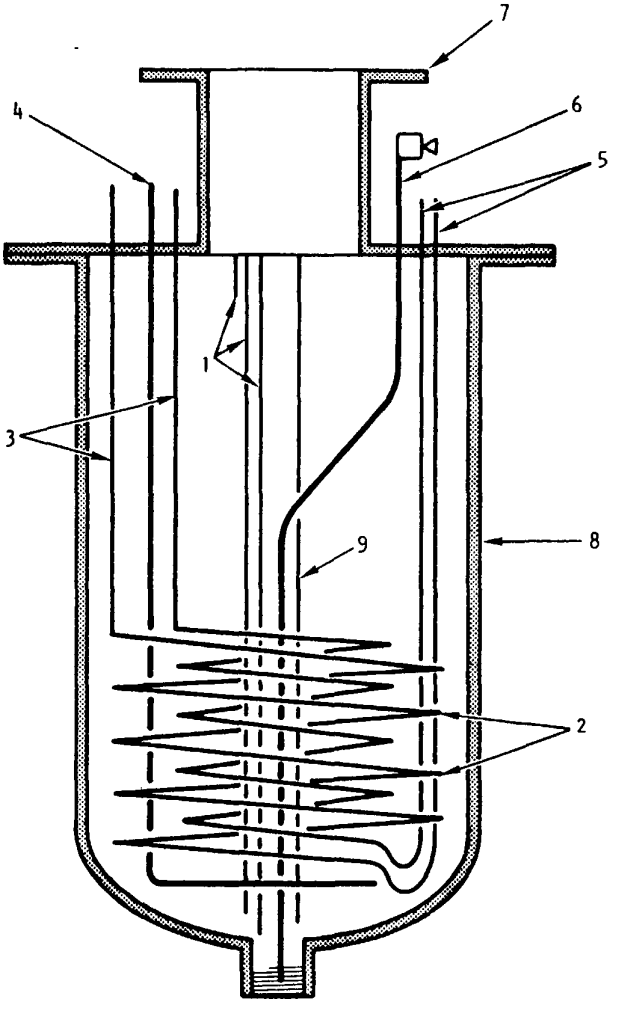

1 $\Delta\rho$ LEGS, 1/4-IN. OD TUBING
2 HEATING COIL, ~3 FT^2
3 100 PSIA STEAM INLET, 1/2-IN. OD TUBING
4 STEAM SPARGER INLET, 1/2-IN. OD TUBING
5 100 PSIA CONDENSATE RETURN, 1/2-IN. OD TUBING
6 JET OUT
7 FLANGED CONNECTION TO PACKED TOWER, 4-IN. NPS
8 8-IN. NPS EVAPORATOR KETTLE
9 TEMPERATURE PROBE, 1/4-IN. OD
10 FLANGED DRAIN/FUTURE CONNECTION, 1-1/2-IN. NPS

Fig. 5-30. Evaporator/stripper internals

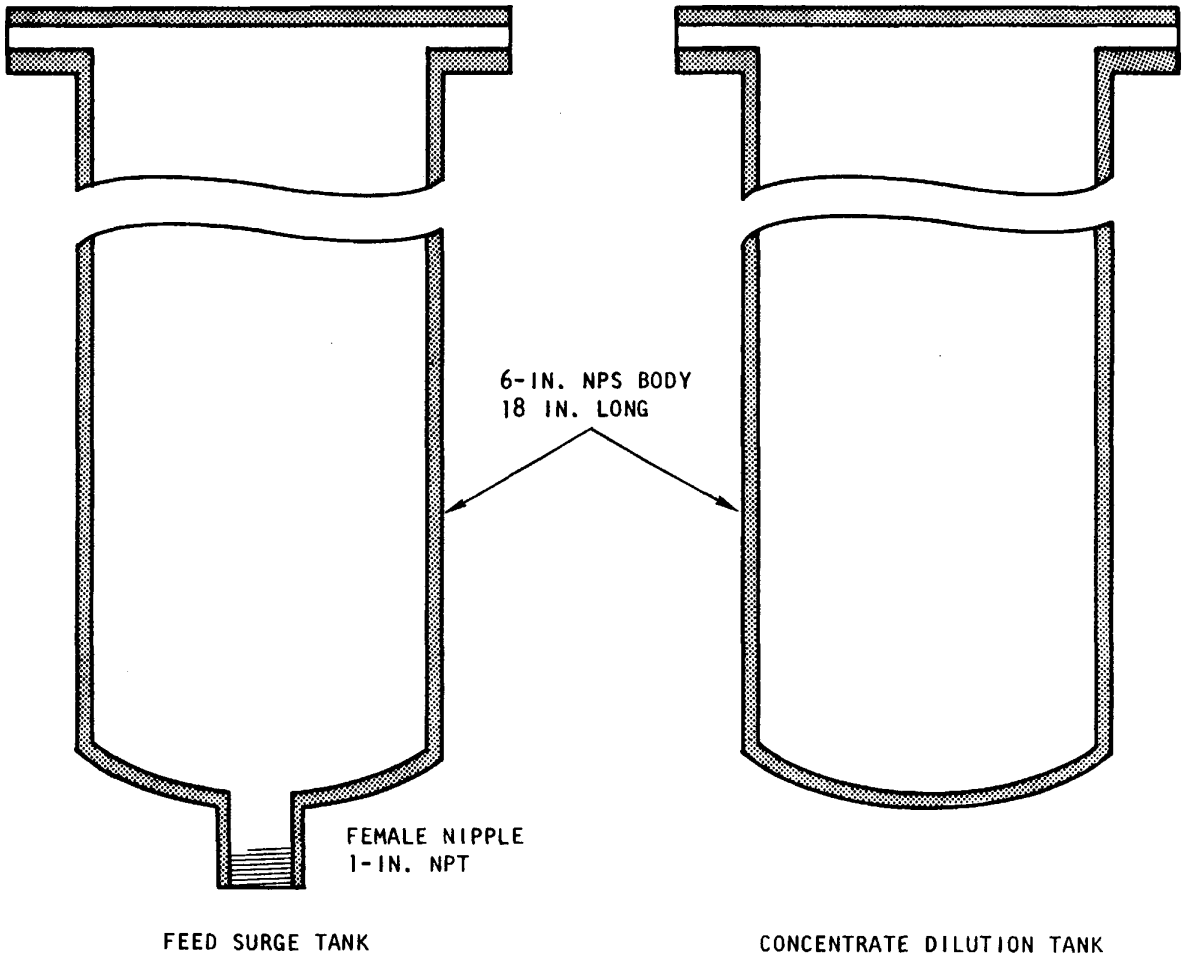

Fig. 5-31. Auxiliary tanks

Interfacing. Interfacing required for the evaporator/stripper system consists primarily of considerations of capacity. The resulting design calls for an evaporator/stripper with a minimum batch capacity of about 10 liters. Existing storage facilities have a capacity on the order of 40 liters for feed, condensate, and diluted product.

Other requirements necessary to incorporate the design into existing facilities will be the use of a liquid transfer system. This will consist of an air lift system to supply feed from the storage facility to the gravity feed surge tank and to transfer the diluted product into the existing storage tank from the dilution tank.

Control and Instrumentation. The control and instrumentation requirements for both continuous and batch operations are as follows:

1. Continuous operation (see Fig. 5-32 for details)

   a. Existing Feed Storage Tank and Feed Surge Tank. Specific gravity and liquid level monitors are in existence (Ref. 5-15). An air lift mechanism will be supplied to transport feed from the storage tank up to the feed surge tank. The transfer rate from storage will be determined by the air rate to the lift controlled by the liquid level in the surge tank.

   b. Evaporator/Stripper. The evaporator/stripper will be equipped with a liquid level indicator controlling feed rate to the vessel, a specific gravity monitor controlling concentrate removal from the vessel, and a temperature indicator controlling the flow of heating steam to the coils. A remote loading station is supplied to control the flow of sparge steam. Flowmeters are supplied on both steam lines and also on feed and concentrate lines.

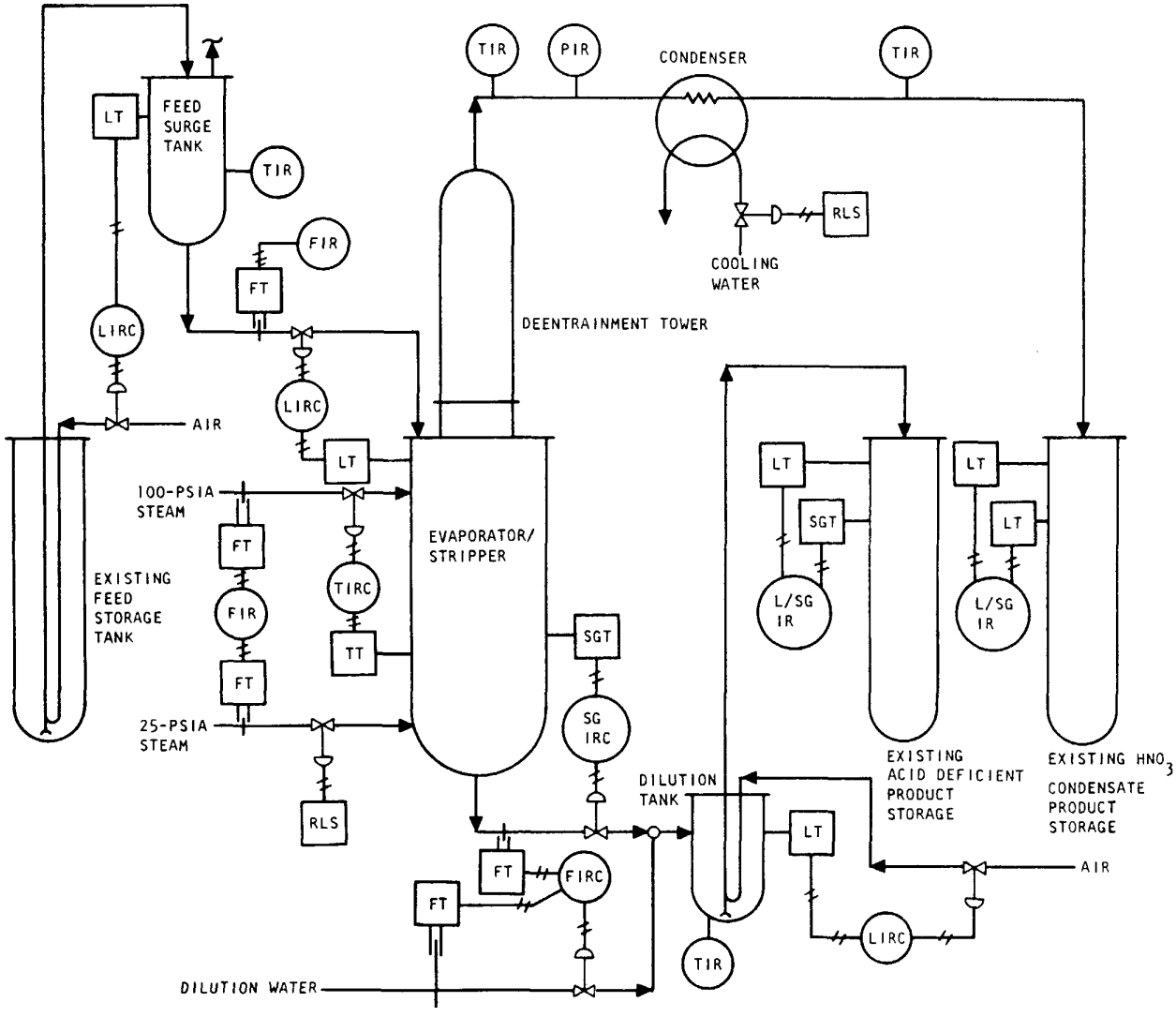

Fig. 5-32. Control and instrumentation

c. Overhead Condenser. The condenser is equipped with a remote loading station to regulate the flow of cooling water.

d. Dilution Tank. The dilution water tank is controlled by the flow of concentrate to the dilution tank. Supply air to an air lift in the dilution tanks is controlled by a liquid level indicator.

e. Condensate and Concentrate Storage Tanks. Both of the storage tanks for the evaporator/stripper products are equipped with existing liquid level and specific gravity indicators.

f. Additional Instruments. Temperature probes are installed for inlet tower feed, overhead condenser product, and diluted product measurements.

2. Batch operation

a. Existing Feed Storage and Feed Surge Tank. Specific gravity and liquid level monitors exist in both tanks. An air lift mechanism will be supplied to transport feed from storage to the evaporator/stripper via the surge tank. The quantity transferred will be measured by the difference in liquid level of storage and evaporator/stripper vessels.

b. Evaporator/Stripper. The evaporator/stripper will use a liquid level indicator and a specific gravity indicator to monitor the process. Flow of heating steam will be controlled manually until a maximum temperature of 135°C is reached. At that temperature steam flow will be controlled by a temperature indicator controller.

Sparging steam flow is controlled via a remote loading station.

c. Overhead Condenser. The overhead condenser is equipped with a remote loading station to control the flow of cooling water to the shell.

d. Dilution Tank. The dilution tank is not used in the batch process. Dilution is accomplished by adding water directly to the evaporator/stripper vessel. Quantity is determined by existing level and specific gravity indicators.

e. Condensate and Concentrate Storage Tanks. Both storage tanks for the evaporator/stripper products are equipped with existing liquid level and specific gravity indicators.

Hazards Analysis. Hazards associated with the operation of the evaporator/stripper system consist primarily of nitric acid and thorium handling.

The safe handling of nitric acid is covered in detail in the General Atomic Company Accident Prevention Manual to which this operation shall conform. Exceptions to the suggested procedures, which are necessary for the operation of the equipment, and the resulting effect on the overall safety of the operation are as follows:

1. Compressed air will be used to transfer the acidic solutions from and to storage. This is possible due to the fact that nitric acid is not flammable.

2. The acidic solution will necessarily come into direct contact with steam heated coils. With nitric acid,

there is little likelihood of fire; however, adequate space is provided for the expansion and evaporation of the acid.

The evaporator/stripper will be housed in an existing facility especially designed for handling and processing nitric acid solutions. Thus, the proposed evaporator/stripper system will be confined to a definite area designed to cope with potential accidents involving nitric acid solutions.

The handling of thorium, which is treated as a radioactive material, falls under all limitations and procedures described in the General Atomic Company Radiological Safety Guide. Adherence to those procedures should be adequate for the proposed system design.

Corrosion Coupons

Four different alloys were fabricated into coupons and installed in the 13-cm-diameter leacher. Information on the different types of alloys is included in Table 5-28. The coupons were installed at four different locations within the leacher (Fig. 5-33) and will be inspected at various time intervals.

TABLE 5-28
CORROSION COUPON ALLOYS USED IN 13-CM-DIAMETER LEACHER

Alloy	Heat No.	Coupon Size	Welding[a]
Incoloy alloy 825	HH4229F	3.099 mm x 26 mm x 74 mm	Incoloy filler metal 65
Incoloy alloy 690	NX10CLH	3.225 mm x 26 mm x 75 mm	Incoloy filler metal 625
304L stainless steel	20316	4.851 mm x 26.5 mm x 76 mm	Welded with 306 ELC wire
ARMCO 22-13-5 stainless steel	031028	Cylindrical shaped, 6.553 mm thick x 62 mm in diameter	ARMCO 22-13-5 wire

[a]All coupons were welded down the center, milled to a smooth surface, and polished with 120 grit.

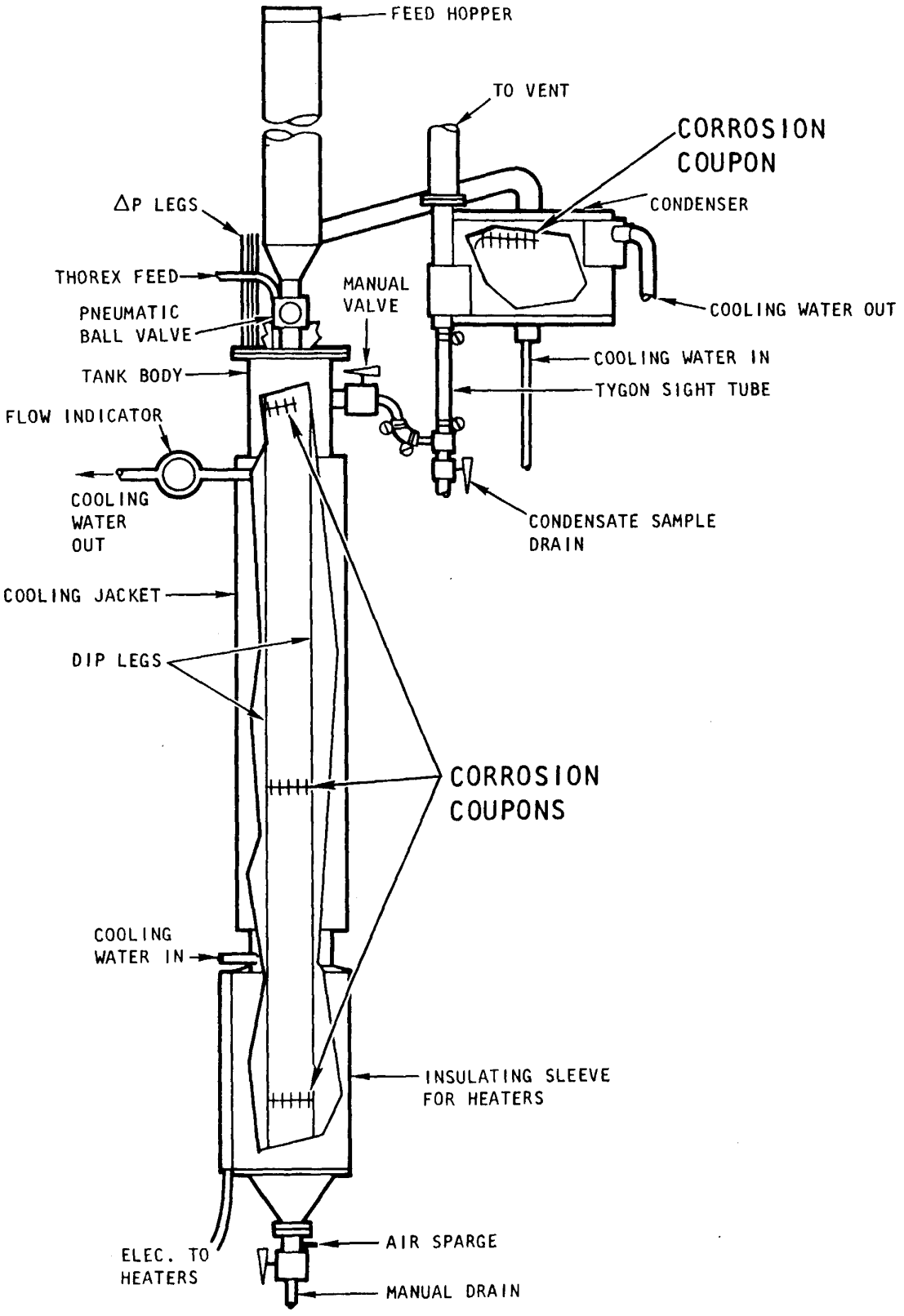

Fig. 5-33. 13-cm-diameter leacher showing positions of related equipment

REFERENCES

5-1 Haws, C. C., B. C. Finney, and W. D. Bond, "Engineering-Scale Demonstration of the Sol-Gel Process," USAEC Report ORNL-4544, Oak Ridge National Laboratory, May 1971.

5-2. Haas, P. A., "Sol-Gel Preparation of Spheres," USAEC Report ORNL-4398, Oak Ridge National Laboratory, September 1969.

5-3. "Annual Progress Report, Chemical Technology Division, Period Ending March 31, 1973," USAEC Report ORNL-4883, Oak Ridge National Laboratory, August 1973.

5-4. Wymore, C. E., I&EC Prod. Research & Development 1, 173 (1962).

5-5. Strausberg, S., General Atomic Company, private communication, January 1974.

5-6. Snider, J. W., Oak Ridge National Laboratory, private communication, February 1974.

5-7. Harrington, F., Oak Ridge National Laboratory, private communication, March 1974.

5-8. Haws, C. C., and J. W. Snider, "A Vertical Tube Furnace for Continuously Calcining Sol-Gel Derived ThO_2-UO_2 at a Rate of 35 Kilograms per Day," USAEC Report ORNL-3894, Oak Ridge National Laboratory, January 1974.

5-9. Furman, F. J., J. T. Meadar and J. D. Sease, "Microsphere Handling Techniques," USAEC Report ORNL-TM-2782, Oak Ridge National Laboratory, March 1970.

5-10. Kunii, D. and O. Levenspiel, Fluidization Engineering, John Wiley, New York, 1969.

5-11. Davidson, J. F., and D. Harrison, Fluidization, Academic Press, New York, 1971.

5-12. Rainey, R. H., "Laboratory Development of the Acid Thorex Process for Recovery of Thorium Reactor Fuel," Nucl. Sci. Eng. 10, 367 (1961).

5-13. Rainey, R. H., "Laboratory Development of the Acid Thorex Process for Recovery of Consolidated Edison Thorium Reactor Fuel," USAEC Report ORNL-3155, Oak Ridge National Laboratory, 1961.

5-14. Kuchler, L., L. Schäfer, and B. Wojtech, "The Thorex Two-Stage Process for Reprocessing Thorium Reactor Fuel with High Burnup," Kerntecknik 13, 319 (1971).

5-15. Kuchler, L., L. Schäfer, and B. Wojtech, "Laboratory and Hot-Cell Experiments on the Applicability of the Acid-Thorex Process for Recovery of Thorium Reactor Fuel with High Burnup," Kerntecknik 12, 327 (1970).

5-16. Nichols, J. P., "Soluble Neutron Poisons as a Primary Criticality Control in Shielded and Contained Radiochemical Facilities," USAEC Report ORNL-3309, Oak Ridge National Laboratory, July 26, 1962.

5-17. Moore, J. G., and R. H. Rainey, "Chemical Feasibility of Nuclear P Poisons in Uranium-Thorium Fuel Processing Systems," Nucl. Sci. Eng. 11, 278 (1961).

BIBLIOGRAPHY FOR CONCEPTUAL FLOWSHEETS AND MATERIAL BALANCES FOR REFABRICATION

Desai, V. J., and M. A. Ammur, "Gelation of Thoria-Urania (sic) Sols," USAEC Report ORNL-MIT-78, Oak Ridge National Laboratory, April 1969.

Haas, P. A., and S. D. Clinton, "Preparation of Thoria and Mixed Oxide Microspheres," USAEC Report ORNL-TM-1281, Oak Ridge National Laboratory, November 1965.

Haas, P. A., F. C. Kitts, and H. Beutler, "Preparation of Reactor Fuels by Sol-Gel Processes," Chem. Eng. Progr., Symp. Ser. No. 80 63, 16 (1967).

Haws, C. C., J. L. Matherne, F. W. Miles, and J. E. Van Cleve, "Summary of the Kilorod Project," USAEC Report ORNL-3681, Oak Ridge National Laboratory, August 1965.

Luina, A. P., P. A. Haas, and C. C. Haws, "Application of Ion Exchange for Recycle of 2-Ethyl-1-Hexanol," USAEC Report ORNL-TM-3226, Oak Ridge National Laboratory, February 1971.

Moore, J. G., "A Sol-Gel Process for Preparing ThO_2-UO_3 Sols," USAEC Report ORNL-4095, Oak Ridge National Laboratory, October 1967.

Pitcher, W. H., and R. S. Dillon, "Sol Properties at Various Stages During Formation of ThO_2-UO_3 Sols," USAEC Report ORNL-MIT-54, Oak Ridge National Laboratory, May 1968.

Snider, J. W., "The Design of Engineering-Scale SOLEX Equipment," USAEC Report ORNL-4256, Oak Ridge National Laboratory, April 1969.

"Quarterly Report, Unit Operations Section, July-September 1967," USAEC Report ORNL-4234, Oak Ridge National Laboratory, July 1969.

"Gas-Cooled Reactor Monthly Programs at Oak Ridge National Laboratory, Monthly Report for October 1973," Oak Ridge National Laboratory Report GCR: 73-13.

TASK VIII
PHYSICS AND FUEL MANAGEMENT

ENDF/B PARTICIPATION

Cross Sections and Codes

Adler-Adler multilevel resolved resonance algorithms were added to the GAND2 and GFE2 cross-section processing codes. The revised codes were used to prepare Pa-233 and U-233 data sets from the ENDF/B Version 3 data file. Several minor problems with the Version 3 data for these nuclides were noted. In the case of Pa-233, a small broad resonance at 0.43 eV probably should not be included because it is now thought to be spurious. Also, the number of degrees of freedom for the p-wave neutron width distribution is incorrectly specified twice in the unresolved resonance data.

The ENDF/B version 3 data for U-233 were found to lack angular distribution data for the n,2n and n,3n reactions and also to have incorrect upper energy limits ("U" values) for the second and third subsections of the fission neutron energy spectrum representation. Detailed comments on these points are being prepared for transmittal to the Cross Section Evaluation Working Group (CSEWG).

A report documenting the GANDY3 unresolved resonance cross-section computation code was prepared and issued (Ref. 8-1). The GANDY3 code will be sent to the Argonne Code Center following AEC patent clearance.

The GFE2 code was extended to treat the unusual fission neutron energy spectrum representation used in the ENDF/B Version 3 data for U-233. The revised versions of the GAND2 and GFE2 neutron cross-

section processing codes used to prepare data from the ENDF/B Version 3 data file are named GAND3 and GFE3. The major revisions include more general nonelastic scattering transfer array algorithms and an Adler-Adler multilevel resolved resonance capability. Documentation and transmittal of the GAND3 and GFE3 codes to the Argonne Code Center is planned.

Preliminary Assessment of the Effect of Plutonium Cross-Section Uncertainties on Plutonium Utilization in HTGRs

A preliminary study of the effect of trans-Pu-241 isotopes on the reactivity lifetime of a Th-Pu HTGR has been made. Although the treatment is quite approximate, it is clear that the effect of the trans-Pu-241 isotopes is small compared to the burnups of U-233, Pu-239, and Pu-241 which essentially determine the end of cycle (EOC) condition.

Data for the most important decay modes were obtained from Nuclear Data (Ref. 8-2).* The only important source of Am-241 is Pu-241, 13.2y → Am-241, 458y → Np-347. Other decay chains of interest include:

$$\text{Am-241}(n,\gamma) \begin{cases} 19\% \rightarrow \text{Am-242m, 152y} \quad \text{Am-242g} \\ 81\% \rightarrow \text{Am-242g, 16h} \begin{cases} 83\% \rightarrow \text{Cm-242, 163d} \rightarrow \text{Pu-238} \\ 17\% \rightarrow \text{Pu-242} \end{cases} \end{cases}$$

$$\text{Pu-242, } 4 \times 10^5\text{y} \rightarrow \text{U-238}$$

$$\text{Pu-243, 5h} \rightarrow \text{Am-243, } 8 \times 10^3\text{y}$$

$$\text{Am-244, 10.1h} \rightarrow \text{Cm-244, 17.6y} \rightarrow \text{Pu-242}$$

*Values for A given in the volumes listed in Ref. 8-2 are A = 241 (1971), A = 242 (1970), and A = 243-261 (1969/1970).

It should be noted that Am-242g, Pu-243, and Am-244 are so short lived that they will be removed through natural decay and not through neutron absorption.

In order to obtain estimates of the various reaction rates near EOC, masses of the various isotopes have been multiplied by their thermal neutron capture and fission cross sections. The masses M, in arbitrary units, were obtained from a calculation by Brogli (Ref. 8-3). The results are shown in Table 8-1.

Nineteen percent of the neutron absorption in Am-241 leads to Am-242m with an enormous fission cross section. This results in as many fission neutrons as absorptions in Am-241 and effectively compensates the negative effect.

The influence of Pu-242 and its neutron chain products will be somewhat reduced from the values given in Table 8-1 due to revised smaller cross sections (Refs. 8-4 through 8-7). Nevertheless, Pu-242, Am-242, and Cm-244 are true poisons with a total $M\sigma_c$ of about 7000, to be reduced perhaps to 5000. On the other hand, the destruction rate of U-233 is about 65,000 compared to a production rate of 22,000. Pu-239 is destroyed at a rate of ∿18,000 with no regeneration, while Pu-241 is removed at a rate of 155,000 with a production rate of perhaps 50,000 to 60,000.

The net removal rate of the fissile isotopes is thus about 150,000 as compared to the poison effect of ∿5000 for Pu-242 and its progeny. This does not mean that the latter should be omitted from fuel cycle calculations but only that high accuracy is not required, since the EOC is essentially determined by the burnup of the fissile isotopes.

CSEWG Thermal Reactor Benchmark Calculations Using ENDF/B Version 3 Data

A series of benchmark calculations recommended by the CSEWG for thermal reactor data testing have been performed using current reactor

TABLE 8-1

RELATIVE REACTION RATES FOR VARIOUS ISOTOPES
IN A Th-Pu HTGR AT END-OF-CYCLE, THERMAL NEUTRONS ONLY
(M = relative masses, arbitrary units)

	M	σ_c (barns)	σ_f (barns)	$M\sigma_c$	$M\sigma_f$
Th-232	3000	7.4		22,000	
U-233	114	46	525	5,250	60,000
Pu-239	18	267	745	4,800	13,400
Pu-240	25	290		7,300[a]	
Pu-241	111	380		42,000	113,000
Pu-242	104	30[b]	1020	3,100	
Am-241	4.05	600		2,450	
Am-242m	0.20	2400	7200	480	1,440
Am-242g	0.03	200	2100		
Am-243	42	85[c]		3,580	
Cm-242	5.4	20		108	
Cm-244	32	13.7	1.1	430	
				∿92,000	∿190,000

(a) This value is grossly distorted due to omission of the effect of the predominant 1-eV resonance. It should be multiplied by a factor of ∿7 to 8.

(b) Newer values are more like 20 b (see McCrosson and Hennelly, Refs. 8-4 and 8-5).

(c) This is a new value (see Simpson et al., Ref. 8-6).

reactor physics calculational methods. These calculations include:

1. Five unreflected spheres of U-235 (as uranyl nitrate) in H_2O, three of them poisoned with boron (ORNL-1/2/3/4/10).

2. Five unreflected spheres of Pu-239 (as plutonium nitrate) in H_2O (PNL-1/2/3/4/5).

3. Two H_2O-moderated lattices of 1.3%-enriched uranium metal rods in a triangular lattice (TRX-1/2).

4. Three D_2O moderated lattices of natural uranium metal rods in a triangular lattice (MIT-1/2/3).

The basic criticality results are compared with those obtained by other laboratories in Table 8-2. Computed activation parameters for the H_2O and D_2O moderated lattices are given in Table 8-3.*

Slightly better agreement between calculation and experiment was obtained than in previously reported calculations using ENDF/B Version 3 data. The longstanding discrepancy between calculated and experimental values of epithermal-to-thermal captures in U-238 persists in these calculations, which were performed using very nearly exact two spatial region resonance cross-section calculations at over 9000 energies. The calculated epithermal-to-thermal capture ratio in U-238 is about 5 to 8% larger than experimentally determined values. Epithermal fission in Pu-239 also appears to be overestimated in these and other calculations based upon the ENDF/B Version 3 data library (because of the systematically high eigenvalues computed for the harder spectrum systems). The Pu-240 resonance cross sections are probably not at fault because similar results have been obtained for systems containing 42% Pu-240 (Ref. 8-8).

---

*The results of other laboratories given in Tables 8-2 and 8-3 are preliminary values reported to the CSEWG and are subject to change.

TABLE 8-2

CRITICALITY (ENDF/B-III)

Benchmark	Description	k_{eff}			
		BAPL[a]	CRNL[a]	SRL[a]	GGA
ORNL	Unref. spheres of uranyl nitrate sol.				
-1	H/U-235=1378; R=34.595 cm	0.9965		0.9988	0.9999
-2	H/U-235=1177; R=34.595 cm	0.9963			0.9995
-3	H/U-235=1033; R=34.595 cm	0.9933			0.9963
-4	H/U-235= 971; R=34.595 cm	0.9947		0.9973	0.9980
-10	H/U-235=1835; R=61.011 cm	0.9931		0.9919	0.9956
TRX	H_2O moderated U lattices				
-1	Mod/Fuel = 2.35	0.9872	0.9808	0.9766	0.9791
-2	Mod/Fuel = 4.02	0.9913	0.9876	0.9859	0.9924
-3	Mod/Fuel = 1.00	0.9889			
-4	Mod/Fuel = 8.11	0.9925			
MIT	D_2O moderated U lattices				
-1	Mod/Fuel = 20.74		0.9801	0.9735	0.9888
-2	Mod/Fuel = 25.88		0.9804	0.9752	0.9925
-3	Mod/Fuel = 34.59		0.9826	0.9788	0.9996
PNL	Unref. spheres of Pu nitrate sol.				
-1	H/Pu-239=698; R=19.509 cm			1.0239	1.0212
-2	H/Pu-239=131; R=19.509 cm			--	1.0158
-3	H/Pu-239=1204; R=22.70 cm			0.9996	1.0012
-4	H/Pu-239=911; R=22.70 cm			1.0111	1.0089
-5	H/Pu-239=578; R=20.1265 cm			1.0197	1.0150

(a) The results of other laboratories shown here are preliminary values reported to the CSEWG and are subject to change.

TABLE 8-3

ACTIVATION PARAMETERS (ENDF/B-III)[a]

Bench-mark	ρ^{28}					δ^{25}					δ^{28}					C*	
	Exp.	BAPL[b]	CRNL[b]	SRL[b]	GGA	Exp.	BAPL	CRNL	SRL	GGA	Exp.	BAPL	CRNL	SRL	GGA	Exp.	GGA
TRX-1	1.311 ±0.020	1.422 (1.08)	1.419 (1.08)	1.454 (1.11)	1.416 (1.08)	0.0981 ±0.001	0.1031 (1.05)	0.1100 (1.12)	0.1024 (1.04)	0.0981 (1.00)	0.0914 ±0.0020	0.0894 (0.98)	0.0878 (0.96)	0.0912 (1.00)	0.0910 (1.00)	0.792 ±0.008	0.829 (1.05)
TRX-2	0.830 ±0.015	0.899 (1.08)	0.874 (1.05)	0.890 (1.07)	0.877 (1.06)	0.0608 ±0.0007	0.0649 (1.07)	0.0665 (1.09)	0.0621 (1.02)	0.0602 (0.99)	0.0667 ±0.0020	0.654 (0.98)	0.0627 (0.94)	0.0651 (0.98)	0.0659 (0.99)	0.646 ±0.002	0.661 (1.02)
MIT-1	0.498 ±0.008	--	0.532 (1.07)	0.568 (1.14)	0.534 (1.07)	0.0447 ±0.0019	--	0.0520 (1.16)	0.0538 (1.20)	0.0473 (1.06)	0.0597 ±0.0020	--	0.0529 (0.89)	0.0600 (1.00)	0.0584 (0.98)	1.017 ±0.023	0.987 (0.97)
MIT-2	0.394 ±0.002	--	0.436 (1.11)	0.466 (1.18)	0.435 (1.10)	0.0310 ±0.0030	--	0.0424 (1.37)	0.0439 (1.42)	0.0385 (1.24)	0.0596 ±0.0017	--	0.0515 (0.86)	0.0580 (0.97)	0.0562 (0.94)	0.948 ±0.020	0.929 (0.98)
MIT-3	0.305 ±0.004	--	0.340 (1.11)	0.362 (1.19)	0.334 (1.10)	0.0248 ±0.0010	--	0.0327 (1.32)	0.0338 (1.36)	0.0295 (1.19)	0.0583 ±0.0012	--	0.0504 (0.86)	0.0561 (0.96)	0.0537 (0.92)	0.859 ±0.016	0.868 (1.01)

[a] Parameters correspond to a thermal cutoff of 0.625 eV.

ρ^{28} = ratio of epithermal-to-thermal U-238 captures.

δ^{25} = ratio of epithermal-to-thermal U-235 captures.

δ^{28} = ratio of U-238 fissions to U-235 fissions.

C^* = ratio of U-238 captures to U-235 fissions.

Ratios of calculated-to-experimental values appear in parentheses.

[b] The results of other laboratories shown here are preliminary values reported to the CSEWG and are subject to change.

The specifications for these CSEWG benchmark situations were supplied by McCrosson (Ref. 8-9). After computation of a k_{eff} value of 0.983 for the PNL-2 benchmark as specified, it was learned that the specifications for this benchmark had been changed (Ref. 8-4). The complete benchmark specifications are included as Appendices A through D.

The methods used to perform these calculations are summarized as follows. The evaluated neutron cross-section data source was the ENDF/B Version 3 data file (Ref. 8-11). The GFE2 code (Ref. 8-12) was used to generate 99 group [GAM-II (Ref. 8-13) group structure] fast neutron data. The GAND2 code (Ref. 8-12) used to generate 9175 energy resonance data covering the 3355 to 2.38 eV energy range (point spacing of 85 meters/sec). The GAND2 code was also used to generate 101 energy [GATHER-II (Ref. 8-14) grid] thermal neutron data for absorber nuclides. The FLANGM code [a local modification of the FLANG-II code (Ref. 8-15)] was used to prepare 101 energy thermal neutron scattering kernels (P_o and P_1) for H in H_2O and D in D_2O from the 1969 ENDF/B scattering law data for these nuclides (materials 1002 and 1004). Effective temperatures for use in the "short collision time" approximation used in the FLANGM code for incident energies greater than 1 eV were obtained from the work of Koppel and Houston (Ref. 8-16). Free gas model thermal neutron scattering kernels for nitrogen, oxygen, and U-238 were prepared with the WTFG code (Ref. 8-17).

These cross sections were then used with the MICROX code (Ref. 8-18) to prepare 19 group cross sections for use in 48 interval P_1, S_4 calculations with the GAC version of the DTF-IV code (Ref. 8-19). The 19 energy group structure is given in Table 8-4.

The MICROX calculations for the uranium and plutonium spheres were one region modified B_1 spectrum calculations using energy-dependent bucklings determined from the geometric sizes plus an energy-dependent extrapolation length (cf. Tables 8-5 and 8-6). The bucklings were adjusted to yield eigenvalues near 1.0 in the MICROX calculation, except

TABLE 8-4

ENERGY GROUP STRUCTURE

Group Number	Lower Energy (eV)	Lower Lethargy
1	1.0×10^{7}	0.0
2	3.68×10^{6}	1.0
3	8.21×10^{5}	2.5
4	1.83×10^{5}	4.0
5	6.74×10^{4}	5.0
6	1.50×10^{4}	6.5
7	3.35×10^{3}	8.0
8	9.61×10^{2}	9.25
9	3.53×10^{2}	10.25
10	1.30×10^{2}	11.25
11	4.79×10^{1}	12.25
12	1.76×10^{1}	13.25
13	3.93	14.75
14	2.37	15.25
15	6.25×10^{-1}	16.59
16	4.14×10^{-1}	17.00
17	1.00×10^{-1}	18.42
18	4.00×10^{-2}	19.34
19	0.0	-

TABLE 8-5

DANCROFF CORRECTION FACTORS

Benchmark	Dancoff Correction Factor	Moderator Cross Section Used in Dancoff Calculation (cm^{-1})
TRX-1	0.1313	1.3243
TRX-2	0.0549	1.3881
MIT-1	0.0055	0.3479
MIT-2	0.0030	0.34817
MIT-3	0.0013	0.34844

TABLE 8-6
ORNL-1 THROUGH ORNL-4 AND ORNL-10 BUCKLINGS

Energy Group No.	Buckling (in units of 10^{-2} cm^{-2})				
	ORNL-1	ORNL-2	ORNL-3	ORNL-4	ORNL-10
1	0.360	Same	Same	Same	0.138
2	0.427	as	as	as	0.154
3	0.517	ORNL-1	ORNL-1	ORNL-1	0.173
4	0.606				0.190
5	0.633				0.195
6	0.646				0.197
7	0.652				0.198
8	0.653				0.199
9	0.653				0.199
10	0.653				0.199
11	0.653				0.199
12	0.653				0.199
13	0.653				0.199
14	0.653				0.199
15	0.663				0.200
16	0.670				0.201
17	0.681				0.203
18	0.687				0.204
19	0.691				0.205
k_∞	1.2053	1.2005	1.1935	1.1939	1.0653
k_{eff}	1.0012	1.0002	1.9966	0.9979	1.0002

for the PNL-2 benchmark which was not adjusted after the change in specification.

The MICROX calculations for the H_2O and D_2O moderated lattices were two space region modified B_1 calculations over the 15-MeV to 0.001-eV energy range using the bucklings given in the benchmark specifications. Dancoff correction factors were computed for the H_2O and D_2O moderated lattices with the GADACO code (Ref. 8-20) and are tabulated in Table 8-7.

TABLE 8-7
PNL-1 THROUGH PNL-5 BUCKLINGS

Energy Group No.	Buckling (in units of 10^{-2} cm^{-2})				
	PNL-1	PNL-2	PNL-3	PNL-4	PNL-5
1	0.815	0.733[a]	0.648	0.671	0.771
2	1.04	0.928	0.808	0.837	0.988
3	1.39	1.26	1.05	1.09	1.32
4	1.80	1.62	1.31	1.36	1.68
5	1.93	1.74	1.40	1.45	1.80
6	2.00	1.80	1.44	1.49	1.87
7	2.03	1.82	1.46	1.51	1.89
8	2.04	1.83	1.46	1.51	1.90
9	2.04	1.83	1.46	1.51	1.90
10	2.04	1.83	1.46	1.51	1.90
11	2.05	1.84	1.46	1.51	1.91
12	2.05	1.84	1.46	1.51	1.91
13	2.05	1.84	1.47	1.52	1.91
14	2.05	1.84	1.47	1.52	1.91
15	2.10	1.89	1.50	1.55	1.95
16	2.13	1.92	1.52	1.58	1.99
17	2.20	1.98	1.56	1.62	2.04
18	2.23	2.00	1.58	1.64	2.08
19	2.26	2.02	1.60	1.65	2.10
k_∞	1.6073	1.6387	1.4588	1.4870	1.6006
k_{eff}	1.0045	1.0449[a]	1.0031	1.0016	1.0058

[a] Bucklings not adjusted after the change in specification for this benchmark.

The aluminum clad was smeared into the H_2O or D_2O. The void region in the TRX-1/2 lattices was explicitly represented in the Dancoff correction factor calculations and smeared into the moderator region in the MICROX calculations.

The P_1 DTF-IV cross sections prepared by the MICROX code include an "extended transport approximation" correction for higher order scattering events (pp. 56-60 of Ref. 8-18). This correction reduced the computed eigenvalue for the PNL-2 benchmark by about 0.005 (only case checked). This correction would be much smaller for the ORNL spheres in which leakage effects are much smaller than in the PNL spheres.

In the case of the D_2O moderated lattices, a DTF-IV calculation was not performed. The results in Tables 8-2 and 8-3 for these lattices are taken directly from the MICROX output.

Typical UNIVAC-1108 (EXEC-8 multiprogramming operating system) running times for such calculations are 3 CPU min for MICROX and 5 CPU min for the GAC version of DTF-IV.

ANALYSIS OF HTGR AND HTLTR EXPERIMENTS

Significant progress has been made toward completion of the final topical report summarizing GAC analyses of the HTGR and HTLTR critical experiments.

ANALYSIS OF REACTOR NOISE AND PULSED-NEUTRON EXPERIMENTS IN LARGE HTGRs

A topical report summarizing the potential usefulness of reactor noise analysis techniques for large HTGRs was completed (Ref. 8-21).

TEST ELEMENT PROGRAM

Fuel Test Element FTE-3

Irradiation History

Fuel test element FTE-3 was irradiated in Peach Bottom Core 2 in core position A03-03 from July 11, 1971 (BOL) at 252 EFPD (Core 2) until January 7, 1972 (EOL) at 385 EFPD. FTE-3 accumulated 133 EFPD under reactor conditions as shown in Fig. 8-1, which gives reactor thermal power and thermal reactor energy versus time and includes shutdowns.

Temperature and Fluence Calculation. Calculated fast and thermal fluence profiles in the axial direction and axial peak fuel and peak center sample temperature distributions are given in Fig. 8-2 for the EOL situation. The axial temperature distribution is based on reactor operation at 95% power [i.e., 109 MW(t)] and 105% flow (i.e., 5×10^5 lb/hr $\hat{=}$ 2.27×10^5 kg/hr). These values reflect operational conditions prevailing throughout the lifetime of FTE-3 (see also Fig. 8-1). The BOL prevailing control rod configuration remained nearly constant until 342 EFPD in Core 2 (90 EFPD for FTE-3 as of October 31, 1971), when a control rod configuration change was realized. After this change the FTE-3 linear heat rate decreased $\sim$11% and then remained constant until EOL.

The BOL and EOL calculations gave nearly the same temperature results because decreasing power was compensated for by decreasing the thermal conductivity of the graphite by assuming 26 Btu/hr-ft-°F (0.1 cal/sec-cm-°C) and 16 Btu/hr-ft-°F (0.07 cal/sec-cm-°C) for BOL and EOL, respectively. Therefore the temperatures shown in Fig. 8-2 approximate fuel temperatures throughout the FTE-3 irradiation lifetime, as far as deducible from thermohydraulic calculations. (Thermocouple results indicate a different behavior, as discussed under Temperature Measurements.)

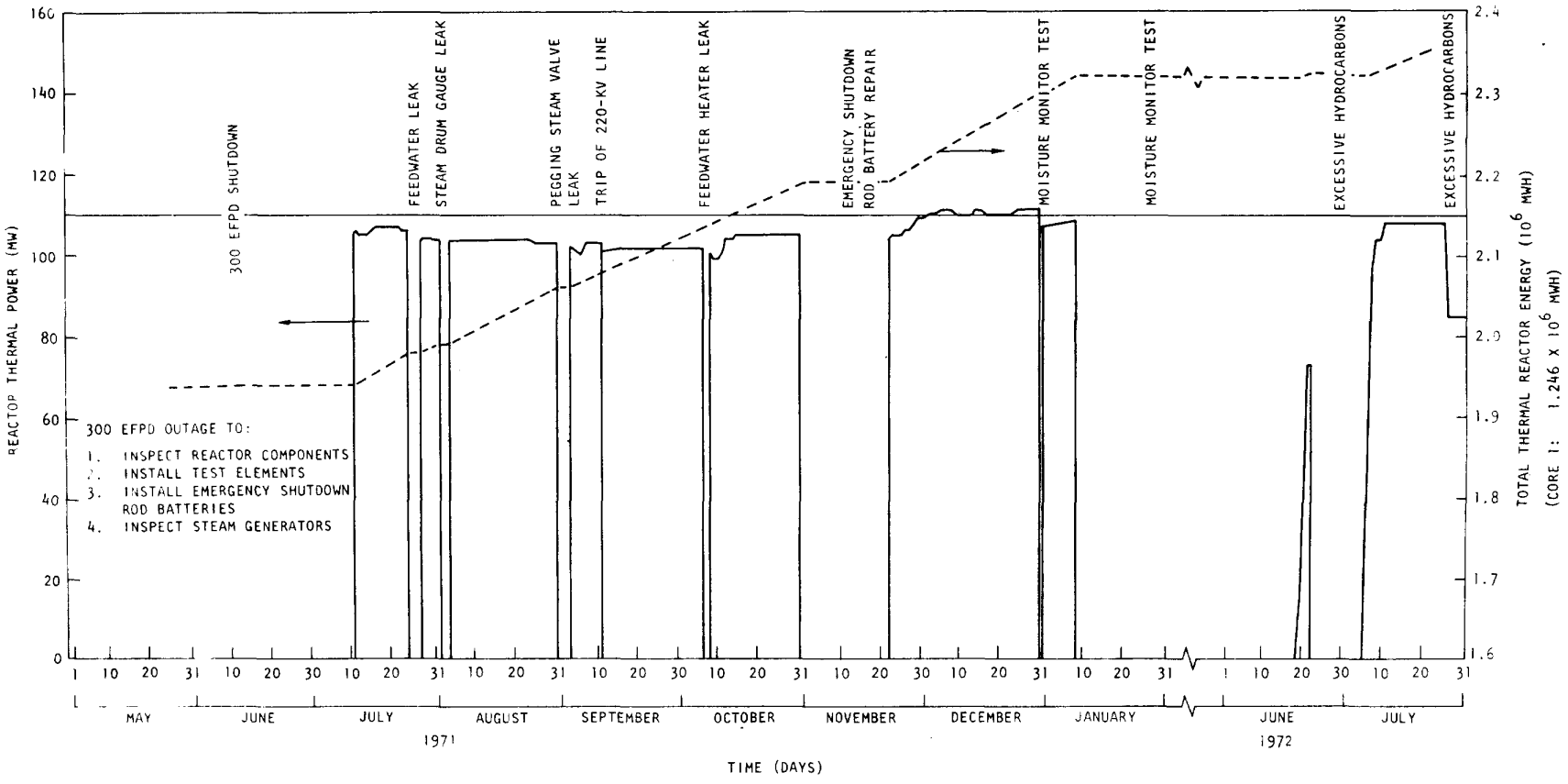

Fig. 8-1. Peach Bottom Unit 1 reactor history

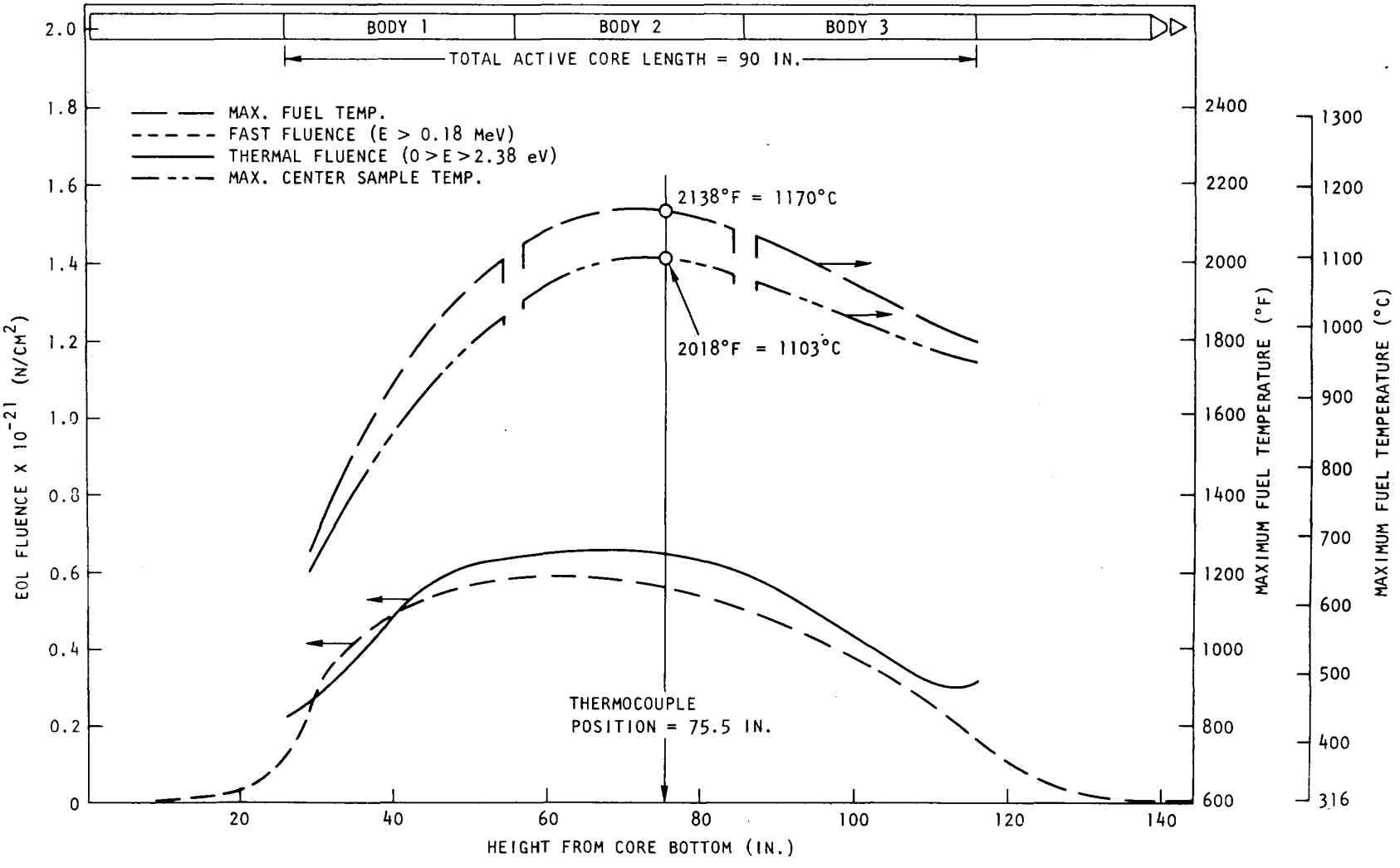

Fig. 8-2. FTE-3 calculated temperature and fluence profiles (EOL)

The maximum fuel temperatures were obtained from the TES code, a one-dimensional code for Peach Bottom test elements (Ref. 8-22), which does not treat the axial interruptions in the fuel where the individual fuel bodies meet. Although these end effects are localized, steep axial thermal gradients at the ends of the fuel bodies can be expected as shown in earlier calculations and as indicated in Fig. 8-2. Fluence distributions are achieved by hand calculations. The following peak values were determined:

EOL peak fast fluence	$\sim 0.6 \times 10^{21}$ n/cm^2 (E > 0.18 MeV)
EOL peak thermal fluence	$\sim 0.66 \times 10^{21}$ n/cm^2 (E $\leq$ 2.38 eV)
EOL* peak fuel temperature	~2138°F (1170°C ± 50°C)
EOL* peak center sample temperature	~2018°F (1103°C ± 50°C)

The axial profiles of the sleeve and coolant temperatures are shown in Fig. 8-3.

Temperature Measurements. FTE-3 was assembled with the following two thermocouples at 75.5 in. total height, (i.e., 49.4 in. active core height):

1 W/Re type near center spine samples (TC-A)
1 C/A type near outer sleeve position (TC-B)

Readings, recorded on a weekly basis, were corrected for:

1. Changes in cold junction temperatures ("standoff pin temperature") for both types (automatically carried out at Peach Bottom).
2. Adjustment in calibration equipment (for W/Re type only), where readings are 40°F too high because of change from W-5%Re/W-26%Re type to W-3%Re/W-25%Re type.
3. Decalibration of W/Re type because of permutation of emf output by neutron bombardment.

*Also average during life.

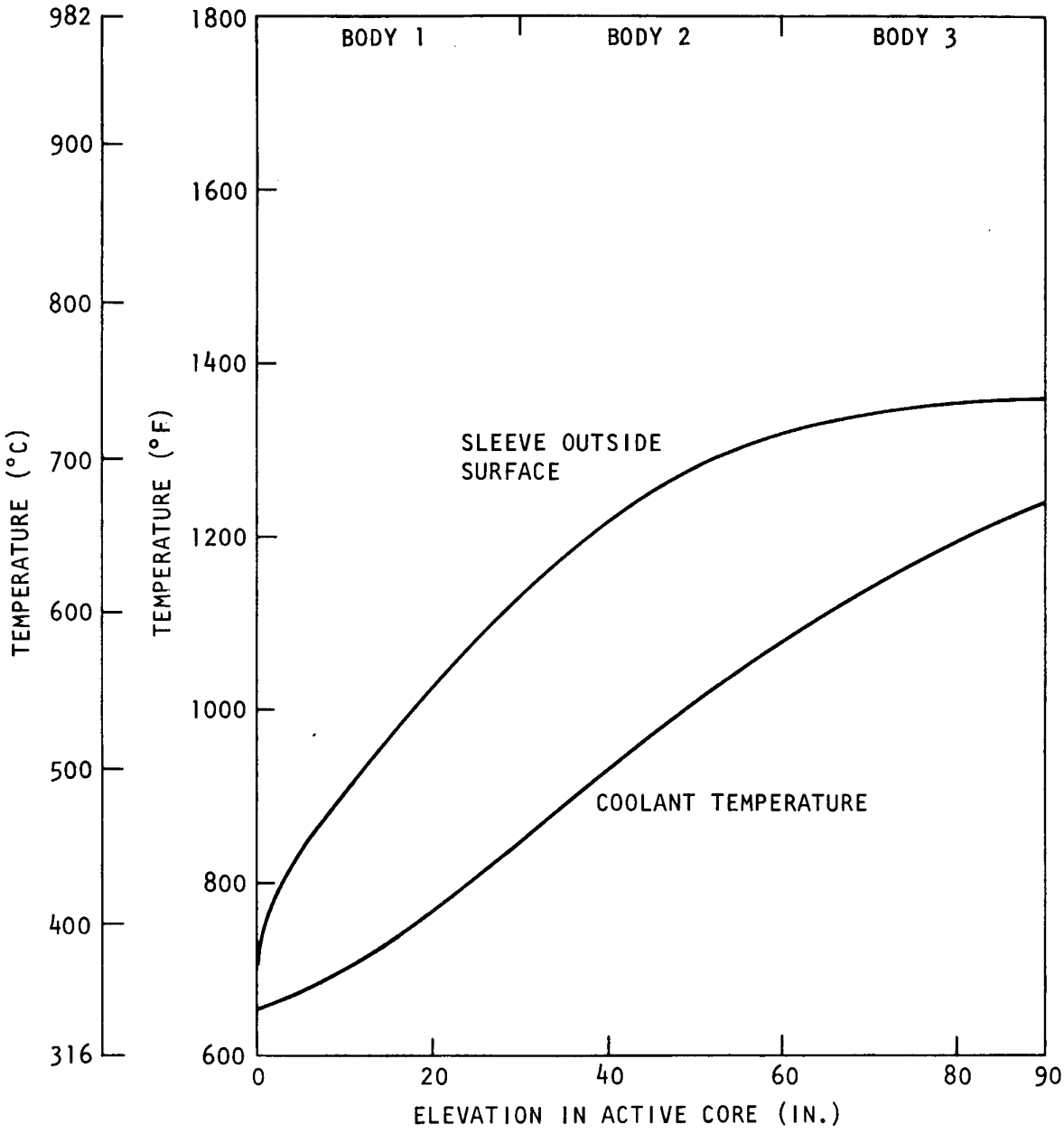

Fig. 8-3. FTE-3 sleeve outside surface and coolant temperatures

The latter is suggested to be a function of thermal fluence, for which the following correction has been derived from capsule experiments [see earlier Quarterly Progress Report Gulf-GA-A12515 (Fig. 8-1) and also Ref. 8-23]:

$$T_a = \frac{T_i - A(\psi)}{B(\psi)} \quad ,$$

where

T_a = actual temperature (corrected signal), °C
T_i = irradiation temperature (uncorrected signal), °C
$A(\psi)$ = $0.183 + \psi \cdot (3.02 - 0.215 \cdot \psi)$, °C
$B(\psi)$ = $0.993 - \psi \cdot (0.201 - 0.009 \cdot \psi)$, dimensionless
ψ = thermal fluence, 10^{21} n/cm^2 (E < 2.38 eV)

The two correction terms $A(\psi)$ and $B(\psi)$ are plotted in Fig. 8-4. The corrected thermocouple readings versus time are shown in Fig. 8-5. Permutation corrections for the W/Re thermocouple are up to 55°C, as also indicated in Fig. 8-5.

Four different time phases can be distinguished, as summarized in Table 8-8. The average readings for the W/Re-type thermocouple decrease with time. For the C/A-type thermocouple, the readings are nearly constant except for a single possible temperature spike at BOL. Comparison of the temperature difference between two corresponding thermocouples and the calculated difference (deduced from Table 8-9) shows poor agreement.

Table 8-9 gives the calculated corrections (Ref. 8-24), for different power factors and lifetimes, by which the peak fuel temperature (at the same axial position as the thermocouples) can be deduced from the thermocouple reading. This has been done for the four different time phases during the FTE-3 irradiation (Table 8-10 and also Fig. 8-5).

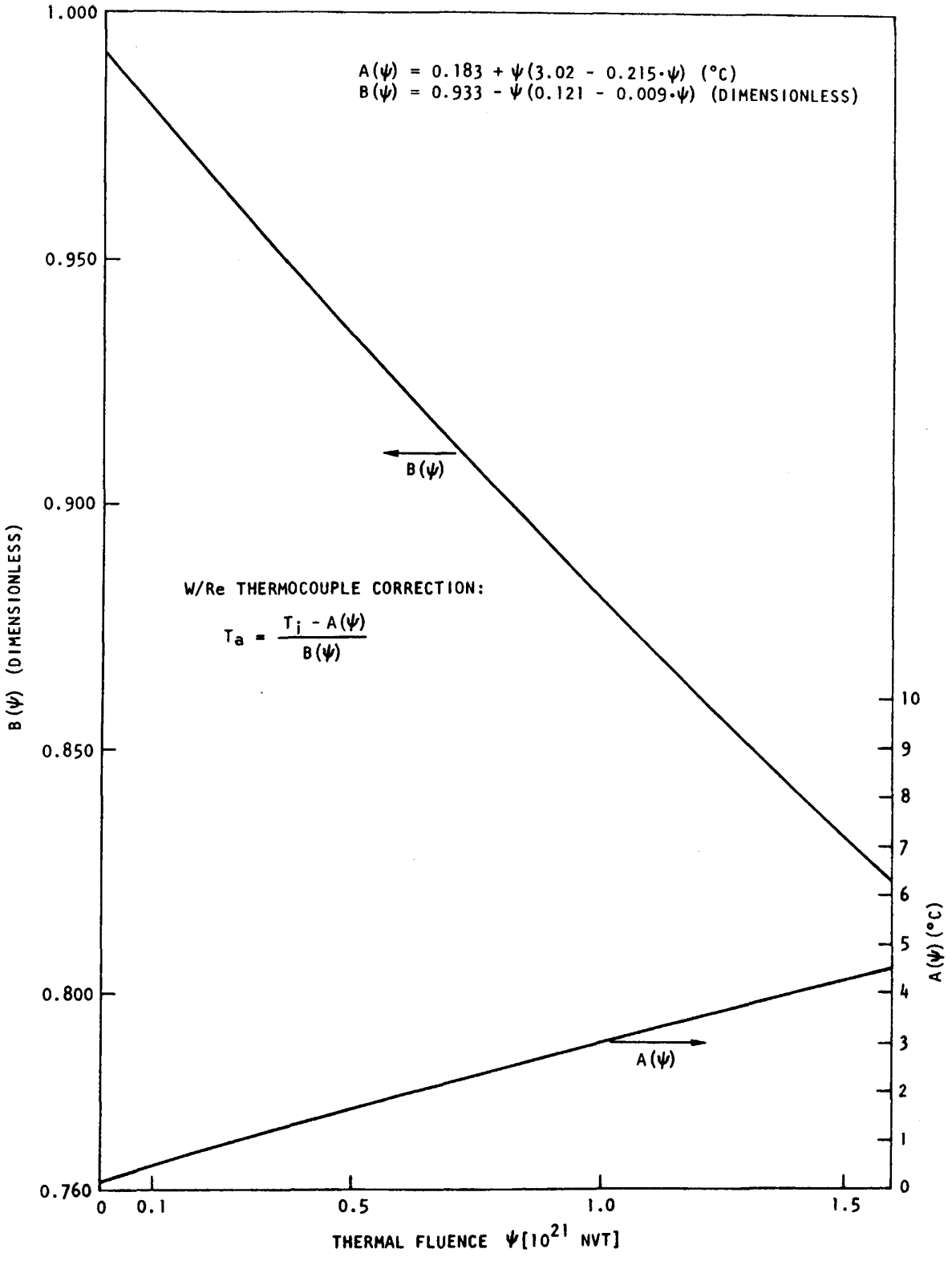

Fig. 8-4. Correction terms for W/Re thermocouple permutation

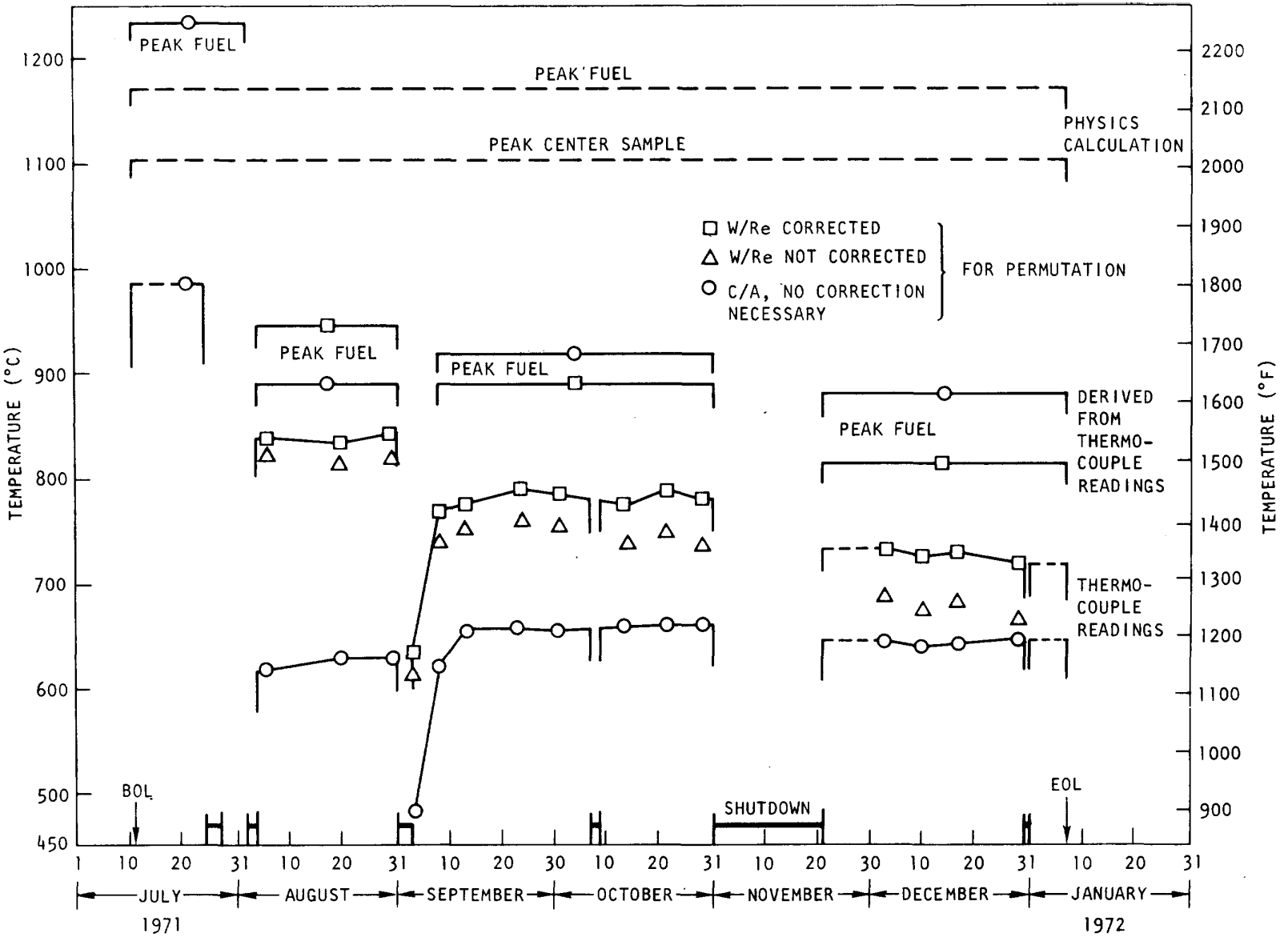

Fig. 8-5. Temperature history from thermocouple readings for FTE-3

TABLE 8-8

FTE-3 AVERAGE THERMOCOUPLE READINGS

Time Phase	Period Covered	Thermocouple Readings				Thermal and Physics Calculations	
		No. of Readings	W/Re (TC-A) (°C)	C/A (TC-B) (°C)	ΔT (°C)	ΔT (°C)	Power Factor
1	7/11/71 - 8/2/71	1	---	985(a)	---	140	0.96
2	8/4/71 - 8/31/71	3	837	624	213	168	0.93
3	9/3/71 - 10/31/71	7	780	652	128	168	0.93
4	11/2/71 - 1/7/72	4	725	641	84	174	0.84

(a) Questionable reading.

TABLE 8-9

ΔT CORRECTION FOR THERMOCOUPLE READINGS AND PEAK FUEL TEMPERATURE
(at Same Axial Level)

	Power Factor = 0.95			Power Factor = 0.85		
	BOL k=25[b]	MOL[a]	EOL k=16	BOL k=25	MOL[a]	EOL k=16
W/Re (TC-A) ΔT, °C	108	98	88	97	88	79
C/A (TC-B) ΔT, °C	248	266	283	222	238	253
ΔT (C/A - W/Re), °C	140	168	195	125	150	174
Time Phase (in Tables 8-8 and 8-10)	1	2,3	---	---	4	---

[a] MOL (middle of life): arithmetrical average of BOL and EOL, chosen because of short irradiation time (0.6×10^{21} n/cm^2, E > 0.18 MeV) for FTE-3.

[b] k = thermal conductivity in Btu/hr-ft-°F.

TABLE 8-10

FTE-3 PEAK FUEL TEMPERATURES (°C) FROM THERMOCOUPLE READINGS (TABLE 8-8) AND CORRECTION (TABLE 8-9)

	1[a]	2	3	4
From W/Re readings	--	945	888	813
From C/A readings	1233[b]	890	918	859
Average	1233[b]	918	898	836

[a] Time phase.

[b] Questionable measurement.

Agreement between the uprated C/A and W/Re thermocouple readings is in the range of 20° to 55°C, which seems to be reasonable considering the raw nature of interpolation used.

The thermocouple-derived peak fuel temperature near BOL confirms the temperature level as derived from physics calculations; however, this is based on only one measurement and is therefore questionable. Otherwise, there must have been a drastic change between time phases 1 and 2 since the peak fuel temperatures for time phases 2, 3, and 4 are at the 900°C level in comparison with 1200°C in phase 1.

The following conclusions can be drawn from the temperature evaluation:

1. The overall tendency is decreasing temperature with time.

2. Thermocouple readings indicate an average (during life) peak fuel temperature of 900°C ± 100°C, which remains in disagreement with a calculated average (during life) peak fuel temperature of 1170°C ± 50°C.

3. The discrepancy between predicted and measured temperatures can be interpreted to mean that power factors are about 30% lower than anticipated (340°C gas entry temperature):

$$\frac{900 - 340}{1170 - 340} = 0.675$$

By this means, temperature profiles in Fig. 8-2 have to be downrated when thermocouple readings are used. This leads to 45°C lower peak center sample temperatures as compared with 67°C as calculated.

4. Preirradiation and postirradiation thermocouple resistance measurements are in very good agreement (see section on Hot Cell results), so that malfunctioning can be excluded. (Misconnection of thermocouples at Peach Bottom can, however, be possible.)

Gamma Scan Results

Upon removal during the 385 EFPD shutdown, FTE-3 was gamma scanned at Peach Bottom for determination of the fueled length. This was done by the Peach Bottom standard procedure, where the fuel element is slowly raised (or lowered) into the charge machine, passing a collimator slit in the radial shielding. Gamma radiation that traverses the collimator path is detected by a scintillation crystal multiplier assembly and amplified. Both the count rate and the element position are recorded simultaneously on a strip chart, from which the actual measurement of the fueled length is obtained.

The gamma scan strip chart for FTE-3 is shown in Fig. 8-6. The average traverse distance (Ref. 8-25) (i.e., averaged over the whole fueled length of 90 in.) is 3.2432 in. ± 0.0036 in., where the +0.0036 in. applies to the bottom end and the -0.0036 in. to the top end of the fueled length. These corrections are caused by the change in the vertical velocity of the fuel element during measurements that originates from the finite thickness of the charge machine lifting tapes, which are wound on a drum.

For FTE-3 with three equal-length fuel bodies, the average transverse distance for each body is:

$$3.2432 \begin{Bmatrix} +0.0024 \text{ in. bottom fuel body} \\ +\ 0 \quad \text{in. center fuel body} \\ -0.0024 \text{ in. top fuel body} \end{Bmatrix} = \begin{Bmatrix} +0.07\% \\ +\ 0 \\ -0.07\% \end{Bmatrix}$$

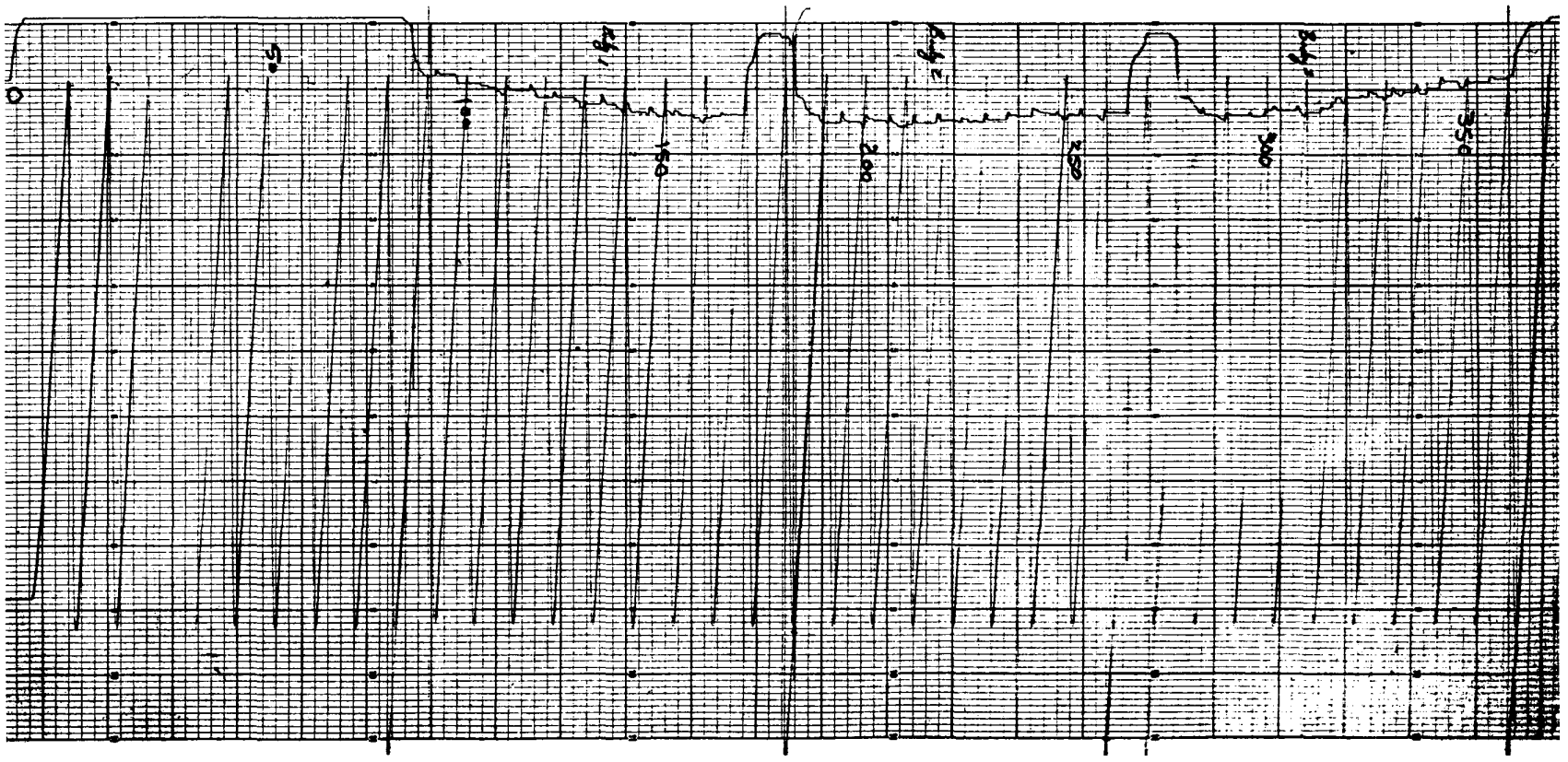

Fig. 8-6. FTE-3 gamma scan trace

The gamma scan results are summarized in Table 8-11 together with comparative measurements. The bottom and top fuel body measurements agree fairly well with length changes deduced from plenum measurements (i.e., the free distance between the fuel stack and the end of the graphite fuel body). Averaged radial and axial fuel rod measurements (i.e., shrinkage values) are up to 100% higher than the plenum measurements because of the different nature of these measurements. One chip between two fuel rods could change a total stack length measurement significantly; concave end cup effects, increased during irradiation, would show up in individual rod measurements but not in overall stack length. Therefore, it is not surprising that the plenum and gamma scan measurements show lower shrinkage values than the radial and axial fuel rod measurements in Table 8-11.

The -0.3% gamma scan result for the center fuel body compared with the -0.8% plenum and -1.4% fuel rod measurements, however, is not only far out of range, but even contradictory to theory and experience. The center body with the highest flux levels should show the highest shrinkage values, especially for short-term irradiations as in FTE-3. All other measurements in Table 8-11 confirm this tendency except this single gamma scan result. Therefore, an evaluation error is suspected. Unfortunately the original gamma-scan strip chart is not available, but even the reduced copy in Fig. 8-6 indicates a value on the order of -1%.

The following conclusions can be drawn from the gamma-scan results:

1. Gamma-scanning gives a reasonable indication of fueled stack length changes during irradiation.

2. Fuel rod dimensional change data should be obtained from individual rod measurements.

TABLE 8-11

FTE-3 FUEL STACK DIMENSIONAL CHANGES

	FTE-3/1 Bottom	FTE-3/2 Center	FTE-3/3 Top
Average fuel stack length[a] (preirradiation), in.	27.330	27.300	27.334
Gamma scan ($\Delta L/L$), %	-0.77	(-0.26)[b]	-0.71
Plenum measurement[a] ($\Delta L/L$), %	-0.59	-0.82	-0.59
Axial fuel rod measurement[a] ($\Delta L/L$), %	-0.82	-1.36	-1.02
Radial fuel rod measurement[a] ($\Delta D/D$), %	-0.90	-1.46	-1.17

[a] Averaged over all six fuel zones.
[b] Suspected evaluation error.

Hot Cell Examinations and Results

Upon arrival from Peach Bottom, the helium-filled aluminum canister containing fuel test element FTE-3 was removed from the Hallam cask and injected into the high level cell without incident. The canister was girdle cut approximately 3/16 in. deep and 30 in. from the bottom end and the piece removed, thereby exposing the thermocouple contacts. Thermocouple resistance readings were made as recorded in Table 8-12. Comparison with preirradiation measurements shows almost no changes, and it can thus be concluded that the operational behavior of the thermocouples was good. Pieces of the canister at the opposite end were subsequently girdle cut and discarded until the element was entirely exposed. A composite photograph of the total element is included as Fig. 8-7.

In order to section the fuel element, it was supported horizontally by a series of U-rollers, which facilitated horizontal and rotational movement. A special extension drill was inserted through the purge gas inlet hole in the upper reflector and a hole was drilled through the porous graphite plug. The fuel bodies were then seated against the bottom connector by using a push rod through this hole and applying force. While the bodies were held down, the upper reflector was removed by plunge cutting through the sleeve at a point about 2 in. below the sleeve-reflector joint. The sleeve was then girdle cut at a point about 16 in. above the sleeve-bottom connector joint. After inspecting the top surface of the graphite cloth at the upper end of the internal trap (see Fig. 8-8) and finding no fuel particles, the bottom section of the lower reflector was removed; 2 in. of the C/A thermocouple cold junction was saved and stored.

The fuel bodies were subsequently removed from the sleeve by inserting a push rod into the upper opening, holding the sleeve, and applying a force. Each individual fuel body was carefully examined externally, and the graphite integrity was assessed. Following visual inspection, the fuel bodies were placed in a special holding fixture to facilitate

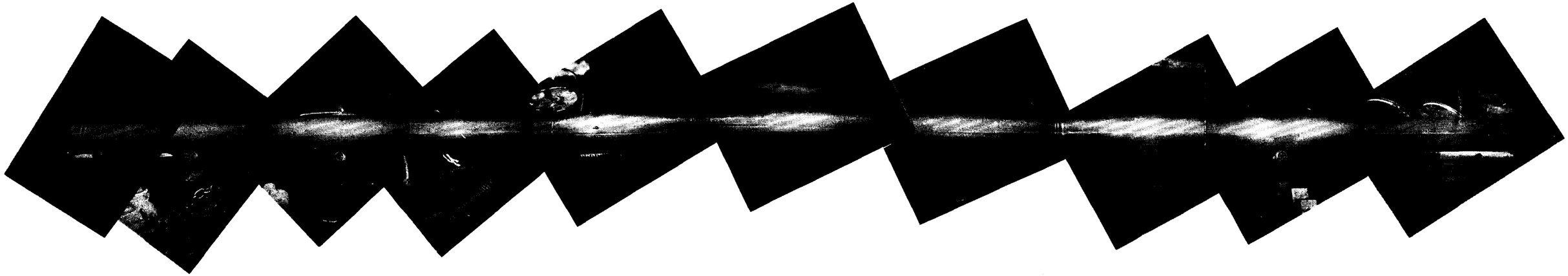

Fig. 8-7. FTE-3 composite photograph of total element (mirror image)

TABLE 8-12

FTE-3 THERMOCOUPLE RESISTANCE MEASUREMENTS[a]

	+ to Ground Circuit (Ω)			- to Ground Circuit (Ω)			Loop (Ω)			
	Pre-Irrad.	Post-Irrad.	ΔΩ	Pre-Irrad.	Post-Irrad.	ΔΩ	Pre-Irrad.	Post-Irrad.	ΔΩ	Remarks
Thermocouple (ARI S/N 22163) W-3%Re/W-25%Re	4.3	4.5	+0.2	11.8	12.0	+0.2	15.3	15.0	-0.3	Satisfactory
Thermocouple B (ARI S/N 22170) C/A	34.1	37.0	+2.9	15.8	15.0	-0.8	48.0	53.0	+5.0	Satisfactory

[a] Accuracy ±1Ω.

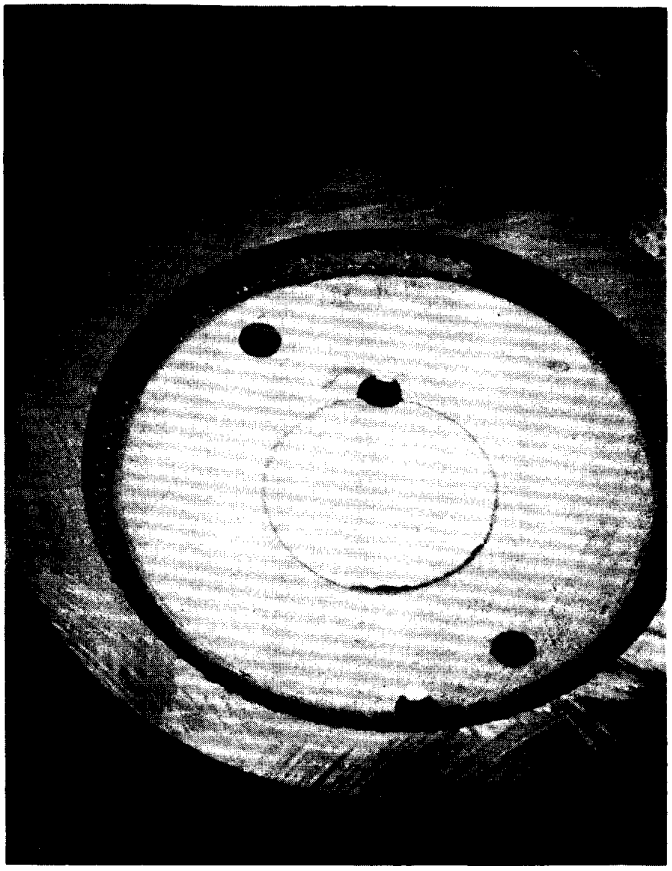

K7311-13

Fig. 8-8. FTE-3 internal trap, upper end view

the removal of the center samples. A hole was drilled through the bottom sample hole plug and a push rod was inserted. When the upper sample hole plug was unscrewed, the distances from the top of the spine samples to the edge of the holes were measured. These measurements are compared with preirradiation measurements in Table 8-13. Changes are in the range to be expected for H-327 graphite except for the spine stack in body 1, which indicates an increase in length. However, this can be related to stack perturbance (e.g., a small chip between two spine samples could have caused this effect). The spine samples were pushed out one at a time, identified, and placed in labeled glass sample bottles. All these operations were carried out over a special pan required to catch any loose fuel particles from the drilled hole. However, none were found. No problems were encountered during the removal or identification of the spine samples. The spine samples are described in Table 8-14.

Upon discharge of the spine samples, the graphite plugs capping the fuel holes were easily removed, and the distances from the top of the fuel rods to the edge of the fuel holes were measured. These measurements are compared with preirradiation measurements in Table 8-15. The overall results were discussed previously, together with gamma scanning of the fuel stack heights. A further analysis for each of the four different fuel rod types will be included in a forthcoming final topical report on FTE-3.

Holes were drilled on the bottom of the fuel bodies to enable the fuel rods to be pushed out with a 1/8-in.-diameter push rod. After all of the fuel rods had been removed, the fuel bodies were sectioned as shown in Fig. 8-9. The graphite slices have been used for autoradiography. Residual stress examinations will be carried out on some of the graphite bodies. Some development work in this area is still necessary and the results will be reported at a later date.

TABLE 8-13

DISTANCE d FROM TOP OF SPINE TO EDGE OF HOLE IN FTE-3

Body No.	Spine Stack Length (in.)	d_1 Preirrad. (in.)	d_2 Postirrad. (in.)	Δd (in.)	ΔG[(a)] (in.)	$\frac{-\Delta d + \Delta G}{L}$ (%)
1	28.58	2.027	2.000	-0.027	-0.008	+0.07
2	28.44	2.052	2.125	+0.073	-0.026	-0.35
3	28.56	2.136	2.188	+0.052	-0.018	-0.24

(a) ΔG = length change of graphite fuel body.

TABLE 8-14

FTE-3 SPINE SAMPLES

Position	Preirrad. Length (in.)	Preirrad. Weight (g)	Sample Type	Ident. No.
Body 1				
1	1.50	32.96	Stress relaxation	33
2	1.50	33.01	Stress relaxation	8
3	1.50	33.79	Stress relaxation	31
4	3.81	78.63	Mechanical test assembly	V1
5	1.26	24.62	Diffusion	3
6	1.26	24.77	Diffusion	11
7	1.26	24.54	Diffusion	24
8	1.25	24.52	Diffusion	30
9	1.26	24.69	Diffusion	42
10	3.81	76.41	Mechanical test assembly	11
11	1.25	24.60	Fission product release	75p
12	1.25	24.79	Fission product release	144p
13	1.25	24.81	Fission product release	24p
14	1.25	24.61	Fission product release	8p
15	1.25	24.98	Fission product release	117p(a)
16	1.25	25.15	Fission product release	120p
17	1.25	25.00	Fission product release	166p
18	1.42	32.42	Graphite spacer	22
	28.58			
Body 2				
1	2.50	57.20	Graphite spacer	23
2	1.25	24.51	Fission product release	61p
3	1.25	24.98	Diffusion	66
4	4.02	93.80	Alternate fuel rod concepts	2C
5	3.98	91.49	Alternate fuel rod concepts	2B
6	3.99	91.79	Alternate fuel rod concepts	2A
7	1.26	102.19	Fission product release	NB-3
8	1.25	24.92	Fission product release	11p
9	1.26	102.20	Fission product release	NB-6
10	1.25	24.69	Fission product release	28p
11	1.26	101.70	Fission product release	Nb-10
12	1.25	24.99	Fission product release	43p
13	1.26	101.58	Fission product release	Nb-14
14	1.25	24.72	Fission product release	147p
15	1.46	33.11	Graphite spacer	24
	28.44			
Body 3				
1	1.96	44.68	Graphite spacer	25
2	5.80	136.81	Thermal stability type 1	K
3	5.75	137.57	Thermal stability type 1	L
4	1.25	26.22	Thermal stability type 2	17
5	1.25	23.79	Thermal stability type 2	23
6	1.25	23.91	Thermal stability type 2	29
7	1.25	24.84	Thermal stability type 2	5
8	1.25	24.70	Thermal stability type 2	11
9	1.26	24.62	Diffusion	5
10	1.26	24.62	Diffusion	16
11	1.26	24.57	Diffusion	45
12	1.26	24.90	Diffusion	63
13	1.26	24.85	Diffusion	55
14	1.25	25.13	Fission product release	58p
15	1.25	24.53	Fission product release	92p
	28.56			

(a) Postirradiation number = 107P.

TABLE 8-15

FTE-3 FUEL STACK MEASUREMENTS

Hole Number	Preirrad. Stack Length, L[a] (Accuracy +0.031/-0.01)	ΔL/L (%)	Plenum (in.)[b] Preirrad.	Plenum (in.)[b] Postirrad.	Δp (in.)	$\frac{-\Delta p + \Delta G}{L}$[c] (%)
Body 1						
1	27.387	-1.01	2.403	2.672	+0.269	-1.01
2	27.391		2.399	-	-	-
3	27.317	-0.45	2.473	2.578	+0.105	-0.41
4	27.304		2.486	2.609	+0.123	-0.48
5	27.310	-0.36	2.480	2.531	+0.051	-0.22
6	27.341		2.449	2.578	+0.129	-0.50
7	27.284	-0.54	2.506	2.641	+0.135	-0.52
8	27.308		2.482	2.625	+0.143	-0.55
	27.330 avg		2.460 avg			-0.59 avg
Body 2						
1	27.367	-1.08	2.473	2.688	+0.215	-0.88
2	27.369		2.421	2.734	+0.313	-1.28
3	27.281	-0.78	2.509	2.703	+0.194	-0.80
4	27.284		2.506	2.688	+0.182	-0.76
5	27.277	-0.62	2.513	2.656	+0.143	-0.62
6	27.292		2.498	2.641	+0.143	-0.62
7	27.292	-0.81	2.498	2.688	+0.190	-0.79
8	27.287		2.503	2.703	+0.200	-0.82
	27.300 avg		2.490 avg			-0.82 avg
Body 3						
1	27.425	-1.06	2.365	2.641	+0.276	-1.08
2	27.422		2.368	2.634	+0.266	-1.04
3	27.305	-0.52	2.485	2.578	+0.093	-0.40
4	27.305		2.485	2.641	+0.156	-0.64
5	27.326	-0.69	2.464	2.625	+0.161	-0.65
6	27.326		2.464	2.634	+0.170	-0.72
7	27.277	-0.49	2.513	2.606	+0.096	-0.42
8	27.285		2.505	2.641	+0.136	-0.56
	27.334 avg		2.456 avg			-0.69 avg

[a] Calculated L via nominal depth = 29.79 +0.03/-0.01 in. minus plenum p. Nominal stack length = 27.16 +0.25/-0.16 in.

[b] Plenum p = distance from top of fuel rod to edge of hole.

[c] ΔG = length change of graphite fuel body.

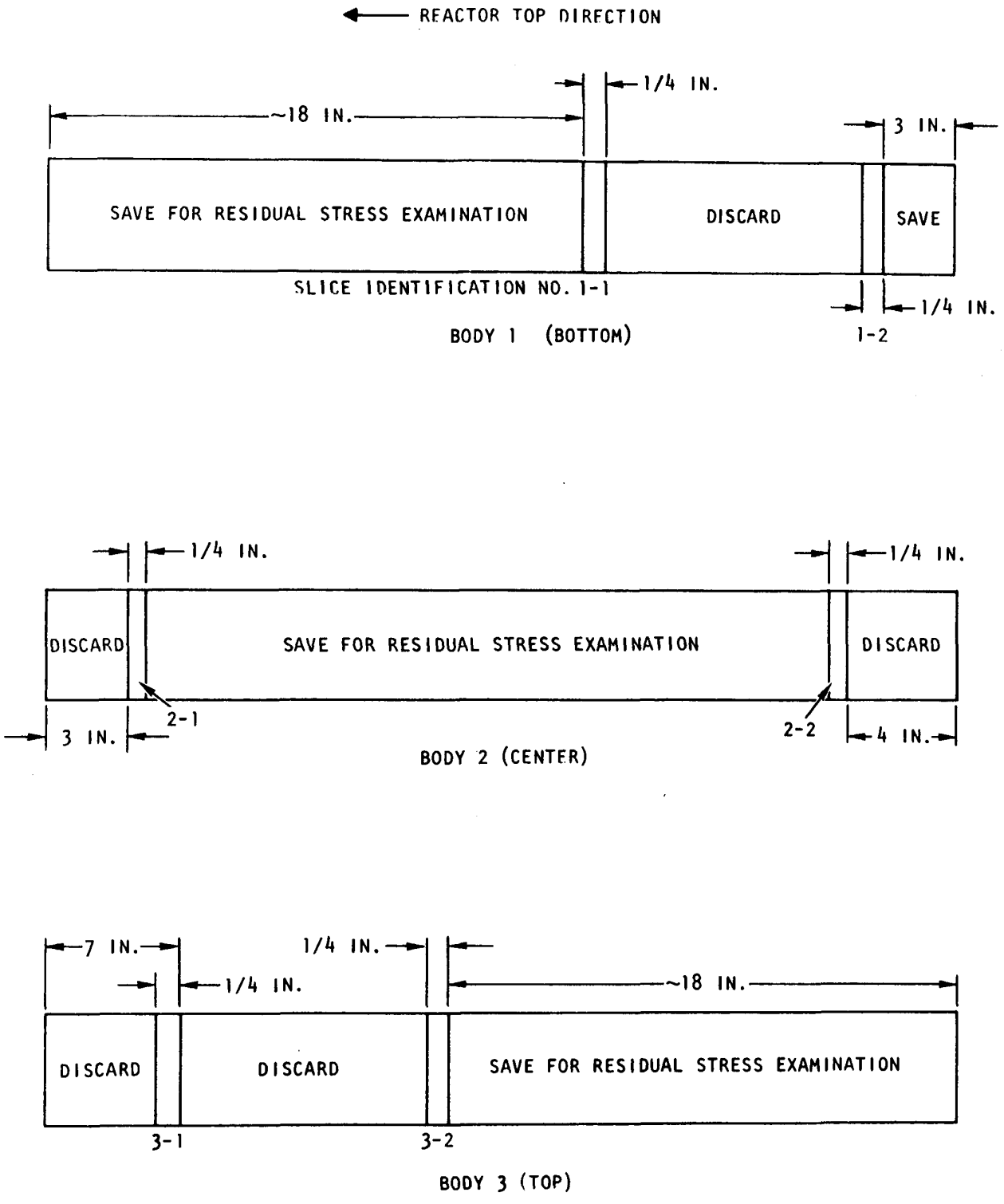

Fig. 8-9. FTE sampling of bodies for inside diameter measurements and autoradiography

REFERENCES

8-1 Mathews, D. R., and P. K. Koch, "GANDY3, A Computer Program for the Evaluation of Effective Cross Sections in the Unresolved Resonance Region," USAEC Report Gulf-GA-A12826, Gulf General Atomic, 1974.

8-2 "Nuclear Data Sheets," Volumes B3 (1969/1970), B4 (1970), and B6 (1971), Academic Press, New York.

8-3 Brogli, R., General Atomic Company, private communication, 1973.

8-4 McCrosson, F. J., "A Practical Model for Generating Resonance Energy Cross Sections for Heavy Nuclei," in Proceedings of the Third Conference on Neutron Cross Sections and Technology, March 15-17, 1971, University of Tennessee, Knoxville, Tennessee, Vol 2, USAEC Report CONF-710301, p. 714.

8-5 Hennelly, E. J., "The Heavy Actinide Cross Section Story," ibid, p. 494.

8-6 Simpson, F. B., et al., Idaho Nuclear Corporation, unpublished data, 1970.

8-7 Berreth, T. R., Idaho Nuclear Corporation, unpublished data, 1970.

8-8 Lloyd, R. C., and E. D. Clayton, "The Criticality of High Burnup Plutonium," Nucl. Sci. Eng. 52, 73 (1973).

8-9 McCrosson, F. J., Savannah River Laboratory, private communication, December 4, 1972.

8-10 McCrosson, F. J., Savannah River Laboratory, private communication, December 6, 1973.

8-11 Ozer, O., and D. Garber (Eds.), "ENDF-201, ENDF/B Summary Documentation," USAEC Report BNL-17541 (ENDF-201), Brookhaven National Laboratory, 1973.

8-12 Archibald, R. J., and D. R. Mathews, "The GAF/GAR/GAND FAst Reactor Cross Section Preparation System, GAND2 and GFE2 - Computer Programs for Preparing Input Data for the GAFGAR, GGC and MICROX Codes from an ENDF/B Format Nuclear Data File," USAEC Report GA-7542, Vol. II, Gulf General Atomic, 1973.

8-13 Joanou, G. D. and J. S. Dudek, "GAM-II - A B_3 Code for the Calculation of Fast Neutron Spectra and Associated Group Constants," General Dynamics, General Atomic Division Report GA-4265, 1963.

8-14 Joanou, G. D., C. V. Smith, and H. A. Vieweg, "GATHER-II, An IBM-7090 Code for the Calculation of Thermal Neutron Spectra and Associated Multigroup Constants," General Dynamics, General Atomic Division Report GA-4132, 1963.

8-15 Honeck, H. C., and D. R. Finch, "FLANG-II(Version 71-1), A Code to Process Thermal Neutron Data from an ENDF/B Tape," USAEC Report DP-1278, Savannah River Laboratory, 1971.

8-16 Koppel, J. U., and D. H. Houston, "Reference Manual for ENDF Thermal Neutron Scattering Data," USAEC Report GA-8774, Gulf General Atomic, 1968.

8-17 Drake, M. K., C. V. Smith, and L. J. Todt, "Description of Auxiliary Codes Used in the Preparation of Data for the GGC-3 Code," General Dynamics, General Atomic Division Report GA-7158, 1967.

8-18 Walti, P., and P. Koch, "MICROX, A Two-Region Flux Spectrum Code for the Efficient Calculation of Group Cross Sections," Gulf General Atomic Report Gulf-GA-A10827, 1972.

8-19 Archibald, R., K. D. Lathrop, and D. Mathews, "1DFX - A Revised Version of the 1DF(DTF-IV) SN Transport Theory Code," Gulf General Atomic Report Gulf-GA-B10820, 1971.

8-20 Walti, P., General Atomic Company,"GADACO - A Code for the Calculation of Dancoff Correction Factors for HTGR Fuel Elements," unpublished data, 1970.

8-21 Borgonovi, G. M., "An Assessment of Noise Analysis Techniques for Large HTGRs," USAEC Report Gulf-GA-B12823, Gulf General Atomic, 1973.

8-22 Vrouwes, J. H.L., and D. L. Hansen, "Thermal Analysis of Fuel Test Elements," General Atomic Company Report GA-A10911, to be published.

8-23 Sandefur, N. L., J. S. Steibel, and R. J. Grenda, "EMF Drift of Cromel/Alumel and W-3%Re/W-25%Re Thermocouples Measured In-Pile to High Neutron Exposures," USAEC Report Gulf-GA-A12501, Gulf General Atomic, May 24, 1973.

8-24 Scheffel, J. W., et al., "Peach Bottom Progress Report No. 2 - Annual Progress Report for the Period Ending June 30, 1972," to be published.

8-25 Scheffel, J. W., et al., "Peach Bottom 150 Full-Power Day Core Examinations," General Atomic Informal Report GAMD-8703, December 31, 1968.

TASK IX

FUEL MATERIALS DEVELOPMENT

FUEL THERMAL STABILITY

A series of thermal gradient tests was conducted on TRISO coated UC_2 particles to characterize UC_2 kernel migration as a function of temperature. The particles in the current test series include particles with 100-μm kernels, particles with 200-μm kernels, and both irradiated and unirradiated particles. The particles being heated are described in Table 9-1.

Kernel migration in carbides in a thermal gradient takes place by the process of carbon solution on the hot side of the kernel and rejection of carbon on the cold side of the kernel (Ref. 9-1). The rate of advance of the hot side of a carbide kernel in a thermal gradient is used to calculate a kernel migration coefficient (KMC), which is defined by the expression

$$KMC = \frac{dx}{dt} T^2 \frac{\Delta T^{-1}}{\Delta X} = KD_o e^{(-\Delta H/RT)} \quad , \qquad (1)$$

where $\frac{dx}{dt}$ = rate of advance of the hot kernel surface

T = temperature, °K

$\frac{\Delta T}{\Delta X}$ = temperature gradient across the kernel

K = constant which depends on material properties

D_o = pre-exponential constant

ΔH = activation energy for carbon diffusion in the fuel kernel

R = gas constant (cal/deg mole)

TABLE 9-1
LOADING PLAN, UC_2 TRISO THERMAL GRADIENT TESTING

UC_2 Batch Number	Uranium Source	Kernel Diameter (μm)	Buffer Thickness (μm)	IPyC Thickness (μm)	SiC Thickness (μm)	OPyC Thickness (μm)	Particle Condition
4000-304	Enriched	97	51	24	19	30	Unirradiated
4000-325	Enriched	93	50	22	20	27	Unirradiated
4413-5E	Enriched	110	53	24	20	23	Unirradiated and irradiated[(a)]
4413-137D	Depleted	200	47	35	18	50	Unirradiated
4423-3D	Depleted	200	41	36	16	50	Unirradiated
4161-01-034	Enriched	179	87	28	25	35	Unirradiated

[(a)] Irradiated in cell 3 thimble 3 of experiment P13L to a burnup of 75% FIMA at a fast neutron dose of 7.8×10^{21} n/cm^2 and an estimated average temperature of 1475°C.

Scott and Stansfield (Ref. 9-2) have measured kernel migration in irradiated and unirradiated carbide particles. The work reported here is a continuation of their work. Carbide fuel thermal gradient experiments in this study will fill data gaps in previous unirradiated UC_2 TRISO particle experiments.

The experimental arrangements and procedures used for thermal gradient testing have been described previously (Ref. 9-2). Kernel migration was induced by heating particles in the temperature range 1260° to 1880°C. Specifically, unirradiated particles were heated from 3 to 2420 hours at average temperatures of 1260°, 1325°, 1525°, 1590°, 1725°, and 1880°C. The heating time was decreased with increasing temperature. Thermal gradients for the unirradiated particle tests ranged from 0.4 to 0.6 °C/μm. The irradiated UC_2 particles were heated for a total of 5574 hours at 1315°, 1390°, or 1460°C at a thermal gradient of approximately 0.024 °C/μm. Kernel migration rates were determined from radiographs by comparing the distance between the fuel kernel and SiC layer, at the hot side of the particles, as a function of time and temperature.

The migration distance was measured as a function of time for each particle heated in these experiments. The range in migration behavior observed in this test series is illustrated in Figs. 9-1a through 9-1c, which show migration distance as a function of annealing time at 1525°C for three particles from batch 4161-01-034. Comparison of the slope of migration distance versus time shown in Figs. 9-1a through 9-1c for the first 250 hours of migration indicates that the initial migration rates were within a factor of 2 of each other for the three particles shown.

The migration behavior of the three particles differed widely, however, for times longer than 250 hours. In one case (Fig. 9-1a), the kernel stopped migrating after 500 hours of heating and a total migration distance of about 88 μm. No more migration had been detected when the test was stopped after 1250 hours. In the second case (Fig. 9-1b), kernel movement was arrested after the kernel migrated approximately 125 μm in 300 hours.

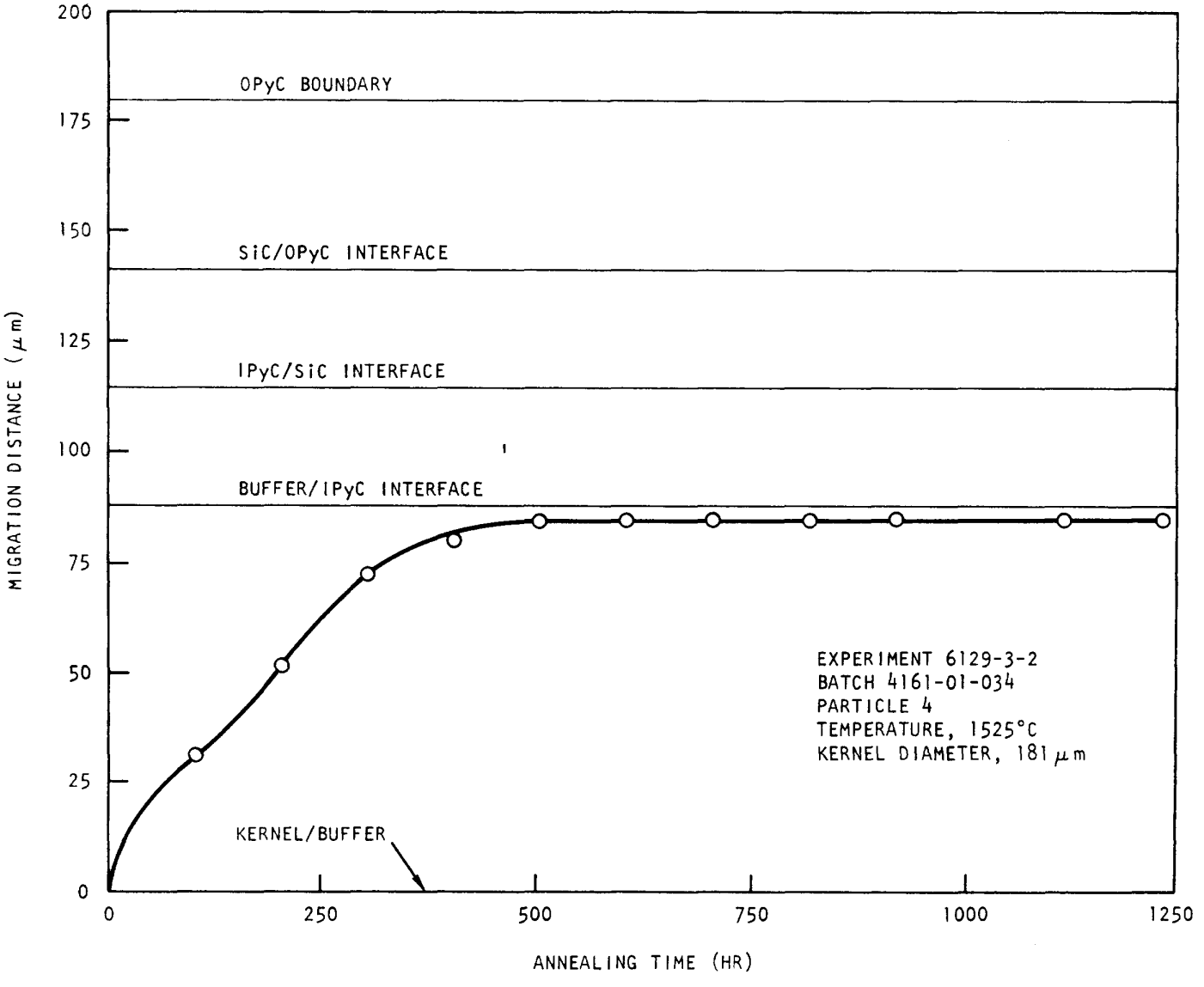

Fig. 9-1. Migration distance versus time: (a) particle 4

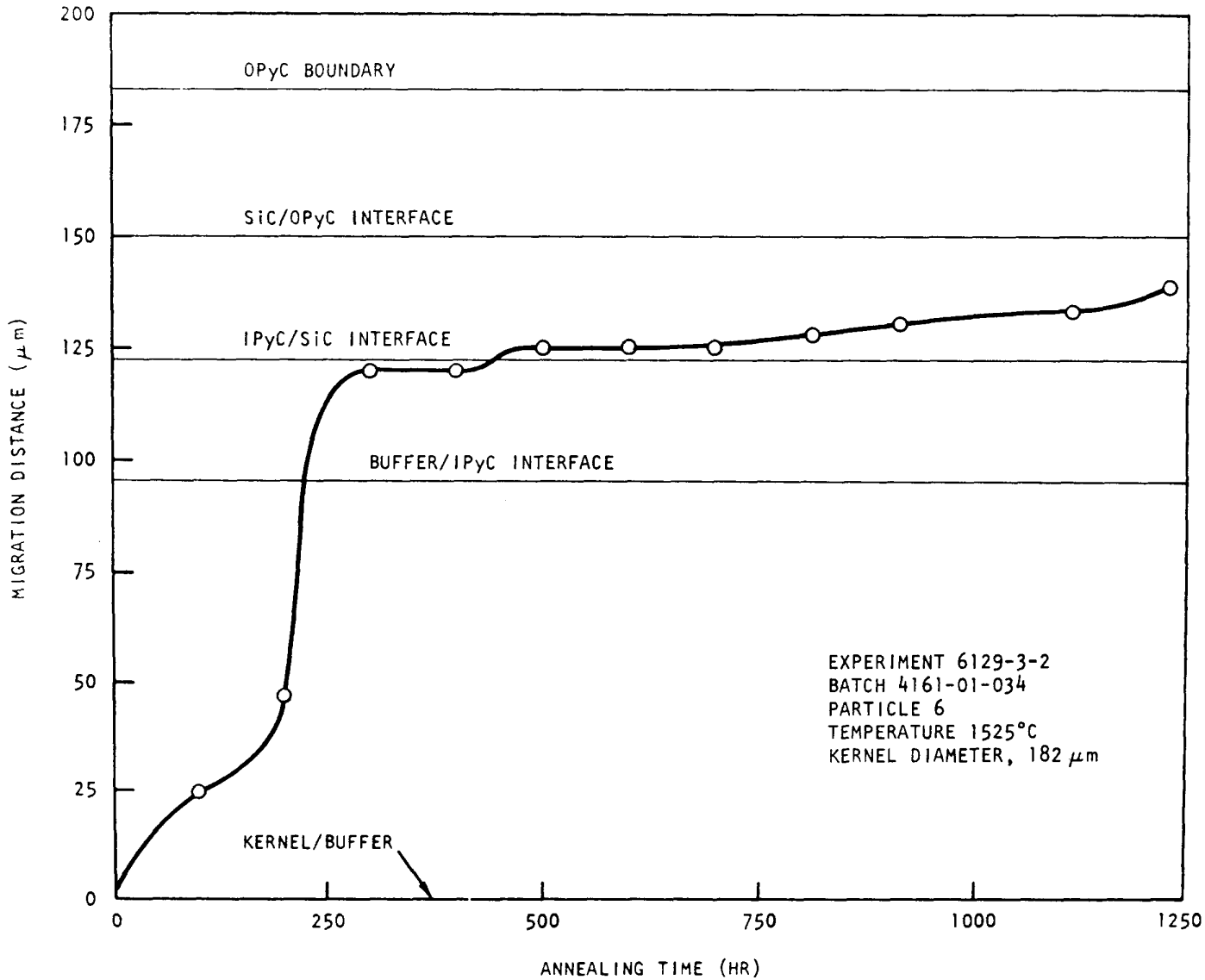

Fig. 9-1. Migration distance versus time: (b) particle 6

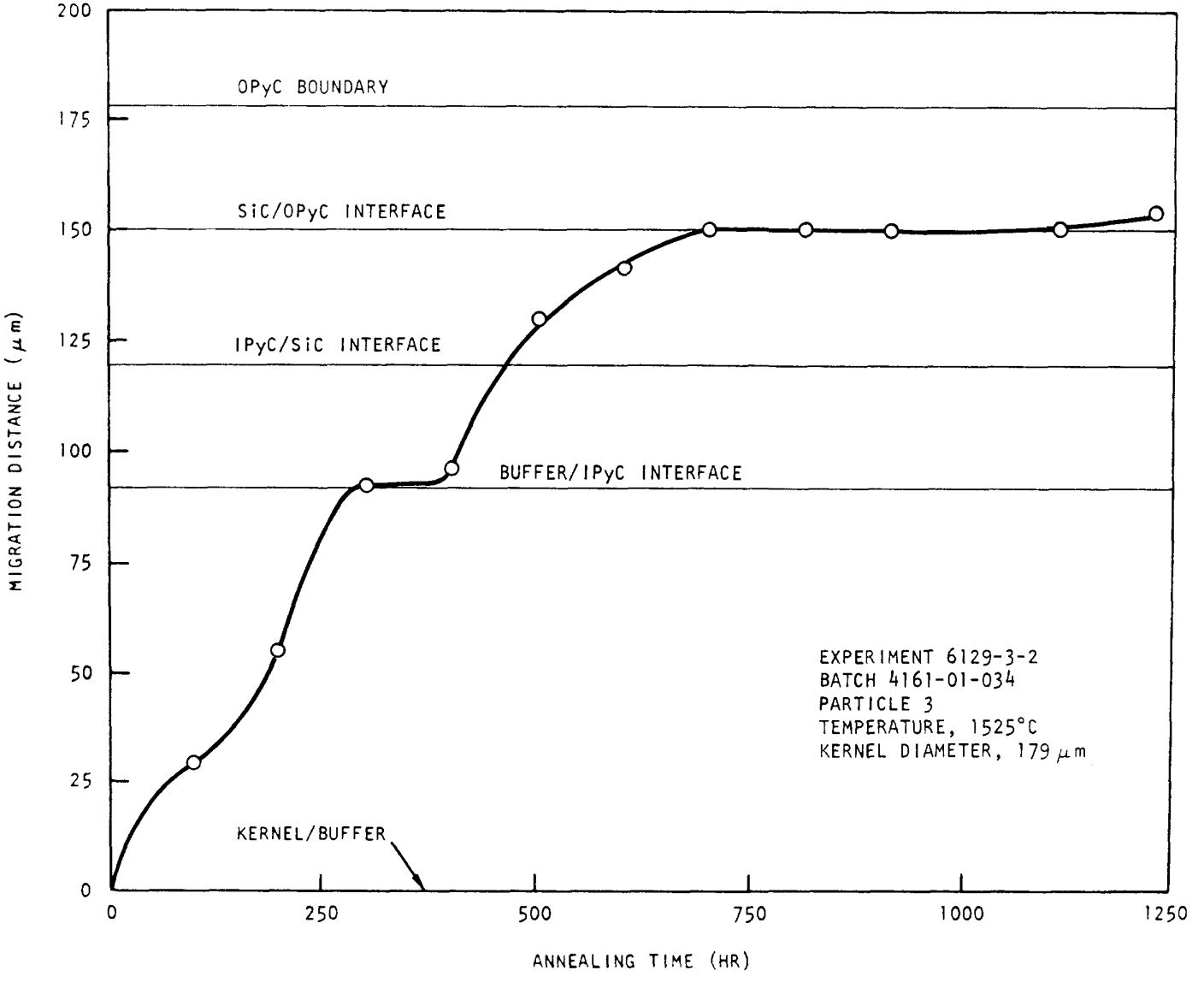

Fig. 9-1. Migration distance versus time: (c) particle 3

Further migration was not detected until nearly 750 hours of heating time had elapsed. In the third case (Fig. 9-1c), kernel movement was interrupted after 95 μm of migration and arrested after 150 μm of migration had occurred in 740 hours of heating. No more migration had been observed when the test was stopped at 1250 hours of heating.

The distances between the kernel and the IPyC/SiC and SiC/OPyC interfaces were determined on the individual particles before heating and are plotted for reference in Figs. 9-1a through 9-1c. It is clear that the migration in particle 6 of batch 4161-01-034 was arrested at the IPyC/SiC interface (Fig. 9-1b), while migration in particle 3 (Fig. 9-1c) was arrested at the SiC/OPyC interface. The interface between the buffer and IPyC layers in these particles is not visible on radiographs due to the presence of the SiC layer. The position of the buffer/IPyC interface can, however, be approximated by subtracting the batch average IPyC thickness from the position of the IPyC/SiC interface in the individual particles. The average IPyC thickness is 28 μm (see Table 9-1). The position of the buffer/IPyC interface, as estimated in this manner, is also shown in Figs. 9-1a through 9-1c. Figure 9-1c shows a short time arrest for particle 3 at the apparent buffer/IPyC interface, while Fig. 9-1a shows an arrest at the buffer/IPyC interface in particle 4 of batch 4161-01-034 that lasted for a total of 750 hours. There is some uncertainty in the position of the buffer/IPyC interface due to the range in IPyC thicknesses deposited during coating. The standard deviation in IPyC thickness for batch 4161-01-034 is 3.98 μm. Therefore, the buffer/IPyC interface on 95% of the particles should be within ±8 μm of the positions shown in Figs. 9-1a through 9-1c. In the two cases discussed, the first arrest occurred within 3 μm of the estimated buffer/IPyC interface.

These data show that kernel migration can be stopped at the interfaces between any of the coating layers in TRISO UC_2 fuels. The reason for these arrests is not clear. The arrests are probably caused by a perturbation in thermal gradient or carbon supply at the coating interfaces. This could be

caused by the random presence of gaps between the coatings, which agrees with the random nature of the observed arrests.

The variation in migration rate with time ($\Delta x/\Delta t$) complicates analysis of the data. In the analysis of large HTGR core thermal performance, it is necessary to predict kernel migration distances up to 55 μm in coated particles with average buffer thicknesses of 85 μm. It is therefore reasonable to use migration rates for approximately 55 μm of migration to determine the KMC for large HTGR-type particles. In the case of batch 4161-01-034, data from particles showing migration distances of 30 to 55 μm were used to define the KMC. This corresponds to kernel migration through 35 to 65% of the buffer layer. The majority of the particles in this test series have approximately 50-μm-thick buffers. In order to be consistent and to avoid possible migration arrests at buffer/IPyC interfaces in these particles, data from particles showing 20 to 35 μm of migration were used to define the KMC if the buffer thickness was 50 μm.

A linear least-squares fit of log KMC versus 1/T is shown in Fig. 9-2 for particles with 100-μm kernels and in Fig. 9-3 for particles with 200-μm kernels. The range of individual data points is indicated in each figure. The apparent activation energy for migration is 84 (±5) kcal/mole and 74 (±3) kcal/mole for particles with 100-μm and 200-μm kernels, respectively. These values agree well with the apparent activation energy of 76 (±9) kcal/mole determined for the migration of UC_2 discs through PyC (Ref. 9-1). Comparison of the KMCs for the 100- and 200-μm particles also shows excellent agreement. Although the average KMCs vary by as much as a factor of 5 (with 200-μm kernels migrating faster), the upper 95% confidence values for KMC are about the same for both size kernels.

Figures 9-2 and 9-3 show two-sided 95% confidence limits for the data fits. This was done to facilitate comparison between KMCs calculated for both unirradiated and irradiated particles. Figure 9-2 shows KMCs calculated from irradiated particle batch 4413-5E (see Table 9-1). With the exception of one datum point, the data from the irradiated particles tested fall

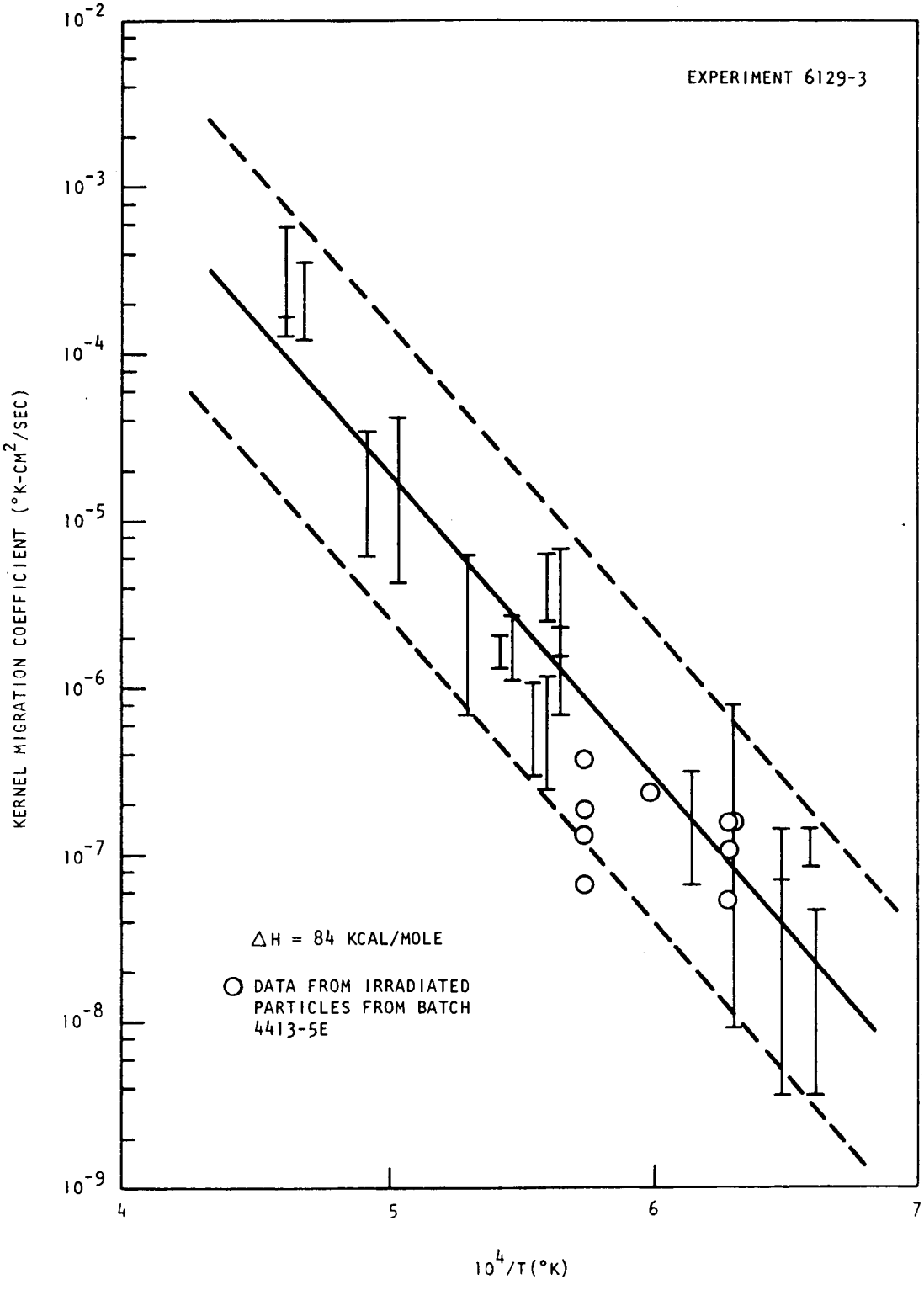

Fig. 9-2. Kernel migration coefficient versus 1/T, 100-μm kernels

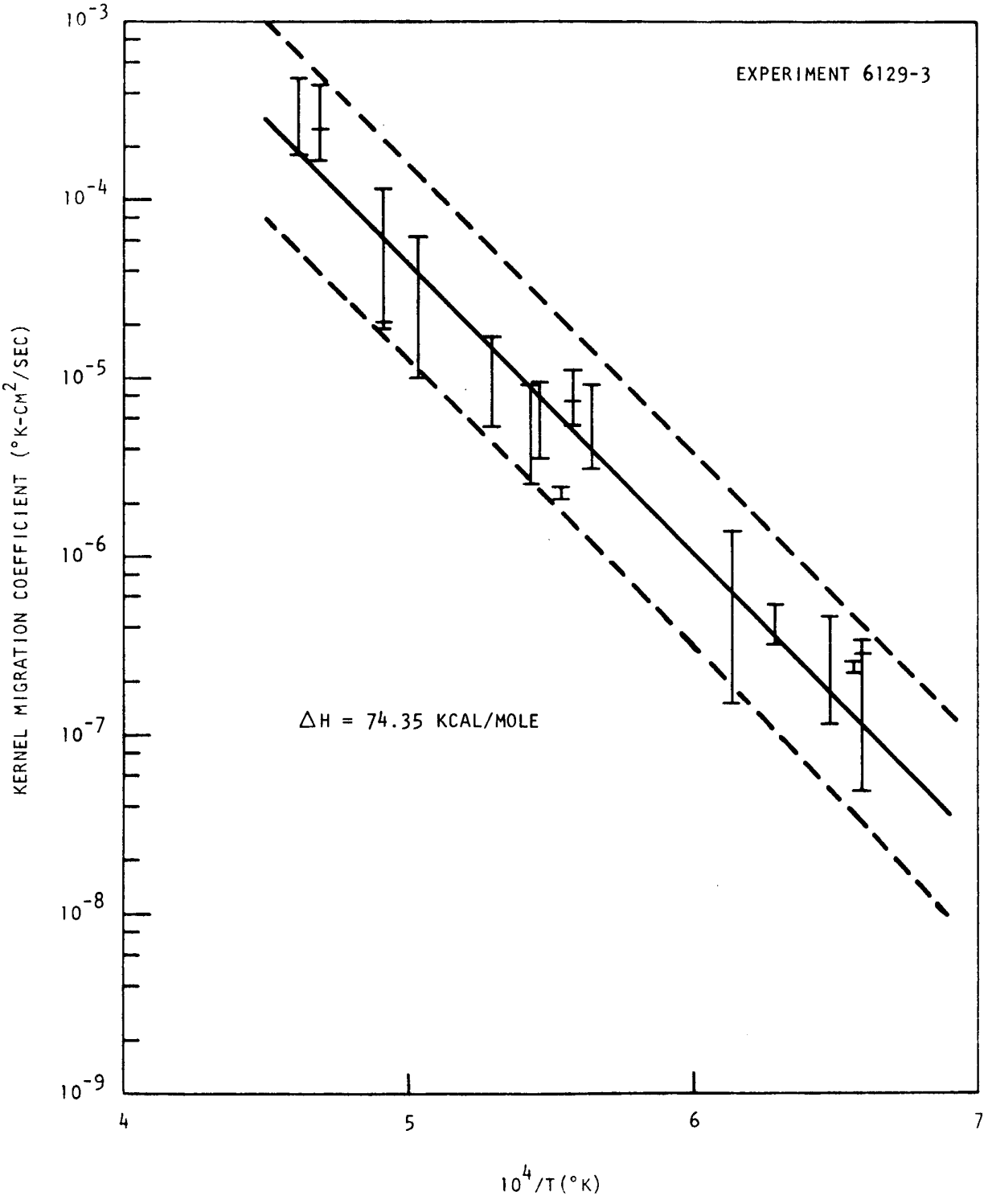

Fig. 9-3. Kernel migration coefficient versus 1/T, 200-μm kernels

within the 95% confidence limits for the unirradiated particle data. Kernel migration rates in irradiated UC_2 fuels appear to be less than or equal to migration rates for unirradiated UC_2 kernels.

FUEL COMPACT THERMAL CONDUCTIVITY

Recent work on thermal conductivity was divided among three major tasks: (1) calibration of a direct heating method for measuring the thermal conductivity of unirradiated fuel compacts, (2) calibration of the Dynatech device for measuring the thermal conductivity of irradiated fuel compacts, and (3) preparation and measurement of unirradiated prototype large HTGR-type fuel compacts.

Direct Heating Technique (Unirradiated Fuel Compacts)

A comparison of the direct heating (Ref. 9-3) and thermal diffusivity (Ref. 9-4) methods for measuring the thermal conductivity of solids has been made to determine the validity of the direct heating method for use in measuring the thermal conductivity of unirradiated fuel compacts.

It was not feasible to make the comparative measurements with a fuel compact because fabricating the thin disc specimens required for the thermal diffusivity apparatus was too difficult. Therefore, a carbon (Grade G.A. from Union Carbide Corporation) was chosen for the comparative measurements. Grade G.A. was selected because it has a low thermal conductivity similar to that of a fuel compact and its conductivity can be increased in a predictable manner by heat treatment.

The comparison of the two techniques was conducted for two conductivity levels, which encompased the range of thermal conductivities expected for unirradiated large HTGR-type fuel compacts. Direct heating measurements were first made on 0.5-in.-diameter by 2.0-in.-long cylinders of G.A. carbon; one cylinder was annealed at 1450°C for 1 hour and another at 1750°C for 1 hour. The thermal conductivities of the carbon in the radial direction were obtained at 900° to 1200°C.

Subsequently, thin discs, 0.40 in. in diameter by 0.050 in. thick, were machined from the direct heating specimens with the parallel faces of the discs parallel to the longitudinal axis of the cylinders. This orientation permits measurements of the thermal conductivity in the same direction as the direct heating measurements. Thermal diffusivity measurements were made on each disc over the temperature range of RT to 800°C. The results of these measurements are shown in Fig. 9-4. The extrapolation of the low-temperature thermal diffusivity data to the higher temperature direct-heat data indicates a very good correlation between the two techniques. The data from both techniques complement each other in both the low and high conductivity ranges, with a difference of about 10% occurring at the low end of the range. This correlation of the two techniques provides an excellent confirmation of the validity of the direct heating method.

Dynatech Device (Irradiated Fuel Rod Compacts)

Initial calibration runs have been completed on the Dynatech device (axial heat flow technique), and the results have been unsatisfactory. The device does not now appear to have the required temperature balancing capabilities for eliminating radial heat flow from and to the specimen; thus, the thermal conductivity values measured are unrealistic. Attempts are now being made to determine if the present device can be modified to prevent radial heat flow from occurring during measurements.

Thermal Conductivity Measurements (Prototype Large HTGR-Type Fuel Rod Compacts)

Eleven types of prototype large HTGR-type fuel rod compacts have been fabricated for thermal conductivity measurements, including compacts with different fuel loadings (Th/U ratios of 11,20, and 40) and different shim loadings (0, 11, 23, and 36 vol. %) loadings, fabricated with several matrix types and cured by two different methods (packed bed and graphite tube). Direct-heating thermal conductivity measurements at 950° to 1250°C have begun, and preliminary data indicate the following:

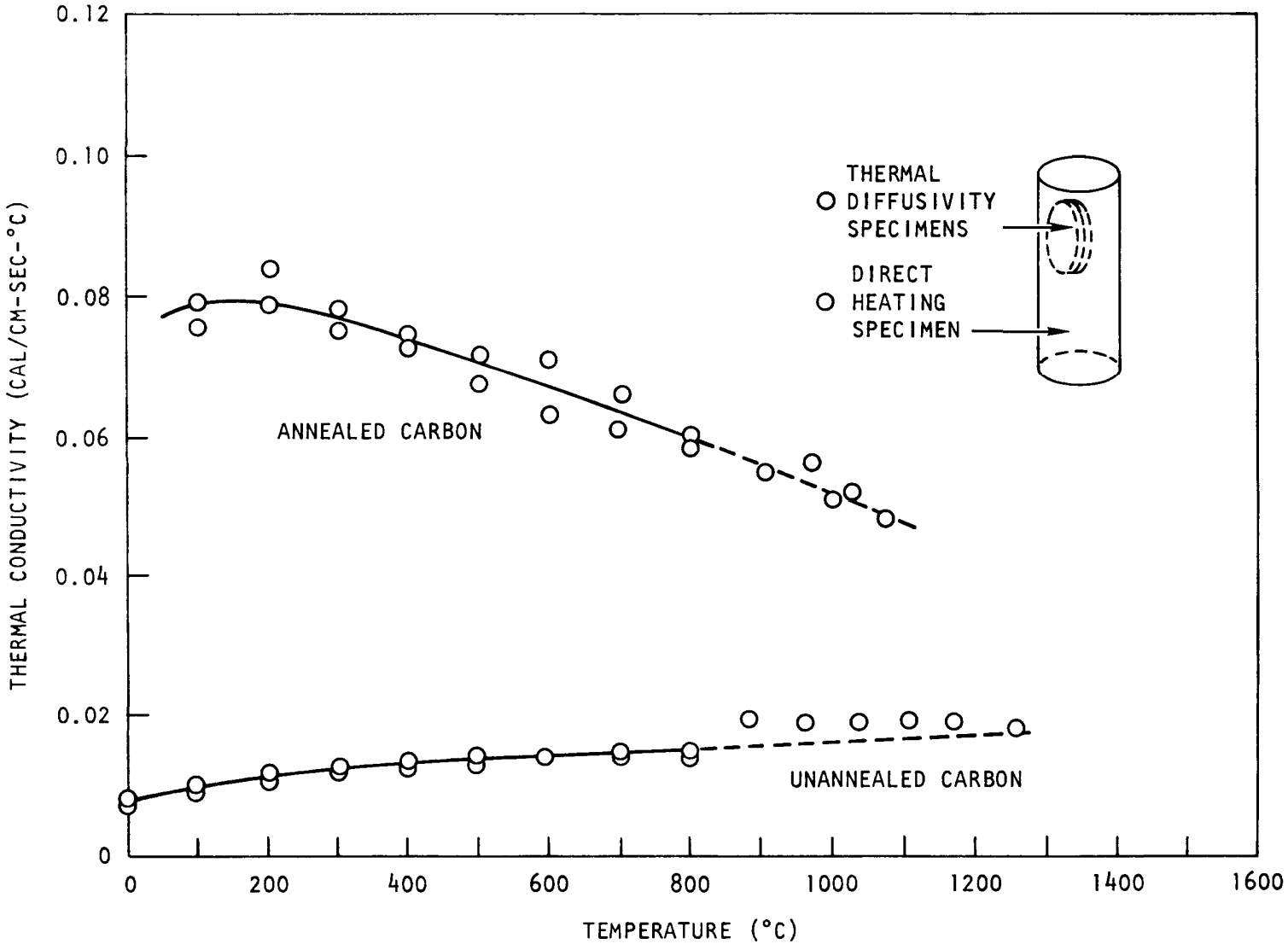

Fig. 9-4. Thermal conductivity versus temperature of unannealed and annealed carbon

1. The thermal conductivity of unshimmed and shimmed compacts decreases with increasing temperature (∿20% decrease from 950° to 1250°C).

2. The thermal conductivity of the compacts increases with increasing shim content, ranging from ∿4 Btu/ft-hr-°F (0.0165 cal/cm-sec-°C) for 0 vol % shim to ∿8 Btu/ft-hr-°F (0.033 cal/cm-sec-°C) for 36 vol % shim at 1250°C.

A topical report (Ref. 9-5) has been written describing the results of this experiment.

FUEL IRRADIATIONS

Capsule P13N

Capsule P13N is the fourth in a series of irradiation tests of candidate HTGR recyclable-type fuels and was the first P-capsule to be monitored for in-pile fission gas release during irradiation. The two primary objectives of this experiment were: (1) to compare oxide, carbide, and resin kernel irradiation performance at very high temperatures (1350° to 1500°C) to moderate fast fluences (approximately 5.5×10^{21} n/cm^2), and (2) to determine coated particle and fuel rod dimensional changes as a function of irradiation temperature, fluence, and particle design.

The capsule contained five cells in which fuel rods and unbonded particle samples were tested. A total of 22 fuel rods, 24 loose particle samples, and 175 piggyback samples were irradiated.

Capsule P13N was inserted in the ETR (I-135W core position) in cycle 114E on January 19, 1972 and completed its scheduled irradiation on January 5, 1973 after 3732 effective full-power hours of operation. It was then shipped to the GAC Hot Cell, where it is currently undergoing postirradiation examination.

Disassembly of the capsule and preliminary examination of all the fuel samples have been completed. The results of the examination of the fuel rod samples, which consisted of visual examination, metallography, and post-irradiation fission gas release measurements (TRIGA activation) were reported in an earlier Quarterly Progress Report (Gulf-GA-A12725).

Particle samples separated from the parent batches tested in the fuel rods according to size and density were irradiated as unbonded particle samples. Visual examination, metallography, fission gas release measurements, and contact microradiography were completed on the 24 unbonded particle samples. Density gradient column studies on selected unbonded particle samples are also planned.

Thermal analysis of the fuel specimens is in progress. Additional results on the irradiation performance of the fuel rod and unbonded particle samples will be reported when the capsule thermal analysis has been completed.

Capsule P13P

Capsule P13P, a companion test to P13N, is the fifth in a series of irradiation tests of candidate HTGR recyclable-type fuels and was also monitored for in-pile fission gas release during irradiation. The two primary objectives of the experiment were: (1) to compare oxide, carbide, and resin kernel irradiation performance at temperatures of 1050° to 1350°C and to fluences of 2.5 to 8.5 x 10^{21} n/cm^2, and (2) to determine coated particle and fuel rod dimensional changes as a function of irradiation temperature, fluence, and particle design. The capsule contained five cells in which 21 fuel rods, 32 unbonded particle samples, and over 150 piggyback samples were tested.

The capsule was inserted in the ETR on April 11, 1972 in the J-10-5E position. Cadmium shield capsules were placed in adjacent holes of the J-10 filler piece to reduce the high peak thermal flux to the P13P design value (2.6 x 10^{14} nv). The capsule completed its scheduled irradiation to

approximately 8 x 10^{21} n/cm^2 (design) in April 1973 and was transferred to the GAC Hot Cell facility. Disassembly of the capsule was completed and the fuel samples are currently undergoing postirradiation examination.

Visual examination and fission gas release measurements were completed on the fuel rod and unbonded particle specimens. Metallographic examination of selected fuel rod and particle specimens is in progress. Visual examination of the six unbonded particle batches of the reference size (200 μm) UC_2 TRISO particles revealed that all six samples survived irradiation with 0% OPyC coating failure. Metallographic examination of fuel rods 1B-21 (irradiated to 6.0 - 7.5 x 10^{21} n/cm^2 at approximately 1050°C) and 3C-25 (irradiated to 7.0 - 8.0 x 10^{21} n/cm^2 at approximately 1350°C) revealed no coating failure of the 200-μm UC_2 TRISO particles under these relatively severe irradiation conditions.

Additional examinations planned include contact microradiography, density gradient column studies, and electrolytic disintegration - acid leach studies.

Capsules P13R and P13S

Capsules P13R and P13S are the seventh and eighth in a series of irradiation tests conducted under the AEC-sponsored HTGR Base Program. Both capsules began their irradiation December 17, 1973 in the E7 position in the GETR. A description of the capsules was given in the previous Quarterly Progress Report (Gulf-GA-A12818).

Operation of capsules P13R and P13S has been very satisfactory to date. Both capsules are estimated to have reached a peak fluence of about 2.0 x 10^{21} n/cm^2 ($E > 0.18$ MeV).

The monitored fuel temperatures in most cases are close to design values, with the exception of the loose particle cells. The loose fissile and fertile particle samples are predicted to have operated approximately

300°C hotter and 100°C cooler, respectively, than the desired temperature of 1075°C for the first cycle. The temperatures of these samples should approach design as the irradiation continues.

Fission gas release values from all cells were initially very low (R/B≈10^{-7} Kr-85m). The R/B values have remained low in all cells operating at 1070°C, indicating no particle failures. P13S, Cell 5, rods being irradiated to 1300° and 1500°C have shown R/B increases to 1 x 10^{-6} and 4 x 10^{-6}, respectively. Cell 1 of P13S has been successfully thermal cycled to 1600°C five times. No increase in R/B has been measured in these rods compared to the companion rods in cell 1 of P13R.

Capsule P13T

Capsule P13T is now scheduled to begin irradiation in the ORR in November 1974. The layout of the capsule is presently being revised to include gel-supported precipitate (GSP) UC_2 kernels.

GAC-ORNL Cooperative Irradiation Capsules

A series of cooperative irradiation tests are being carried out with ORNL in their irradiation facilities. These irradiations include tests in the HFIR target position (HT-capsules), the HFIR beryllium-reflector position (HRB-capsules), and the ORR facility.

Capsule P13Q

Capsule P13Q is designed to demonstrate the performance of fuel rods fabricated using candidate large-HTGR processes and materials. The capsule is presently being irradiated in the E-3 position of the ORR. A description of the fuel was given in the previous Quarterly Progress Report (Gulf-GA-A12818).

Reported temperatures indicated that body 1 and body 2 were operating close to design (1150°C) and body 3 was running about 175°C lower than

design (1150°C). Thermal analysis of the in-pile data has begun, and initial results indicate that the power could be 30 to 40% low; this means the temperatures could be as much as 100°C lower than reported.

Capsule P13Q is estimated to have reached a fast fluence of 4.6×10^{21} n/cm^2 ($E > 0.18$ MeV). Fission gas release values have remained relatively constant and at levels below 10^{-6} (R/B Kr-85m).

Capsules HRB-4 and HRB-5

Capsules HRB-4 and HRB-5 represent a cooperative GGA-ORNL irradiation effort designed to evaluate the irradiation performance of fuel rods fabricated using candidate processes and materials for large HTGR startup and recycle fuel systems. Capsules HRB-4 and HRB-5 are companion capsules and were inserted in the beryllium-reflector position of the HFIR on October 8, 1972. Both capsules were designed to operate isothermally with a 1250°C axial (centerline) temperature and were monitored for in-pile fission gas release during irradiation. Capsule HRB-5 was discharged from the HFIR in February 1973, after completing its scheduled irradiation (5 cycles) to a peak fast neutron fluence of 4.7×10^{21} n/cm^2 ($E > 0.18$ MeV). Capsule HRB-4 was discharged from the HFIR in July 1973, after completing its scheduled irradiation (11 cycles) to a peak fast neutron fluence of approximately 10.5×10^{21} n/cm^2.

The GAC samples in each capsule consisted of six fuel rods (two each of three different types) having nominal dimensions of 0.05 x 1.00 in. These samples included rods fabricated with three different graphite fillers, one binder, and two types of graphite shim material. All rods were fabricated by the admix compaction process and were carbonized and high-fired in H-327 graphite tubes to simulate in-block curing. A description of the fuel rods tested in capsules HRB-4 and HRB-5 was given in a previous Quarterly Progress Report (Gulf-GA-A12422).

Metallographic examination of the six HRB-4 fuel rods revealed the occurrence of fissile and fertile particle OPyC coating failure. This

failure was attributed to matrix-coating interaction where the PyC coatings had bonded to the matrix material and were torn as the matrix pulled away from the particles during irradiation. This phenomenon is being investigated further and will be reported in more detail when the metallographic examination of the companion HRB-5 fuel rods has been completed.

Capsule HRB-6

Capsule HRB-6 represents a cooperative GGA-ORNL irradiation effort designed to evaluate the irradiation performance of fuel rods fabricated using candidate processes and materials for large HTGR startup and recycle fuel systems. The six GGA fuel rods tested in this experiment contained a blend of $(Th,U)C_2$ TRISO/ThO_2 BISO/inert carbon BISO particles. These rods were fabricated using the hot injection process and were cured in-place in H-451 graphite. A more complete description of the fuel rods tested in capsule HRB-6 was given in an earlier Quarterly Progress Report (Gulf-GA-A12515).

The capsule was designed to operate isothermally with a 1250° axial (centerline) temperature and was designed to be swept with helium to monitor for in-pile fission gas release during irradiation. Capsule HRB-6 was discharged from the HFIR in September 1973 after completing eight irradiation cycles to a peak fast neutron fluence of approximately 8×10^{21} n/cm^2 ($E > 0.18$ MeV).

The six GGA fuel rods were found to be in good condition during the preliminary examination conducted at ORNL. The fuel rods have been shipped to the GAC Hot Cell facility where the postirradiation examination is in progress. Visual and metallographic examinations, fission gas release measurements, and electrolytic disintegration - acid leach studies are to be performed.

Capsules HT-12, HT-13, HT-14, and HT-15

Capsules HT-12 through HT-15 are a series of four irradiation experiments designed to test the irradiation behavior of unbonded, BISO coated, ThO_2 fertile fuel particles. All capsules have completed irradiation and have been transferred to the GAC Hot Cell facility, where examination of the fuel samples is currently in progress. Visual examination, radiography, metallography, and density gradient column separations are being used to evaluate the particle samples.

Capsules HT-17, HT-18, and HT-19

General Atomic Company ThO_2 coated particle samples from experiments HT-17 through HT-19 are now in the Hot Cell awaiting postirradiation examination.

Capsules HT-24, HT-25, and HT-26

A third series of HT-capsule experiments is scheduled to begin irradiation during May/June 1974. These tests are designed to investigate fertile particle coating attributes and designs. The prime objective of the samples will be to investigate OPyC coatings deposited from mixed gas (propylene-acetylene) on BISO ThO_2 particles. OPyC attribute variables will be density and coating rate. The samples will be selected from particle batches fabricated for capsules P13R and P13S. These samples will duplicate variables tested in HT-17 through HT-19, which were propylene coated ThO_2 BISO particles.

One sample irradiated in previous HT-capsules (HT-17 through HT-19) will be included as a standard for comparison. Also, two batches of TRISO coated fertile particles will be irradiated in order to determine the effect of coating rate on OPyC failure. (OPyC will be deposited from propylene for direct comparison with results from HT-17 through HT-19.)

A total of eight different coating batches will be irradiated at two nominal temperatures, 900° and 1100°C. Table 9-2 lists the samples proposed for testing in capsules HT-24 through HT-26, and Table 9-3 gives the design irradiation exposures for each of the capsules.

REFERENCES

9-1. Gulden, T. D., "Carbon Thermal Diffusion in the UC_2-Carbon System," J. Am. Ceram. Soc. 55, 14 (1972).

9-2. Scott, C. B., and O. M. Stansfield, "Stability of Irradiated Coated-Particle Fuels in a Thermal Gradient," Gulf General Atomic Report GA-A12081, September 1972.

9-3. Powell, R. W., and F. H. Schofield, Proc. Phys. Soc. Lond. 51, 153 (1939).

9-4. Parker, W. J., R. J. Jenkins, C. P. Builer, and G. L. Abbott, J. Appl. Phys. 32, 1679 (1961).

9-5. Johnson, W. R., "Thermal Conductivity of Large HTGR Fuel Compacts," General Atomic Company Report GA-A12910, March 15, 1974.

TABLE 9-2
SAMPLES SELECTED FOR IRRADIATION IN HT-24 THROUGH HT-26

Sample Number (Parent Batch)	Kernel		OPyC		Total Particle			Design for HT-Particles	
	Diameter (μm)	Standard Deviation	Density (g/cm^3)	Coating Rate (μm/min)	Diameter (μm)	Standard Deviation	Density (g/cm^3)	Size (μm)	Density (g/cm^3)
6542-21-015[a]	492	25	1.73	7.8	833	41	3.46	790/833	3.45
6542-22-015[a]	503	26	1.80	4.0	831	42	3.50	790/833	3.45
6542-22-015[a]	500	23	1.81	7.6	833	37	3.53	790/833	3.45
6542-23-015[a]	476	33	1.92	6.5	812	44	3.56	790/833	3.45
6542-24-015[a]	511	23	1.94	6.6	844	36	3.55	833/895	3.45
6542-01-010[b]	500	13	1.80	10.0	828	31	3.59	790/833	3.45
6252-02[c]	486		1.80	4-6	(d)	(d)	(d)	(d)	(d)
6252-03[c]	486		1.80	6-8	(d)	(d)	(d)	(d)	(d)

[a] OPyC deposited from mixed gas.

[b] Standard used for comparing HT-17 through HT-19 with HT-24 through HT-26.

[c] TRISO particles.

[d] Not determined; properties presently being determined.

TABLE 9-3
EXPECTED IRRADIATION CONDITIONS FOR FERTILE PARTICLE SAMPLES
IN HT-24 THROUGH HT-26

Sample Number	Holder	Temperature (°C)	Estimated Fast Neutron Exposure (10^{21} n/cm^2)		
			HT-24	HT-25	HT-26
6542-01-01	27	1250	3.9	8.6	13.9
	40	900	3.1	6.9	11.0
6542-21-01	29	1250	3.9	8.6	13.8
	42	900	2.9	6.5	10.4
6542-22-01	30	1250	3.9	8.5	13.7
	43	900	2.8	6.2	10.0
6542-22-02	32	1250	3.8	8.4	13.5
	45	900	2.6	5.8	9.4
6542-23-01	33	1250	3.8	8.3	13.4
	46	900	2.5	5.6	9.0
6542-24-01	35	1250	3.7	8.2	13.1
	48	900	2.3	5.2	8.3
6542-02	36	1250	3.6	8.1	12.9
	49	900	2.2	4.9	7.9
6542-03	38	1250	3.5	7.8	12.5
	51	900	2.0	4.3	6.9

TASK XI
GRAPHITE RESEARCH

INTRODUCTION

Work during the present quarter was divided among three major tasks: (1) characterization of production-size graphites, (2) graphite irradiations, and (3) statistical measurements of graphite strength.

GRAPHITE CHARACTERIZATION

Two additional nuclear graphites from the Union Carbide Corporation were received and are undergoing preliminary examinations. These materials are designated TS-1240, a near-isotropic graphite, and TS-1111, a needle-coke graphite. These materials were extruded as 18-in.-diameter logs and manufactured with the intent of meeting GAC's material specifications for core graphite.

Preliminary evaluation of these materials is under way. Density, thermal conductivity, and impurity data are shown in Tables 11-1, 11-2, and 11-3, respectively.

Grade TS-1240 appears satisfactory as a candidate material for large HTGRs with respect to density and impurity levels. Additional in-depth evaluations have begun on this material. Grade TS-1111 also appears to be satisfactory as a needle-coke candidate.

TABLE 11-1
DENSITY OF TS-1240 AND TS-1111 GRAPHITES

Graphite Grade	Location in Log[a]	Density (g/cm^3)		
		Mean	Maximum	Minimum
TS-1240	MLC	1.73	1.74	1.72
(Log 5651-72)	EC	1.73	1.75	1.70
	MLE	1.75	1.77	1.73
	EE	1.74	1.77	1.71
TS-1240	MLC	1.81	1.81	1.80
(Log 5651-75)	EC	1.82	1.82	1.81
	MLE	1.81	1.83	1.80
	EE	1.80	1.82	1.78
TS-1111	MLC	1.70	1.71	1.69
(Log 5651-69)	EC	1.69	1.72	1.69
	MLE	1.70	1.72	1.66
	EE	1.70	1.71	1.68

[a]MLC = Mid-length center, EC = end center, MLE = mid-length edge, and EE = end edge.

TABLE 11-2
THERMAL CONDUCTIVITY OF GRAPHITE TS-1240 (LOG 5651-72)

Orientation	Thermal Conductivity (cal/cm-sec-°C)				
	22°C	200°C	400°C	600°C	800°C
Perpendicular	0.235	0.213	0.183	0.161	0.134
Parallel	0.245	0.223	0.193	0.158	0.136

TABLE 11-3
IMPURITY CONTENT (IN PPM) OF GRAPHITES TS-1240 AND TS-1111

Graphite	Location in Log(a)	Ash	B	Fe	V	Ti	S
TS-1240 (Logs 5651-72 and 5651-75)	MLC	98	0.75	<10	13	20	9
	EC	71	0.75	<10	15	18	17
	MLE	89	0.75	<10	13	15	13
	EE	92	<0.5	<10	13	13	17
	Average of whole log	88	0.7	<10	14	17	14
TS-1111 (Log 5651-69)	MLC	85	<0.5	<10	9	15	7
	EC	92	<0.5	<10	8	8	11
	MLE	45	<0.5	<10	10	10	10
	EE	63	<0.5	<10	9	8	8
	Average of whole log	72	<0.5	<10	9	10	9

(a) MLC = mid-length center, EC = end center, MLE = mid-length edge, and EE = end edge.

CAPSULE IRRADIATIONS

Capsule OG-1

The OG-1 graphite irradiation capsule completed irradiation in the C-3 position of the Oak Ridge Reactor (ORR) on December 2, 1973 and was removed from the reactor after having completed three cycles of irradiation (cycles 113 to 115). The capsule was disassembled at ORNL and the graphite crucibles (sample holders) and their contents were returned to GAC for examination and measurement of the graphite samples.

Neutron fluences along the capsule were measured from the activation of flux monitors. The monitors were located at 28 positions (four monitors at NW, NE, SE, and SW positions in each of seven axial locations). Fast fluences were determined from iron and titanium monitors using the $^{54}Fe(n,p)^{54}Mn$ and the $^{46}Ti(n,p)^{46}Sc$ reactions and assuming cross sections of 46.5 mb and 6.85 mb, respectively. Thermal fluences were determined from cobalt monitors, using the $^{59}Co(n,\gamma)^{60}Co$ reaction and assigning a cross section of 36.8 b. The measured fluences (after averaging the NW, NE, SE, and SW data) are shown in Fig. 11-1.

Analysis of the temperature records is not yet complete, but preliminary examination shows that the time-averaged centerline temperatures of the crucibles fell within 50°C of the design temperatures (600° to 1400°C). Radial temperature gradients were higher than expected, with the temperature drop between the centerline and the outside falling in the range 100° to 150°C for most crucibles. Both chromel-alumel and tungsten-rhenium thermocouples were used in the assembly of the capsule, and a comparison of the thermocouple records should provide data on the decalibration of the tungsten-rhenium thermocouples. Preliminary data indicate that decalibration in the OG-1 capsule was much less marked than in previous irradiations in the GETR.

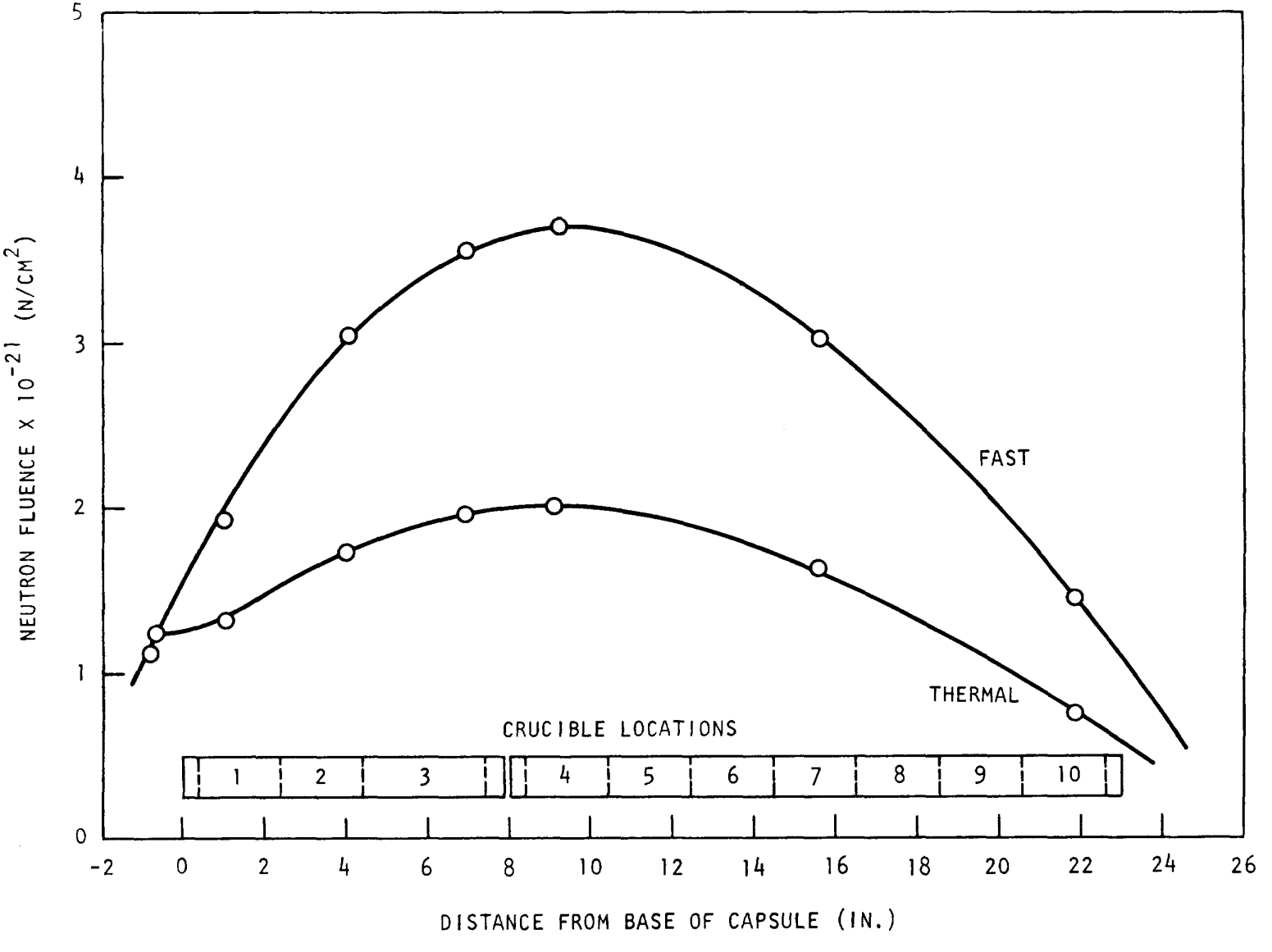

Fig. 11-1. Measured neutron fluences in capsule OG-1

Postirradiation Measurements

Capsule OG-1 contained approximately 100 tensile samples (0.25-in. diameter x 0.9-in. long) of both production-grade H-327 (needle-coke) graphite and preproduction H-451 (near-isotropic petroleum coke) graphite. Half the samples will be held for tensile testing to failure, and half will be reloaded into capsule OG-2 for further irradiation. In addition to the tensile samples, the capsule contained over 400 0.45-in.-long dimensional samples of H-451, about half of which will be reirradiated; over 200 samples of H-327 graphite (including 56 reirradiations), about half to be irradiated in OG-2; and 70 samples of H-429, a prototype of H-451, which received one irradiation in a previous capsule and will be reirradiated in capsule OG-2 to provide early full-exposure data on near-isotropic petroleum-coke-based material. Other specimens irradiated in capsule OG-1 include dimensional samples of P_3JHAN (a French full-sized nuclear-grade graphite) and 2020 (a very fine-grained graphite made by the Stackpole Carbon Company), samples of boronated graphite, fuel matrix material, and discs of H-451 and H-327 graphite for thermal diffusivity measurements.

Dimensional Changes

Measurement of the postirradiation dimensions is complete, and the data are being entered into the GRAFT data storage and retrieval program. The full data will be reported when checking and verification are complete and when analysis of the temperature records is finalized. Preliminary data for the near-isotropic petroleum-coke-based graphites H-451 and H-429 show behavior resembling that of Gilsocoke-based graphites, with much better dimensional stability than needle-coke-based graphites. The near-isotropic material contracts in both directions, with contraction perpendicular to extrusion averaging 0.6 times the contraction parallel to extrusion. Parallel shrinkages in H-451 graphite average 0.2% for an irradiation temperature of $\sim$600°C and a fast fluence of 2×10^{21} n/cm^2 ($E > 0.18$ MeV), 0.6% for $\sim$950°C and 3×10^{21} n/cm^2, 1.1% for $\sim$1100°C and 3.7×10^{21} n/cm^2,

and 3% for 1300° to 1400°C and 3.6 x 10^{21} n/cm^2. Irradiation of H-429 graphite to 6.6 x 10^{21} n/cm^2 at 1300° to 1500°C produces parallel shrinkage of around 3%, indicating that even at this high temperature "turnaround" and the onset of expansion do not occur until higher fluences are reached.

Thermal Expansivity

The thermal expansivity of 72 samples of H-451, H-429, and H-327 graphites irradiated in the OG-1 capsule was measured between room temperature and 100°C lower than the irradiation temperature using a silica dilatometer. The mean expansivities between room temperature and 500°C are tabulated in Table 11-4. The expansivities of H-451 and H-429 are plotted as a function of fast neutron fluence in Figs. 11-2 and 11-3, and those of H-327 are shown in Fig. 11-4. The irradiation-induced changes in the expansivity of H-451 and H-429 are quite small compared with those of Gilsocoke-based graphites. For irradiation temperatures of about 650° and 825°C, the thermal expansivity increases by about 0.5 x 10^{-6} °C^{-1} in both parallel and perpendicular directions for a fluence of 2 x 10^{21} n/cm^2 (E > 0.18 MeV). At higher temperatures the changes are smaller; there is some indication of a net decrease in expansivity after irradiation to 6.6 x 10^{21} n/cm^2 at 1425° to 1500°C. The thermal expansivity of H-327 graphite increases by about 0.5 x 1-$^{-6}$ °C^{-1} in the parallel direction for a fluence of 2 to 3 x 10^{21} n/cm^2 at 575° to 650°C and 875° to 975°C, but remains unchanged in the perpendicular direction.

Tensile Testing

Apparatus for tensile testing selected samples from OG-1 has been set up. Cylindrical samples (0.25-in. diameter by 0.9 in. long) will be tested, and strains will be measured with an extensometer to enable Young's modulus to be calculated. About 50 samples each of irradiated H-451 graphite and H-327 graphite will be tested.

TABLE 11-4

THERMAL EXPANSIVITY OF GRAPHITE SAMPLES IRRADIATED IN CAPSULE OG-1

Graphite Grade	Sample No.	Log Location and Orientation	Crucible No.	Hole No.	Mean Irradiation Temperature(a) (°C)	Fast Neutron Fluence x 10^{-21} (n/cm^2, E > 0.18 MeV)	Coefficient of Thermal Expansion, 22°-500°C (°C^{-1} x 10^6)
H-451	.341.	C	5	6	1425	3.6	3.49
H-451	.342.	C	5	6	1425	3.6	3.73
H-451	.343.	C	5	7	1425	3.6	3.69
H-451	.466.	C	5	6	1425	3.6	4.30
H-451	.467.	C	5	6	1425	3.6	4.37
H-451	.468.	C	5	7	1425	3.6	4.16
H-429	.141.	C	5	16	1425-1500	6.6	3.58
H-429	.142.	C	5	16	1425-1500	6.6	3.38
H-429	.143.	C	5	17	1425-1500	6.6	3.05
H-429	.161.	C	5	16	1425-1500	6.6	4.16
H-429	.162.	C	5	16	1425-1500	6.6	4.07
H-429	.163.	C	5	17	1425-1500	6.6	4.29
H-451	.583.	E	4	2	1175	3.7	3.49
H-451	.584.	E	4	2	1175	3.7	3.55
H-451	.585.	E	4	3	1175	3.7	3.64
H-451	.683.	E	4	2	1175	3.7	3.70
H-451	.684.	E	4	2	1175	3.7	4.01
H-451	.685.	E	4	3	1175	3.7	3.78
H-429	404	E	4	30	1100-1275	6.3	3.77
H-429	405	E	4	30	1100-1275	6.3	3.67
H-429	406	E	4	40	1100-1275	6.3	3.66
H-429	434	E	4	30	1100-1275	6.3	4.70
H-429	435	E	4	30	1100-1275	6.3	4.52
H-429	436	E	4	40	1100-1275	6.3	4.37
H-451	.596.	E	7	2	975	3.1	3.33
H-451	.597.	E	7	3	975	3.1	3.38
H-451	.598.	E	7	4	975	3.1	3.58
H-451	.696.	E	7	2	975	3.1	4.11
H-451	.697.	E	7	3	975	3.1	4.25
H-451	.698.	E	7	4	975	3.1	4.44
H-451	.371.	C	8	7	925	2.6	3.52
H-451	.372.	C	8	7	925	2.6	3.75
H-451	.373.	C	8	8	925	2.6	3.61
H-451	.496.	C	8	7	925	2.6	4.39
H-451	.497.	C	8	7	925	2.6	4.15
H-451	.498.	C	8	8	925	2.6	4.16

TABLE 11-4 (continued)

Graphite Grade	Sample No.	Log Location and Orientation	Crucible No.	Hole No.	Mean Irradiation Temperature(a) (°C)	Fast Neutron Fluence x 10^{-21} (n/cm^2, E > 0.18 MeV)	Coefficient of Thermal Expansion, 22°-500°C (°C^{-1} x 10^6)
H-429	389	C	8	16	900	3.4	3.70
H-429	390	C	8	16	900	3.4	3.90
H-429	391	C	8	16	900	3.4	4.06
H-429	419	C	8	15	900	3.4	4.93
H-429	420	C	8	15	900	3.4	5.19
H-429	421	C	8	15	900	3.4	5.16
H-451	.613.	E	9	2	825	2.1	3.92
H-451	.614.	E	9	3	825	2.1	3.83
H-451	.615.	E	9	4	825	2.1	4.09
H-451	.713.	E	9	2	825	2.1	5.04
H-451	.714.	E	9	3	825	2.1	4.85
H-451	.715.	E	9	4	825	2.1	4.78
H-451	.303.	C	1	2	650	2.2	3.98
H-451	.304.	C	1	3	650	2.2	3.80
H-451	.305.	C	1	4	650	2.2	3.72
H-451	.428.	C	1	2	650	2.2	4.82
H-451	.429.	C	1	3	650	2.2	4.89
H-451	.430.	C	1	4	650	2.2	4.73
H-327	.222.	E	7	2	975	3.1	1.97
H-327	.223.	E	7	3	975	3.1	1.96
H-327	.224.	E	7	4	975	3.1	1.93
H-327	.272.	E	7	2	975	3.1	3.10
H-327	.273.	E	7	3	975	3.1	3.38
H-327	.274.	E	7	4	975	3.1	3.27
H-327	176	C	8	19	875-900	3.4	2.03
H-327	177	E	8	19	875-900	3.4	2.27
H-327	174	C	8	19	875-900	3.4	3.18
H-327	175	E	8	19	875-900	3.4	3.70
H-327	.1.	C	1	2	650	2.2	1.84
H-327	.2.	C	1	3	650	2.2	1.87
H-327	.201.	E	1	40	575	2.2	1.72
H-327	.202.	E	1	40	575	2.2	1.65
H-327	.101.	C	1	2	650	2.2	3.47
H-327	.102.	C	1	3	650	2.2	3.25
H-327	.251.	E	1	40	575	2.2	3.55
H-327	.252.	E	1	40	575	2.2	3.54

(a) Preliminary estimate of mean irradiation temperature.

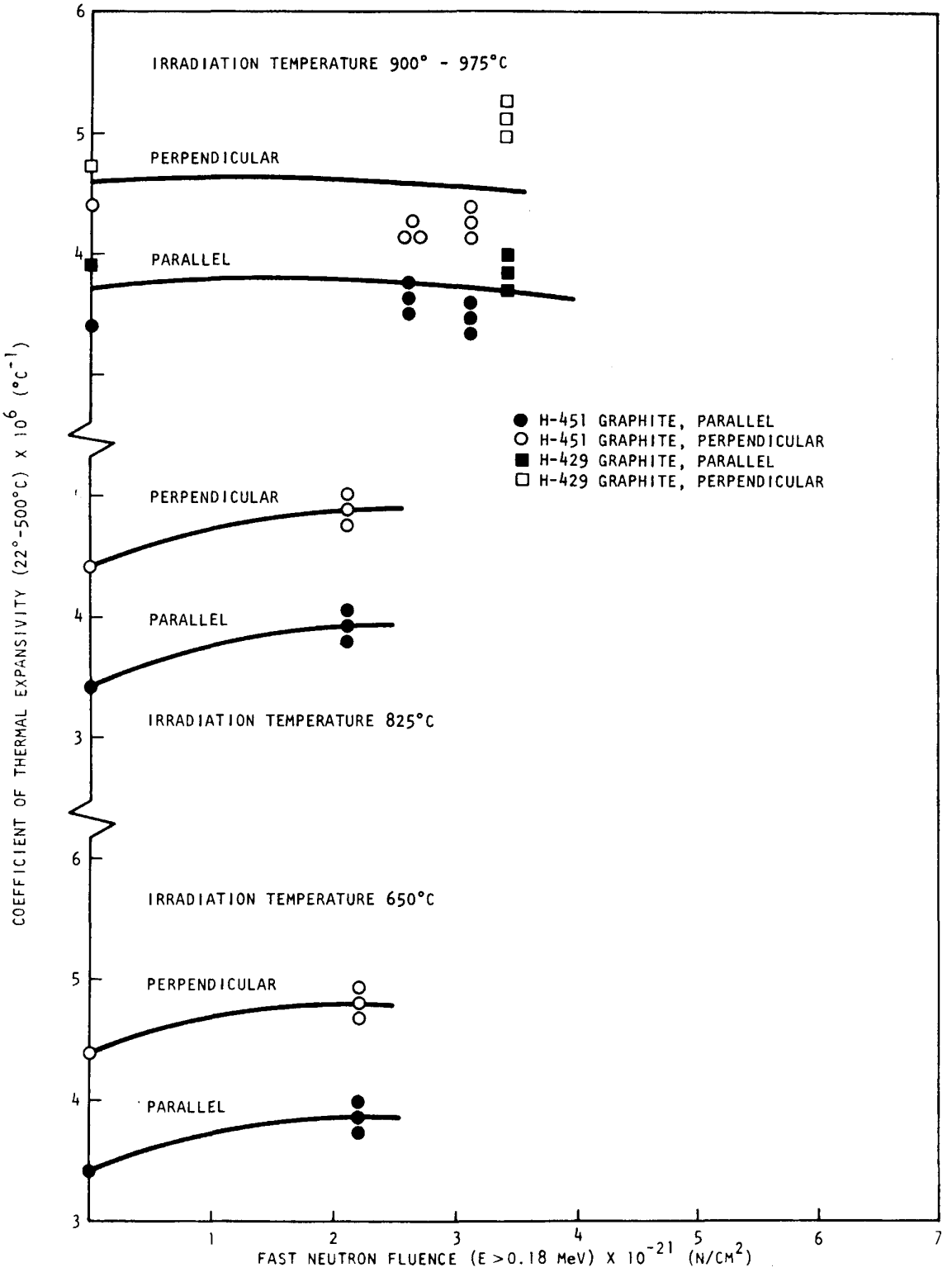

Fig. 11-2. Thermal expansivity of near-isotropic petroleum coke based graphite as a function of neutron fluence at 650°, 825°, and 900° to 975°C

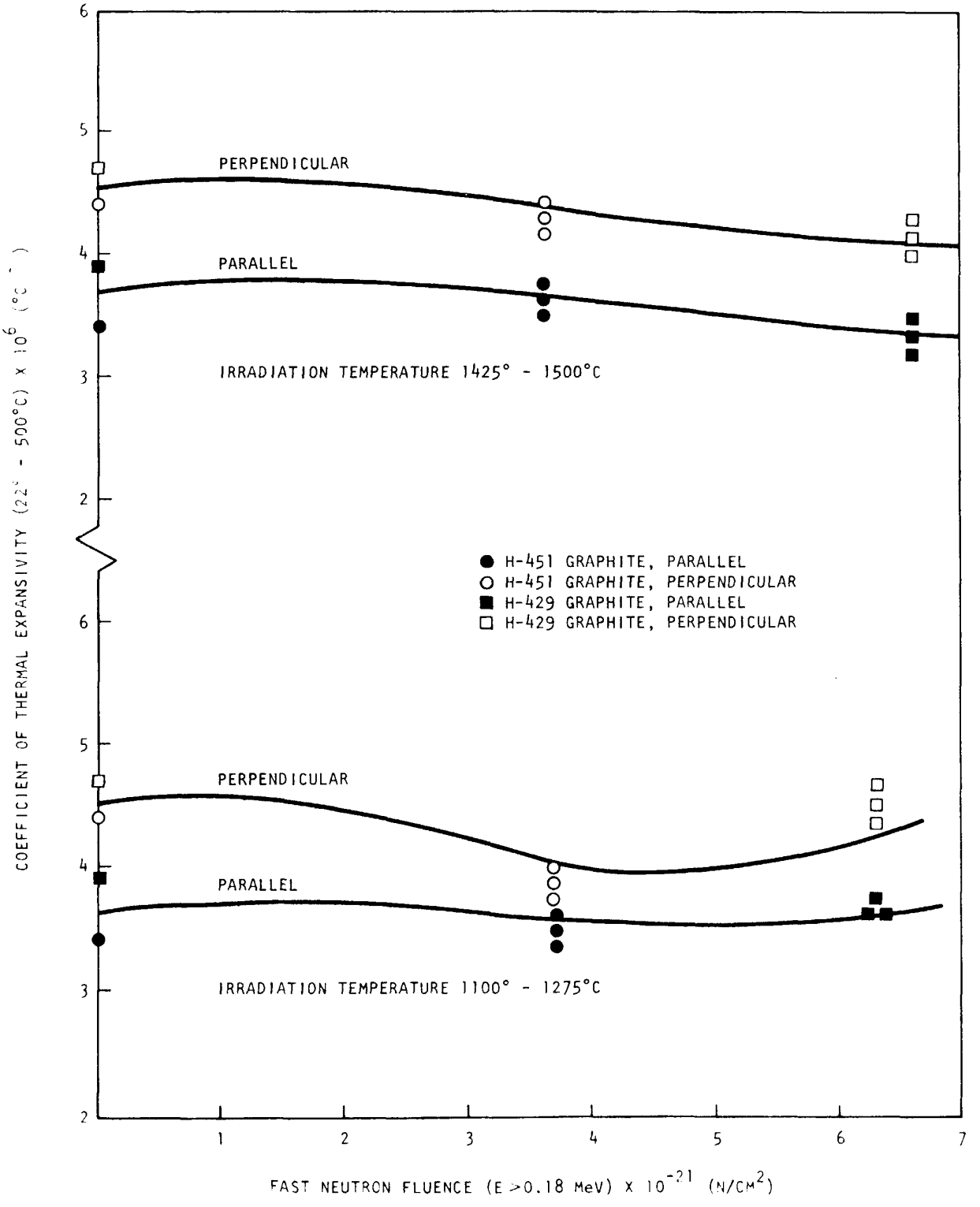

Fig. 11-3. Thermal expansivity of near-isotropic petroleum coke based graphite as a function of neutron fluence at 1100° to 1275°C and 1425° to 1500°C

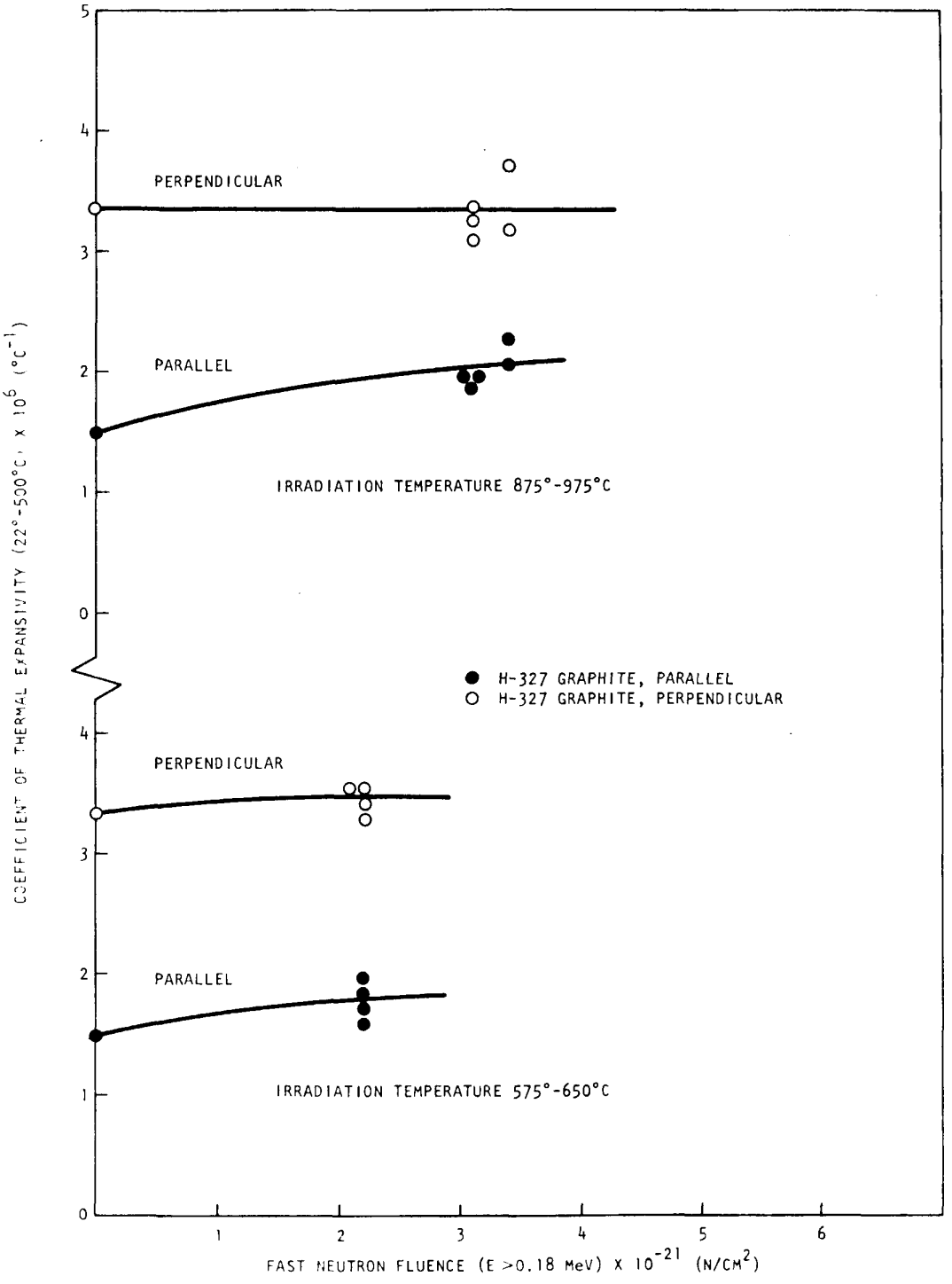

Fig. 11-4. Thermal expansivity of needle-coke-based H-327 graphite as a function of neutron fluence at 575° to 650°C and 875° to 975°C

Thermal Conductivity

The thermal conductivity of discs of irradiated graphite (0.4-in. diameter by 0.05 in. thick) from the OG-1 capsule will be measured by the heat pulse method. About 50 discs of H-327 and H-451 graphites will be measured and reirradiated in capsule OG-2. About half will be measured at room temperature only and half will be measured at temperatures up to 800°C.

Capsule OG-2

The thermal and mechanical design of the second capsule in the OG-series will be identical to that of OG-1, and the capsule will be irradiated in the same facility (C-3 position in the Oak Ridge Reactor) as OG-1. Owing to delays in procuring metallic components, it is likely that assembly of the capsule will be delayed beyond the original insertion date, and startup will have to be postponed by one reactor cycle until early July.

Although the overall design remains unchanged from OG-1, changes are being made in the patterns of holes drilled in the crucibles for the graphite test samples. This change results from a decision to use a single size (0.25-in. diameter x 0.9 in. long) for all future virgin samples and to use the same specimen for dimensional, thermal expansivity, and tensile measurements. However, in order to reirradiate samples made for earlier capsules, it will be necessary to retain some holes to accommodate 0.2-in.-diameter cylinders. The hole-pattern changes will increase the number of holes for 0.25-in. samples at the expense of holes for 0.2-in. samples.

The test plan for capsule OG-2 is based on the following considerations:

1. About half the H-451 dimensional and tensile samples from OG-1 will be retained for destructive testing and half will be reencapsulated in OG-2 for additional neutron exposure. The samples of H-429 (a prototype for H-451), which have already received two increments of fluence, will be reirradiated to provide early full-exposure data.

2. About half the H-327 tensile and dimensional samples from OG-1 will be held for destructive testing and half will be reirradiated. A limited number of virgin tensile samples of H-327 will be irradiated in OG-2. It is anticipated that these tests will complete the necessary work on H-327 graphite and will provide a body of data sufficient for future purposes.

3. Most samples of the French production nuclear graphite P_3JHAN from OG-1 will be reirradiated to provide data for comparison with European results.

4. About 100 virgin tensile/dimensional samples each of the most recent preproduction grade H-451 and Union Carbide TS-1240 will be irradiated.

5. Some 0.12-in.-diameter samples of 2020 and other fine-grained experimental graphites will be irradiated in piggyback positions.

6. Sixteen dimensional samples of H-451 graphite from OG-1 will be transposed between crucibles 1 and 6 to investigate the effects of changing irradiation temperature.

The types and numbers of graphite samples to be tested are summarized in Table 11-5; the breakdown according to crucible and test temperature is shown in Table 11-6.

TABLE 11-5
SAMPLES TO BE IRRADIATED IN CAPSULE OG-2

Grade	No. Samples	Size (in.)	Previous Irradiations	Tests to be Performed	Comments
H-451 (preproduction II)	96	0.25 x 0.9	-	Tensile, dimensional, CTE	First production materials of H-451
H-451 (preproduction I)	50	0.25 x 0.9	OG-1	Tensile, dimensional, CTE	Higher fluence mechanical properties
H-451 (preproduction I)	200	0.2 x 0.45	OG-1	Dimensional, CTE	Higher fluence dimensional changes, temperature history effects
H-429 (prototype of H-451)	70	0.2 x 0.45	GEH-13-422 OG-1	Dimensional, CTE	Full-exposure data on prototype of H-451
H-451 (preproduction I)	61	0.2 x 0.9	OG-1	Fatigue	--
H-327 (production)	46	0.25 x 0.9	-	Tensile, dimensional, CTE	To complete data on H-327
H-327 (production)	46	0.25 x 0.9	OG-1	Tensile, dimensional, CTE	
H-327 (production)	70	0.2 x 0.45	OG-1	Dimensional, CTE	
H-327 (production)	28	0.2 x 0.45	GEH-13-422 OG-1	Dimensional, CTE	
TS-1240 (production)	98	0.25 x 0.9	-	Tensile, dimensional, CTE	First measurements on UCC TS-1240
P_3JHAN	68	0.2 x 0.45	OG-1	Dimensional, CTE	To compare with European data on French production-grade nuclear graphite
2020 (production)	102	0.12 x 0.45	OG-1	Dimensional	Data on representative fine-grain, high-strength material (these small samples occupy "piggyback" space)
H-451 (preproduction I)	36	0.05 x 0.45	OG-1	Thermal conductivity	
H-327 (production)	15	0.05 x 0.45	OG-1	Thermal conductivity	
TS-1240 (preproduction)	36	0.05 x 0.45	-	Thermal conductivity	
Pyrocarbon	4	-	OG-1	Miscellaneous	
Silicon carbide	4	-	OG-1	Miscellaneous	
Carbon insulating material	-	-	-	Miscellaneous	
Boronated graphite	28	-	-	Miscellaneous	

TABLE 11-6

LOCATION BY CRUCIBLE OF SAMPLES TO BE IRRADIATED IN CAPSULE OG-2

Grade	Size (in.)	Previous Irradiations	Tests to be Performed	Number of Samples by Crucible									
				1[a]	2	3	4	5	6	7	8	9	10
				700°C	800°C	1000°C	1200°C	1400°C	1100°C	1000°C	900°C	800°C	600°C
H-451 (preproduction II)	0.25 x 0.9	-	Tensile, dimensional, CTE	24		24		24			24		
H-451 (preproduction I)	0.25 x 0.9	OG-1	Tensile, dimensional, CTE	8		18		8		8			8
H-451 (preproduction I)	0.2 x 0.45	OG-1	Dimensional, CTE[b]	32[b]	32	12	14	8	24[b]	20	12	28	18
H-429 (prototype of H-451)	0.2 x 0.45	GEH-13-422 OG-1	Dimensional, CTE				12	22			28		8
H-451 (preproduction I)	0.2 x 0.9	OG-1	Fatigue			42			19				
H-327 (production)	0.25 x 0.9	-	Tensile, dimensional, CTE		28				18				
H-327 (production)	0.25 x 0.9	OG-1	Tensile, dimensional, CTE		10		8		10		8	10	
H-327 (production)	0.2 x 0.45	OG-1	Dimensional, CTE	20	20	12				18			
H-327 (production)	0.2 x 0.45	GEH-13-422 OG-1	Dimensional, CTE								12		16
TS-1240 (preproduction)	0.25 x 0.9	-	Tensile, dimensional, CTE				26			20		28	24
P_3JHAN	0.2 x 0.45	OG-1	Dimensional, CTE			12		8	16			24	8
2020 (production)	0.12 x 0.45	OG-1	Dimensional	12	16	24	8	2			12	16	12
H-451 (preproduction I)	0.05 x 0.45	OG-1	Thermal conductivity	12				12		12			
H-327 (production)	0.05 x 0.45	OG-1	Thermal conductivity	5				5		5			
TS-1240 (preproduction)	0.05 x 0.45	-	Thermal conductivity	12				12		12			
Pyrocarbon		OG-1	Miscellaneous				1	1		1	1		
Silicon carbide		OG-1	Miscellaneous				1	1	1	1			
Carbon insulating material		-	Miscellaneous							1			
Boronated graphite		-	Miscellaneous				14			8			6

[a] Crucible number.

[b] Sixteen dimensional samples of previously irradiated H-451 from OG-1 will be switched between cell 1 and cell 6 to provide data on the effect of changing irradiation temperature.

ORNL-GAC Cooperative Irradiation Studies

Graphite Screening Tests (Capsules HT-20 through HT-23 at ORNL)

ORNL will screen near-isotropic graphites in the end positions of four ORNL HT-type HFIR capsules. The capsules, scheduled to begin irradiation in April 1974, are designed to operate between 910° and 960°C to fluences of ∿1.5, 3, 5, and 8 x 10^{21} n/cm^2 (E > 0.050 MeV). Several small crucibles containing PyC samples from GAC will also be included in each capsule. Graphites included are H-327, H-451, H-451L, TS-1240, and an experimental graphite fabricated by GAC and ORNL from a near-isotropic coke supplied by AirCo Speer.

Shim Particle Screening Tests (Capsules HT-24 and HT-25 at ORNL)

ORNL will conduct two HT-type capsule irradiations in HFIR to screen candidate shim particles for large HTGR fuel compact development. These capsules are tentatively scheduled to begin irradiation in May 1974 and are designed to operate between 840° and 1010°C to fluences of 4 to 8 x 10^{21} n/cm^2 (E > 0.050 MeV). BISO inert particle compacts containing low and intermediate loadings of four candidate GAC shim types and one ORNL-fabricated shim type will be tested. Two small crucibles containing PyC samples will also be included in the capsules. Fabrication of trial samples containing GAC's candidate shim types (Poco, GLCC 1099, Lonza, and Ringsdorff) has begun at ORNL. ORNL has fabricated several shim candidates.

STATISTICAL MEASUREMENTS OF GRAPHITE STRENGTH

A statistical study of the strength of H-451 graphite is being planned. A single log of production-grade H-451 graphite will be cut into slabs; 80 tensile samples including three sizes (0.5-in. diameter x 3 in. long, 0.375-in. diameter x 2 in. long, and 0.25-in. diameter x 0.9 in. long) and 80 bend samples (0.25-in. diameter x 2 in. long) will be machined in both parallel and perpendicular directions from each of four log locations.

The samples will be mechanically tested at room temperature. The statistical distribution of strengths within each batch, and the relationship between the median strengths of batches of samples with different sizes, will be compared with the predictions of the Weibull theory for the strength of brittle solids.

APPENDICES

APPENDIX A (TASK VIII): BENCHMARKS ORNL-1 THROUGH ORNL-4 AND ORNL-10

APPENDIX B (TASK VIII): BENCHMARKS PNL-1 THROUGH PNL-5

APPENDIX C (TASK VIII): BENCHMARKS TRX-1 THROUGH TRX-4

APPENDIX D (TASK VIII): BENCHMARKS MIT-1, MIT-2, AND MIT-3

APPENDIX A (TASK VIII)

BENCHMARKS ORNL-1 THROUGH ORNL-4 AND ORNL-10

GENERAL DESCRIPTION

This series of benchmarks consists of five unrelated spheres of U-235 (as uranyl nitrate) in H_2O, three of them poisoned with boron. Critical compositions and volumes were determined. These benchmarks are useful for testing H_2O fast scattering data, the U-235 fission spectrum, thermal capture and fission of U-235, and thermal absorption of hydrogen.

PHYSICAL PROPERTIES

Benchmarks ORNL-1 through ORNL-4 have a radius of 34.595 cm; ORNL-10 has a radius 61.011 cm.

	Concentration (10^{24} atoms/cm^3)				
Material	ORNL-1	ORNL-2	ORNL-3	ORNL-4	ORNL-10
B-10	0	1.0286×10^{-6}	2.0571×10^{-6}	2.5318×10^{-6}	0
H	0.66228	0.066148	0.066070	0.066028	0.066394
O	0.033736	0.033800	0.033865	0.033902	0.033592
N	1.869×10^{-4}	2.129×10^{-4}	2.392×10^{-4}	2.548×10^{-4}	1.116×10^{-4}
U-234	5.38×10^{-7}	6.31×10^{-7}	7.16×10^{-7}	7.62×10^{-7}	4.09×10^{-7}
U-235	4.8066×10^{-5}	5.6206×10^{-5}	6.3944×10^{-5}	6.7959×10^{-5}	3.6185×10^{-5}
U-236	1.38×10^{-7}	1.63×10^{-7}	1.84×10^{-7}	1.97×10^{-7}	2.20×10^{-7}
U-238	2.807×10^{-6}	3.281×10^{-6}	3.734×10^{-6}	3.967×10^{-6}	1.985×10^{-6}

CALCULATIONAL METHOD

It is suggested that the multiplication factor be calculated with multigroup S_n ($n \geq 4$) or equivalent P_ℓ theory.

The measured k values (Ref. A-1) and "corrected" experimental k values (Ref. A-2) are shown below. The corrections were evaluated by Staub et al. (Ref. A-2) to account for newer β values, the thin aluminum shells, distortion of the spherical shape, fill tubes, and room return.

	Measured k	Corrected Measured k
ORNL-1	1.00118	1.00026
-2	1.00073	0.99975
-3	1.00090	0.99994
-4	1.00028	0.99924
-10	1.00129	1.00031

COMMENTS AND DOCUMENTATION

The experiments are described in Ref. A-1. The experimental k values are for a sphere without container. Ref. A-2 presents a detailed analysis of these systems including a discussion of cross-section sensitivities and uncertainties in the analysis, both systematic and random.

REFERENCES

A-1. Gwin, R., and D. W. Magnuson, "Eta of U-233 and U-235 for Critical Experiments," Nucl. Sci. Eng. 12, 364 (1962).

A-2. Staub, A., et al., "Analysis of a Set of Critical Homogeneous U-H_2O Spheres," Nucl. Sci. Eng. 34, 263 (1968).

APPENDIX B (TASK VIII)

BENCHMARKS PNL-1 THROUGH PNL-5

GENERAL DESCRIPTION

This series of benchmarks consists of five unreflected spheres of plutonium nitrate solutions with hydrogen/Pu-239 atom ratios ranging from 124 to 1204. Critical volumes for the various solutions were measured. In one experiment the critical buckling was determined. These benchmarks are useful for testing H_2O thermal scattering data and cross sections for thermal neutron capture and fission by Pu-239.

PHYSICAL PROPERTIES

PNL-1 and PNL-2 have H/Pu-239 atom ratios of 698 and 124 [131 for PNL-2 (rev)], respectively; each contains 4.6 wt % Pu-240 and has an effective radius of 19.509 cm.

	Concentration (10^{24} atoms/cm^3)		
Material	PLN-1	PNL-2	PNL-2 (rev)[a]
H	0.06544	0.06126	0.064164
O	0.03459	0.03979	0.039768
N	6.216×10^{-4}	4.720×10^{-3}	4.7204×10^{-3}
Pu-239	9.375×10^{-5}	4.135×10^{-4}	4.141×10^{-4}
Pu-240	4.502×10^{-6}	1.985×10^{-5}	1.9844×10^{-5}

[a] Per personal communication from F. J. McCrosson, Savannah River Laboratory, December 6, 1973.

Benchmarks PNL-3 and PNL-4 have H/Pu-239 atom ratios of 1204 and 911, respectively; each contains 4.20 wt % Pu-240 and has an effective radius of 22.70 cm.

Material	Concentration (10^{24} atoms/cm^3)	
	PNL-3	PNL-4
H	0.06495	0.06041
O	0.03441	0.03712
N	7.393×10^{-4}	1.775×10^{-3}
Fe	1.294×10^{-6}	1.520×10^{-6}
Pu-239	5.395×10^{-5}	6.633×10^{-5}
Pu-240	2.355×10^{-6}	2.895×10^{-6}

Benchmark PNL-5 has an effective radius of 20.1265 cm, a H/Pu-239 atom ratio of 578, and contains 4.17 wt % Pu-240.

Material	Concentration (10^{24} atoms/cm^3)
H	0.06028
O	0.03710
N	2.737×10^{-3}
Fe	1.930×10^{-6}
Pu-239	0.043×10^{-4}
Pu-240	4.520×10^{-6}

CALCULATION METHOD

It is suggested that multiplication constants k be calculated using S_n theory ($n \geq 4$) with approximately 50 mesh points per sphere. Experimental data for PNL-1 includes a geometric buckling of 0.02182 cm^{-2}; hence, this benchmark may be analyzed using B_ℓ theory with $\ell \geq 1$.

EXPERIMENTAL DATA

The compositions and dimensions specified above were experimentally derived for criticality (k = 1). A geometric buckling of 0.02182 ± 0.00015 cm^{-2} was derived for PNL-1.

COMMENTS AND DOCUMENTATION

The experimental conditions associated with benchmarks PNL-1 and PNL-2 are given in Ref. B-1. Recent calculations for these two benchmarks with ENDF/B-II data are described in Ref. B-2. Reference B-3 documents the experimental conditions associated with PNL-3, PNL-4, and PNL-5. In all five experiments, the plutonium nitrate solutions were enclosed in stainless steel walled spheres. The effective radii quoted under Physical Properties were derived by the experimenters (Refs. B-1 and B-3) and specify critical sizes for solutions without stainless steel walls.

REFERENCES

B-1. Lloyd, R. C., et al., "Criticality Studies with Plutonium Solutions," Nucl. Sci. Eng. 25, 165 (1966).

B-2. Hansen, L. E., and E. D. Clayton, "Theory-Experiment Tests Using ENDF/B Version II Cross-Section Data," Trans. Am. Nucl. Soc. 15, 309 (1972).

B-3. Kruesi, F. E., et al., "Critical Mass Studies of Plutonium Nitrate Solution," USAEC Report HW-24514, General Electric, Hanford Atomic Products Operation, 1952.

APPENDIX C (TASK VIII)

BENCHMARKS TRX-1 THROUGH TRX-4

GENERAL DESCRIPTION

These benchmarks are H_2O-moderated lattices of slightly enriched (1.3%) uranium rods with diameters of 0.4915 cm in a triangular pattern. Measured lattice parameters include ρ^{28}, δ^{25}, δ^{28}, and C*; B^2 was measured for TRX-1 and TRX-2, but not for TRX-3 and TRX-4 which are two-region lattices. These lattices directly test cross sections for U-238 capture and U-235 fission, both thermal and epithermal, and U-238 fast fission. They are sensitive to U-238 inelastic scattering, the U-235 fission spectrum, and the H_2O cross sections.

INFINITE LATTICE CALCULATION

Physical Properties (Cylindrical Geometry)

Region	Outer Radius (cm)	Isotope	Concentration (10^{24} atoms/cm^3)
Fuel	0.4915	U-235	6.253×10^{-4}
		U-238	4.7205×10^{-2}
Void	0.5042		
Clad	0.5753	Al	6.025×10^{-2}
Moderator	(a)	H	6.676×10^{-2}
		O-16	3.338×10^{-2}

(a) Lattice spacings of 1.8060, 2.1740, 1.4412, and 2.8824 cm, respectively, for TRX-1 through TRX-4.

Suggested Method of Calculation

Monte Carlo, multigroup S_n ($n \geq 4$) or equivalent P_ℓ, or integral transport theory. An accurate treatment of resonance absorption is essential.

LEAKAGE CALCULATION

To account for leakage use a homogenized multigroup B_ℓ calculation with a total buckling $B^2 = 0.0057$ cm^{-2} for TRX-1 and $B^2 = 0.005469$ cm^{-2} for TRX-2. This is not suitable for TRX-3 and TRX-4, which are two-region lattices.

An alternative treatment of leakage, applicable to all four lattices, is to cylinderize them and calculate radial shapes explicitly using multigroup S_n or P_ℓ theory. In all four lattices the axial buckling is 0.000526 cm^{-2} [height = 122 cm (48 in)]; all are fully reflected. Core perimeters are as nearly circular as possible.

TRX-1: 764 fuel rods

TRX-2: 578 fuel rods

TRX-3: A hexagonal array of 169 UO_2 rods was removed from the center of the driver lattice (pitch 1.806 cm), leaving 1432 rods. A hexagonal array of 217 metal rods (pitch 1.4412 cm) was centered in the opening.

TRX-4: Every other rod of the TRX-3 inner lattice was removed, leaving 61 metal rods (pitch 2.8824 cm). 1809 UO_2 driver rods were now required.

Dimensions of Cylinderized TRX Lattices

Composition	Outer radius (cm)			
	TRX-1	TRX-2	TRX-3	TRX-4
Homogenized test lattice cells	26.2093	27.4419	11.1467	11.8198
Water gap	-	-	12.3268	12.3268
Homogenized driver lattice cells	-	-	37.9406	42.1717
Reflector		Large		

Properties of UO_2 Driver Lattice (TRX-3 and TRX-4)

Region	Outer Radius (cm)	Isotope	Concentration (10^{24} atoms/cm^3)
Fuel	0.4864	U-235	3.112×10^{-4}
		U-238	2.3127×10^{-2}
		O-16	4.6946×10^{-2}
Void	0.5042	-	
Clad	0.5753	Al	6.025×10^{-2}
Moderator	(a)	H	6.676×10^{-2}
		O-16	3.338×10^{-2}

(a) Triangular pitch lattice with spacing of 1.8060 cm.

Experimental Data

	TRX-1	TRX-2	TRX-3	TRX-4
Pitch, cm	1.8060	2.1740	1.4412	2.8824
Water/fuel vol. ratio	2.35	4.02	1.00	8.11
Number of rods	764	578	217	61
B^2, 10^{-4} cm^{-2}	57±1	54.69±0.36	-	-
ρ^{28}	1.311±0.02	0.830±0.015	3.01±0.05	0.466±0.01
δ^{25}	0.0981±0.001	0.0608±0.0007	0.230±0.003	0.0352±0.0004
δ^{28}	0.0914±0.002	0.0667±0.002	0.163±0.004	0.0452±0.0007
C*	0.792±0.008	0.646±0.002	1.255±0.011	0.526±0.004

NOTE: Parameters correspond to thermal cutoff of 0.625 eV and were measured at core center.

ρ^{28} = ratio of epithermal-to-thermal U-238 captures.

δ^{25} = ratio of epithermal-to-thermal U-235 fissions.

δ^{28} = ratio of U-238 fissions to U-235 fissions.

C* = ratio of U-238 captures to U-235 fissions.

COMMENTS AND DOCUMENTATION

Parameter measurements are described in Refs. C-1 and C-2. Measurements of thermal disadvantage factors (Ref. C-3) and fast advantage factors (Ref. C-4) are also available. Reference C-5 shows some additional details about the lattices, fuel rods, etc. Cadmium cutoff energies and foil perturbation were given careful attention.

REFERENCES

C-1. Hardy, J., Jr., D. Klein, and J. J. Volpe, "A Study of Physics Parameters in Several Water-Moderated Lattices of Slightly Enriched and Natural Uranium," USAEC Report WAPD-TM-931, Westinghouse Atomic Power Division, March 1970.

C-2. Hardy, J., Jr., D. Klein, and J. J. Volpe, Nucl. Sci. Eng. 40, 101 (1970).

C-3. Volpe, J. J., J. Hardy, Jr., and D. Klein, Nucl. Sci. Eng. 40, 116 (1970).

C-4. Hardy, J., Jr., D. Klein, and R. Dannels, Nucl. Sci. Eng. 26, 462 (1966).

C-5. Brown, J. R., et al., "Kinetics and Buckling Measurements in Lattices of Slightly Enriched U or UO_2 Rods in H_2O," USAEC Report WAPD-176, Westinghouse Atomic Power Division, January 1958.

APPENDIX D (TASK VIII)

BENCHMARKS MIT-1, MIT-2, AND MIT-3

GENERAL DESCRIPTION

These benchmarks consist of D_2O-moderated lattices of natural uranium rods with diameters of 2.565 cm positioned in a triangular lattice pattern. The associated lattice spacings are 11.43, 12.70, and 14.605 cm. Measured lattice parameters include B^2, ρ^{28}, δ^{25}, δ^{28}, and C*. These lattices are useful for testing D_2O cross-section data and cross sections for thermal and epithermal U-235 fission, thermal and epithermal U-238 neutron capture, and U-238 fast fission.

INFINITE LATTICE CALCULATION

Physical Properties (Cylindrical Geometry)

Region	Outer Radius (cm)	Composition	
		Isotope	Concentration (10^{24} atoms/cm^3)
Fuel	1.283	U-235	3.489×10^{-4}
		U-238	4.750×10^{-2}
Clad	1.354	Al	6.049×10^{-2}
Moderator	(a)	H-1	1.850×10^{-4}
		H-2	6.641×10^{-2}
		O-16	3.321×10^{-2}

(a) Lattice spacings of 11.32, 12.70 and 14.605 cm (benchmarks MIT-1, MIT-2, and MIT-3, respectively).

Suggested Method of Calculation

Monte Carlo, S_n ($n \geq 4$), or integral transport theory. An accurate treatment of resonance absorption is essential.

AXIAL LEAKAGE CALCULATION

To account for leakage, use the following geometric bucklings in B_ℓ calculations with $\ell \geq 1$:

Benchmark	Pitch (cm)	B^2 (10^6 cm^{-2})
MIT-1	11.43	848
MIT-2	12.70	865
MIT-3	14.605	815

A less desirable way to account for axial leakage is to use the following critical heights, h:

Benchmark	h (cm)	λ_{tr} (cm)
MIT-1	103.8	2.845
MIT-2	102.9	2.769
MIT-3	106.2	2.692

These heights have been derived from measured material bucklings using

$$B^2 = \left(\frac{\pi}{h + 2}\right)^2 ,$$

when the extrapolation distances, ε, have been determined using the relation

$$\varepsilon = 0.71\ \lambda_{tr} .$$

The values for the transport mean free patch λ_{tr} were obtained using leakage-corrected integral transport theory and ENDF/B-III cross sections.

EXPERIMENTAL DATA

Parameter	Pitch (cm)		
	11.43	12.70	14.605
B^2, 10^6 cm^{-2}	848 ± 10	865 ± 10	815 ± 8
ρ^{28}	0.498 ± 0.008	0.394 ± 0.002	0.305 ± 0.004
δ^{25}	0.0447 ± 0.0019	0.031 ± 0.003	0.0248 ± 0.0010
δ^{28}	0.0597 ± 0.0020	0.0596 ± 0.0017	0.0583 ± 0.0012
C*	1.017 ± 0.023	0.948 ± 0.020	0.859 ± 0.016

NOTE: Parameters correspond to thermal cutoff of 0.625 eV.

ρ^{28} = ratio of epithermal-to-thermal U-238 captures.

δ^{25} = ratio of epithermal-to-thermal U-235 fissions.

δ^{28} = ratio of U-238 fissions to U-235 fissions.

C* = ratio of U-238 captures to U-235 fissions.

COMMENTS AND DOCUMENTATION

The physical properties of the lattices and the experimental facilities are described in Ref. D-1. The measured lattice parameters are documented in Ref. D-2. With regard to the latter, no mention is made of the cadmium cutoff energy to be associated with the δ^{25}, ρ^{28} measurements. Apparently the experiments employed 20-mil Cd covers (Refs. D-3 and D-4); hence, the values reported in Ref. D-2 correspond to a cutoff energy of approximately 0.55 eV. The experimental values for δ^{25} and ρ^{28} recorded here have been adjusted from a 0.555-eV cutoff energy to a 0.625-eV cutoff using ENDF/B cross sections.

REFERENCES

D-1. Palmedo, P. F., et al., "Measurements of the Material Bucklings of Lattices of Natural Uranium Rods in D_2O," USAEC Report NYO-9660 (MITNE-13), Massachusetts Institute of Technology, 1962.

D-2. Thompson, T. J., et al., "Heavy Water Lattice Project Final Report," Massachusetts Institute of Technology Report MIT-2344-12, 1967.

D-3. Kaplan, Irving, et al., "Heavy Water Lattice Project Annual Report, September 30, 1963," USAEC Report NYO-10,212 (MITNE-46), Massachusetts Institute of Technology, 1963.

D-4. Driscoll, M. J., Massachusetts Institute of Technology, private communication, 1972.

APPENDIX E

PROJECT REPORTS PUBLISHED DURING THE QUARTER

Borgonovi, G. M., "An Assessment of Noise Analysis Techniques for Large HTGRs," USAEC Report Gulf-GA-B12823, Gulf General Atomic Company, 1973.

Mathews, D. R., and P. K. Koch, "GANDY 3 - A Computer Program for the Evaluation of Effective Cross Sections in the Unresolved Resonance Region," USAEC Report GA-A12826, General Atomic Company, January 1974.

Gulden, T. D., J. L. Scott, and C. Moreau, "Present Thorium-Cycle Fuel Concepts and Performance Limitations," General Atomic Company Report GA-A12877, February 1974.